STIC-ILL

From: Canella, Karen
Sent: Sunday, February 03, 2002 9:00 PM
To: STIC-ILL
Subject: ill order 09/815,340

Art Unit 1642 Location 8E12(mail)

Telephone Number 308-8362

Application Number 09/815,340

1. Trends in Cell biology, 2001 Jan, 11(1):18-21
2. Clinical Cancer Research, 2000 Aug, 6(8):3215-3221
3. Mutation Research, 1997 Apr 29, 375(2):157-165
4. american Journal of Hematology, 1985 Mar, 18(3):243-249.
5. PNAS, 1989 Apr, 86(7):2276-2280
6. Genes and Development, 1996 Oct 15, 10(20):2621-2631
7. Cancer, 1975 Jun, 35(6):1664-1677
8. Mutation Research, 1978, 57(3): 313-324
9. Environ Mutagen, 1981, 3(1):53-64
10. Nucleic Acids Research, 2001 Mar 15, 29(6):1300-1307
11. Oncogene:
    1998 Oct 29, 17(17):2187-2193
    2000 Jan 20, 19(3):403-409
12. Molecular endocrinology, 1999 Jan, 13(1):156-166
13. Gene, 1999 Nov 29, 240(2):317-324
14. Science, 1999 Jul 16, 285(5426)418-422
15. Biochemistry and Molecular biology international, 1999 May, 47(5):891-897
16. Journal of Clinical Endocrinology and Metabolism, 1999 Mar, 84(3):1149-1152
17. Journal of biological chemistry:
    1999 Jan 29, 274(5):3151-3158
    2000 Nov 24, 275(47):36502-36505 ***
18. Gene 2000 May 2, 248(1-2):41-50
19. Molecular endocrinology, 2000 Aug, 14(8):1137-1146
20. Cancer Letters, 2001 Feb 10, 163(1):131-139
21. Brain Pathology, 2001 Jul, 11(3):328-341

Oncogene (1998) 17, 2187-2193

http://www.stockton-press.co.uk onc

hpttg, a human homologue of rat *pttg*, is overexpressed in hematopoietic neoplasms. Evidence for a transcriptional activation function of hPTTG

África Domínguez[1], Francisco Ramos-Morales[1,2], Francisco Romero[1], Rosa M Rios[1], François Dreyfus[3], María Tortolero[1] and José A Pintor-Toro[2]

[1]*Departamento de Microbiología, Facultad de Biología, Universidad de Sevilla. Apdo. 1095. 41080-Sevilla, Spain;* [2]*Instituto de Recursos Naturales y Agrobiología, Apdo. 1052. 41080-Sevilla, Spain;* [3]*Service hématologie, Hôpital Cochin, Rue du Fb St Jacques. 75015 Paris, France*

We have isolated a human cDNA clone encoding a novel protein of 22 kDa that is a human counterpart of the rat oncoprotein PTTG. We show that the corresponding gene (*hpttg*) is overexpressed in Jurkat cells (a human T lymphoma cell line) and in samples from patients with different kinds of hematopoietic malignancies. Analysis of the sequence showed that hPTTG has an amino-terminal basic domain and a carboxyl-terminal acidic domain, and that it is a proline-rich protein with several putative SH3-binding sites. Subcellular fractionation studies show that, although hPTTG is mainly a cytosolic protein, it is partially localized in the nucleus. In addition we demonstrate that the acidic carboxyl-terminal region of hPTTG acts as a transactivation domain when fused to a heterologous DNA binding domain, both in yeast and in mammalian cells.

Keywords: PTTG; oncogene; transcription; tumorigenesis

Introduction

Cancer is a disease of genes that arises via a multistep process in which a normal somatic cell progresses to a fully malignant tumor through a recurrent mechanism of clonal expansion triggered by genetic lesions (Vogelstein and Kinzler, 1993). These lesions include mutations, but also aberrant expression, of protooncogenes or tumor suppressor genes.

Gene transcription is a key regulatory point in diverse developmental processes such as cell growth, differentiation, apoptosis and transformation. The transcription factors are often tightly regulated and the activities of these proteins can be modified at a variety of levels. Their inappropriate expression may subvert normal programs of cell proliferation, differentiation, and survival. Genes coding for transcription factors are the most frequently affected by altered expression in acute leukemias, emphasizing the critical role of these regulatory molecules in blood cells development (Shivdasani and Orkin, 1996). Activation of transcription factors such as *myc*, *hox11*, *lmo1*, *lmo2*, *tall*, *lyl1*, *tal2*, *aml1*, *cbfβ*, *mll* and *pbx* is involved in acute leukemias (reviewed in Hwang and Baer, 1995; Look, 1997). However, a much larger number of genes are probably involved in primary and secondary processes responsible for the acquisition of the phenotype of tumor cells. Identification of these genes and analysis of their functions is helping efforts to understand the mechanisms of tumorigenesis, as well as the normal physiology of eukaryotic cells.

The rat protein PTTG (Pei and Melmed, 1997) was identified because of the differential expression of its mRNA in pituitary tumor cells. Its overexpression was able to induce cell transformation *in vitro* in mouse 3T3 cells, and tumor formation in nude mice.

Now we have cloned a human cDNA homologue of *pttg*. This gene, named *hpttg*, is overexpressed in Jurkat cells as well as in leukocytes from patients with different kinds of hematopoietic neoplasms or myelodysplastic syndromes. In contrast, its expression in samples obtained from normal donors is very low or undetectable. Analysis of the sequence showed that the protein contains an amino-terminal basic domain and a carboxyl-terminal acidic domain. In many eukaryotic transcription activators, the presence of an acidic region in the carboxyl terminus correlates with the transactivation domain (Ptashne, 1988). Importantly, we demonstrate that the acidic C-terminal region of hPTTG acts as a transactivation domain when fused to a heterologous DNA binding domain.

Results

Molecular cloning of human pttg *cDNA*

After screening a Jurkat cell oligo(dT) cDNA library by the yeast two-hybrid system with Grb3-3 (an isoform of Grb2) as a bait, several positive clones were isolated (Ramos-Morales *et al.*, 1997). The cDNA insert from one of these clones (g24) contained a 700 base pairs (bp) insert and carried a poly-A tail as expected. An open reading frame was detected in these sequence but the first ATG codon was not preceded of any in-frame stop codon. In order to obtain additional sequence, a screening of a λgt11 human thymus oligo(dT) cDNA library was performed using the insert from clone g24 as a probe. Three clones were obtained and the cDNA inserts were subcloned into pBluescript and sequenced. The three clones were different in size but identical in the overlapping sequence.

As shown in Figure 1a, the longest sequence comprises 787 bp and contains an open reading frame of 609 bp. The presence of an in-frame stop codon upstream of the predicted initiation codon indicates

Correspondence: JA Pintor-Toro
The first two authors contributed equally to this work
Received 9 March 1998; revised 18 May 1998; accepted 18 May 1998

that the complete coding sequence was present in this clone as well as in g24. The predicted protein sequence consists of 202 amino acids and has a calculated molecular mass of 22 024 daltons and a pI of 6.55.

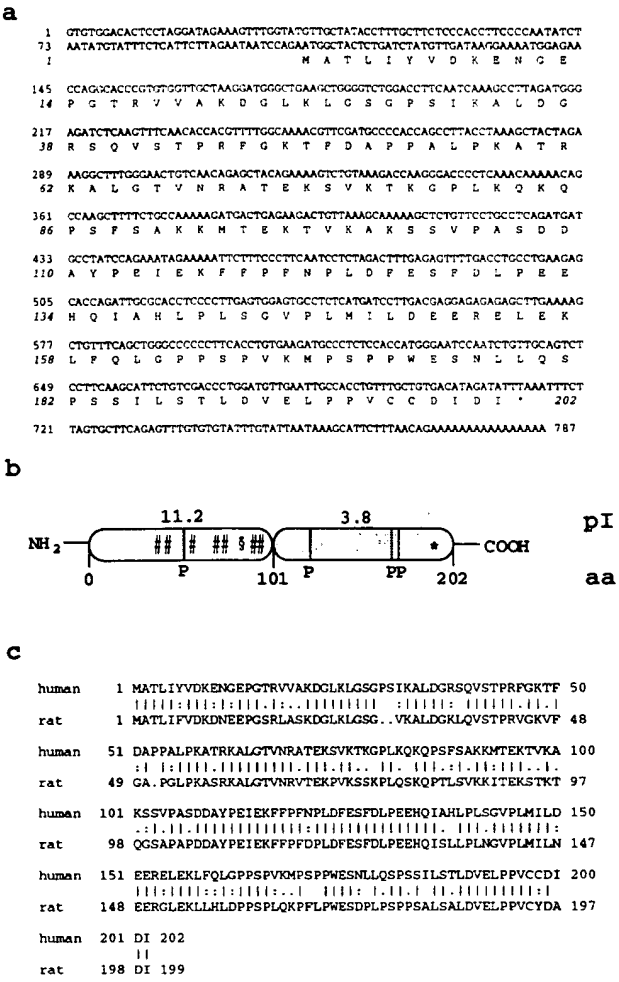

Figure 1 Cloning and sequencing of *hpttg*. (**a**) cDNA and predicted amino acid sequence of *hpttg*. The sequence is available from EMBL/GenBank under accession number AJ223953. (**b**) Schematic representation of hPTTG protein. The protein can be divided in two domains, an amino-terminal domain with isoelectric point 11.2 and a carboxyl-terminal domain with isoelectric point 3.8. Putative motifs are indicated as follows: P: Pro-X-X-Pro motif (putative SH3-binding motif), #: Protein kinase C phosphorylation site, §: cyclic-AMP and cyclic-GMP dependent protein kinase phosphorylation site, *: Casein kinase phosphorylation site. (**c**) Amino acid sequence alignment of human and rat PTTG. A BESTFIT comparison is shown. Both sequences are 72% identical and 82% similar

The PROSITE Dictionary of Protein Sites and Patterns revealed consensus motifs for cyclic AMP and cyclic GMP dependent protein kinase phosphorylation, casein kinase II phosphorylation and protein kinase C phosphorylation. The secondary structure and charge display of the protein was predicted using the programs PeptideStructure and Pepstats (not shown). According to these analyses, the protein can be divided in an amino-terminal basic domain (amino acids 1 to 101) of pI 11.2 and a carboxyl-terminal acidic domain (amino acids 102 to 202) of pI 3.8. It is of note the high content in prolines (12%) and the presence of several proline motifs that could mediate interaction with SH3 domain containing proteins (Figure 1b).

When the cDNA sequence was used to search the EMBL and GenBank data bases for homologous sequences, 79% identity was found with a recently isolated rat gene, *pttg*, that is exclusively expressed in pituitary tumor cell lines but not in normal pituitary (Pei and Melmed, 1997). The predicted human PTTG protein was 72% identical and 82% similar to the rat protein (Figure 1c). A search on the EST division of GenBank revealed many partial human sequences identical to g24. There were not human EST sequences more similar to rat *pttg* than the sequence contained in g24, so it probably corresponds to the human counterpart of *pttg*. To confirm this, g24 insert was used to screen a λZAPII rat testis oligo(dT) cDNA library. All clones obtained were identical to rat *pttg* in the coding region.

Table 1 summarizes the results obtained when the predicted amino acid sequence of the new protein was used in a similarity search performed on databases SWISSPROT+TREMBL+TREMBLNEW with the Washington University version of the program BLASTP. The accession number, species, name, per cent of identity and similarity and length of similar segments are given for the ten sequences producing the highest scores. The highest score corresponds to rat PTTG. Most of the rest are histones or other DNA-binding proteins, including a known transcription factor: mouse stromelysin PDGF responsive element binding protein transcription factor (Sanz *et al*., 1995).

In vitro *transcription and translation of human* pttg *and analysis of expression by Western blotting*

To molecularly characterize the human PTTG (hPTTG) protein, a set of experiments was performed. First, as shown in Figure 2a, translation of the *in vitro* transcribed g24 clone generated a product

Table 1 Sequences producing high-scoring segment pairs after a similarity search with hPTTG using database SWALL and program BLASTP

Accession number	*Species*	*Name*	*% Identity*	*% Similarity*	*Length of segments*
P97613	*Rattus norvegicus*	Pituitary tumor-specific	72	82	202
Q13078	*Homo sapiens*	AR1 DNA-binding protein	29	43	194
O01332	*Caenorhabditis elegans*	F46A8.6	32	57	71
Q08864	*Volvox carteri*	Histone H1-I	30	43	105
Q60792	*Mus musculus*	Stromelysin PDGF responsive element binding protein transcription factor	29	42	175
D1023837	*Homo sapiens*	KIAA0292 (fragment)	29	43	194
E274710	*Alnus glutinosa*	AG13 protein precursor	27	51	103
P19375	*Strongylocentrotus purpuratus*	Histone H1, early embrionic	35	50	68
Q02539	*Homo sapiens*	Histone H1.1	34	49	93
P43277	*Mus musculus*	Histone H1.3	32	46	92

of apparent molecular mass of approximately 29 kDa on SDS-PAGE. Next, hPTTGΔC124, a fragment of clone g24, was subcloned into a pGEX-4T-2 bacterial expression vector in order to overproduce a glutathione-S-transferase (GST) fusion protein containing amino acids 1 to 123 from human PTTG. A polyclonal antiserum was raised in rabbit against the GST fusion protein. The resulting immune rabbit serum (anti-hPTTG) reacted strongly with the fusion protein and with both GST and hPTTG moieties obtained after thrombin treatment (Figure 2b). The expression of *hpttg* was assessed in Jurkat cells by Western blotting with the rabbit polyclonal serum. Nonidet P-40 lysates were resolved by SDS-PAGE, transferred to a nitrocellulose filter, and revealed with the polyclonal serum anti-hPTTG. A band of apparent molecular mass of 29 kDa was observed, confirming the result obtained by *in vitro* transcription and translation of clone g24 (Figure 2c).

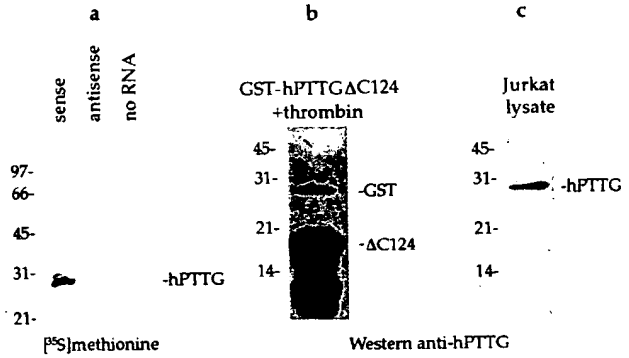

Figure 2 hPTTG protein analysis. (**a**) *In vitro* transcription and translation of hPTTG. *In vitro* transcription and translation of hPTTG product was analysed by SDS-PAGE on a 10% polyacrylamide gel. (**b**) Analysis of bacterial fusion proteins with anti-hPTTG rabbit serum. 1 μg of GST plus thrombin-released hPTTGΔC124 was electrophoresed, blotted, and probed with anti-hPTTG rabbit serum. The bands of lower molecular weight decorated by the antibody are the result of partial degradation of hPTTGΔC124 and are also detected by Coomassie blue staining. (**c**) Immunoblot analysis of cell extracts. A Nonidet P-40 lysate from 5×10^5 Jurkat cells was electrophoresed on a 15% polyacrylamide gel, transferred to nitrocellulose filter, and immunoblotted with anti-hPTTG serum using the ECL system. Molecular weight markers are indicated in kDa

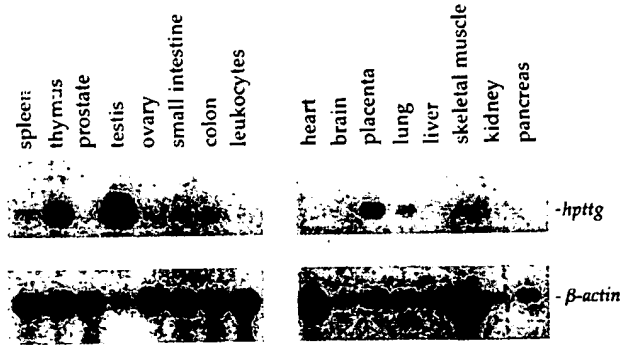

Figure 3 Northern blot analysis in normal tissues. Northern blot of poly(A)$^+$ RNA from the indicated human adult tissues (Clontech) with g24 cDNA and human β-actin cDNA (bottom panel shows relative amounts of RNA on each lane)

Tissue distribution of human pttg

To investigate the expression of human *pttg* (*hpttg*), Northern blot analysis of mRNA from different human adult tissues was performed with g24 insert as a probe. As seen in Figure 3, a single band of about 900 bp was observed in some tissues. High level of expression is observed in testis, thymus and placenta. Very low or undetectable expression levels were observed in spleen, prostate, ovary, peripheral blood leukocytes, heart, brain, liver, skeletal muscle, kidney and pancreas.

hpttg *is overexpressed in hematopoietic tumors*

The low expression of *hpttg* in leukocytes (some expression is observed after long exposure in the Northern blotting), together with the fact that g24 clone was obtained from Jurkat cells, prompted us to compare the expression of this mRNA in normal T lymphocytes and Jurkat T cells. Northern blot analysis showed a high expression in Jurkat cells whereas it was not detected in isolated peripheral T lymphocytes (Figure 4, left panel). Next the expression of *hpttg* was assessed in samples from patients with leukemia, lymphoma or myelodysplastic diseases (Figure 4, right panel). Twenty out of 28 patients (70%) expressed detectable levels of *hpttg*, in contrast with healthy donors, indicating that overexpression of this gene is correlated with hematopoietic diseases.

Subcellular localization of hPTTG

The localization of hPTTG was examined in Jurkat cells by subcellular fractionation. Western blot experiments performed on cytosol and nuclear fractions showed that hPTTG is mainly located in the cytosol. However, it is also partially localized in the nucleus (Figure 5). Quantification of the bands by scanning densitometry shows that about 15% of hPTTG is present in the nucleus of Jurkat cells. This

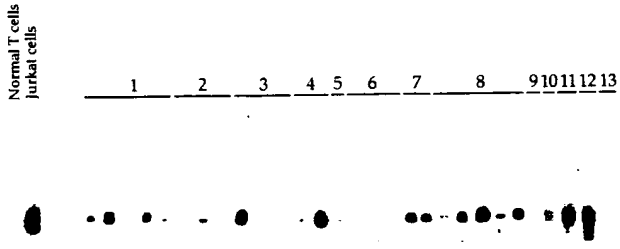

Figure 4 Overexpression of *hpttg* in hematopoietic neoplasms. Left panel: Expression of *hpttg* in Jurkat cells and normal T lymphocytes. Equal amounts of total RNA from Jurkat cells and isolated T lymphocytes from normal donors were used for Northern blot analysis. Right panel: Expression of *hpttg* in hematopoietic neoplasms. Total RNA from samples isolated from patients with the following hematopoietic diseases were used for Northern blot analysis: 1, plasmocytomas; 2, acute monoblastic leukemias; 3, acute myelomonocytic leukemia; 4, acute erythroleukemia; 5, acute promyelocytic leukemia; 6, chronic myelomonocytic leukemia (chronic phase); 7, refractory anemia with ringed sideroblasts; 8, refractory anemia with excess blasts; 9, thrombocytemia; 10, follicular lymphoma; 11, Hodgkin's lymphoma; 12, lymphoplasmoide lymphoma. RNA from normal perypheral blood leukocytes is included in 13. RNA concentrations were determined by optical density and equal amounts of each sample were loaded. g24 cDNA was used as a probe

estimation largely exceeds the 1% calculated of maximal contamination of cytosolic proteins in the nuclear fraction (see the Materials and methods section).

hPTTG exhibits transcriptional activity in yeast

The similarity of hPTTG to DNA-binding proteins together with the partial nuclear localization of the protein and the presence of an excess of negative charged residues in the C-terminal region, may suggest a function of hPTTG in transcription activation. In order to investigate this possibility, g24 insert was subcloned into the two-hybrid vector pGBT9 to obtain a fusion between Gal4 DNA-binding domain and hPTTG. *Saccharomyces cerevisiae* strain HF7c, containing *his3* and *lacZ* reporter genes under the control of Gal4-responsive elements, was transformed with plasmid pGBT9-hPTTG alone and tested for growth on selective medium and for β-galactosidase activity. pGBT9-hPTTG was able to induce β-galactosidase activity and to promote growth of HF7c in selective medium even when this medium was supplemented with 5 mM 3-amino-1,2,4-triazole (Figure 6). In order to elucidate the domain involved in this activation two subclones were made in the vector pGBT9. As seen in Figure 6, strain HF7c transformed with pGBT9-hPTTGΔN122 (lacking amino acids 1–122) was still able to grow in selective medium, whereas the same strain carrying plasmid pGBT9-hPTTGΔC124 (lacking amino acids 124–202) was not. These results show that the carboxyl-terminal domain of hPTTG is able to display a strong transcriptional activity in yeast.

hPTTG transcriptional activity in mammalian cells

To rule out the possibility that hPTTG activates transcription only in the yeast system, we examined the transcriptional activity of this protein using a mammalian cell line, Cos-7. g24 insert was subcloned into the vector pGAL4. Cos-7 cells were cotransfected with this plasmid and with the pGAL4-4TK-luc luciferase reporter plasmid. As seen in Figure 7, hPTTG shows transcriptional activity of the same level than the activity displayed by GAL4-VP16 (Sadowski *et al*., 1988), a strong transcriptional activator used as a positive control. Subclones hPTTGΔN122 and hPTTGΔC124 were also prepared in the vector pGAL4. Subclone hPTTGΔN122 showed the same transcriptional activity as the full length hPTTG whereas subclone hPTTGΔC124 was not able to activate transcription to a detectable level (Figure 7). Similar results were obtained in mouse NIH3T3 cells (not shown). These results confirm and extend the data obtained in yeast.

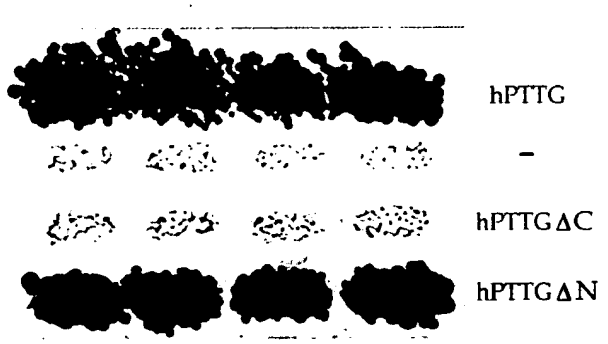

Figure 6 Transcriptional activation by hPTTG in yeast. Hf7c reporter strain was transformed with pGBT9 alone (–), pGBT9-hPTTG (hPTTG), pGBT9-hPTTGΔC124 (hPTTGΔC) or pGBT9-hPTTGΔN122 (hPTTGΔN). Growth in the absence of histidine and with 5 mM of 3-amino-1,2,4-triazole indicates transactivation. Each patch represents an independent transformant. There are four patches for every strain

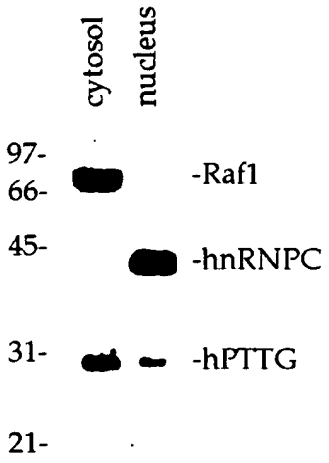

Figure 5 Detection of hPTTG in cytosol and nuclear fractions of Jurkat cells. Subcellular fractions from 5×10^5 Jurkat cells were separated on SDS–PAGE, transferred to nitrocellulose membrane and then probed with anti-hPTTG polyclonal antibody. The same filter was reblotted with anti-Raf1 polyclonal antibody and anti-hnRNP C monoclonal antibody, respectively, to control the purity of the fractions. Exposure of 2 min using epichemiluminescence Western immunoblotting system (ECL, Amersham)

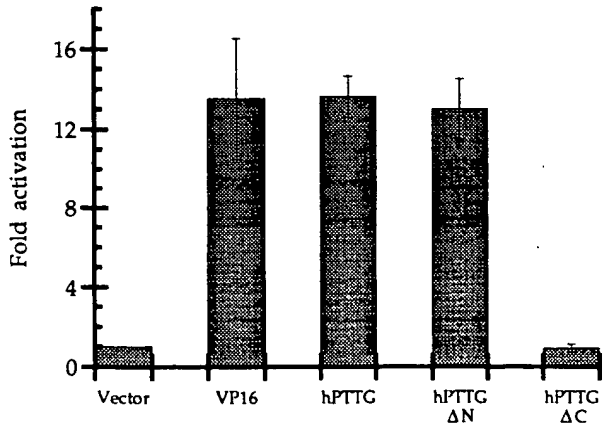

Figure 7 Transcriptional activation by hPTTG in mammalian cells. Different protein regions were fused to the GAL4 DNA binding domain and tested for activation by cotransfection of Cos-7 cells with a GAL4 site-dependent reporter plasmid driving expression of the luciferase gene. pGAL4-VP16 (VP16) contains the activation sequences of the VP16 protein. pGAL4-hPTTG (hPTTG) contains full length hPTTG protein. pGAL4-hPTTGΔN122 (hPTTGΔN) fuses 80 carboxyl-terminal residues from hPTTG to GAL4 DNA-binding domain. pGAL4-hPTTGΔC124 (hPTTGΔC) comprises 123 amino-terminal residues from hPTTG. Luciferase values from at least three independent transfections are plotted as fold activation over control

Discussion

In this study we report the isolation and characterization of a human counterpart of the rat gene *pttg* (for pituitary tumor-transforming gene) (Pei and Melmed, 1997). *pttg* mRNA is highly expressed in GC and GH_4 rat pituitary tumor cell lines but not in normal pituitary or osteogenic sarcoma cells. Transfection experiments in mouse 3T3 cells and injection of transfected cells into athymic nude mice showed that *pttg* is a potent transforming gene.

We have isolated *hpttg* cDNA from a Jurkat cDNA library. This fact together with the low expression observed in normal peripheral blood leukocytes prompted us to investigate the expression of this gene in normal T lymphocytes, Jurkat T cells and samples from healthy donors and from patients with leukemia or other hematopoietic neoplastic disorders. Our data show that *hpttg* is overexpressed not only in Jurkat cells but also in a high proportion of the primary tumors examined, indicating that this is not an artifact of cell culture. These results show an aberrant expression of the *hpttg* gene in leukemic cells and suggest the involvement of this gene in leukemogenesis.

The mechanism that leads to ectopic expression of hPTTG is unknown. However, chromosomal translocations are present in a high proportion of leukemias. These structural rearrangements may activate proto-oncogenes that are silent or expressed at low levels in the progenitors cells of a particular lineage by placing them under the control of potent enhancer elements within the regulatory region of a gene that is normally highly expressed. Chromosomal translocations are found in 65% of acute leukemias (Look, 1997); a chromosome translocation to the IgH locus, most frequently into a switch region, is a nearly universal event in myeloma cell lines, and it appears to be equally frequent in primary tumor samples (Hallek *et al*., 1998). Studies of chromosome abnormalities associated with T cell acute leukemias have implicated an increasing number of different protooncogenes (Hwang and Baer, 1995). Chromosomal mapping of the *hpttg* gene in normal and leukemic cells could help to understand the cause of its aberrant expression.

Among adult tissues examined, testis is the only tissue that expresses rat *pttg*. We have studied 16 human adult tissues and we show that *hpttg* is expressed at high level in testis but also in thymus and placenta. Interestingly these organs are immune privileged sites. Immune privilege is a mechanism to protect some organs against dangerous and unwanted immune reactions (see Streilein (1993) for a review). Expression of FasL (the ligand for Fas/APO-1/CD95, a member of the TNF receptor superfamily) has been recently involved in immune privilege (Bellgrau *et al*., 1995; Griffith *et al*., 1995). This mechanism may also account for the ability of tumor cells to evade immune destruction. A relationship between overexpression of hPTTG and immune privilege would be an attractive mechanism to explain the tumorigenic potential of hPTTG that deserves further studies. On the other hand, comparison of the high expression observed in thymus with the undetectable levels observed in normal T cells suggests a role of hPTTG in normal hematopoietic development.

Transcriptional activators are typically composed of distinct domains including separable DNA-binding and activation domains (for a review, see Triezenberg, 1995). This feature allows the use of a heterologous binding domain to study the activation domains when the physiological targets of a transcription factor have not been defined. This approach has been used to identify transcriptional domains in the oncoproteins BRCA1 (Chapman and Verma, 1996; Monteiro *et al*., 1996) and BRCA2 (Milner *et al*., 1997). By using the same approach, we show that the C-terminal portion of hPTTG (amino acids 123–202) is able to activate transcription of the *his3* and *lacZ* genes in *S. cerevisiae* HF7c as well as the luciferase gene in mammalian cells, all driven by GAL4 responsive elements. Interestingly, the activation observed in mammalian cells has the same level as that displayed by VP16, used for comparison, and considered as a very strong activator (Sadowski *et al*., 1988). These results provide insight into the potential function of the hPTTG protein. They suggest that this protein has the ability to stimulate transcription.

The activation domains have been classified depending on whether they are rich in acidic amino acids, glutamine or proline. Several mammalian proteins containing acidic-rich and/or proline-rich activation domains have been shown to stimulate transcription in *S. cerevisiae* (Lech *et al*., 1988; Metzger *et al*., 1988; Sadowski *et al*., 1988; Schena and Yamamoto, 1988; Struhl, 1988) and in *Schizosaccharomyces pombe* (Remacle *et al*., 1997). The domain of hPTTG that shows transactivation capacity (amino acids 123–202), although rich in proline, seems to belong to the acidic-rich class since it contains 19% of acidic amino acids and has a net charge of −12.

Subcellular fractionation studies indicated that hPTTG is mainly cytoplasmic and partially localized in the nucleus. The controls of the purity of subcellular fractions included in Figure 5 demonstrate that there is no significant leakiness from one fraction to another and so the nuclear proportion of hPTTG is low but significant. A modulation of this localization could occur under proper conditions. This behaviour is observed in known transcriptional activators. The Stat proteins, for instance, are cytoplasmic in non-stimulated cells. In response to IFN-α treatment, Stat 1α, Stat 1β and Stat 2 become tyrosine-phosphorylated and migrate to the nucleus where they join a 48 kDa DNA-binding protein and subsequently direct the transcription at IFN-α responsive elements (Darnell, 1997).

Definite confirmation that transcriptional activation exhibited by hPTTG is physiologically relevant must await the demonstration of its DNA-binding activity, or its interaction with a DNA-binding protein, together with the identification of its target genes.

Materials and methods

Two-hybrid screen

A cDNA library from Jurkat cell polyadenylated RNA constructed in fusion with Gal4-activation domain in pGAD1318 (Hannon *et al*., 1993) was used (Bartel *et al*., 1993). *S. cerevisiae* strain Hf7c (*MAT* **a** *trpl-901 leu2-3,112 his3-200 ura3-52 lys-801 ade2-101 canr gal4-542 gal80-538 LYS2::GAL1-HIS3 URA3::Gal4 binding site-CYC1-lacZ*)

was grown at 30°C in YPD medium containing 1% yeast extract, 2% polypeptone and 2% glucose, and it was sequencially transformed with pGBT-Grb3-3 and the Jurkat cell cDNA library by the lithium acetate method (Sherman *et al.*, 1986). Double transformants were plated on yeast drop-out medium lacking tryptophan and leucine (Sherman *et al.*, 1986). They were grown for 3 days at 30°C and then colonies were patched on the same medium and replica-plated on Whatman 40 filters, to test the β-galactosidase activity (Breeden and Nasmyth, 1985), and on yeast drop-out media lacking tryptophan and leucine and supplemented with 5 mM 3-amino-1,2,4-triazole (Sherman *et al.*, 1986) (the Gal4-Grb3-3 fusion protein had a weak transcriptional activity if yeast grew only in selective medium). Positive clones were rescued and tested for specificity by retransformation into Hf7c either with pGBT-Grb3-3 or with irrelevant targets.

cDNA cloning and sequence analysis

Clone g24, obtained after screening by the two-hybrid system, was subcloned in pGBT9 for transactivation experiments in yeast, and in pGAL4 for transactivation experiments in Cos-7 cells. The entire g24 insert was used as a probe to hybridize against a human thymus cDNA λgt11 library. The clones obtained were isolated and subcloned into pBluescript plasmid. The nucleotide sequence was determined by using an automated sequencer from Pharmacia.

Nucleic acids and protein sequences were analysed by the University of Wisconsin Genetics Computer Group sequence analysis software package version 8.1 for UNIX computers (Devereux *et al.*, 1984). Comparisons to known sequences were performed by BLAST (Altschul *et al.*, 1990) on the Internet server. Secondary structure analysis was conducted with the software programs Pepstats and PeptideStructure (Kyte and Doolittle, 1982; Chou and Fasman, 1978; Garnier *et al.*, 1978).

Patients

Peripheral blood, bone marrow or lymph nodes samples were obtained from patients who had been referred to the Hematology Department at Hôpital Cochin (Paris). All specimens were collected before the initiation of therapy and were obtained from patients with hematopoietic disorders. The diagnosis was established on the basis of morphologic and cytochemical staining, and the patients were classified according to the criteria of the French-American-British committee.

mRNA preparation and Northern blot analysis

A poly(A)$^+$ RNA blot from Clontech was hybridized with ^{32}P-labeled cDNA insert from clone g24 and washed as described in the manufacturer's instructions. The membrane was stripped and rehybridized to a human β-actin cDNA control probe. Peripheral blood or bone marrow cells were isolated after Ficoll-Hypaque density gradient centrifugation and washed three times in Hank's balanced salt solution. RNA was extracted by the guanidium thiocyanate procedure. After precipitation in ethanol at −20°C, RNA pellets were resuspended in water. RNA concentrations were determined by optical density, and samples were frozen at −80°C until use. RNA samples (10 μg of total RNA) were denatured in glyoxal, dimethyl sulfoxide and phosphate buffer at 60°C during 10 min, size-fractionated by electrophoresis through 1% agarose gel and transferred to nylon membrane. Membranes were hybridized with random ^{32}P-labeled probe and washed under stringent conditions. The probe used in this study was the cDNA insert from clone g24.

Preparation of GST fusion proteins and rabbit anti-hPTTG fusion protein antibodies

A fusion protein containing the complete insert from g24 was constructed at the carboxyl terminus of GST using the prokaryotic expression vector pGEX-4T-2. The subclone GST-hPTTGΔC124 (lacking aminoacids 124–202) was also generated. Plasmids were transformed in *Escherichia coli* strain DH5α. Expression of the GST fusion proteins was induced by the addition of 1 mM isopropyl-β-D-thiogalactoside and the fusion proteins were isolated from bacterial lysates by affinity chromatography with glutathione-agarose beads (Sigma). hPTTG was released from the fusion protein by treatment with 1% (w/w) thrombin in cleavage buffer (50 mM Tris-HCl, pH 7.5, 150 mM NaCl, 2.5 mM $CaCl_2$) for 2 h at 25°C. A polyclonal antibody was generated in rabbit using the GST-hPTTGΔC124 fusion protein. The antiserum obtained after the fourth immunization, named anti-hPTTG, was used in the experiments described.

Electrophoresis and immunoblot analyses

Proteins were separated by SDS–PAGE on 10%, 12% or 15% acrylamide gels (Laemmli, 1970) and stained with Coomassie brilliant blue. Gels were electrophoretically transferred to nitrocellulose filters (Towbin *et al.*, 1979) and immunoblot analyses were carried out as described (Rios *et al.*, 1994).

Cell culture, lysis and subcellular fractionation

Simian Cos-7 cells were cultured in Dulbeco's modified Eagle's medium (DMEM) supplemented with 10% foetal calf serum. Jurkat cells were cultured in RPMI medium supplemented with 10% foetal calf serum. 2 mM L-glutamine, 100 U/ml penicillin and 100 μg/ml streptomycin were included in all culture media. All cells were mantained in a 5% CO_2 humidified atmosphere at 37°C. For cell lysis, 2×10^7 to 10^8 cells per ml were incubated at 4°C in NP40 buffer (10 mM Tris-HCl (pH 7.4), 150 mM NaCl, 10% glycerol, 1% NP40, 1 mM vanadate, 1% aprotinin, 1 mM PMSF, 1 μg/ml pepstatin and 1 μg/ml leupeptin) for 20 min. The extract was centrifuged at 20 000 *g* for 20 min and the supernatant was stored at −80°C.

Jurkat cell cytosol and nuclear fractions were prepared essentially as previously described (Dignam *et al.*, 1983). Monoclonal anti-hnRNP C (4F4) antibodies (provided by Dr G Dreyfuss, University of Pennsylvania) (Dreyfuss *et al.*, 1984) and polyclonal anti-Raf1 antibody (Santa Cruz Biotechnology, Inc., Santa Cruz, USA) were used in Western blot to control the purity of the fractions. Quantification of the bands by scanning densitometry indicated that 99% of Raf1, a cytosolic marker, was found in the cytosol, whereas 98% of hnRNPC, a exclusively nuclear protein, was recovered in the nuclear preparation.

Transactivation assays in mammalian cells

Cos-7 cells were grown until confluent. Cells were cotransfected with plasmids pGAL4 (Moriggl *et al.*, 1997), pGAL4-VP16, pGAL4-hPTTG, pGAL4-hPTTGΔN122 or pGAL4-hPTTGΔC124 all together with reporter plasmid pGAL4-4TK-luc (Moriggl *et al.*, 1997). Cells were harvested 48 h after transfection. Cells were lysed and extracts were assayed for luciferase activity as described (Seth *et al.*, 1992).

Acknowledgements
We thank S Gisselbrecht and S Fischer for helpful discussions. This work was supported by grants from Ministerio de Educación y Ciencia of Spain (SAF96-0275) and from DGUI of the Junta de Andalucia.

References

Altschul SF, Gish W, Miller W, Myers EW and Lipman DJ. (1990). *J. Mol. Biol.*, **215**, 403–410.

Bartel PL, Chien CT, Sternglanz R and Fields S. (1993). *Cellular interactions in development: a practical approach*. Hartley DA (ed.). Oxford University Press: Oxford, pp. 153–179.

Bellgrau D, Gold D, Selawry H, Moore J, Franzusoff A and Duke RC. (1995). *Nature*, **377**, 630–632.

Breeden L and Nasmyth K. (1985). *Cold Spring Harb. Symp. Quant. Biol.*, **50**, 643–650.

Chapman MS and Verma IM. (1996). *Nature*, **382**, 678–679.

Chou PY and Fasman GD. (1978). *Adv. Enzymol. Relat. Areas Mol. Biol.*, **47**, 45–148.

Darnell JJ. (1997). *Science*, **277**, 1630–1635.

Devereux J, Haeberli P and Smithies O. (1984). *Nucleic Acids Res.*, **12**, 387–395.

Dignam JD, Lebovitz RM and Roeder RG. (1983). *Nucleic Acids Res.*, **11**, 1475–1489.

Dreyfuss G, Choi YD and Adam SA. (1984). *Mol. Cell Biol.*, **4**, 1104–1114.

Garnier J, Osguthorpe DJ and Robson B. (1978). *J. Mol. Biol.*, **120**, 97–120.

Griffith TS, Brunner T, Fletcher SM, Green DR and Ferguson TA. (1995). *Science*, **270**, 1189–1192.

Hallek M, Bergsagel PL and Anderson KC. (1998). *Blood*, **91**, 3–21.

Hannon GJ, Demetrick D and Beach D. (1993). *Genes Dev.*, **7**, 2378–2391.

Hwang LY and Baer RJ. (1995). *Curr. Opin. Immunol.*, **7**, 659–664.

Kyte J and Doolittle RF. (1982). *J. Mol. Biol.*, **157**, 105–132.

Laemmli UK. (1970). *Nature*, **227**, 680–685.

Lech K, Anderson K and Brent R. (1988). *Cell*, **52**, 179–184.

Look AT. (1997). *Science*, **278**, 1059–1064.

Metzger D, White JH and Chambon P. (1988). *Nature*, **334**, 31–36.

Milner J, Ponder B, Hughes-Davies L, Seltmann M and Kouzarides T. (1997). *Nature*, **386**, 772–773.

Monteiro AN, August A and Hanafusa H. (1996). *Proc. Natl. Acad. Sci. USA*, **93**, 13595–13599.

Moriggl R, Berchtold S, Friedrich K, Standke GJ, Kammer W, Heim M, Wissler M, Stocklin E, Gouilleux F and Groner B. (1997). *Mol. Cell. Biol.* **17**, 3663–3678.

Pei L and Melmed S. (1997). *Mol. Endocrinol.*, **11**, 433–441.

Ptashne M. (1988). *Nature*, **335**, 683–689.

Ramos-Morales F, Dominguez A, Rios RM, Barroso SI, Infante C, Schweighoffer F, Tocque B, Pintor-Toro JA and Tortolero M. (1997). *Biochem. Biophys. Res. Commun.*, **237**, 735–740.

Remacle JE, Albrecht G, Brys R, Braus GH and Huylebroeck D. (1997). *EMBO. J.*, **16**, 5722–5729.

Rios RM, Tassin AM, Celati C, Antony C, Boissier MC, Homberg JC and Bornens M. (1994). *J. Cell. Biol.*, **125**, 997–1013.

Sadowski I, Ma J, Triezenberg S and Ptashne M. (1988). *Nature*, **335**, 563–564.

Sanz L, Moscat J and Diaz-Meco MT. (1995). *Mol. Cell. Biol.*, **15**, 3164–3170.

Schena M and Yamamoto KR. (1988). *Science*, **241**, 965–967.

Seth A, Gonzalez FA, Gupta S, Raden DL and Davis RJ. (1992). *J. Biol. Chem.*, **267**, 24796–24804.

Sherman F, Fink GR and Hicks JB. (1986). *Methods in yeast genetics*. Cold Spring Harbor Laboratory, Cold Spring Harbor, NY.

Shivdasani RA and Orkin SH. (1996). *Blood*, **87**, 4025–4039.

Streilein JW. (1993). *Curr. Opin. Immunol.*, **5**, 428–432.

Struhl K. (1988). *Nature*, **332**, 649–650.

Triezenberg SJ. (1995). *Curr. Opin. Genet. Dev.*, **5**, 190–196.

Towbin H, Staehlin T and Gordon J. (1979). *Proc. Natl. Acad. Sci. USA*, **76**, 4350–4354.

Vogelstein B and Kinzler KW. (1993). *Trends Genet.*, **9**, 138–141.

STIC-ILL

From: Canella, Karen
Sent: Sunday, February 03, 2002 9:00 PM
To: STIC-ILL
Subject: ill order 09/815,340

Art Unit 1642 Location 8E12(mail)

Telephone Number 308-8362

Application Number 09/815,340

1. Trends in Cell biology, 2001 Jan, 11(1):18-21
2. Clinical Cancer Research, 2000 Aug, 6(8):3215-3221
3. Mutation Research, 1997 Apr 29, 375(2):157-165
4. american Journal of Hematology, 1985 Mar, 18(3):243-249.
5. PNAS, 1989 Apr, 86(7):2276-2280
6. Genes and Development, 1996 Oct 15, 10(20):2621-2631
7. Cancer, 1975 Jun, 35(6):1664-1677
8. Mutation Research, 1978, 57(3): 313-324
9. Environ Mutagen, 1981, 3(1):53-64
10. Nucleic Acids Research, 2001 Mar 15, 29(6):1300-1307
11. Oncogene:
    1998 Oct 29, 17(17):2187-2193
    2000 Jan 20, 19(3):403-409
12. Molecular endocrinology, 1999 Jan, 13(1):156-166
13. Gene, 1999 Nov 29, 240(2):317-324
14. Science, 1999 Jul 16, 285(5426)418-422
15. Biochemistry and Molecular biology international, 1999 May, 47(5):891-897
16. Journal of Clinical Endocrinology and Metabolism, 1999 Mar, 84(3):1149-1152
17. Journal of biological chemistry:
    1999 Jan 29, 274(5):3151-3158
    2000 Nov 24, 275(47):36502-36505 ***
18. Gene 2000 May 2, 248(1-2):41-50
19. Molecular endocrinology, 2000 Aug, 14(8):1137-1146
20. Cancer Letters, 2001 Feb 10, 163(1):131-139
21. Brain Pathology, 2001 Jul, 11(3):328-341

Structure, Expression, and Function of Human Pituitary Tumor-Transforming Gene (PTTG)

Xun Zhang, Gregory A. Horwitz, Toni R. Prezant, Alberto Valentini, Masahiro Nakashima, Marcello D. Bronstein, and Shlomo Melmed

Cedars-Sinai Research Institute-UCLA School of Medicine
(X.Z., G.A.H., T.R.P., A.V., M.N., S.M.)
Los Angeles, California 90048

Neuroendocrine Unit (M.D.B.)
Division of Functional Neurosurgery
University of São Paulo Medical School
São Paulo, SP, Brazil 01406-100

Despite advances in characterizing the pathophysiology and genetics of pituitary tumors, molecular mechanisms of their pathogenesis are poorly understood. Recently, we isolated a transforming gene [pituitary tumor-transforming gene (PTTG)] from rat pituitary tumor cells. Here we describe the cloning of human PTTG, which is located on chromosome 5q33 and shares striking sequence homology with its rat counterpart. Northern analysis revealed PTTG expression in normal adult testis, thymus, colon, small intestine, brain, lung, and fetal liver, but most abundant levels of PTTG mRNA were observed in several carcinoma cell lines. Stable transfection of NIH 3T3 cells with human PTTG cDNA caused anchorage-independent transformation *in vitro* and induced *in vivo* tumor formation when transfectants were injected into athymic mice. Overexpression of PTTG in transfected NIH 3T3 cells also stimulated expression and secretion of basic fibroblast growth factor, a human pituitary tumor growth-regulating factor. A proline-rich region, which contains two PXXP motifs for the SH3 domain-binding site, was detected in the PTTG protein sequence. When these proline residues were changed by site-directed mutagenesis, PTTG *in vitro* transforming and *in vivo* tumor-inducing activity, as well as stimulation of basic fibroblast growth factor, was abrogated. These results indicate that human PTTG, a novel oncogene, may function through SH3-mediated signal transduction pathways and activation of growth factor(s). (Molecular Endocrinology 13: 156–166, 1999)

0888-8809/99/$3.00/0
Molecular Endocrinology

INTRODUCTION

Tumorigenesis is a multistep process, involving activation of oncogenes, growth factors, and their receptors, or the inactivation of tumor suppressor genes (1). Abnormal gene expression in tumor cells is associated with several characteristics that differ from normal cells, such as cell differentiation (2), DNA repair (3), cell-cell communication (4, 5), cell-matrix interaction (6), tumor invasion, motility and metastasis (7, 8), angiogenesis (9), and apoptosis (10). Despite major advances in studying these characteristics, understanding tumorigenesis as a continuous, multifunctional process is still limited.

Pituitary tumors are well differentiated adenomas accounting for ~10% of intracranial neoplasms, and clinically silent pituitary microadenomas are encountered in up to 23% of unselected adult autopsies (11, 12). These monoclonal adenomas are either nonfunctioning and do not secrete pituitary trophic hormones or are functioning and secrete one or more hormones including PRL, GH, ACTH, or rarely, glycoprotein hormones. These hypersecretory syndromes are associated with hypogonadism, infertility, acromegaly, Cushing's disease, or rarely, hyperthyroidism (13). Most pituitary tumors are histologically benign. True pituitary carcinomas are extremely rare, and documentation of distant metastasis is the sole diagnostic criterion for malignancy (14).

Pituitary tumor pathogenesis has been extensively studied (15). Several intrinsic mutations resulting in activation of tumor-promoting genes as well as inactivation of tumor suppressor genes have been described, including G protein ($G_s\alpha$) mutations (16, 17), rarely occurring *ras* mutations in invasive tumors (18, 19), loss of heterozygosity involving the 11q13 region (20), loss of purine-binding factor gene (nm23) expression (21), and, in mouse models, disruption of RB (22)

a

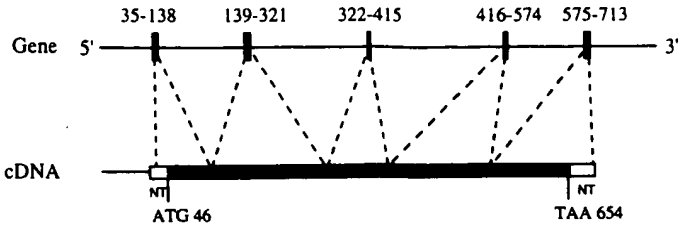

b

```
  1  GCGGCCTCAG ATGAATGCGG CTGTTAAGAC CTGCAATAAT CCAGAATGGC
 51  TACTCTGATC TATGTTGATA AGGAAAATGG AGAACCAGGC ACCCGTGTGG
101  TTGCTAAGGA TGGGCTGAAG CTGGGGTCTG GACCTTCAAT CAAAGCCTTA
151  GATGGGAGAT CTCAAGTTTC AACACCACGT TTTGGCAAAA CGTTCGATGC
201  CCCACCAGCC TTACCTAAAG CTACTAGAAA GGCTTTGGGA ACTGTCAACA
251  GAGCTACAGA AAAGTCTGTA AAGACCAAGG GACCCCTCAA ACAAAAACAG
301  CCAAGCTTTT CTGCCAAAAA GATGACTGAG AAGACTGTTA AAGCAAAAAG
351  CTCTGTTCCT GCCTCAGATG ATGCCTATCC AGAAATAGAA AAATTCTTTC
401  CCTTCAATCC TCTAGACTTT GAGAGTTTTG ACCTGCCTGA AGAGCACCAG
451  ATTGCGCACC TCCCCTTGAG TGGAGTGCCT CTCATGATCC TTGACGAGGA
501  GAGAGAGCTT GAAAAGCTGT TTCAGCTGGG CCCCCCTTCA CCTGTGAAGA
551  TGCCCTCTCC ACCATGGGAA TCCAATCTGT TGCAGTCTCC TTCAAGCATT
601  CTGTCGACCC TGGATGTTGA ATTGCCACCT GTTTGCTGTG ACATAGATAT
651  TTAAATTTCT TAGTGCTTCA GAGTTTGTGT GTATTTGTAT TAATAAAGCA
701  TTCTTTAACA GATAAAAAAA AAAAAAAAAA
```

c

```
  1 MATLIYVDKE NGEPGTRVVA KDGLKLGSGP SIKALDGRSQ VSTPRFGKTF
 51 DAPPALPKAT RIKALGTVNR TEKSVKTKGP LKDKDPSFSA KKMTEKTVKA
101 KSSVPASDDA YPEIEKFFPF NPLDFESFDL PEEHQIAHLP LSGVPLMILD
151 EERELEKLFQ LGPPSPVKMP SPPWESNLLQ SPSSILSTLD VELPPVCCDI
201 DI*
```

Fig. 1. Human PTTG Genomic and cDNA Structure

a, Human PTTG genomic structure, with numbering according to the cDNA sequence in panel b. The translation initiation (ATG) and stop (TAA) codons in the cDNA are indicated. NT, Nontranslated region. b, Nucleotide sequence of human PTTG cDNA. The translation initiation and stop codons for the open reading frame are *bold and underlined*. The in-frame stop codon upstream of the initiation codon is *bold and italicized*. c, Amino acid sequence of PTTG protein deduced from the coding region of cDNA. The basic amino acid-rich domain is *underlined*, and the basic amino acid residues are *bold and italicized*. The proline-rich motifs are *bold*.

and cyclin-dependent kinase inhibitors (23, 24). However, only G protein mutations have reproducibly been identified in a subset of sporadic GH-secreting pituitary adenomas (25). The molecular etiology of these tumors remains elusive, and other mechanisms may be invoked in pituitary tumorigenesis. Recently, a novel pituitary tumor-transforming cDNA (PTTG) was isolated in our laboratory from rat GH4 pituitary tumor cells (26). Overexpression of rat PTTG resulted in cell transformation *in vitro* and induced *in vivo* tumor formation in athymic mice.

We now characterize the human pituitary tumor-transforming gene (PTTG). It is abundantly expressed in malignant tumor cells, as well as in some normal tissues, and potently transforms cells both *in vitro* and *in vivo*. Overexpression of PTTG in transfected NIH 3T3 cells increases basic FGF mRNA level as well as stimulates its secretion. As point mutations in a proline-rich region near the PTTG C terminus abrogate its transforming ability and block basic FGF production, PTTG function in tumorigenesis may involve intracellular SH3 signals and growth factor production.

RESULTS

Molecular Cloning of Human PTTG

An open reading frame containing 609 bp was revealed in the positive clones obtained from human fetal liver cDNA library using a 0.6-kb rat PTTG cDNA as screening probe (Fig. 1b). The presence of an in-

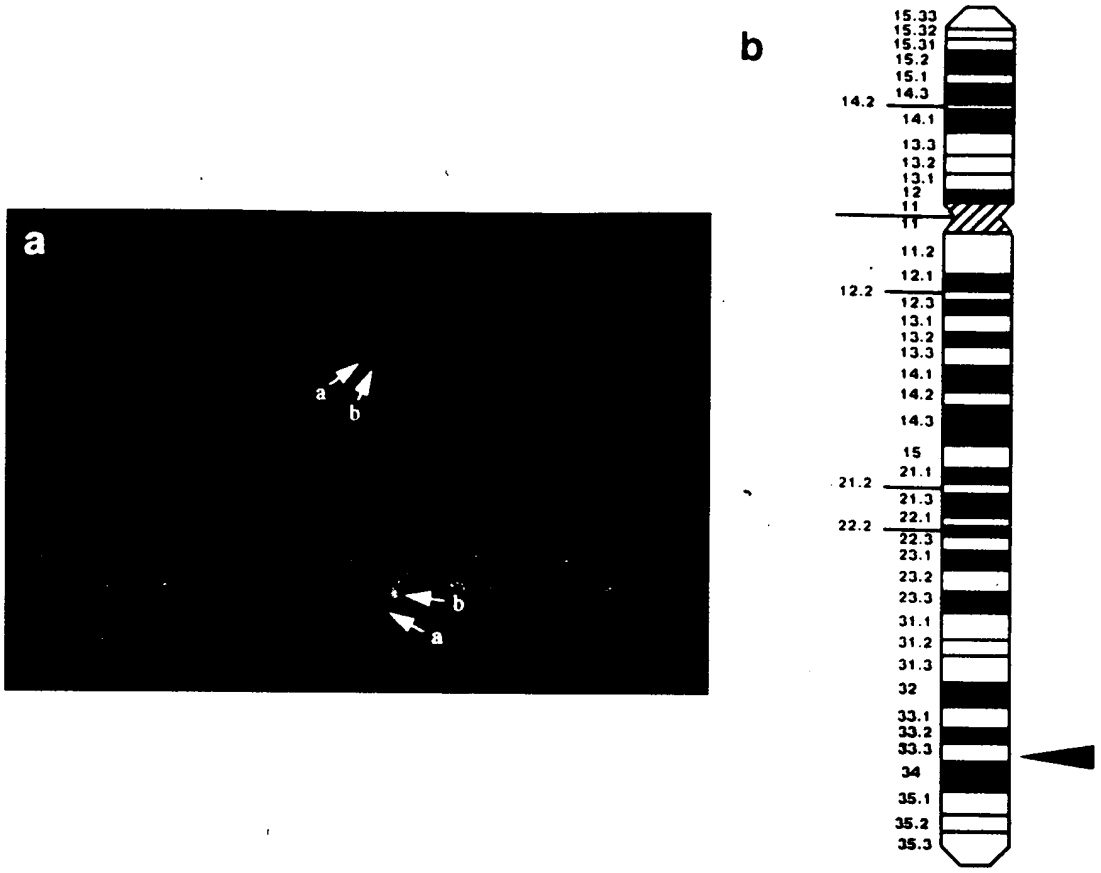

Fig. 2. Chromosomal Localization as Determined by FISH

a, Metaphase chromosomes hybridized with human PTTG probe (*arrow a*) and 5q21 control probe (*arrow b*). b, Ideogram illustrating the chromosomal position of human PTTG at 5q33 according to the International System for Human Cytogenetic Nomenclature 1995. *Arrow* indicates human PTTG position.

frame stop codon before the predicted initiation codon suggests that it is complete. The homology between DNA sequences of this open reading frame and the coding region of rat PTTG is 85%. Amino acid sequence comparison between the translated product of this cDNA and rat PTTG protein reveals 77% identity and 89% homology. Since all positive clones were sequenced and no other cDNA fragment with higher homology was detected in the library, it appears that these cDNA clones represent human homologs of rat PTTG.

GenBank search did not reveal a known protein with structural similarity to PTTG. However, we detected a basic amino acid-rich region near the N terminus (from position 58 to 101, with 32% basic amino acid residues) and a proline-rich region near the C-terminus of human PTTG protein (Fig. 1c). This proline-rich region contains two PXXP motifs consistent with the previously identified SH3-binding site (27). The presence of these functional motifs suggests that human PTTG protein may be involved in SH3 domain-mediated signal transduction pathways (28, 29).

The human PTTG cDNA was used to screen a human genomic library, and positive genomic clones were subjected to sequence analysis. The results were compared with the cDNA sequence of human PTTG and revealed four introns within the coding region (Fig. 1a).

Chromosomal Localization of Human PTTG

DNA from the Stanford Human-Hamster G3 Radiation Hybrid Mapping Panel was used as template in PCR reactions with PTTG-specific primers. The amplified products were sequenced to confirm that they indeed contain human PTTG sequences. By electronic analysis at the Stanford Human Genome Center website, PTTG was localized to 21.01 centirads from the marker D5S2576 with a LOD score of 8.48. According to neighboring Genethon markers in the SCIENCE96 Transcription Map, this marker is most likely located within the interval 5q32–34 of chromosome 5.

This mapping result was further confirmed by fluorescence *in situ* hybridization (FISH), using a 16-kb human genomic fragment containing PTTG as a probe. The initial experiment resulted in specific labeling of the distal long arm of a group B chromosome, which was believed to be chromosome 5 based on its

size, morphology, and banding pattern. In a second experiment, a probe previously mapped to 5q21 was cohybridized with PTTG, resulting in specific labeling of the middle and distal long arm of chromosome 5, respectively (Fig. 2a). Among a total of 80 metaphase cells analyzed, 63 exhibited specific labeling, showing that human PTTG is located at a position that is 84% the distance from the centromere to the telomere of chromosome arm 5q, an area corresponding to band 5q33 according to the International System for Human Cytogenetic Nomenclature 1995. Thus, the results concur and localize PTTG to 5q33 (Fig. 2b).

Tissue Distribution of Human PTTG mRNA

The expression pattern of human PTTG mRNA in normal human adult and fetal tissues and in several human carcinomas is depicted in Fig. 3. A strong mRNA signal of approximately 0.8 kb was detected in human fetal liver (Fig. 3b). In normal human adult tissues, abundant PTTG expression was evident in testis. Strong expression was also observed in thymus, and weak expression signals were seen in colon, small intestine, brain, placenta, and pancreas (Fig. 3a). Interestingly, when human malignant tumor cells were tested, PTTG was found to be highly expressed in all cell lines examined (Fig. 3c). PTTG mRNA was also detected in several human pituitary tumors, including nonfunctioning, PRL-secreting, and ACTH-secreting tumors (Fig. 3d). No mutations of the PTTG-coding region in tumors were detected by RT-PCR followed by sequence analysis (data not shown).

Effects of Human PTTG Overexpression on Cell Transformation and Tumor Induction

Since a GeneBank search revealed no known proteins structurally similar to PTTG, its role in tumor formation is as yet unclear. However, the presence of a proline-rich region containing PXXP motifs near the C terminus of PTTG protein suggests that it may be involved in SH3-mediated intracellular signal transduction pathways. To explore the function of this domain and its relationship to PTTG-transforming ability, we constructed human PTTG mutants by PCR-based site-directed mutagenesis. The following amino acid residues in the SH3-binding motifs were mutated: P163A, P170L, P172A, and P173L. Mutant cDNA, as well as wild-type PTTG cDNA, was cloned into the mammalian expression vector under control of the cytomegalovirus (CMV) promoter and stably transfected into NIH 3T3 cells. Overexpression of wild-type and mutant PTTG in each transfected cell line was confirmed by Northern analysis, RT-PCR followed by direct sequence analysis, and Western blot (Fig. 4). The point mutations did not change protein expression or susceptibility to proteolysis, since PTTG protein with the same molecular weight was expressed in each transfected cell type at similar levels, as shown by Western blot (Fig. 4c). The transforming ability of these cells was tested in an anchorage-independent growth assay. We found that NIH 3T3 cells overexpressing PTTG formed large colonies (numbers ranged from 198 ± 6 to 267 ± 23 colonies per plate, mean ± SD) on soft agar, while control NIH 3T3 cells containing the same expression vector but lacking PTTG cDNA insert did not induce significant colony foci under the same conditions (22 ± 1 colonies per plate) (Table 1). In contrast, the number and size of colonies formed from NIH 3T3 cells expressing mutant PTTG were greatly reduced (ranging from 57 ± 6 to 60 ± 5 colonies per plate) (Table 1 and Fig. 5). Furthermore, when these cells were injected subcutaneously into athymic nude mice, PTTG-overexpressing cells caused tumor formation within 2 weeks in all five injected animals (tumor weights ranged from 560 to 1000 mg) (Fig. 6). In five mice injected with control transfectants (expression vector alone), only one developed a much smaller tumor weighing only 100 mg. As expected, when cells expressing mutant PTTG were injected into nude mice, no tumor formation was observed even after 3 weeks of injection (Fig. 6), consistent with the results obtained in the anchorage-independent growth assay. These results thus demonstrate the *in vitro* transforming activity and *in vivo* tumor-inducing potential of human PTTG and also strongly suggest that signaling protein(s) containing SH3 domain(s) mediate PTTG action.

Stimulation of Basic FGF Expression and Secretion by Human PTTG

As PTTG-expressing NIH 3T3 cells were able to induce solid tumor growth *in vivo*, PTTG may activate growth factor and/or angiogenesis pathways. To test this hypothesis, we examined the expression of two important angiogenic factors, vascular endothelial growth factor (VEGF) and basic fibroblast growth factor (bFGF), in the PTTG-transfected NIH 3T3 cells. Northern analysis showed that, although no difference in VEGF mRNA expression was found in control and PTTG-transfected cells (data not shown), bFGF mRNA levels in PTTG-transfected cells were increased compared with mock-transfected control cells (Fig. 7a). In the cells transfected with mutant PTTG, the abundance of bFGF mRNA transcripts was low, similar to that observed in the control cells.

To further confirm bFGF regulation by PTTG at the protein level, enzyme-linked immunosorbent assay (ELISA) was performed to examine bFGF levels in conditioned culture medium. As shown in Fig. 7b, bFGF levels were markedly higher in the conditioned medium collected from wild-type human PTTG transfectants cultured for 72 h than those from control and mutant transfectants. Differences of total protein concentrations in these cultures were less than 10%. Therefore, PTTG not only enhances bFGF mRNA levels, but also stimulates bFGF secretion. The PTTG proline-rich region containing two SH3-binding motifs appears critical for this function.

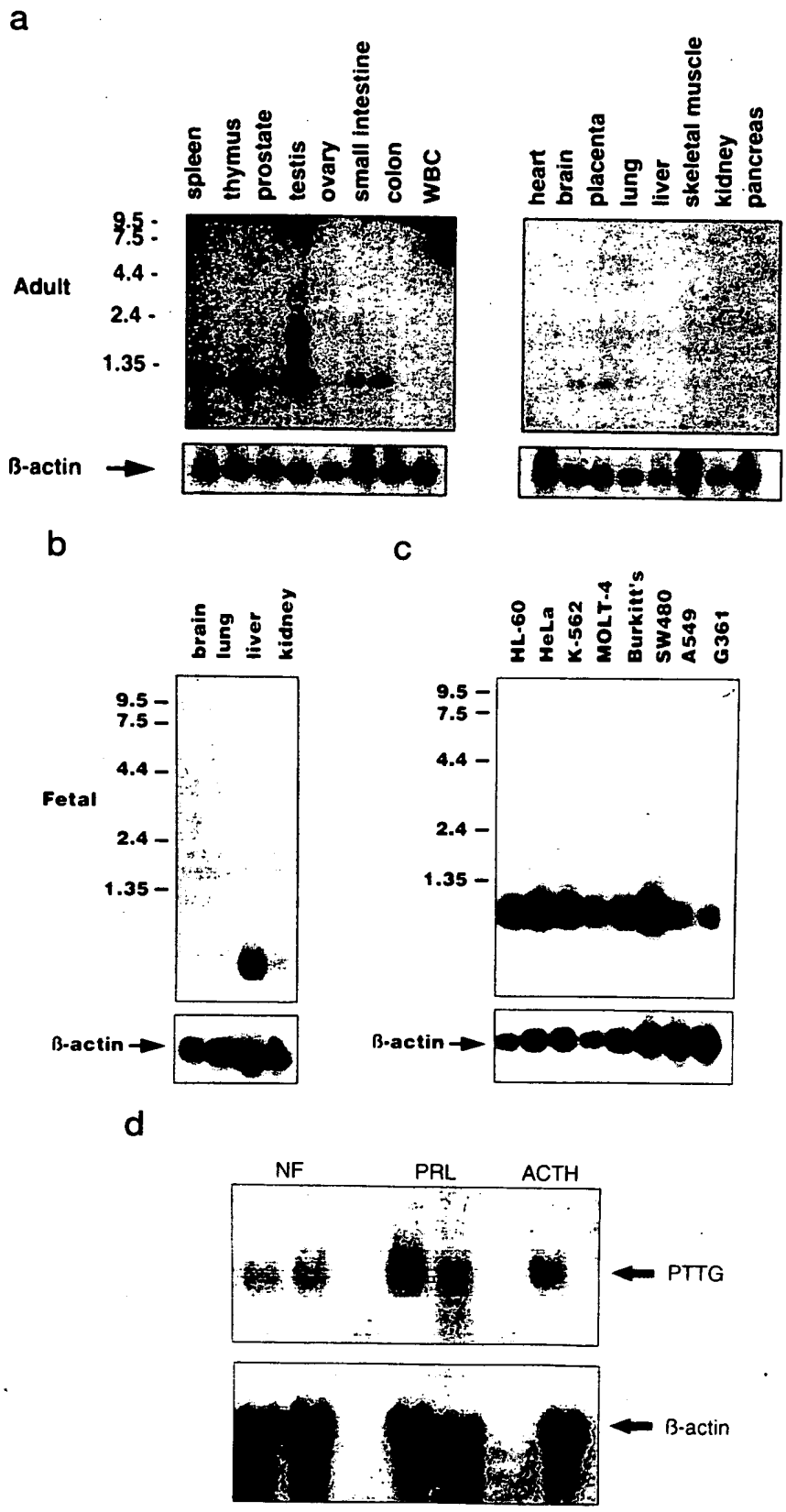

Fig. 3. Tissue Distribution of Human PTTG mRNA

Two micrograms of poly A^+ RNA derived from the indicated tissues were loaded in each lane. *Top panel* shows result of Northern hybridization to PTTG cDNA probe, and *bottom panel* shows hybridization to β-actin probe (control). a, Normal human adult tissues. b, Normal human fetal tissues. c, Human cancer cells. From *left to right*: promyelocytic leukemia HL-60; HeLa cell

DISCUSSION

We have isolated a human gene that shows a striking structural similarity (85% identity for cDNA and 89% similarity for amino acid sequences) to rat PTTG. Human PTTG is located on chromosome 5, at position 5q33. Like its rat counterpart, it induces cell transformation *in vitro* and *in vivo*.

In normal adult rat tissues, PTTG expression is restricted to the testis (26). The normal tissue distribution of human PTTG is also limited; however, it is not restricted to testis but is also expressed in thymus, colon, small intestine, and, weakly, in brain and placenta, indicating that it may also play a role in certain normal cellular functions. The expression of human PTTG in fetal liver, but not in adult liver, suggests that it is differentially regulated and possibly functions during development. Interestingly, PTTG is highly expressed in all carcinoma cell lines tested, suggesting that it is a common and important factor for most malignant tumor types.

The chromosomal location of human PTTG, 5q33, is associated with reports of recurrent neoplastic abnormalities, including myeloid leukemia, chronic myeloproliferative disorder, myelodysplastic syndrome, squamous cell carcinoma, and lipoma (30). Using RT-PCR and direct sequencing, we examined PTTG in several human carcinoma cell lines, including cervix carcinoma HeLa cell, choriocarcinomas JEG-3 and JAR, breast adenocarcinoma MCF-7, osteogenic sarcoma U-2 OS, hepatocellular carcinoma Hep 3B, lung carcinoma EY, and thyroid carcinoma TC-1. Although no mutation was detected within the PTTG coding region, PTTG expression levels were high in all carcinoma cell lines tested. Thus, putative mutations in the gene-regulatory regions may cause PTTG dysregulation, and enhanced PTTG expression may mediate neoplastic cell transformation. We also found that PTTG mRNA was expressed in several pituitary tumors, indicating that it may be involved in pituitary tumorigenesis. Interestingly, PTTG mRNA levels in benign pituitary tumors, in general, were much lower than in malignant carcinomas (31). Therefore, although it seems that tumor PTTG expression correlates with malignancy, further confirmation is needed.

The transforming ability and high level of PTTG expression in malignant tumors demonstrate its involvement in tumorigenesis, although mechanisms of PTTG action and its relationship to other oncogene or tumor suppressor gene products is yet unclear. The presence of a basic amino acid-rich region and a proline-rich region in PTTG protein provide insights regarding its function. Basic amino acid-rich domains have been suggested as a nuclear localization signal (31–33), although the subcellular localization of PTTG is still undetermined. The proline-rich region of the human PTTG protein contains two PXXP motifs, which are potential binding sites for SH3-domains (27), important mediators of intracellular signal transduction (28, 34). Several proteins have recently been identified to contain PXXP motifs and bind to SH3 domains, such as GDP/GTP exchange factor SOS (35, 36), protein kinases JNK and phosphatidylinositol 3-kinase (37, 38), and the Abl oncogene product (39, 40). We report here that point mutations in the PXXP motif of human PTTG abrogated its transforming and tumor-inducing activity, despite expression of PTTG mRNA and protein in these mutants. Thus, this PXXP motif is important for PTTG-mediated transformation. Alternatively, another mechanism for the function of this region could involve serine phosphorylation of adjacent regions (41).

Interestingly, PTTG induces bFGF production at both the mRNA and protein levels. bFGF is a major activating factor for angiogenesis (42, 43), a necessary process for the expansion of the primary tumor mass as well as tumor metastasis (9, 44, 45). This is also in concurrence with our finding that transfected cells overexpressing PTTG cause formation of solid tumors in nude mice. Increased bFGF expression has been reported in several human tumors, such as pancreatic carcinoma (46), endometrial adenocarcinoma (47), advanced renal cell carcinoma (48), primary breast cancer (49), and pituitary tumors (50), in which it is considered a stimulating growth factor (51). Considering that the bFGF receptor is a protein tyrosine kinase and that PTTG increases bFGF production, we propose that one of the mechanisms of tumorigenesis by PTTG involves an SH3 protein interacting with PTTG, stimulating gene transcription and secretion of bFGF, and resulting in cell transformation and tumor formation. This hypothesis is supported by our observation that mutations of the proline-rich region, the potential SH3-binding site, abrogate bFGF production as well as cell transformation. These results establish human PTTG as a potent tumor-promoting factor whose functions involve bFGF production and cell transformation.

MATERIALS AND METHODS

Library Screening

A human fetal liver cDNA library (CLONTECH, Palo Alto, CA) was screened as described (51), using a 0.6-kb radioactively labeled cDNA fragment containing the entire rat PTTG coding region as a probe. The cDNA inserts from positive clones were subcloned into plasmid pBluescript-SK (Stratagene, La Jolla, CA) and subjected to sequence analysis using a Se-

S3; chronic myelogenous leukemia K-562; lymphoblastic leukemia MOLT-4; Burkitt's lymphoma Raji; colorectal adenocarcinoma SW480; lung carcinoma A549; melanoma G361. d, Pituitary tumors. NF, Nonfunctioning tumor; PRL, PRL-secreting tumor; ACTH, ACTH-secreting tumor.

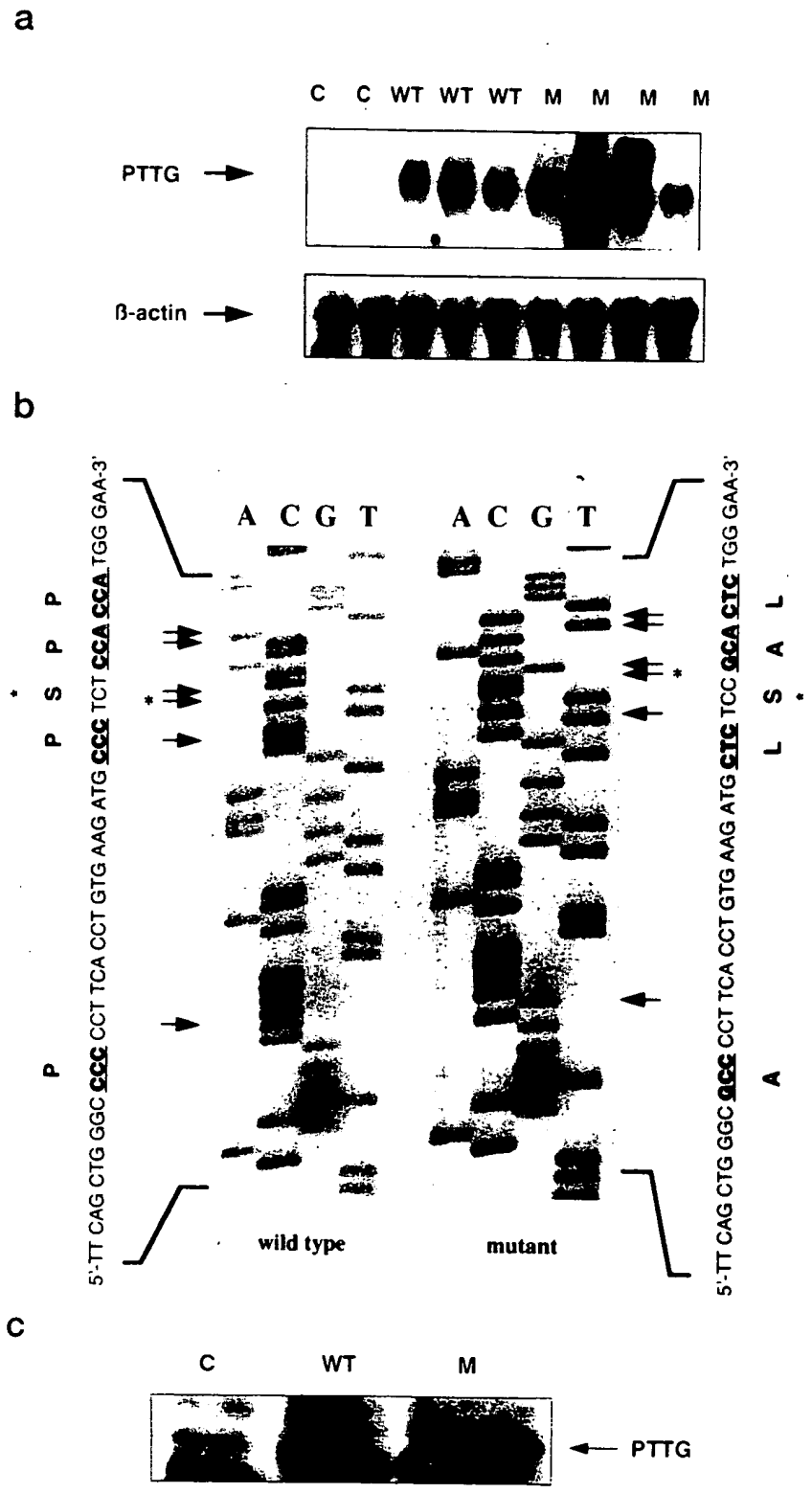

Fig. 4. Wild-Type and Mutant PTTG Expression in Transfected NIH 3T3 Cells

a, A representative Northern blot in which 20 μg total RNA from each cell line were used to hybridize with human PTTG cDNA probe (*top panel*) or β-actin probe (*bottom panel*). b, A representative sequencing gel from RT-PCR followed by direct sequence analysis showing wild-type PTTG and mutant PTTG expression in a respective transfectant. The *arrows* point to nucleotide changes. A silent mutation (*) was introduced to obtain equal melting points for the different primers. c, A representative Western blot in which 40 μg protein extracted from each transfectant were analyzed using a purified anti-PTTG polyclonal antibody. C, Cell lines transfected with vector alone; WT, cell lines transfected with wild-type PTTG expression vector; M, cell lines transfected with mutant PTTG expression vector.

quenase kit (United States Biochemical Corp., Cleveland, OH) and SequeGel System (National Diagnostics, Atlanta, GA).

A human genomic library (Stratagene, La Jolla, CA) was screened according to the manufacturer's protocol, using the radioactively labeled human cDNA clone containing the complete coding region as a probe. DNA from each positive phage clone was purified using Lambda DNA preparation kit (Qiagen, Valencia, CA) and sequenced with a thermocycle sequencing kit (Amersham, Arlington Heights, IL) and SequaGel System (National Diagnostics).

Table 1. Colony Formation by PTTG-Expressing Cells in Soft Agar

Cell Line	Colonies/10^4 Cells (mean ± SEM)
Vector alone	22 ± 1
Wild-type PTTG-1	198 ± 6
Wild-type PTTG-2	267 ± 23
Mutant PTTG-1	57 ± 6
Mutant PTTG-2	60 ± 5

Each transfectant cell line was plated in three different plates and scored on the 14th day. Only colonies consisting of 60 or more cells were scored. Vector, NIH 3T3 cell line stably transfected with vector only; wild type PTTG, NIH 3T3 cell line stably transfected with wild-type PTTG expression vector; mutant PTTG, NIH 3T3 cell line stably transfected with PXXP motif-mutated PTTG (P163A, P170L, P172A, and P173L) expression vector.

Determination of Human PTTG Chromosomal Location

Chromosomal localization of human PTTG was determined by PCR analysis of the Stanford Human-Hamster G3 Radiation Hybrid (RH) Mapping Panel (Research Genetics, Huntsville, AL) as well as by FISH. DNA from 83 samples in the G3 RH mapping panel were amplified in 20-μl reactions containing 50 ng DNA, 1.75 U Expand High Fidelity enzyme (Boehringer-Mannheim, Indianapolis, IN), 1× reaction buffer with 1.5 mM $MgCl_2$, 0.2 mM deoxynucleoside triphosphates (dNTPs), and 300 nM human PTTG-specific primers, 5′-CTGCCT-CAGATGATGCCTATCCAG-3′and 5′-CAAGCTCTCTCTCCTCGTCAAGG-3′. The PCR reactions were performed for 35 cycles of 94 C, 15 sec; 60 C, 30 sec; 68 C, 2.5 min. PCR products were visualized in 1% agarose gels stained with ethidium bromide and scored as positive ("1") if a strong (~3.5-kb PCR product) was visualized, negative ("0") if the band was not visualized, or ambiguous if a weak band was observed. The same results were obtained when the panel was again amplified with GIBCO-BRL (Gaithersburg, MD) *Taq* DNA polymerase. These data were submitted electronically to the Stanford Human Genome Center website to determine linkage to previously mapped markers. The FISH was performed at GenomeSystem, Inc. (St. Louis, MO). Briefly, a 16-kb human genomic fragment containing PTTG was labeled with digoxigenin dUTP by nick translation. Labeled probe was combined with sheared human DNA and hybridized to normal metaphase chromosomes derived from phy-

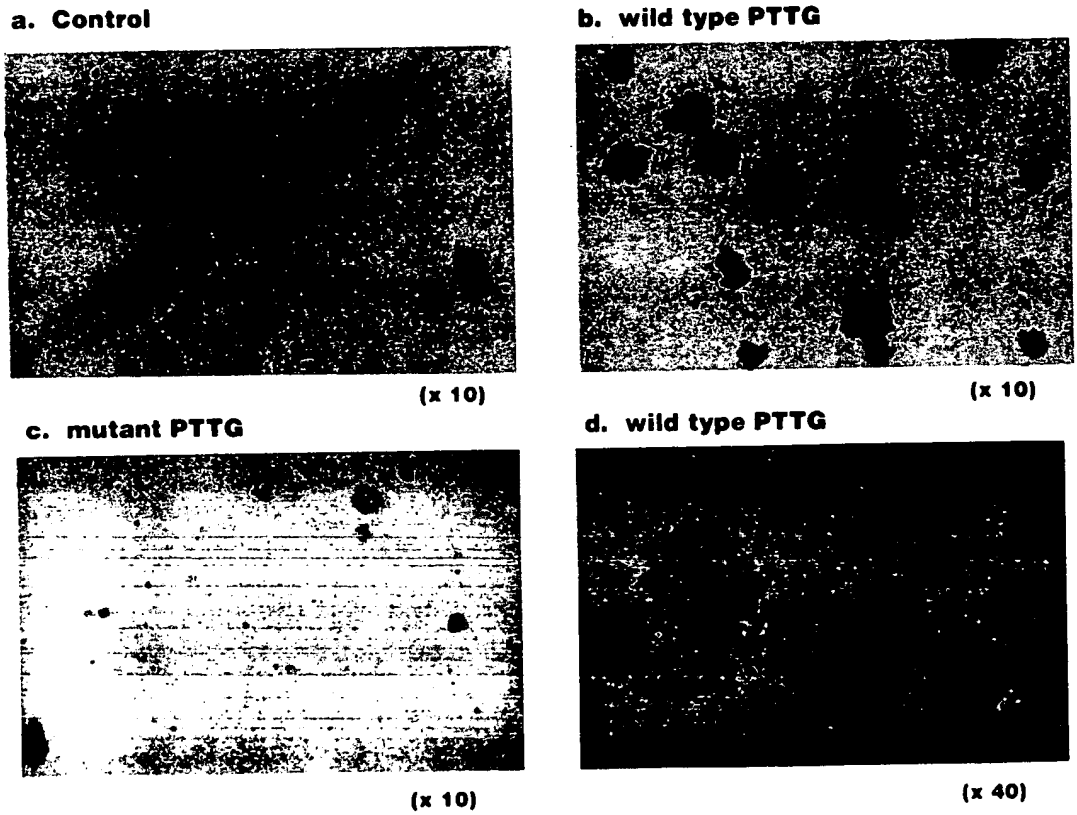

Fig. 5. Colony Formation of NIH 3T3 Cells Transfected with Wild-Type and Mutant PTTG Expression Vector on Soft Agar
a, Cells transfected with vector pCI-neo alone. b, Cells transfected with vector pCI-neo containing wild-type PTTG cDNA. c, Cells transfected with vector pCI-neo containing PTTG cDNA mutated in the proline-rich region (P163A, P170L, P172A, and P173L). d, High magnification of colonies formed from cells transfected with vector pCI-neo containing wild-type PTTG cDNA.

Tumor weight (mg)		
Vector (n=5)	wtPTTG (n=5)	mPTTG (n=4)
100	1000	none
none	560	none
none	670	none
none	770	none
none	940	

Fig. 6. Tumor Formation Induced by Human PTTG-Expressing Cells in Nude Mice

Each mouse was injected subcutaneously with 3×10^5 control, wild-type PTTG-overexpressing, or mutant PTTG-overexpressing cells. After 2 weeks, mice were photographed and killed, and their tumors were excised and weighed. Vector, Cell line transfected with vectors only; wt PTTG, cell line transfected with wild-type human PTTG expression vectors; mPTTG, cell line transfected with mutant human PTTG expression vector; None, no detectable tumor. The mouse on the *left* was injected with control cells transfected with vector only. The mouse in the *middle* was injected with cells transfected with wild-type PTTG expression vector. The mouse on the *right* was injected with cells transfected with mutant PTTG expression vector.

tohemagglutinin-stimulated peripheral blood lymphocytes. Specific hybridization signals were detected by incubating the hybridized slides in fluoresceinated antidigoxigenin antibodies followed by counterstaining with 4,6-diamidino-2-phenylindole (DAPI).

Northern Blot Analysis

RNA blots (CLONTECH, Palo Alto, CA) derived from normal human adult and fetal tissue, as well as from malignant tumor cell lines and fresh pituitary tumor specimens, were hybridized with a 0.7-kb radiolabeled human cDNA fragment containing the complete coding region. Northern blot analysis was performed using ExpressHyb Solution (CLONTECH) or QuickHyb Solution (Stratagene, La Jolla, CA) according to the manufacturer's protocol.

Western Blot Analysis

An antirat PTTG polyclonal antibody was developed as described previously (26). This antibody was purified by a PTTG affinity column that couples 10 mg synthetic antigenic peptide with HiTrap *N*-hydroxysuccinimide-activated column (Pharmacia, Piscataway, NJ) according to manufacturer's protocol. The affinity column was washed with 75 mM Tris-HCl, pH 8.0, until no protein appeared in the eluent. The purified antibody was eluted with 0.1 M glycine, 0.5 M NaOH, pH 2.7, and neutralized with each volume of 2 N Tris-HCl, pH 8.0. Western blot was performed as described previously (26) using this purified antibody (1:100 dilution).

Stable Transfection of Human PTTG into NIH 3T3 Cells

The complete coding region of human PTTG cDNA was subcloned in frame into mammalian expression vectors pBK-CMV (Stratagene) or pCI-neo (Promega, Madison, WI) and transfected into NIH 3T3 fibroblast cells with Lipofectamine (GIBCO-BRL) according to the manufacturer's protocol. Twenty-four hours after transfection, cells were serially di-

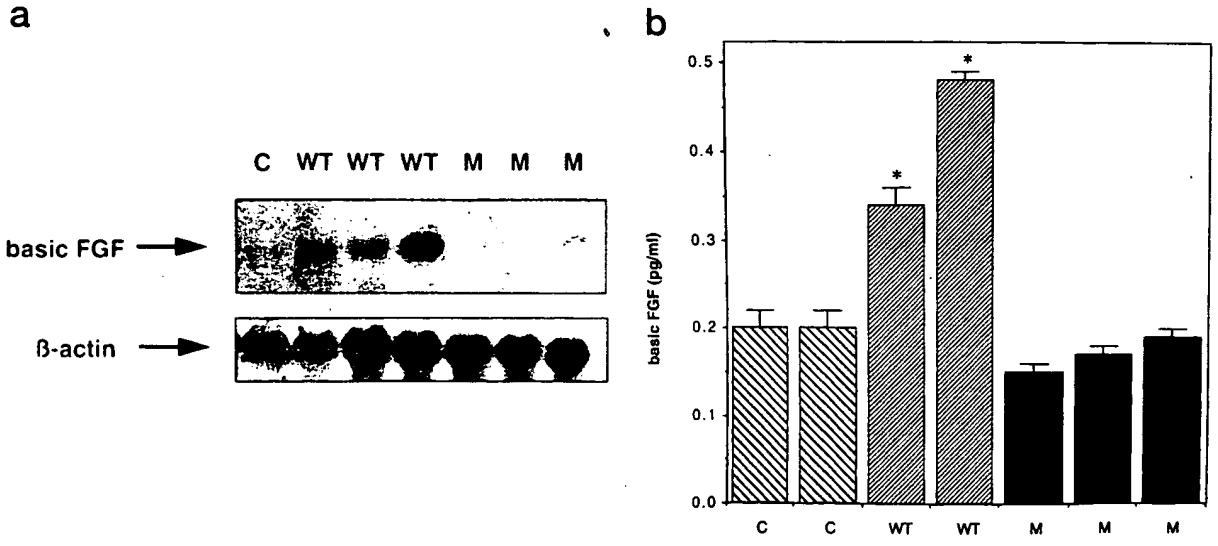

Fig. 7. Human PTTG Stimulates bFGF Production

a, A representative Northern blot in which 20 μg total RNA from each cell line were used to hybridize with human bFGF cDNA probe (*top panel*) or β-actin probe (*bottom panel*). b, bFGF concentration in conditioned medium derived from each PTTG transfectant cultured for 72 h as measured by ELISA. C, Cell lines transfected with vector alone; WT, cell lines transfected with wild-type PTTG expression vector; M, cell lines transfected with mutant PTTG (P163A, P170L, P172A, and P173L) expression vector.

tted and grown in selection medium containing 1 mg/ml G418 for 2 weeks. Individual clones were isolated and maintained in selection medium. Total RNA was isolated from human PTTG-transfected cell lines as well as from control cells in which the vector pBK-CMV or pCI-neo had been transfected. Overexpression of human PTTG in each transfected cell line was confirmed by Northern blotting.

Site-Directed Mutagenesis

Point mutations on the proline-rich domain of PTTG peptide were generated by PCR-based site-directed mutagenesis. Two synthetic oligonucleotides, 5′-GATGCTCTCCG-CACTCTGGGAATCCAATCTG-3′ and 5′-TTCACAAGTT-GAGGGGCGCCCAGCTGAAACAG-3′, which would cause amino acid changes P163A, P170L, P172A, and P173L, were used to amplify human PTTG cDNA cloned into pBlue-Script-SK vector (Stratagene). The amplified cDNA containing these mutations was then cloned into pCI-neo (Promega) and used in stable transfection. Expression of mutated PTTG product in transfected cells was confirmed by Northern analysis and RT-PCR followed by direct sequence analysis.

In Vitro and *in Vivo* Transformation Assay

Control and human PTTG-transfected cells were tested for anchorage-independent growth in soft agar (53). Three milliliters of soft agar (20% 2× DMEM, 50% DMEM, 10% FBS, and 20% 2.5% agar, melted and mixed at 45 C) were added to 35-mm tissue culture dishes. Ten thousand cells were mixed with 1 ml soft agar and added to each dish. Cells were incubated for 2 weeks before colonies were counted and photographed. For *in vivo* transformation, 1×10^5 control or human PTTG-transfected cells were resuspended in 400 μl PBS and injected subcutaneously into nude mice (five mice for each group). After two weeks, animals were photographed and tumors were excised and weighed.

Hybridization with VEGF and bFGF cDNA Probes

The cDNA probes for VEGF and bFGF were generated by RT-PCR using specific primers according to the published sequences (54, 55). These cDNAs generated from PCR were cloned and confirmed by sequence analysis. Total RNAs from cultured cells were extracted using Trizol Reagent (GIBCO-BRL) and used in Northern analysis as described previously (56).

ELISA of bFGF in Conditioned Medium

bFGF concentration in cell culture medium was assayed using Quantikine HS Human FGF Basic Immunoasssay Kit (R&D Systems, Minneapolis, MN) according to the manufacturer's protocol. Cells (1×10^5) were plated in 100-mm cell culture dishes. After 72 h, the culture medium was collected, and 1 ml was lyophilized and resuspended in 200 μl PBS for ELISA assay.

Acknowledgments

We thank Drs. S. G. Ren and X. Li for technical help.

This work was supported by NIH Grant DK-50238 (S.M.), Institutional Training Grant DK-7682 (X.Z.), and the Doris Factor Molecular Endocrinology Laboratory.

Received July 23, 1998. Re-revision received October 5, 1998. Accepted October 8, 1998.

Address requests for reprints to: Shlomo Melmed, Academic Affairs, Cedars-Sinai Medical Center, 8700 Beverly Boulevard, Room 2015, Los Angeles, California 90048. E-mail: melmed@csmc.edu.

REFERENCES

1. Weinberg RA 1995 The molecular basis of oncogenes and tumor suppressor genes. Ann NY Acad Sci 758:331–338
2. Pawson T, Hunter T 1994 Signal transduction and growth control in normal and cancer cells. Curr Opin Gene Dev 4:1–4
3. Sancar A 1994 Mechanisms of DNA excision repair. Science 266:1954–1956
4. Hirschi KK, Xu C, Tsukamoto T, Sager R 1996 Gap junction genes Cx26 and Cx43 individually suppress the cancer phenotype of human mammary carcinoma cells and restore differentiation potential. Cell Growth Differ 7:861–870
5. Loewenstein WR, Rose B 1992 The cell-cell channel in the control of growth. Semin Cell Biol 3:59–79
6. Giancotti FG, Ruoslahti E 1990 Elevated levels of the alpha 5 beta 1 fibronectin receptor suppress the transformed phenotype of Chinese hamster ovary cells. Cell 60:849–859
7. Muller BM, Yu YB, Laug WE 1995 Overexpression of plasminogen activator inhibitor 2 in human melanoma cells inhibits spontaneous metastasis in *scid/scid* mice. Proc Natl Acad Sci USA 92:205–209
8. Stetler-Stevenson WG, Aznavoorian S, Liotta LA 1993 Tumor cell interactions with the extracellular matrix during invasion and metastasis. Annu Rev Cell Biol 9:541–573
9. Hanahan D, Folkman J 1996 Pattern and emerging mechanisms of the angiogenic switch during tumorigenesis. Cell 86:353–346
10. Wyllie AH 1995 The genetic regulation of apoptosis. Curr Opin Gen Dev 5:97–104
11. Kontogeorgos G, Kovacs K, Horvath E, Scheithauer BW 1991 Multiple adenomas of the human pituitary. A retrospective autopsy study with clinical implications. J Neurosurg 74:243–247
12. Molitch ME, Russell EJ 1990 The pituitary "incidentaloma." Ann Intern Med 112:925–931
13. Melmed S, Braunstein GD, Chang RJ, Becker DP 1986 Pituitary tumors secreting growth hormone and prolactin. Ann Intern Med 105:238–253
14. Pernicone PJ, Scheithauer BW, Sebo TJ, Kovacs KT, Horvath E, Young Jr WF, Lioyd RV, Davis DH, Guthrie BL, Schoene WC 1997 Pituitary carcinoma: a clinicopathological study of 15 cases. Cancer 79:804–812
15. Shimon I, Melmed S 1997 Pituitary tumor pathogenesis. J Clin Endocrinol Metab 82:1675–1681
16. Lyons J, Landis CA, Harsh G, Vallar L, Grunewald K, Feichtinger H, Duh QY, Clark OE, Kawasaki E, Bourne HR, McCormick F 1990 Two G protein oncogenes in human endocrine tumors. Science 249:655–659
17. Vallar L, A Spada A, Giannattasio G 1987 Altered G_s and adenylate cyclase activity in human GH-secreting pituitary adenomas. Nature 330:566–568
18. Karga HJ, Alexander JM, Hedley-Whyte ET, Klibanski A, Jameson JL 1991 *ras* mutations in human pituitary tumors. J Clin Endocrinol Metab 74:914–919
19. Pei L, Melmed S, Scheithauer B, Kovacs K, Prager D 1994 H-*ras* mutations in human pituitary carcinoma metastasis. J Clin Endocrinol Metab 78:842–846
20. Bale AE, Norton JA, Wong EL, Fryburg JS, Maton PN, Oldfield EH, Streeten E, Aurbach GD, Brandi ML, Friedman E, Spiegel AM, Taggart RT, Marx SJ 1991 Allelic loss on chromosome 11 in hereditary and sporadic tumors related to familial multiple endocrine neoplasia type 1. Cancer Res 51:1154–1157
21. Takino H, Herman V, Weiss M, Melmed S 1995 Purine-

binding factor (nm23) gene expression in pituitary tumors: marker of adenoma invasiveness. J Clin Endocrinol Metab 80:1733–1738
22. Jacks T, Fazeli A, Wschmitt EM, Bronson RT, Goodell MA, Weinberg RA 1992 Effects of an RB mutation in the mouse. Nature 359:295–300
23. Nakayama K, Ishida N, Shirane N, Inomata A, Inoue T, Shishido N, Horii I, Loh DY, Nakayama K 1996 Mice lacking p27(Kip1) display increased body size, multiple organ hyperplasia, retinal dysplasia, and pituitary tumors. Cell 85:707–720
24. Fero ML, Rivkin M, Tasch M, Porter P, Caroe CE, Firpo E, Polyak K, Tsai LH, Broudy V, Perlmutter RM, Kaushansky K, Roberts JM 1996 A syndrome of multiorgan hyperplasia with features of gigantism, tumorigenesis, and female sterility in p27(Kip1)-deficient mice. Cell 85:733–744
25. Boggild MD, Jenkinson S, Pistorello M, Boscaro M, Scanarini M, McTernan P, Perrett CW, Thakker RV, Clayton RN 1994 Molecular genetic studies of sporadic pituitary tumors. J Clin Endocrinol Metab 78:387–392
26. Pei L, Melmed S 1997 Isolation and characterization of a pituitary tumor-specific transforming gene. Mol Endocrinol 11:433–441
27. Yu H, Chen JK, Feng S, Dalgarno DC, Brauer AW, Schreiber SL 1994 Structural basis for the binding of proline-rich peptides to SH3 domains. Cell 76:933–945
28. Pawson T 1995 Protein modules and signalling network. Nature 373:573–580
29. Cohen GB, Ren R, Baltimore D 1995 Modular binding domains in signal transduction proteins. Cell 80:237–248
30. Strausberg RL, Dahl CA, Klausner RD 1997 New opportunities for uncovering the molecular basis of cancer. Nat Genet 15:415–416
31. Zhang X, Horwitz GA, Heaney AP, Nakashima M, Prezant TR, Bronstein MD, Melmed S, Pituitary tumor transforming gene in pituitary adenomas. J Clin Endocrinol Metab, in press
32. Romac JMJ, Graff DH, Keene JD 1994 The U1 small nuclear ribonucleoprotein (snRNP) 70K protein is transported independently of U1 snRNP particles via a nuclear localization signal in the RNA-binding domain. Mol Cell Biol 14:4662–4670
33. Vives E, Brodin P, Lebleu B 1997 A truncated HIV-1 Tat protein basic domain rapidly translocates through the plasma membrane and accumulates in the nucleus. J Biol Chem 272:16010–16017
34. Pawson T, Scott JD 1997 Signaling through scaffold, anchoring, and adapter proteins. Science 278:2075–2080
35. Olivier JP, Raabe T, Henkemeyer M, Dickson B, Mbamalu G, Margolis B, Schlessinger J, Hafen E, Pawson T 1993 A *Drosophila* SH2-SH3 adapter protein implicated in coupling the sevenless tyrosine kinase to an activator of *ras* guanine nucleotide exchange, Sos. Cell 73:179–191
36. Tanaka S, Morishita T, Hashimoto Y, Hattori S, Nakamura S, Shibuya M, Matuoka K, Takenawa T, Kurata T, Nagashima K, Matsuda M 1994 C3G, a guanine nucleotide-releasing protein expressed ubiquitously, binds to the Src homology 3 domains of CRK and GRB2/ASH protein. Proc Natl Acad Sci USA 91:3443–3447
37. Kharbanda S, Saleem A, Shafman T, Emoto Y, Taneja N, Rubin E, Weichselbaum R, Woodgett J, Avruch J, Kyriakis J, Kufe D 1995 Ionizing radiation stimulates a Grb2-mediated association of the stress-activated protein kinase with phosphatidylinositol 3-kinase. J Biol Chem 270:18871–18874
38. Wang J, Auger KR, Jarvis L, Shi Y, Roberts TM 1995 Direct association of Grb2 with the p85 subunit of phosphatidylinositol 3-kinase. J Biol Chem 270:12774–12780
39. Ren R, Ye ZS, Baltimore D 1994 Abl protein-tyrosine kinase selects the Crk adapter as a substrate using SH3-binding sites. Genes Dev 8:783–795
40. Feller SM, Knudsen B, Hanafusa H 1994 c-Abl kinase regulates the protein binding activity of c-Crk. EMBO J 13:2341–2351
41. Kreegipuu A, Blom N, Brunak S, Jarv J Statistical analysis of protein kinase specificity determinants. FEBS Lett 430:45–50
42. Folkman J, Klagsbrun M 1987 Angiogenic factors. Science 235:442–447
44. Friesel RE, Maciag T 1995 Molecular mechanisms of angiogenesis: fibroblast growth factor signal transduction. FASEB J 9:919–925
44. Liotta LA, Steeg PS, Stetler-Stevenson WG 1991 Cancer metastasis and angiogenesis: an imbalance of positive and negative regulation. Cell 64:327–336
45. Folkman J, Watson K, Ingber D, Hanahan D 1989 Induction of angiogenesis during the transition from hyperplasia to neoplasia. Nature 339:58–61
46. Yamanaka Y, Friess H, Buchler M, Beger HG, Uchida E, Onda M, Kobrin MS, Korc M 1993 Overexpression of acidic and basic fibroblast growth factors in human pancreatic cancer correlates with advanced tumor stage. Cancer Res 53:5289–5296
47. Gold LI, Saxena B, Mittal KR, Marmor M, Goswami S, Nactigal L, Korc M, Demopoulos RI 1994 Increased expression of transforming growth factor β isoforms and basic fibroblast growth factor in complex hyperplasia and adenocarcinoma of the endometrium: evidence for paracrine and autocrine action. Cancer Res 54:2347–2358
48. Duensing S, Grosse J, Atzpodien J 1995 Increased serum levels of basic fibroblast growth factor (bFGF) are associated with progressive lung metastases in advanced renal cell carcinoma patients. Anticancer Res 15:2331–2334
49. Relf M, LeJeune S, Scott PAE, Fox S, Smith K, Leek R, Moghaddam A, Whithouse R, Bicknell R, Harris AL 1997 Expression of the angiogenic factors vascular endothelial cell growth factor, acidic and basic fibroblast growth factor, tumor growth factor β-1, platelet-derived endothelial cell growth factor, placenta growth factor, and pleiotrophin in human primary breast cancer and its relation to angiogenesis. Cancer Res 57:963–969
50. Zimmering MB, Katsumata N, Sato Y, Brandi ML, Aurbach GD, Marx SJ, Friesen HG 1993 Increased basic fibroblast growth factor in plasma from multiple endocrine neoplasia type 1: relation to pituitary tumor. J Clin Endocrinol Metab 76:1182–1187
51. Ray D, Melmed S 1997 Pituitary cytokine and growth factor expression and action. Endocr Rev 18:206–228
52. Sambrook J, Fritsch EF, Maniatis T 1989 Molecular Cloning, ed. 2. Cold Spring Harbor Laboratory Press, Cold Spring Harbor, NY
53. Cowley S, Paterson H, Kemp P, Marshall CJ 1994 Activation of MAP kinase is necessary and sufficient for PC 12 differentiation and for transformation of NIH 3T3 cells. Cell 77:841–852
54. Breier G, Albrecht U, Sterrer S, Risau W 1992 Expression of vascular endothelial growth factor during embryonic angiogenesis and endothelial cell differentiation. Development 114:521–532
55. Hebert JM, Basilico C, Goldfarb M, Haub O, Martin GR 1990 Isolation of cDNAs encoding four mouse FGF family members and characterization of their expression pattern during embryogenesis. Dev Biol 138:4545–463
56. Shimon I, Huttner A, Said J, Spirina OM, Melmed S 1996 Heparin-binding secretory transforming gene (*hst*) facilitates rat lacotrope cell tumorigenesis and induces prolactin gene transcription. J Clin Invest 97:187–195

STIC-ILL

RC 261-C6

From: Canella, Karen
Sent: Sunday, February 03, 2002 9:00 PM
To: STIC-ILL
Subject: ill order 09/815,340

Art Unit 1642 Location 8E12(mail)

Telephone Number 308-8362

Application Number 09/815,340

1. Trends in Cell biology, 2001 Jan, 11(1):18-21
2. Clinical Cancer Research, 2000 Aug, 6(8):3215-3221
3. Mutation Research, 1997 Apr 29, 375(2):157-165
4. american Journal of Hematology, 1985 Mar, 18(3):243-249.
5. PNAS, 1989 Apr, 86(7):2276-2280
6. Genes and Development, 1996 Oct 15, 10(20):2621-2631
7. Cancer, 1975 Jun, 35(6):1664-1677
8. Mutation Research, 1978, 57(3): 313-324
9. Environ Mutagen, 1981, 3(1):53-64
10. Nucleic Acids Research, 2001 Mar 15, 29(6):1300-1307
11. Oncogene:
    1998 Oct 29, 17(17):2187-2193
    2000 Jan 20, 19(3):403-409
12. Molecular endocrinology, 1999 Jan, 13(1):156-166
13. Gene, 1999 Nov 29, 240(2):317-324
14. Science, 1999 Jul 16, 285(5426)418-422
15. Biochemistry and Molecular biology international, 1999 May, 47(5):891-897
16. Journal of Clinical Endocrinology and Metabolism, 1999 Mar, 84(3):1149-1152
17. Journal of biological chemistry:
    1999 Jan 29, 274(5):3151-3158
    2000 Nov 24, 275(47):36502-36505 ***
18. Gene 2000 May 2, 248(1-2):41-50
19. Molecular endocrinology, 2000 Aug, 14(8):1137-1146
20. Cancer Letters, 2001 Feb 10, 163(1):131-139
21. Brain Pathology, 2001 Jul, 11(3):328-341

Alteration of DNA Ploidy Status and Cell Proliferation Induced by Preoperative Radiotherapy Is a Prognostic Factor in Rectal Cancer

Guido Lammering, Mohiuddin M. Taher, Hans-Helmut Gruenagel, Franz Borchard, and Rainer Porschen[1]

Department of Radiation Oncology, Medical College of Virginia, Virginia Commonwealth University, Richmond, Virginia 23298 [G. L., M. M. T.]; Department of Radiation Oncology, Heinrich-Heine University Düsseldorf, Düsseldorf, Germany [G. L.]; Department of Surgery, Evangelic Hospital of Düsseldorf, Düsseldorf, Germany [H. H. G.]; Department of Pathology, Municipal Hospital, Aschaffenburg, Germany [F. B.]; and Department Internal Medicine I, University Hospital, D-72076 Tübingen, Germany [R. P.]

ABSTRACT

To identify predictors of prognosis after preoperative radiotherapy, DNA ploidy and cell proliferation were investigated in 116 patients with rectal cancer. For flow cytometry, a nuclear suspension was prepared by pepsin digestion of paraffin samples of biopsies taken before preoperative radiotherapy (15 × 2 Gy) and also of the resected rectal tumors after radiotherapy. The median follow-up period was 6 years. The proportion of tumor necrosis was evaluated in histological sections before and after irradiation. There was a significant decrease (74 to 48%) in aneuploid tumors after radiation. Of 86 patients with aneuploid biopsies, 28 revealed no reduction in the proportion of aneuploid tumor cells [group AN(=/↑)], and 58 showed a reduction (mean 48.9%) or complete elimination of aneuploid tumor cells [group AN(↓/∅)]. The incidence of local or distal failure was significantly reduced in the group AN(↓/∅) (7.8%/20%), compared with the group AN (=/↑) (27%/54%) and the group of constant diploid tumors (n = 22; 13.6%/31.8%; P = 0.034). There was a trend of decreased recurrence rate in diploid tumors with a reduced fraction of cells in S-phase after radiotherapy. Survival was significantly increased in group AN(↓/∅) (P < 0.0001). In a multivariate regression analysis, variables of independent prognostic significance were increased proportion of necrosis after irradiation and DNA ploidy group and the postoperative tumor stage. These results suggest that alterations in tumor DNA ploidy and cell proliferation induced by preoperative radiotherapy might help to identify patients likely to benefit from preoperative radiation in rectal cancer.

Received 8/10/99; revised 3/17/00; accepted 5/9/00.

The costs of publication of this article were defrayed in part by the payment of page charges. This article must therefore be hereby marked *advertisement* in accordance with 18 U.S.C. Section 1734 solely to indicate this fact.

[1] To whom requests for reprints should be addressed, at Medizinische Universitätsklinik und Poliklinik, Otfried-Müller-Strasse 10, D-72076, Tübingen, Germany.

INTRODUCTION

Cancer of the rectum is a common visceral tumor that for decades has been managed primarily by surgery alone. Survival and local recurrence rates in rectal carcinoma after curative surgical resection have remained static for many years. Recent studies, evaluating pre- and postoperative radiotherapy with cumulative doses between 25 and 50 Gy, could demonstrate a significant reduction in local recurrence and (1, 2), in combining postoperative radiotherapy with chemotherapy, an increased survival (3). When comparing pre- and postoperative radiotherapy modalities at similar doses, preoperative radiotherapy appears to be more efficient in reducing local failure rate (4), and recently, one study has shown improved survival over surgery alone (5).

Several studies have been reported on flow cytometric DNA measurement in human tumor biopsies to obtain prognostic data from tumor ploidy and cell proliferation. In head and neck (6), cervix (7), and bladder (8) cancers, it has been suggested that tumors with an aneuploid DNA content might dispose of higher radiosensitivity than diploid tumors. As an impact of preoperative radiotherapy, the prevalence of DNA aneuploidy was significantly lower in irradiated esophagus carcinomas compared with nonirradiated cases (9). Furthermore, radiobiological investigations have shown that cell proliferation influences the radiosensitivity of tumor cells considerably (10). Tumors with a higher proliferative activity show a higher response to radiotherapeutic treatment. Thus, the aim of the current study was to determine whether flow cytometric analysis of DNA ploidy and cell proliferation and their changes induced by radiotherapy are of prognostic value in preoperatively irradiated rectal cancer.

MATERIALS AND METHODS

Patients and Tissue Samples. One hundred and sixteen patients (51 men and 65 women) with a histologically proven localized adenocarcinoma of the rectum, treated by curative resection after preoperative irradiation at the Department of Surgery, Evangelic Hospital of Düsseldorf in Germany between 1980 and 1988 were included in this study. Mean age of the patients was 64.5 years (range, 38–87 years). The preoperative radiation therapy consisted of a total dose of 30 Gy delivered to the midplane of the pelvis through opposing anterior-posterior fields given in a daily fraction of 2 Gy, according to the regimen of a randomized trial conducted by the European Organization for Research and Treatment of Cancer (1), for tumors within 10 cm of the anal verge, and additional perineal field was used for irradiation. After an average time of 14.2 ± 9.8 days, 76 and 24% of the patients underwent anterior and abdomino-perineal resection, respectively. Table 1 shows the postoperative tumor characteristics. All pathological diagnosis and classification of

Table 1 Tumor characteristics of irradiated adenocarcinomas of the rectum (n = 116)

	No.	%
Tumor location from anal verge		
4 to <7 cm	49	42.2
7 to <12 cm	53	45.7
≥12 cm	14	12.1
Grading		
G1/2	95	81.9
G3	21	18.1
Tumor size		
<3 cm	69	59.5
3–6 cm	41	35.3
>6 cm	5	4.3
Tumor invasion		
$pT_{1/2}$	98	84.4
$pT_{3/4}$	18	15.5
Lymph node metastasis		
pN_0	77	66.4
$pN_{1/2}$	39	33.6
Tumor stage		
I	69	59.5
II/III	47	40.5

variables were reevaluated according to the TNM[2] staging (11) and the WHO grading system (12). Postirradiated tumor size ranged from 0.5 to 8 cm (median, 3.0 cm).

For these investigations, the whole tumor tissue was available in formalin-fixed, paraffin-embedded blocks. The mean number of biopsies before irradiation taken from different tumor regions during endoscopy was 4.7 ± 1.0, whereas the average number of paraffin blocks was 1.2 ± 0.6. The mean number of blocks embedding the resected tumor was 2.5 ± 0.9. Follow-up data were obtained from the charts of the patients, and the patients' data were stored in a follow-up computer program. Up-to-date information on survival or death and the cause of death was obtained from the local tumor register, the proper registration offices, the family doctors, or the patients themselves. For three patients, the cause of the death could not determined. Four patients died postoperatively; 9 patients showed incomplete or irregular follow-up. Complete follow-up was available in 103 patients (88.8%) with a mean period of 75 months (median, 73.2 months; range, 4.3–157 months).

Flow Cytometry. Formalin-fixed, paraffin-embedded tumor tissue was prepared and stained for flow cytometric analysis according to the modified procedure described by Hedley *et al.* (13). To enrich the proportion of tumor cells, the localized tumor region was microdissected from stroma tissue in paraffin blocks. Afterward, 150–200-μm sections were cutoff from the blocks to decrease nuclear debris (14). The average proportion of the tissue sample occupied by the resected tumor was 20% (range, 7–80%), whereas the analyzed proportion of the tumor biopsies before radiation was approximately 30–40%. Sections were treated with xylene over a period of 24 h to remove the paraffin and then rehydrated in ethanol and washed with distilled water. To prepare a nuclear suspension, sections were incubated in a 0.5% pepsin solution (pH 1.5, 37°C) for 90 min. After filtration through a 50-μm nylon mesh, nuclei were washed twice in PBS and then centrifuged. The nuclear pellet was resuspended in a 0.1% NP40-trisodium citrate solution (15) and treated with RNase solution (40 μg/ml). Finally the nuclear DNA was stained with propidium iodide (50 μg/ml) to analyze on a flow cytometer (Becton Dickinson, San Jose, CA), equipped with an argon laser using excitation at 488 nm. A total of 10,000 cells were used for cell cycle analysis using the Cellfit Software (Becton Dickinson, San Jose, CA). The flow cytometric parameters evaluated included DNA ploidy, the fractions of the cell cycle compartments, and the DI (where DI represents the ratio of the aneuploid G_1-G_0-DNA peak channel to the diploid G_1-G_0-DNA peak channel). Samples were defined as aneuploid only if there was more than one G_0-G_1 peak in the DNA histogram. In these tumors, the first peak on the left of the histogram was considered to represent diploid G_0-G_1 cells. For multiple paraffin blocks, the mean values of the S-phase fraction, the DI and the aneuploid G_0-G_1 peak were used. Evaluation of S-phase fraction was not possible in 20 aneuploid tumors because of overlapping of the diploid G_2-M cells in the channel area of the aneuploid S-phase cells in the histogram. The mean coefficient of variation of the G_1 peak in this study was 6.5 ± 1.8%.

Quantification of Necrosis. The extent of necrosis in the tumors was evaluated semiquantitatively by histopathological examination of all H&E-stained sections of every paraffin block of the biopsies and the resected tumors by one observer without knowledge of the patients' outcome. The proportion of necrosis was classified in 5% gradation (ex: 0, 5, 10, and 15–100%). For the biopsy necrosis gradation, it was necessary to start with 2%, indicating a minimal proportion of necrosis. The mean number of biopsies on one histological section was 3.9 ± 1.6 with an average of 1.2 ± 0.6 sections. Because the resected tumors were fixed in a mean number of 2.5 ± 0.9 paraffin-embedded blocks, 2.5 ± 0.9 sections of each tumor were available. The mean values of the proportion of necrosis in all histological sections before and after irradiation were used for each tumor.

Statistical Analysis. Possible associations between flow cytometric results and clinicopathological characteristics were determined using the χ^2 test. Yates correction was applied for a number of cases between 40 and 60 in a four-field table. Differences between mean values were analyzed using the Student's t test. Data analysis was performed with the SPSS statistical software package (SPSS, Inc., Chicago, IL). The Kaplan-Meier product-limit method was used to estimate survival or disease-free probabilities, with statistical interference's on actuarial curves made using the Breslow and the log-rank test. Patients dying as a result of postoperative complications (within 30 days) were excluded from the survival analysis. All patients with incomplete or missing follow-up had to be excluded for the calculations of local or distant recurrences. To determine independent prognostic factors, multivariate analysis was calculated using the Cox proportional hazards regression model. Results

[2] The abbreviations used are: TNM, Tumor-Node-Metastasis; AN(↓/∅), group of tumors with a reduced or eliminated proportion of aneuploid cells after radiotherapy; AN(=/↑), group of tumors with a constant or increased proportion of aneuploid cells after radiotherapy; DIDI, group of tumors with diploidy before and after radiotherapy; DI, DNA index; PCNA, proliferative cell nuclear antigen; SPF, S-phase fraction.

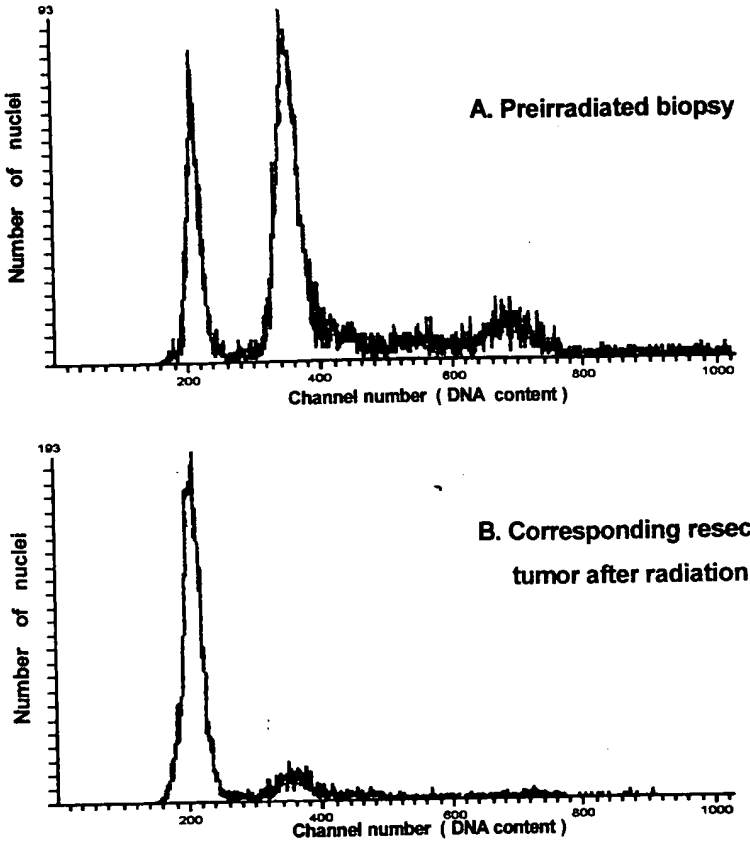

Fig. 1 DNA flow cytometric histograms of the biopsy before and the corresponding resected specimen after preoperative radiotherapy in rectal cancer. Both samples are classified as aneuploid because of a separate peak, representing the aneuploid G_1 population with a DI of 1.66. The proportion of the aneuploid G_1 population is reduced from 46% in the pretreatment biopsy to 11.4% in the resected tumor after irradiation. *A*, biopsy; *B*, resected tumor.

are presented as mean ± SD. Only $P < 0.05$ was considered statistically significant.

RESULTS

Ploidy and S-Phase Analysis. There are no reports available associating the DNA ploidy and preoperative radiotherapy as a prognostic tool. Speculations have been made that changes in ploidy status induced by radiation may be a useful predictor for clinical outcome in various cancers. In this study, we analyzed DNA ploidy and their alterations before and after irradiation of each tumor and compared those findings with the clinical follow-up. In the preirradiated biopsies, DNA aneuploidy was detected in 86 of 116 (74%) tumors. After radiotherapy, however, the number of aneuploid tumors decreased to 56 (48%; $\chi^2 = 16.33$; $P < 0.0001$). The distribution of the DI was similar before and after radiation. Compared with a mean DI of 1.67 ± 0.28 in the preirradiated hyperdiploid biopsies, the mean DI in the irradiated resected aneuploid tumors decreased to 1.55 ± 0.26, being clustered around triploid levels. After radiotherapy, 24 tumors (28%) showed a decrease in the proportion of aneuploid cells compared with the pretreatment values (mean reduction, 49.8%; range, 16.7–92.2%). A representative analysis of the data is given in Fig. 1. In contrast, 28 (33%) preirradiated aneuploid tumors revealed a constant or increased proportion of aneuploid cells after radiotherapy [mean increase, 64%; range, 0–262%; group AN(=/↑)]. Of these 52 tumors with a decrease or increase in the amount of aneuploid tumor cells, 35 tumors (67%) consistently showed this alteration among all analyzed samples in the posttreatment assessment. However, for the rest (33%), the decrease or increase was consistent in two of three samples. Thirty-four tumors (39%) even demonstrated a complete elimination of aneuploid cells [group AN(↓/∅)]. The percentage of tetraploid pretreatment tumors (DI, 1.8–2.2) was significantly higher in the group of tumors with an eliminated aneuploidy (41.2%) after radiotherapy than in the remaining aneuploid tumors (17.3%; $P = 0.042$). From 30 preirradiated diploid tumors, nearly all (26 of 30; 87%) remained diploid (group DIDI).

Tumor cell proliferation was determined by measuring the SPF. All 26 constant diploid cases and 32 of 52 pre- and posttreatment aneuploid cases (61%) provided analyzable S-phase data. Of the 26 constant diploid tumors, 17 (65%) revealed a constant or increased SPF [S-phase (=/↑)] with a mean increase of 73% (range, 12–430%). Only 9 tumors (35%) showed a decreased SPF [S-phase (↓)] in the posttreatment samples [mean decrease, 44% (range, 5 to 71%)]. The mean pretreatment SPF in group S-phase (↓) (10.4 ± 2.4%) was significantly higher than in the group S-phase (=/↑) (5.9 ± 2.3%; $P < 0.0001$).

Compared with a mean S-phase fraction of 7.4% (median, 6.8 ± 3.1%) for all diploid cases before treatment, the 32 aneuploid cases showed a significantly higher mean value of 19.5% (median, 20.3 ± 6.1%; $P < 0.0001$). Fourteen aneuploid tumors (44%) revealed a constant or increased SPF (mean

Table 2 Local or distal recurrence rates in correlation to different flow cytometric variables

Flow cytometric variables	No.	Local recurrence		Distant metastasis	
		No. (%)	P^a	No. (%)	P^a
Ploidy group					
AN (=/↑)	26	7 (27.0)	0.034	14 (53.9)	0.009
AN (↓/∅)	51	3 (7.8)		10 (20.0)	
DIDI	22	3 (13.6)		7 (31.8)	
Pretreatment ploidy					
Diploid	26	4 (15.4)	NS	8 (30.8)	NS
Aneuploid	77	10 (13.0)		20 (26.0)	
Pretreatment DI					
<1.3 (hyperdiploid)	12	1 (8.3)	NS	7 (58.3)	0.004
1.3–1.8 (peri-/ triploid)	43	6 (14.0)		16 (37.2)	
>1.8–2.2 (peri-/ tetraploid)	20	3 (15.0)		1 (5.0)	
Pretreatment aneuploidy					
<20.3 SPF	29	6 (20.7)	NS	9 (31.0)	NS
>20.3 SPF	29	2 (6.9)		4 (13.7)	
Pretreatment diploidy					
<6.6 SPF	13	2 (15.4)	NS	5 (38.5)	NS
>6.6 SPF	13	2 (15.4)		3 (23.1)	
Pre- and posttreatment diploid tumors					
SPF (↓)	7	1 (14.3)	NS	0 (0.0)	0.036
SPF (=/↑)	16	2 (12.5)		7 (43.8)	
Pre- and posttreatment aneuploid tumors					
SPF (↓)	15	1 (6.7)	NS	4 (26.7)	NS
SPF (=/↑)	14	1 (7.1)		8 (57.1)	

[a] All *P*s are based on the χ^2 test. NS, not significant.

increase, 43.3%; range, 0–99%). In 18 aneuploid tumors (56%), a mean decrease of 31.3% (range, 6.6–62%) was observed. The pretreatment fraction of the S-phase was significantly higher in the group of tumors with a reduced SPF after irradiation (23 ± 3.4% *versus* 15 ± 5.5%; $P < 0.0001$).

Characterization of Necrosis in Tumors. In biopsies, the overall percentage of necrosis was 1.6%. In the resected postirradiated tumors, the mean proportion of necrosis increased to 9.3%. The ploidy groups showed a visible difference in the increase of necrosis after radiotherapy. The group of tumors with a reduced or eliminated aneuploidy after irradiation [group AN (↓/∅)] showed the highest increase of necrosis with a mean of 10.9%, followed by the group AN (=/↑) with an increase of 6.2%. The lowest increase was observed in the group of constant diploid tumors (group DIDI; mean, 3.4%).

There was no significant relationship between the two ploidy groups [AN (↓/∅); AN (=/↑)] and clinicopathological characteristics, such as sex, age, localization, tumor differentiation, or lymph node metastasis. The association with the invasion of the primary tumor was of borderline statistical significance ($P = 0.07$). A decrease or elimination in the proportion of aneuploid cells is related to a significant increase of tumor necrosis ($P = 0.0001$).

Correlation with Clinical Follow-Up. During follow-up, 28 patients (27.2%) developed distant metastases, 10 relapsed locally (9.7%), and 4 relapsed locally and distally (3.9%). In total, the incidence of local recurrence was 13.5% ($n = 14$). Table 2 shows the recurrence rates in relation to different ploidy groups, pretreatment ploidy, pretreatment hyperdiploid DIs, pretreatment SPF, and changes in the SPF after irradiation. Although the pretreatment ploidy status was of no influence on recurrence, however, the changes in the proportion of aneuploidy induced by radiotherapy showed a significant impact on the number of local as well as distant recurrences. The preirradiated near-diploid tumors (DI < 1.3) relapsed distally in >50%, compared with 37.2% in the group of peri-/triploid tumors (DI, 1.3 to <1.8) and only 5% in the group of peri-/tetraploid tumors (DI, >1.8–2.2; $P < 0.004$). There was no significant influence on local or distant outcome between the different percentage of S-phase in the pretreatment diploid tumors, but for the alterations in the S-phase fraction after radiotherapy, a significant difference in the number of distant metastases could be observed (Table 2). In contrast, a pretreatment SPF of >20.3% in the aneuploid tumors showed a visible significant decreased overall recurrence rate.

Correlation with Patients' Survival. Forty-four patients (40.4%) died because of cancer-related causes, and 13 (11.9%) died because of intercurrent diseases. After exclusion of postoperative deaths ($n = 4$) and deaths of unknown causes ($n = 3$), the overall 5-year survival rate was 63.3%. Mean overall survival time of the study population ($n = 109$) related to cancer-related causes was 8.8 ± 0.5 years. Median survival time could not be achieved, because <50% of the patients died within the follow-up period. In univariate survival analysis sex, age, tumor location, tumor size, presence of lymph node metastasis, and grading were of no prognostic significance in this study group. In addition, the variables related to surgical treatment, such as the type of resection used, the period of time between the end of radiotherapy and surgery, and the distance between the edge of the tumor and the margin of bowel resection, showed no significant difference in overall survival. In the clinicopathological variables, only TNM stage and the pT category were significantly associated with overall survival. When compared with stage I with II/III, the 5-year survival rate (65%

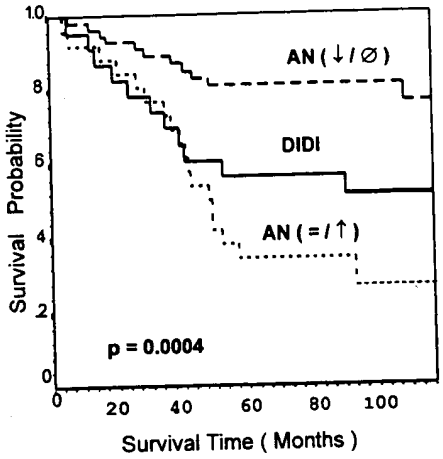

Fig. 2 Survival curves for cumulative survival in 105 patients with preoperatively irradiated carcinoma of the rectum, stratified into three different ploidy groups. AN (↓ /∅), n = 56; DIDI, n = 23; AN (=/ ↑), n = 26. P = 0.0004 (log-rank test).

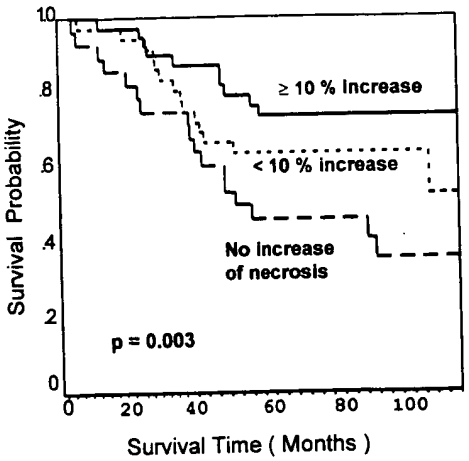

Fig. 3 Survival curves for cumulative survival in 106 patients with rectal cancer according to the increase of necrosis in histological sections after preoperative radiation (increase of necrosis ≥10%, n = 41; increase of necrosis, >0 to <10%, n = 37; no increase of necrosis, 0%, n = 28). P = 0.003 (log-rank test).

versus 51.7%) differed significantly (P = 0.044) as well as $pT_{1/2}$ compared with $pT_{3/4}$ (5-year survival rate, 65% *versus* 50%; P = 0.05). The group of patients with a reduced or eliminated proportion of aneuploid cells in tumor [group (AN (↓ /∅)] showed the highest survival benefit, followed by the group of patients with constant diploid tumors (group DIDI) and the group with no decrease in the proportion of aneuploid cells [group AN(=/ ↑); 5-ysr 81.2%; 56.5%; 34.6%; P = 0.0004; Fig. 2]. The pretreatment aneuploid group had a nonsignificant tendency to improved survival (aneuploid: 5-year survival rate, 65.4%; diploid: 5-year survival rate, 55.1%). The reduction in SPF of diploid tumors was also associated with a tendency to a better prognosis (5-year survival rate, 72.6% *versus* 50%; P = 0.14), but the significance level could not be reached because of a small case number. The group of patients with tumors showing an increase of necrosis of >10% after radiotherapy had a more favorable prognosis (5-year survival rate, 74%) than patients with <10% increase (5-year survival rate, 63.9%) or patients with no increase of necrosis in the tumors (5-year survival rate, 46.4%; P = 0.003; Fig. 3 represents the related survival curves).

Multivariate Cox Regression Analysis. The only variables of independent prognostic significance by multivariate regression analysis were tumor TNM stage, DNA ploidy group, and increase of necrosis (Table 3).

Table 3 Multivariate Cox regression analyses of clinicopathological and flow cytometric characteristics for overall survival in preoperatively irradiated rectal cancer

	Overall survival (n = 102) P
Sex	
Male *vs.* Female	NS[a]
Age	
≤64.7 yr *vs.* >64.7 yr	NS
TNM stage	
Stage I *vs.* II/III	0.038
Histological grade	
Grade 1/2 *vs.* 3	NS
Tumor location from anal verge	
4 to <7 cm *vs.* 7 to <12 cm *vs.* ≥12 cm	0.056
Ploidy group	
AN (=/ ↑) *vs.* AN (↓ /∅) *vs.* DIDI	0.048
Increase of necrosis	
0% *vs.* <10% *vs.* ≥10%	0.017

[a] NS, not significant.

DISCUSSION

In this report, we found that changes in the ploidy status and cell proliferation, determined by flow cytometry, as a result of preoperative irradiation are of predictive value in the prognosis of patients with rectal cancer. This is the first study to compare ploidy status and cell proliferation before and after irradiation and to correlate the alterations with the clinical outcome of the patients. Previous investigations of DNA ploidy in colorectal cancer were mainly conducted in the operatively resected tumors without any previous neoadjuvant therapy. Thus, a direct comparison of these investigations only exists to our flow cytometric results of the pretreatment biopsy samples. Usage of stored tumor material offers the advantage that long-term follow-up is available. Other investigators have shown, in comparative studies of fresh and paraffin-embedded tumor tissue, that the determination of DNA ploidy is accurate and a reliable method (16, 17). In the present study, aneuploidy was observed in 86 of 116 preirradiated rectal adenocarcinomas (74%). This percentage is in accordance with most of the results of several other studies of rectal cancer (18–20). Slight differences in percentage of aneuploidy result from the fact that in Anglo-American studies the colon and rectal cancers were often evaluated together. This led to a decrease in the overall percentage of aneuploid tumors, which was also shown by Costa *et al.* (20) and Rognum *et al.* (21), who have observed that aneuploid tumors are more frequently represented in distal sections of the

large bowel. In accordance with other authors (22–24), the pretreatment nondiploid rectal carcinomas tended to cumulate around the triploid level with a mean DI of 1.67.

As described previously, we classified tumors as aneuploid only after evaluating all excised biopsies or paraffin blocks of these tumors if at least one showed a separate peak in the DNA histogram. In consideration of the known heterogeneity in solid carcinomas (25), Quirke *et al.* (26) reported that if only one excisional biopsy of a colorectal carcinoma was taken and analyzed by flow cytometry, the probability of determining aneuploid cells is 72% accurate. With an average count of 4.7 excisional biopsies/tumor before radiation and 2.5 paraffin blocks containing the resected tumor after irradiation, the chances to overlook aneuploid cells in our study are therefore minimal. The heterogeneity in solid carcinomas does not only influence the results of ploidy analyses but also the results of cell cycle compartment analyses (27). For that reason, the proportion of SPF in diploid colorectal cancers described in previous studies ranged from 5.8% to 11.7% (23, 27), compared with 7.4% in the present study. The mean SPF of pretreatment aneuploid carcinomas was calculated to be significantly higher (19.5%) than for diploid carcinomas, confirming the data of most other reports (22, 28).

Clinical studies of irradiated solid cancers showed that the percentage of aneuploid tumors was clearly reduced by irradiation (29–31). For example, in esophageal cancer, the rate of DNA aneuploidy was significantly reduced by irradiation (71% *versus* 47%; Ref. 9); however, this comparison was done in two separate groups of patients with and without preoperative irradiation. These results are confirmed in the present study, showing a reduction in aneuploidy from 74 to 48% after irradiation as an intraindividual comparison. The reduction in the number of aneuploid tumors presumably reflects that aneuploid cells undergo apoptotic cell death after DNA damage. Mohr *et al.* (31) reported that loss of aneuploidy was associated with an increase of necrosis in histological sections. Moreover, aneuploid carcinomas appear to be more radiosensitive, because in this study the increase of necrosis after irradiation was observed more frequently in aneuploid than in diploid tumors. In addition, survival of patients was significantly improved after induction of necrosis after irradiation.

The influence of the aneuploid DI in determining the likelihood of radiosensitivity is beyond dispute. Tetraploid bladder cancers are reported to have a greater responsiveness to irradiation with a more favorable clinical outcome (8, 32). This observation is in accordance to our results, showing that the percentage of tetraploid tumors was significantly higher in the group of aneuploid tumors with an eliminated aneuploidy. Furthermore, tetraploid tumors relapsed distally significant less frequently (5%) than near diploid (58%) or triploid tumors (37%). Therefore, it can be hypothesized that DNA tetraploidy might be an indicator for response to preoperative radiotherapy in rectal cancer. This assumption, however, still has to be supported by prospective studies.

Because radiation effects are seen mainly in tissues with a high rate of cell turnover (33), Kubouchi *et al.* (34) have noted that radiosensitivity in rectal cancer depends on the proliferative activity of cells. This study revealed a correlation between reduction in PCNA activity after radiotherapy in the patients with high initial levels of PCNA activity. This could be confirmed in the present study, in which the groups of diploid as well as aneuploid tumors with a reduced SPF after irradiation were found to have a significantly higher initial proportion of SPF. However, there was no significant influence on local or distant failure between the different percentage of S-phase in the pretreated diploid tumors, whereas a trend for improved survival was found in patients with diploid tumors, who had a reduced SPF after radiotherapy. Accordingly, in aneuploid tumors an initial SPF of <20.3 (median as cutoff; Table 2) was associated with a significantly higher recurrence rate and this led to a borderline significant lower 5-year disease-free survival rate (data not shown).

The apoptotic cell death after DNA damage to aneuploid tumor cells after irradiation results in an elimination or decrease of aneuploidy. The tumors with a reduced or eliminated proportion of aneuploid cells after radiation rarely relapsed locally (5.8%) compared with constant diploid tumors (13.6%) or tumors with an increased proportion of aneuploid tumor cells (27%). Furthermore, the clinical outcome was significantly different between these three defined ploidy groups. Therefore, 67% of the preirradiated aneuploid tumors [group (AN ($\downarrow$ /$\varnothing$)] seem to have a higher radiosensitivity with a more favorable prognostic trend in contrast to the other 33% with an increased proportion of aneuploidy despite radiation. Several cell kinetic studies reported that response to radiation depends on multiple intrinsic and extrinsic factors (33). These factors, influencing radiosensitivity in a complicated still unknown way, might explain the differences in radioresponsiveness within the aneuploid tumors.

In this study, no significant difference in overall survival was observed for the tumor characteristic location and lymph node metastasis. This observation is in contrast to several studies (35, 36), defining tumor location and lymph node status as important prognostic factors in rectal cancers. Thus, preoperative radiotherapy seems to eliminate the prognostic meaning of these factors, which was also concluded by Sarashina *et al.* (37). The TNM stage and pT category were still of significant predictive value.

In conclusion, we propose that detection of alterations in the proportion of aneuploid cells after irradiation has a good prognostic value in preoperatively irradiated rectal cancer, and these results will help to distinguish between radiosensitive and radioresistant tumors. In addition, changes in the cell proliferation rate after radiotherapy might be helpful in detecting patients likely to benefit from preoperative radiotherapy. Further investigations of cell cycle kinetics during radiotherapy will be required to elucidate the precise mechanisms of tumor response to radiation and to optimize the individualized application of radiotherapy.

REFERENCES

1. Gerard, A., Buyse, M., Nordlinger, B., Loyquen, J., Pene, F., Kempf, P., Bosset, J. F., Gignoux, M., Arnaud, J. P., DeSaive, C., *et al.* Preoperative radiotherapy as adjuvant treatment in rectal cancer. Ann. Surg., *208:* 606–614, 1988.

2. Kodner, J., Shemesh, E. I., Myerson, R., *et al.* Preoperative irradiation for rectal cancer improved local control and long-term survival. Ann. Surg., *209:* 194–199, 1989.

3. Krook, J. E., Moertel, C. G., Gunderson, L. L., Eieand, H. S., Collins, R. T., Beart, R. W., Kubista, T. P., Poon, M. A., Meyers, W. C., Maillard, J. A., *et al.* Effective surgical adjuvant therapy for high risk rectal carcinoma. N. Engl. J. Med., *324:* 709–715, 1991.

4. Glimelius, B., Isacsson, U., Jung, B., *et al.* Radiotherapy in addition to radical surgery in rectal cancer: evidence for a dose-response effect favoring preoperative treatment. Int. J. Radiat. Oncol. Biol. Phys., *2:* 281–287, 1997.

5. Swedish Rectal Cancer Trial. Improved survival with preoperative radiotherapy in resectable rectal cancer. N. Engl. J. Med., *336:* 980–997, 1997.

6. Franzen, G., Klintenberg, C., Olofsson, J., and Risberg, B. DNA measurements as an objective predictor of response to irradiation? A review of 24 squamous cell carcinomas of the oral cavity. Br. J. Cancer, *53:* 643–651, 1986.

7. Dyson, J. E. D., Joslin, C. A. F., Rothwell, R. I., *et al.* Flow cytometric evidence for the differential radioresponsiveness of aneuploid and diploid cervix tumours. Radiother. Oncol., *8:* 263–272, 1987.

8. Wijkstrom, H., and Tribukait, B. Deoxyribonucleic acid flow cytometry in predicting response to radical radiotherapy of bladder cancer. J. Urol., *144:* 646–650, 1990.

9. Porschen, R., Bevers, G, Remy, U., *et al.* Influence of preoperative radiotherapy on DNA ploidy in squamous cell carcinomas of the esophagus. Gut, *34:* 1086–1090, 1993.

10. Streffer, C., Van Beuningen, D., Gross, E., *et al.* Predictive assays for the therapy of rectum carcinoma. Radiother. Oncol., *5:* 303–310, 1986.

11. Hermanek, P., Sobin, L. H. TNM Classification of Malignant Tumours, Ed. 4. Berlin: Springer-Verlag, 1987.

12. Jass, J. R., and Sobin, L. H. Histological typing of intestinal tumours. International Histological Classification of Tumours, Ed. 2. Geneva: WHO. Berlin: Springer-Verlag, 1989.

13. Hedley, D. W., Friedlände, M. L., Taylor, I. W., Rugg, C. A., and Musgrove, E. A. Method for analysis of cellular DNA content of paraffin-embedded pathological material using flow cytometry. J. Histochem. Cytochem., *31:* 1333–1335, 1983.

14. Stephenson, R. A., Gay, H., Fair, W., and Melamed, M. R. Effect of section thickness on quality of flow cytometric DNA content determinations in paraffin-embedded tissues. Cytometry, *7:* 41–44, 1986.

15. Vindelov, L. L., Christensen, I. J., and Nissen, N. I. A detergent-trypsin method for the preparation of nuclei for flow cytometric DNA analysis. Cytometry, *3:* 323–327, 1983.

16. McIntire, T. L., Goldey, S. H., Benson, N. A., and Braylan, R. C. Flow cytometric analysis of DNA in cells obtained from deparaffinized formalin-fixed lymphoid tissues. Cytometry, *8:* 474–478, 1987.

17. Schutte, B., Reynders, M. M. J., Bosman, F. T., and Blijham, G. H. Flow cytometric determination of DNA ploidy level in nuclei isolated from paraffin-embedded tissue. Cytometry, *6:* 26–30, 1985.

18. Jones, D. J., Moore, M., and Schofield, P. F. Refining the prognostic significance of DNA ploidy status in colorectal cancer: a prospective flow cytometric study. Int. J. Cancer, *41:* 206–210, 1988.

19. Enblad, P., Glimelius, B., Bengtsson, A., Porter, J., and Pahlman, L. The prognostic significance of DNA content in carcinoma of the rectum and rectosigmoid. Acta Chir. Scand., *153:* 453–458, 1987.

20. Costa, A., Faranda, A., Scalmati, A., Quagliuolo, V., Colella, G., Ponz de Leon, M., and Silvestrini, R. Autoradiographic and flow cytometric assessment of cell proliferation in primary colorectal cancer: relationship to DNA ploidy and clinicopathological features. Int. J. Cancer, *50:* 719–723, 1992.

21. Rognum, T. O., Thorud, E., and Lund, E. Survival in large bowel carcinoma patients with different DNA ploidy. Br. J. Cancer, *56:* 633–636, 1987.

22. Kouri, M., Pyrhonen, S., Mecklin, J. P., Jarvnen, H., Laasoner, A., Franssila, K., and Nordling, S. The prognostic value of DNA-ploidy in colorectal carcinoma: a prospective study. Br. J. Cancer, *62:* 976–981, 1990.

23. Hiddemann, W., Von Bassewitz, D. B., Kleinemeier, H. J., Schulte-Brochteibeck, E., Hauss, J., Lingemann, B., Buchner, T., and Grundmann, E. DNA stemline heterogeneity in colorectal cancer. Cancer (Phila.), *58:* 258–263, 1986.

24. Giaretti, W., and Santi, S. Tumor progression by DNA flow cytometry in human colorectal cancer. Int. J. Cancer, *45:* 597–603, 1990.

25. Kallioniemi, O. P. Comparison of fresh and paraffin-embedded tissue as starting material for DNA flow cytometry and evaluation of intratumor heterogeneity. Cytometry, *9:* 164–169, 1988.

26. Quirke, P., Dyson, J. E., Dixon, M. F., Bird, C. C., and Joslin, C. A. Heterogeneity of colorectal adenocarcinoma evaluated by flow cytometry and histopathology. Br. J. Cancer, *51:* 99–106, 1985.

27. Bauer, K. D., Lincoln, S. T., Vera-Roman, J. M., Wallemark, C. B., Chimiel, J. S., Madurski, M. L., Murad, T., and Scarpelli, D. G. Prognostic implications of proliferative activity and DNA aneuploidy in colonic adenocarcinomas. Lab. Investig., *57:* 329–334, 1987.

28. Meyer, J. S., and Prioleau, P. G. S-Phase fractions of colorectal carcinomas related to pathologic and clinical features. Cancer (Phila.), *48:* 1221–1228, 1981.

29. Yu, J. M., Zhang, H., Wang, S. Q., Miao, H. Q., Yang, L. H., Chen, Y. T., and Tian, G. D. DNA ploidy analysis of effectiveness of radiation therapy for cervical carcinoma. Cancer (Phila.), *68:* 76–78, 1991.

30. Toyota, K., Nagamori, S., Kashiwagi, A., *et al.* Flow cytometric analysis of the DNA content in the urinary bladder cancers treated by radical cystectomy and pre-operative irradiation. Nippon Hinyokika Gakkai Zasshi, *83:* 2050–2057, 1992.

31. Mohr, C., Molls, M., Streffer, C., and Pelzer, T. Prospective flow cytometric analysis of head and neck carcinomas. Prognostic relevance of DNA content and S-fraction. J. Cranio-Maxillo-Fac. Surg., *20:* 8–13, 1992.

32. Jacobsen, A. B., Lunde, S., Ous, S., Melvik, J. E., Pattersen, E. O., Kaalhus, O., and Fossa, S. D. T2/T3 bladder carcinomas treated with definitive radiotherapy with emphasis on flow cytometric DNA ploidy values. Int. J. Radiat. Oncol. Biol. Phys., *17:* 923–929, 1989.

33. Denekamp, J. Cell kinetics and cancer therapy. Springfield, IL: Charles C. Thomas, 1982.

34. Kubouchi, T., Kimura, K., Nakajiama, A., Katoh, K., Eiraku, H., Majima, T., Wada, T. Sumi, T., Sakamoto, N., and Ebihara, Y. DNA ploidy and proliferating cell nuclear antigen positively rate as predictive indication of effectiveness of preoperative radiation. Gan. To Kagaku Ryoho, *21:* 82–88, 1994.

35. Pescatori, M., Mattana, C., Maria, G., Ferrara, A., and Lucibello, L. Outcome of colorectal cancer. Br. J. Surg., *74:* 370–372, 1987.

36. McDermott, F. T., Hughes, E. S., Pihl, E., Johnson, W. R., and Price, A. B. Local recurrence after potentially curative resection for rectal cancer in a series of 1008 patients. Br. J. Surg., *72:* 34–37, 1985.

37. Sarashina, H., Inoue, I., Saitoh, N., *et al.* Untersuchung zur präoperativen Strahlentherapie beim Rektumkarzinom. Strahlenther. Onkologie., *167:* 361–365, 1991.

STIC-ILL

Adams only 20

From: Canella, Karen
Sent: Sunday, February 03, 2002 9:00 PM
To: STIC-ILL
Subject: ill order 09/815,340

Art Unit 1642 Location 8E12(mail)

Telephone Number 308-8362

Application Number 09/815,340

1. Trends in Cell biology, 2001 Jan, 11(1):18-21
2. Clinical Cancer Research, 2000 Aug, 6(8):3215-3221
3. Mutation Research, 1997 Apr 29, 375(2):157-165
4. american Journal of Hematology, 1985 Mar, 18(3):243-249.
5. PNAS, 1989 Apr, 86(7):2276-2280
6. Genes and Development, 1996 Oct 15, 10(20):2621-2631
7. Cancer, 1975 Jun, 35(6):1664-1677
8. Mutation Research, 1978, 57(3): 313-324
9. Environ Mutagen, 1981, 3(1):53-64
10. Nucleic Acids Research, 2001 Mar 15, 29(6):1300-1307
11. Oncogene:
    1998 Oct 29, 17(17):2187-2193
    2000 Jan 20, 19(3):403-409
12. Molecular endocrinology, 1999 Jan, 13(1):156-166
13. Gene, 1999 Nov 29, 240(2):317-324
14. Science, 1999 Jul 16, 285(5426)418-422
15. Biochemistry and Molecular biology international, 1999 May, 47(5):891-897
16. Journal of Clinical Endocrinology and Metabolism, 1999 Mar, 84(3):1149-1152
17. Journal of biological chemistry:
    1999 Jan 29, 274(5):3151-3158
    2000 Nov 24, 275(47):36502-36505 ***
18. Gene 2000 May 2, 248(1-2):41-50
19. Molecular endocrinology, 2000 Aug, 14(8):1137-1146
20. Cancer Letters, 2001 Feb 10, 163(1):131-139
21. Brain Pathology, 2001 Jul, 11(3):328-341

Article title	Molecular cloning of pituitary tumor transforming gene 1 from ovarian tumors and its expression in tumors
Article identifier	0304383501000519
Authors	Puri_R Tousson_A Chen_L Kakar_S_S
Journal title	Cancer Letters
ISSN	0304-3835
Publisher	Elsevier Ireland
Year of publication	2001
Volume	163
Issue	1
Supplement	0
Page range	131-139
Number of pages	9
User name	Adonis
Cost centre	
PCC	$20.00
Date and time	Tuesday, February 05, 2002 9:08:40 PM

ELSEVIER

Cancer Letters 163 (2001) 131–139

CANCER Letters

www.elsevier.com/locate/canlet

Molecular cloning of pituitary tumor transforming gene 1 from ovarian tumors and its expression in tumors

Rashmi Puri[a], Albert Tousson[b], Leilei Chen[a], Sham S. Kakar[a,*]

[a]*James Graham Brown Cancer Center, University of Louisville, Louisville, KY, USA*
[b]*Department of Cell Biology, University of Alabama at Birmingham, Birmingham, AL, USA*

Received 28 September 2000; received in revised form 6 November 2000; accepted 10 November 2000

Abstract

Pituitary tumor transforming gene 1 (PTTG1) recently cloned from human testis is a potent oncogene and is highly expressed in all the tumors analyzed to date. However, primary structure of PTTG1 and the cell types that express PTTG1 in tumors remained undescribed. We have used the reverse transcriptase-polymerase chain reaction technique to clone PTTG1 from ovarian tumors. Nucleotide sequencing of the PTTG1 cDNAs from various ovarian tumors showed identity with that of the human testis PTTG1. To determine the cell types that express PTTG1 in normal and tumor tissues, we performed in situ hybridization using digoxigenin-labeled cRNA as a probe. Our studies revealed a high level of expression of PTTG1 mRNA in both seminomatous and non-seminomatous testicular tumors; epithelial, sex-cord and stromal cell, and germ cell tumors of the ovary; and invasive ductal, ductal in situ and infiltrating ductal carcinoma of the breast. In normal tissues, expression of PTTG1 mRNA was very low or undetectable except in testis, where PTTG1 mRNA was found to be localized to spermatocytes and spermatids. Tumors that expressed high levels of PTTG1 mRNA also exhibited high levels of expression of basic fibroblast growth factor (bFGF), suggesting a correlation between PTTG1 and bFGF expression, and further suggesting that the PTTG1 protein may be involved in tumor angiogenesis and mitogenesis.

Keywords: In situ hybridization; Pituitary tumor transforming gene 1; Tumor; Cloning

1. Introduction

Tumorigenesis typically involves multiple genetic changes, which can take the form of mutation or an alteration in the expression of the gene that is not associated with mutation of the functional domains of the gene. These changes in oncogenes, tumor suppressor genes, and genes that encode proteins associated with the regulation of the cell cycle culminate in unrestrained cellular growth, tissue invasion, and ultimately, metastasis. The composition of the tumorigenesis cascade varies with the type of tumor and the critical elements of the cascades that have yet to be described in many tumors, including those of the ovary. Several mechanisms that contribute to tumorigenesis in ovarian cancers have been described including mutations or overexpression of the HER-2/neu, *fms*, *Akt-2* proto-oncogenes, *p53* suppressor gene, and transforming growth factors. The HER-2/neu gene is overexpressed in approximately 20–30% of ovarian cancers and in one third of breast cancers. Although amplification of the HER-2/neu gene is associated with a poor prognosis in breast cancer [1], a number of studies, have

* Corresponding author. Department of Medicine, 570 Preston Street, Baxter Biomedical Research Building, Room 204C, University of Louisville, Louisville, KY 40202, USA. Tel.: + 1-502-852-0812; fax: +1-502-852-2356.
E-mail address: sskaka01@louisville.edu (S.S. Kakar).

0304-3835/01/$ - see front matter
PII: S0304-3835(00)00688-1

failed to identify an adverse effect of HER-2/neu overexpression on the overall survival of patients with ovarian cancer [2]. Alterations in members of the *myc* family of proto-oncogenes have been reported to play a major role in the pathogenesis of several human cancers [3–5]. Again, although 10% of ovarian cancers have been shown to overexpress the *c-myc* gene, no apparent relationship between c-myc amplification and the grade of tumor differentiation or prognosis in patients with ovarian cancer has been reported. Mutation of the *p53* suppressor gene, which is located on chromosome 17p13.1, is one of the most frequent genetic changes in human tumors and has been described in a variety of tumors including cancers of the colon, lung, breast, and endometrium. At least 50% of ovarian cancers exhibit alterations of the *p53* gene and overexpress the transformant protein [6,7]. These mutations of *p53* are less frequent in the early stages of ovarian cancer than in advanced stages, however, and it is only in advanced-stage disease that mutations of p53 have been associated with adverse prognosis. Thus, alterations in p53 may be a relatively late event in the progression of ovarian cancer [8].

Recently, using a mRNA differential display PCR expression technique, Pei and Melmed [9] cloned a novel oncogene, the pituitary tumor transforming gene (PTTG) from rat pituitary tumor, and showed that overexpression of this gene in mouse fibroblast cells (NIH 3T3) results in cellular transformation in vitro and promotes tumor formation in vivo. Subsequently, we and others cloned PTTG from human tissue and defined its primary structure [10–14]. The PTTG family consists of at least three homologous genes. The PTTG1 gene contains five exons and four introns, and is located on human chromosome 5q35.1 [15]. Both PTTG2 and PTTG3 are intronless genes that are located on chromosomes 4p15.1 and 8q13.1, respectively [16,17]. Northern blot and reverse transcriptase–polymerase chain reaction (RT-PCR) analysis of the mRNA revealed a high level of expression of PTTG1 mRNA in various human tumors including tumors of the pituitary gland, adrenal gland, liver, kidney, endometrium, uterus, and ovary and in cell lines derived from various tumors [10–13]. The expression of PTTG1 mRNA was either very low or undetectable in all of the normal tissues tested except for the testis.

The predicted PTTG1 gene product is a highly hydrophilic protein that contains two proline rich-motifs at its C-terminus. As is the case for rat PTTG, overexpression of the human PTTG1 gene induces cellular transformation in vitro, and promotes tumor formation in nude mice [10,12]. Furthermore, transfection of PTTG1 into NIH 3T3 cells results in an increase in expression of basic growth factor (bFGF) and inhibition of chromatid separation [12,14] with mutation of the proline-rich motif abolishing the transforming ability of PTTG1 and blocking bFGF production [12]. Thus, PTTG1 may promote tumorigenesis by affecting angiogenesis and/or mitogenesis through its regulatory effect on bFGF.

Neither the primary structure of PTTG1 nor its cellular expression in the various tumors has been described to date. In this study, we cloned and sequenced PTTG1 cDNAs from various ovarian tumors and determined the cellular expression of PTTG1 in tumors derived from ovary, breast and testis. We also determined the expression of bFGF in these tumors.

2. Materials and methods

2.1. Cloning of PTTG1 from ovarian tumors

To clone PTTG1 from ovarian tumors, we used the RT-PCR technique as described previously [18]. Total RNA from four different ovarian tumors was prepared using the UltraspecIII RNA isolation system from Biotecx (Houston, TX). The integrity of RNA was determined by fractionation on agarose gel and staining with ethidium bromide. Total RNA from each tumor (2 μg) was subjected to first strand cDNA synthesis using an oligo(dT) primer and AMV reverse transcriptase (Promega, Madison, WI). A 5-μl aliquot from the 20-μl reaction volume was then used in PCR amplification using the GeneAmp kit (PE Applied Biosystem, Branchburg, NJ). The reaction conditions for PCR were initial denaturation at 95°C for 5 min, denaturation at 95°C for 1 min, annealing at 54°C for 1 min, and extension at 72°C for 1 min for 30 cycles with final extension at 72°C for 7 min after the last cycle of amplification. The oligonucleotide primers used for PCR amplification were sense 5′-AAGACCTGCAATAATCCAGA-3′ and antisense 5′-CACACAAACTCTGAAGCACT-3′

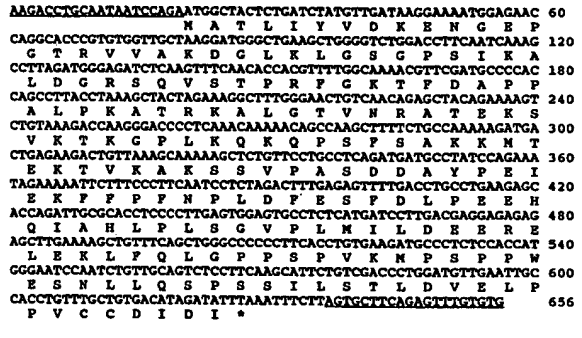

Fig. 1. Nucleotide and deduced amino acid sequence of the PTTG1 cDNAs from ovarian tumors. The underlined nucleotides designate the oligonucleotide primers used for PCR.

selected from 5′ and 3′ untranslated regions of the PTTG cDNA sequence (Fig. 1). A 10-μl aliquot of the reaction mixture from each sample was fractionated on a 1.5% agarose gel and stained with ethidium bromide. To identify contamination of the RNA samples with genomic DNA, RNA from each tissue was subjected to PCR without inclusion of the reverse transcriptase step. The PCR product from each sample was subcloned into the pCR4.0 TOPO TA cloning vector (Invitrogen, Carlsbad, CA). Plasmid DNA from the recombinant clones was prepared using the Plasmid Purification System from Qiagen (Chatsworth, CA). Complete nucleotide sequencing of the four independent clones for each tumor was performed on both strands using an automatic DNA sequencer.

2.2. *Tissue collection and preparation of sections*

Normal and tumor tissues were obtained from The Tissue Procurement Facility of the Comprehensive Cancer Center, the University of Alabama at Birmingham, AL. These tissues were collected at the time of biopsy or autopsy (3–12 h after death) and were immediately frozen in liquid nitrogen and then stored at −80°C. All human tissue specimens were obtained and analyzed with approval from the University of Alabama at Birmingham Human Studies Review Board. The tissue sections (10 μm) thick were cut and mounted on Super Frost Plus glass slides (Fisher Scientific, Atlanta, GA) and stored at −80°C.

2.3. *Preparation of digoxigenin-labeled cRNA probes*

The PTTG1 cDNA representing the sequence from nucleotides 21 to 319 (Fig. 1) was amplified by PCR using the specific oligonucleotide primers: sense 5′-ATGGCTACTCTGATCTATG-3′ and anti-sense 5′-GCTTTTAACAGTCTTCTCAGT-3′ as described above. The human PTTG cDNA was used as a template. The amplified product was then subcloned into the pCR4.0 TOPO TA cloning vector. The recombinant clones were isolated and sequenced to confirm the authenticity of the sequence and to determine orientation. The plasmid DNA was linearized with *Pst*I restriction endonuclease to transcribe sense cRNA using T3 RNA polymerase, and with *Not*I to transcribe antisense cRNA using T7 RNA polymerase. The cRNA transcripts were digoxigenin-labeled by in vitro transcription using a DIG RNA Labeling kit (Roach Diagnostics Corp., Indianapolis, IN).

2.4. *In situ hybridization*

The frozen sections were thawed at room temperature and air-dried. The sections were fixed in 4% paraformaldehyde (pH 7.4–7.5) for 20 min, and then treated with 0.2 N HCl for 10 min to suppress endogenous alkaline phosphatase activity. The sections were washed twice with 1 × phosphate-buffered saline (PBS) for 5 min each and digested with proteinase K (1 μg/ml) for 15 min at 37°C in proteinase K buffer (100 mM Tris–HCl, 50 mM EDTA, pH 8.0). The enzyme digestion was stopped by rinsing the sections with PBS and refixing with 4% paraformaldehyde for 10 min. After rinsing the sections with PBS, the tissues were acetylated with freshly prepared 0.25% acetic anhydride in 0.1 M triethanolamine (pH 8.0). The sections were then dehydrated in a graded series of ethanol, delipidated in chloroform and washed twice with absolute alcohol. The sections were prehybridized at 42°C for 1 h in prehybridization solution containing 50% formamide, 2 × Denhardt's solution, 20 × SSC, 10% dextran sulfate, 400 μg/ml tRNA, 400 μg/ml salmon sperm DNA, and 20 mM dithiothreitol. The hybridization solution containing labeled RNA probes (2 μg/slide) was heated at 65°C for 5 min and then chilled on ice for 5 min. The sections were hybridized in hybridization solution containing digoxigenin-labeled cRNA (2 μg/ml). Hybridization was performed at

42°C overnight. Post-hybridization treatments were as follows: two washes with 2 × SSC for 10 min each at room temperature; digestion with RNase A (10 μg/ml) at 37°C for 30 min; a wash with 2 × SSC; two washes with 0.2 × SSC for 15 min each; a wash with 0.1 × SSC for 30 min at 55°C; a wash with 0.1 × SSC and finally a wash with Buffer A (100 mM Tris–HCl, 150 mM NaCl, pH 7.5). The sections were incubated in blocking solution (Buffer A containing 0.3% Triton X-100, and 2% normal goat serum) for 1 h at room temperature. The sections were incubated with alkaline phosphatase-conjugated anti-digoxigenin Fab fragment antibody (Roach Diagnostics Corp.) diluted 1:500 in Buffer A for 2 h at room temperature. After incubation, the sections were washed twice with Buffer A for 10 min each and then once with Buffer B (100 mM Tris–HCl, 100 mM NaCl, 50 mM $MgCl_2$, pH 9.5) for 10 min. The sections were incubated with 5-bromo-4 choloro-3-indolyl phosphate (BCIP)/nitroblue tetrazolium (NBT) (Sigma Chemical, St. Louis, MO) at room temperature for 2 h. The reaction was terminated by washing the sections with Buffer C (0.5 M Tris–HCl, 0.5 M EDTA, pH 8.0) for 5min. The sections were mounted in Aqua Mount (Fisher Scientific) and were examined using an Olympus XO microscope.

2.5. Immunohistochemical staining for bFGF

For immunocytohistochemical analysis, the frozen tissue sections were thawed at room temperature. The sections were incubated at 95°C in 0.01 mol/l sodium citrate buffer (pH 6.0) for 20 min to optimize antigen retrieval. Non-specific antibody binding was blocked by incubating the sections in 5% non-fat skim milk powder in Tris-buffered saline/0.1% Tween-20 (TBS/T) for 60 min. The sections were incubated with monoclonal antibody to basic fibroblast growth factor (clone FB-8, Sigma) diluted 1:100 at room temperature for 1 h as described by Heaney et al. [19]. Controls included sections incubated with no primary antibodies. After several rinses in TBS/T, sections were incubated with biotinylated mouse anti-goat

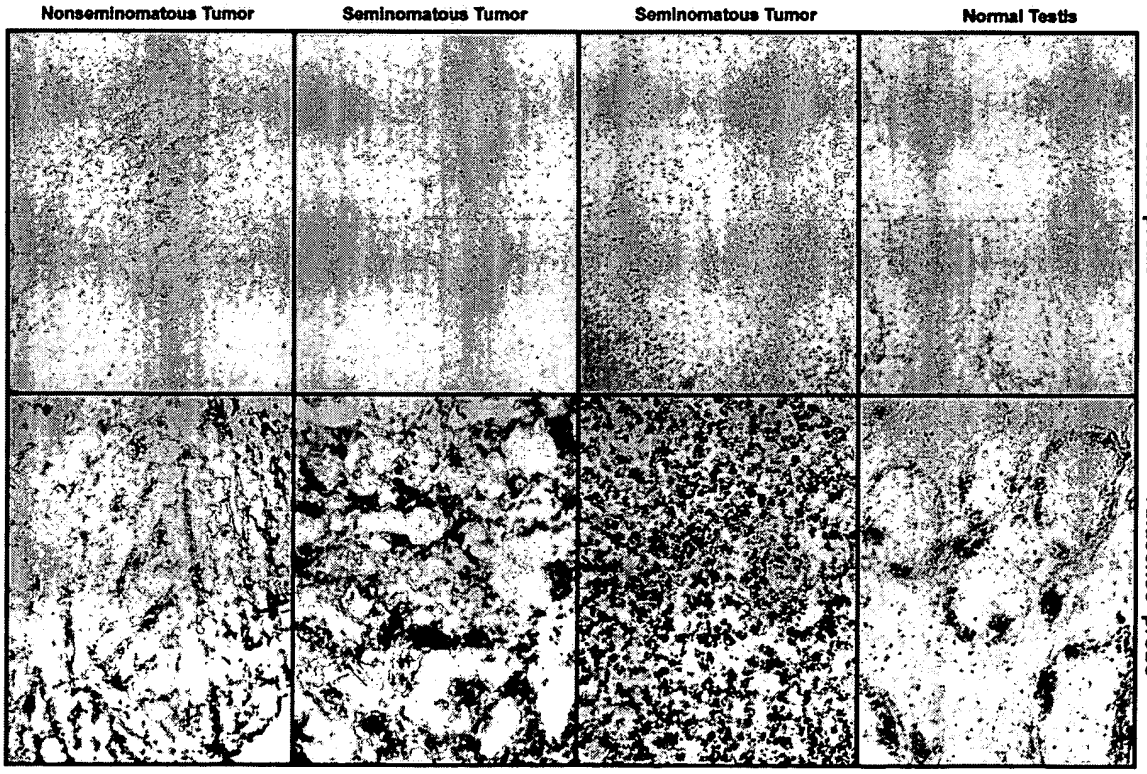

Fig. 2. In situ hybridization of the human PTTG1 in normal testis and testicular tumors. Sections were hybridized with either sense or antisense probes corresponding to PTTG1 cDNA. Notably, the level of expression was considerably higher in tumors than that observed in normal tissues.

secondary antibody for 30 min at room temperature. The sections were rinsed three times in TBS/T, and then incubated with streptavadin-horseradish peroxidase conjugate (Vector Laboratories Inc., Burlingame, CA) for 30 min. After washing three times with TBS/T, the sections were incubated with diaminobenzidine tetrahydrochloride for 3 min at room temperature. The sections were then rinsed with H_2O followed by a rinse with hematoxylin. The sections were mounted in Aqua Mount (Fisher Scientific) and examined using an Olympus XO microscope.

3. Results and discussion

We have demonstrated previously that PTTG1 is an oncogene and is upregulated in human malignancies including tumors of the pituitary gland, adrenal gland, liver, kidney, endometrium, uterus, and ovary and cell lines derived from various tumors [10]. It was therefore of interest to determine the primary structure of the PTTG1 expressed in tumors. In the studies presented here, we used ovarian tumors as our model and used the RT-PCR technique to clone the PTTG1 from these tumors. As shown in Fig. 1, the PTTG1 cDNAs cloned from various ovarian tumors are composed of 656 nucleotides and encode a protein of 202 amino acids. The nucleotide sequences of all the clones were identical with each other and with the human testis PTTG1 cDNA sequence [10], suggesting that the primary structure of PTTG1 is unaltered in ovarian tumors. As anticipated, it appears that the mechanism underlying the role of PTTG1 in tumorigenesis in ovarian tumors is not loss of function due to mutation but rather overexpression.

To characterize the cellular expression of PTTG1, a range of normal tissues as well as tumor tissues were examined using the in situ hybridization technique with antisense PTTG1 cRNA as a probe. The condi-

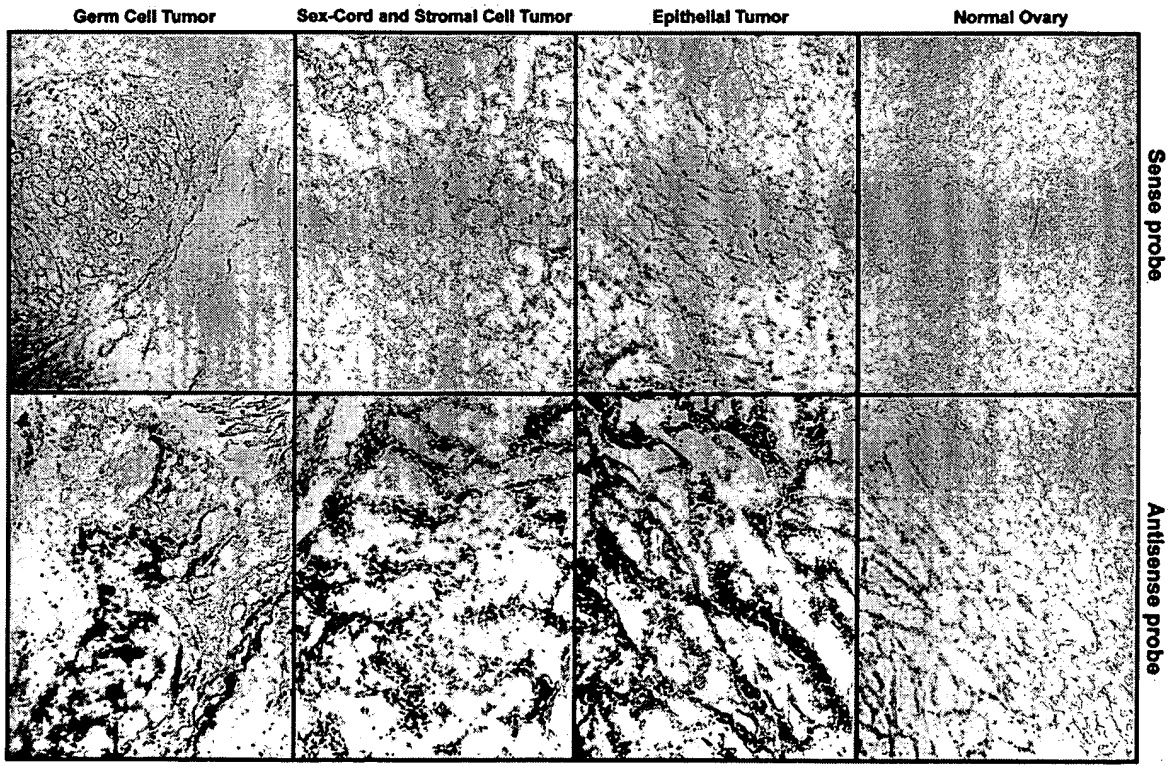

Fig. 3. In situ hybridization of the human PTTG1 in normal ovary and ovarian tumors. Sections were hybridized with either sense or antisense probes corresponding to PTTG1 cDNA. Notably, the level of expression was considerably higher in tumors than that observed in normal tissues.

tions such as temperature of hybridization, length of hybridization and washing of unhybridized probe were optimized to obtain a high signal with low background. As shown in Fig. 2, a hybridization signal was detected in normal testis. The signal appear to be specific, since no signal was detected with the sense probe. Testis is composed of numerous cell types that are both proliferating and differentiating. Maturation of germ cells proceeds through several ordered stages, with the stage of maturation increasing from the base of the seminiferous tubules toward the tubule lumen. A strong hybridization signal was observed in spermatocytes and spermatids, whereas only a weak hybridization signal was observed in Leydig cells, suggesting high levels of expression of PTTG1 mRNA in spermatocytes and spermatids and a low level of expression in Leydig cells. These results are consistent with those of Pei [20] who, using similar techniques, showed high levels of expression of PTTG1 mRNA in spermatocytes and spermatids in rat testis. Thus, PTTG1 may play a role in spermatogenesis in the normal testis. Most testicular tumors originate from germ cells. In situ hybridization of the testicular tumors showed strong hybridization signals in all the testicular tumor tissues analyzed including seminomatous and non-seminomatous testicular tumors. The hybridization signals were distributed homogeneously throughout the tumor tissue. No signal was observed in these tumors with the sense probe.

Ovarian cancer develops predominately from the malignant transformation of a single cell type, with transformation of the surface epithelium occurring in ~90% of malignant ovarian cancers. In our previous studies, using RT-PCR analysis, we showed high levels of expression of PTTG1 mRNA in ovarian mucinous carcinoma, poorly differentiated ovarian adenocarcinoma and granulosa cell tumors [10]. As shown in Fig. 3, in situ hybridization of the various ovarian tumors with the antisense PTTG1cRNA probe revealed strong signals in the epithelial tumor, sex-

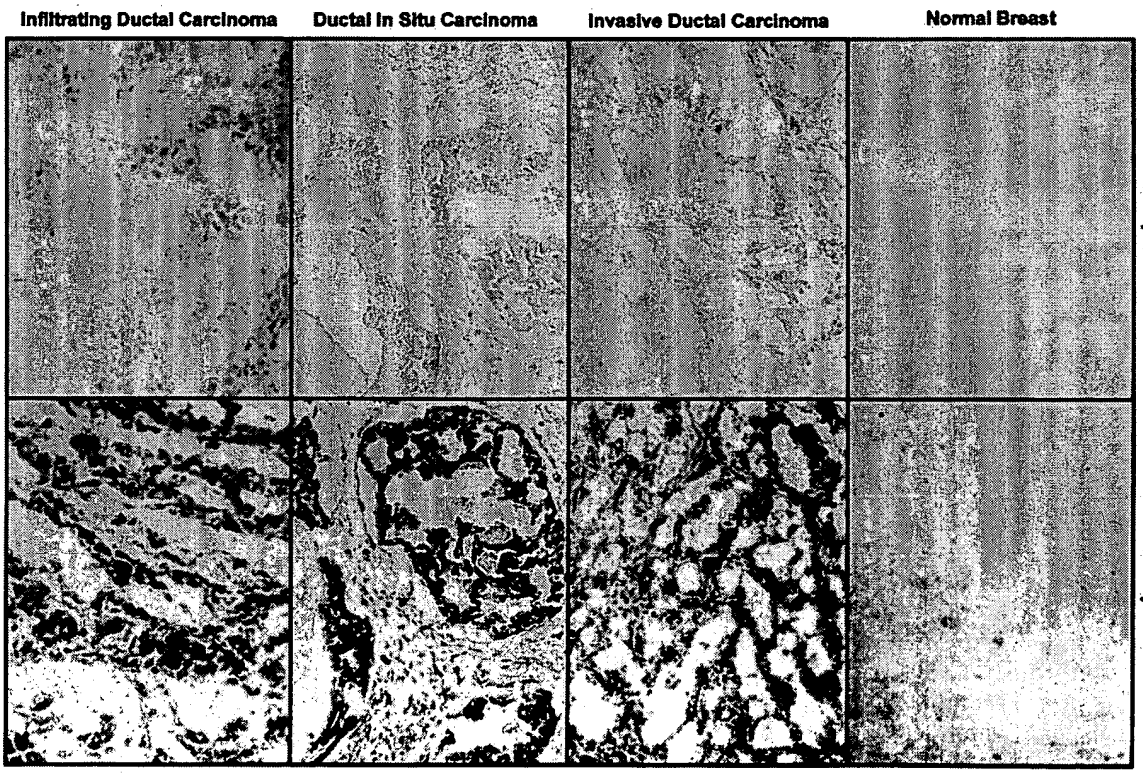

Fig. 4. In situ hybridization of the human PTTG1 in normal breast and breast tumors. Sections were hybridized with either sense or antisense probes corresponding to PTTG1 cDNA. Notably, the level of expression was considerably higher in tumors than that observed in normal tissues.

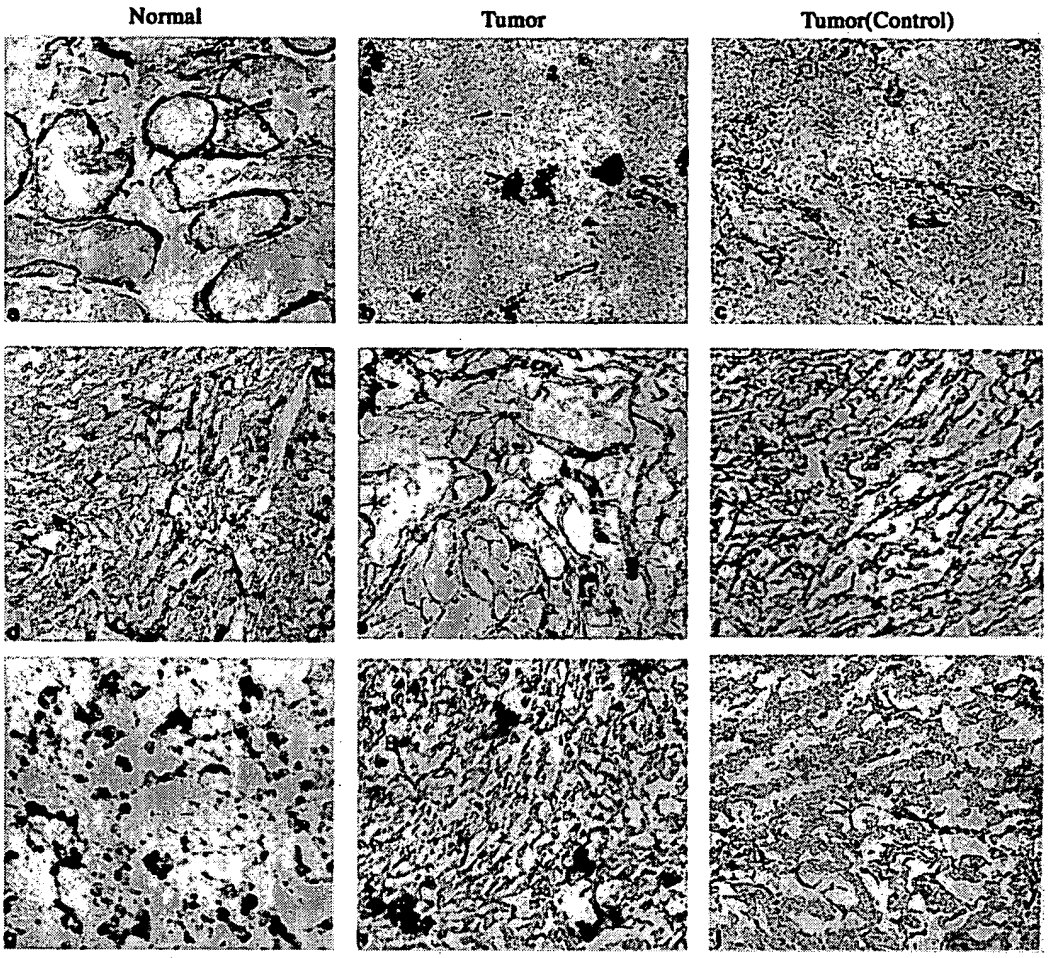

Fig. 5. Pattern of bFGF immunoreactivity in human normal and tumor tissues. bFGF immunoreactivity in normal testis (a), testicular tumor (b); normal ovary (d), ovarian tumor (e), normal breast (g) and breast tumor (h) detected with a monoclonal bFGF antibody. Negative controls: immunohistochemical staining reaction in testicular tumor (c), ovarian tumor (f) and breast carcinoma (i).

cord and stromal cell tumor, and germ cell tumor. The hybridization signal was distributed widely throughout the tumor specimen. Hybridization signals were not observed in any of the cells of the normal ovary nor were they observed using the sense probe. The present results confirm our previous findings and suggest high levels of expression of PTTG1 mRNA in epithelial as well as germ cell ovarian tumors, with the absence, or only low levels of expression of PTTG1 in the normal ovary.

Similar studies were accomplished using breast cancer specimens representing either invasive or non-invasive (generally known as in situ) tumors. Infiltrating ductal carcinoma, an invasive cancer, that penetrates the wall of a duct, and infiltrates into stroma. This is the most common form of breast cancer, representing approximately 70% of all cases. Infiltrating lobular carcinoma, an invasive cancer that has spread through the wall of a lobule, accounts for approximately 8% of all breast cancers. non-invasive breast cancers include ductal carcinoma in situ (also called intraductal carcinoma) and lobular carcinoma in situ, which account for approximately 10% of all breast cancer cases. In situ hybridization of the breast tumor tissues using the antisense PTTG1 cRNA showed high levels of expression of PTTG1 mRNA in all the breast cancers analyzed including infiltrating ductal carcinoma, ductal in situ carcinoma, and invasive ductal carcinoma (Fig. 4).

Signals were not observed in any of the cells of normal breast tissues, suggesting the absence, or only low levels of expression, of PTTG1 mRNA in normal breast, and enhancement of its expression in non-invasive and invasive tumors.

In our previous studies, we demonstrated that overexpression of PTTG1 in NIH 3T3 cells induces a transformed phenotype [10]. However, the molecular mechanisms through which PTTG1 contributes to cellular transformation remain unknown. Recently, Zou et al. [10] showed that overexpression of PTTG causes inhibition of chromatid separation which may lead to genetic instability, and thereby result in tumorigenesis. Zhang et al. [12] also showed an increase in secretion and expression of bFGF upon expression of PTTG1 in NIH 3T3 cells. The bFGF growth factor is a major activating factor for mitogenesis and angiogenesis [21,22]. Increased expression of bFGF has been reported in several human tumors, including those of the breast, pituitary, endometrium, and ovary [23–26]. To determine if the expression of bFGF is associated with PTTG1 expression in human tumors, we performed immunohistochemical analysis of the bFGF protein in normal and tumor tissues. As shown in Fig. 5, using a monoclonal bFGF antibody, only low levels of bFGF protein were observed in normal testis, ovary, and breast, with higher levels in testicular, ovarian, and breast tumors. In the tumors, the distribution of bFGF protein was not homogeneous; rather, groups of cells showed intense immunostaining, suggesting an autocrine or paracrine regulatory effect on the expression of bFGF. These results are consistent with those of Heaney et al. [19,27] who showed higher levels of expression of bFGF in colorectal and pituitary tumors. The concordant increase in expression of PTTG mRNA and bFGF in tumors indicates that the PTTG1 protein may play an important role in the generation of the malignant phenotype through upregulating the expression and secretion of bFGF.

Acknowledgements

This work was supported by a grant CA82511 from the National Cancer Institute. We wish to thank Dr Fiona Hunter for her editorial assistance and comments.

References

[1] D.J. Slamon, W. Godolphin, L.A. Jones, J.A. Holt, S.G. Wong, D.E. Keith, W.J. Levin, S.G. Stuart, J. Udove, A. Ullrich, H.M.F. Press, Studies of the HER-2/neu proto-oncogene in human breast and ovarian cancer, Science 244 (1989) 707–712.

[2] A. Berchuck, A. Kamel, R. Whitaker, B. Kerns, G. Olt, R. Kinney, J.T. Soper, R. Dodge, D.L. Clarke-Pearson, P. Marle, S. Mckenzie, S. Yin, R.C. Bast, Overexpression of Her-2/neu is associated with poor survival in advanced epithelial ovarian cancer, Cancer Res. 50 (1990) 4087–4091.

[3] G. Klein, E. Klein, Evolution of tumors and the impact of molecular oncology, Nature 315 (1985) 190–195.

[4] K. Marcu, Regulation of expression of the c-myc proto-oncogene, Bioassays 6 (1985) 28–32.

[5] R. Collum, F. Alt, Are myc proteins transcription factors, Cancer Cells 2 (1990) 69–75.

[6] M.E. Kohler, J. Marks, R.W. Wiseman, I.J. Jacobs, A.M. Davidoff, D.L. Clarke-Pearson, J.T. Soper, R.C. Bast, A. Berchuck, Spectrum of mutation and frequency of allelic deletion of the p53 gene in ovarian cancer, J. Natl. Cancer Inst. 85 (1993) 1513–1519.

[7] J. Kupryjanczyk, A.D. Thor, R. Beauchamp, V. Merritt, S.M. Edgerton, D.A. Bell, D.W. Yandell, p53 gene mutations and protein accumulation in human ovarian cancer, Proc. Natl. Acad. Sci. USA 90 (1993) 4961–4965.

[8] B.J. Milner, L.A. Allan, D.M. Eccles, H.C. Kitchener, R.C. Leonard, K.F. Kelly, D.E. Parkin, N.E. Haites, p53 mutation is a common genetic event in ovarian carcinoma, Cancer Res. 53 (1993) 2128–2132.

[9] L. Pei, S. Melmed, Isolation and characterization of a pituitary tumor- transforming gene (PTTG), Mol. Endocrinol. 11 (1997) 403–411.

[10] S.S. Kakar, L. Jennes, Molecular cloning and characterization of the tumor transforming gene (TUTR1): a novel gene in human tumorigenesis, Cytogenet. Cell Genet. 84 (1998) 211–216.

[11] A. Dominguez, F. Ramos-Morales, F. Romero, R.M. Rios, F. Dreyfus, M. Tortolero, J.A. Pintor-Toro, hPTTG, a human homologue of rat pttg, is overexpressed in hematopoietic neoplasms. Evidence for a transcriptional activation function of hPTTG, Oncogene 17 (1998) 2187–2193.

[12] X. Zhang, G.A. Horwitz, T.R. Prezant, A. Valentini, M. Nakashima, M.D. Bronstein, S. Melmed, Structure, expression, and function of human pituitary tumor-transferring gene (PTTG), Mol. Endocrinol. 13 (1999) 156–166.

[13] I.A. Lee, C. Seong, I.S. Choe, Cloning and expression of human cDNA encoding human homologue of pituitary tumor transforming gene, Biochem. Mol. Biol. Int. 47 (1999) 891–897.

[14] H. Zou, T.J. McGarry, T. Bernal, M.W. Krischner, Identification of a vertebrate sister-chromatid separation inhibitor involved in transformation and tumorigenesis, Science 285 (1999) 418–422.

[15] S.S. Kakar, Molecular cloning, genomic organization, and

identification of the promoter for the human pituitary tumor transforming gene (PTTG), Gene 240 (1999) 317–324.
[16] L. Chen, R. Puri, E.J. Lefkowitz, S.S. Kakar, Identification of the human pituitary tumor transforming gene (hPTTG) family: molecular structure, expression, and chromosomal localization, Gene 248 (2000) 41–50.
[17] T. Prezant, P. Kadioglu, S. Melmed, An intronless homolog of human proto-oncogene hPTTG is expressed in pituitary tumors: evidence for hPTTG family, J. Clin. Endocrinol. Metab. 84 (1999) 1149–1152.
[18] S.S. Kakar, L. Jennes, Expression of gonadotropin-releasing hormone and gonadotropin-releasing receptor mRNAs in various non-reproductive human tissues, Cancer Lett. 98 (1985) 57–62.
[19] A. Heaney, R. Singson, C.J. McCabe, V. Nelson, M. Nakashima, S. Melmed, Expression of pituitary-tumor transforming gene in colorectal tumors, Lancet 355 (2000) 716–719.
[20] L. Pei, Pituitary tumor-transforming gene protein associates with ribosomal protein S10 and a novel human homologue of DnaJ in testicular cells, J. Biol. Chem. 274 (1999) 3151–3158.
[21] J. Folkman, M. Klagsbrun, Angiogenic factors, Science 235 (1987) 442–447.
[22] R.E. Friesel, T. Maciag, Molecular mechanisms of angiogenesis: fibroblast growth factor signal transduction, FASEB J. 9 (1995) 919–925.
[23] M. Relf, S. LeJeune, P.A. Scott, S. Fox, K. Smith, R. Leek, A. Moghaddam, R. Whitehouse, R. Bicknell, A.L. Harris, Expression of the angiogenic factors vascular endothelial cell growth factor, acidic and basic fibroblast growth factor, tumor growth factor β-1, platelet-derived endothelial cell growth factor, placenta growth factor, and pleiotrophin in human primary breast cancer and its relation to angiogenesis, Cancer Res. 57 (1997) 963–969.
[24] L.I. Gold, B. Saxena, K.R. Mittal, M. Marmor, S. Goswami, L. Nactigal, M. Korc, R.I. Demopoulos, Increased expression of transforming growth factor β isoforms and basic fibroblast growth factor in complex hyperplasia and adenocarcinoma of the endometrium: evidence for paracrine and autocrine action, Cancer Res. 54 (1994) 2347–2358.
[25] M.B. Zimering, N. Katsumata, Y. Sato, M.L. Brandi, G.D. Aurbach, S.J. Marx, H.G. Friesen, Increased basic fibroblast growth factor in plasma from multiple endocrine neoplasia type 1: relation to pituitary tumor, J. Clin. Endocrinol. Metab. 76 (1993) 1182–1187.
[26] J. Fujimoto, S. Ichigo, M. Hori, H. Sakaguchi, T. Tamaya, Expression of basic fibroblast growth factor and its mRNA in advanced ovarian cancers, Eur. J. Gyncol. Oncol. 18 (1997) 349–352.
[27] A. Heaney, G.A. Horwitz, Z. Wang, R. Singson, S. Melmed, Early involvement of estrogen-induced pituitary tumor transforming gene and fibroblast growth factor expression in prolactinoma pathogenesis, Nat. Med. 5 (1999) 1317–1321.

STIC-ILL

From: Canella, Karen
Sent: Sunday, February 03, 2002 9:00 PM
To: STIC-ILL
Subject: ill order 09/815,340

Art Unit 1642 Location 8E12(mail)

Telephone Number 308-8362

Application Number 09/815,340

1. Trends in Cell biology, 2001 Jan, 11(1):18-21
2. Clinical Cancer Research, 2000 Aug, 6(8):3215-3221
3. Mutation Research, 1997 Apr 29, 375(2):157-165
4. american Journal of Hematology, 1985 Mar, 18(3):243-249.
5. PNAS, 1989 Apr, 86(7):2276-2280
6. Genes and Development, 1996 Oct 15, 10(20):2621-2631
7. Cancer, 1975 Jun, 35(6):1664-1677
8. Mutation Research, 1978, 57(3): 313-324
9. Environ Mutagen, 1981, 3(1):53-64
10. Nucleic Acids Research, 2001 Mar 15, 29(6):1300-1307
11. Oncogene:
    1998 Oct 29, 17(17):2187-2193
    2000 Jan 20, 19(3):403-409
12. Molecular endocrinology, 1999 Jan, 13(1):156-166
13. Gene, 1999 Nov 29, 240(2):317-324
14. Science, 1999 Jul 16, 285(5426)418-422
15. Biochemistry and Molecular biology international, 1999 May, 47(5):891-897
16. Journal of Clinical Endocrinology and Metabolism, 1999 Mar, 84(3):1149-1152
17. Journal of biological chemistry:
    1999 Jan 29, 274(5):3151-3158
    2000 Nov 24, 275(47):36502-36505 ***
18. Gene 2000 May 2, 248(1-2):41-50
19. Molecular endocrinology, 2000 Aug, 14(8):1137-1146
20. Cancer Letters, 2001 Feb 10, 163(1):131-139
21. Brain Pathology, 2001 Jul, 11(3):328-341

Expression of Bcl-x_L and loss of p53 can cooperate to overcome a cell cycle checkpoint induced by mitotic spindle damage

Andy J. Minn,[1,2] Lawrence H. Boise,[1] and Craig B. Thompson[1–4]

[1]Gwen Knapp Center for Lupus and Immunology Research, [2]The Committee on Immunology, [3]Howard Hughes Medical Institute, Department of Medicine, and Department of Molecular Genetics and Cell Biology, The University of Chicago, Chicago, Illinois 60637 USA

During somatic cell division, faithful chromosomal segregation must follow DNA replication to prevent aneuploidy or polyploidy. Damage to the mitotic spindle is one potential mechanism that interferes with chromosomal segregation. The accumulation of aneuploid or polyploid cells resulting from a disrupted mitotic spindle is presumably prevented by cell cycle checkpoint controls. In the course of studying cells that overexpress the apoptosis-inhibiting protein Bcl-x_L, we found that these cells have an increased rate of spontaneous tetraploidization, suggesting that apoptosis may play an important role in eliminating cells that fail to complete mitosis properly. When cells expressing Bcl-x_L are treated with mitotic spindle inhibitors, a significant percentage reinitiate DNA replication and become polyploid. Nevertheless, the majority of cells expressing Bcl-x_L undergo a prolonged p53-dependent cell cycle arrest following mitotic spindle damage. Unexpectedly, p53 expression is not induced in mitosis, nor does it influence M-phase arrest. Instead, cells with mitotic spindle damage only transiently arrest in M phase, and despite failing to complete mitosis, appear to proceed to G_1. During this subsequent growth factor-dependent phase, p53 is induced and mediates cell cycle arrest. In cells that do not overexpress Bcl-x_L, elimination of the p53-dependent growth arrest with a dominant negative mutant also results in polyploidy after mitotic spindle damage, but under these conditions most cells die by apoptosis. Expression of Bcl-x_L and abrogation of p53 cooperate to allow rapid and progressive polyploidization following mitotic spindle damage. Our results suggest that suppression of apoptosis by *bcl-2*-related genes and loss of p53 function can act cooperatively to contribute to genetic instability.

[*Key Words*: Apoptosis; checkpoint control; mitosis; mitotic spindle; p53; Bcl-x_L]

Received April 4, 1996; revised version accepted August 28, 1996.

During cell division, the orderly execution of DNA replication and chromosomal segregation, which define the S and M phases of the cell cycle, respectively, must occur with great fidelity. To ensure the interdependency of S phase and M phase, cells have developed mechanisms to monitor the completion of each process and halt cell cycle progression if either process is interrupted by cellular damage. Presumably, arresting damaged cells gives them a chance to repair and/or prevents their further expansion. Cell cycle checkpoint controls are genetic pathways that include proteins that sense damage, arrest the cell cycle, initiate repair, and cause apoptosis (Murray 1994, 1995). The importance of genes involved in these pathways is emphasized by the increasing evidence that mutations in checkpoint control genes contribute to tumorigenesis and by the fact that cancer cells often have karyotypic abnormalities (Hartwell and Kastan 1994).

p53 is one of the best-studied proteins involved in cell cycle checkpoint controls and is found to be mutated in over half of all human cancers (Hollstein et al. 1991). After DNA damage, p53 is induced and acts as a sequence-specific transcription factor (Cox and Lane 1995; Haffner and Oren 1995). The cyclin dependent kinase inhibitor $p21^{Waf1/Cip1}$ is a direct transcriptional target of p53 transactivation and is partly responsible for arresting cells in G_1 (El-Deiry et al. 1993; Harper et al. 1993; Deng et al. 1995). Gadd45 is another transcriptional target and is involved in stimulating DNA repair (Smith et al. 1994). Besides its role in a G_1 checkpoint, p53 also has

[4]Corresponding author.

been implicated in having a role in G_2/M. Fibroblasts null for p53 rapidly become aneuploid and polyploid in culture (Harvey et al. 1993), and after mitotic spindle damage these cells continue DNA replication in the absence of cell division and become polyploid (Cross et al. 1995). Interestingly, arrest after mitotic spindle damage is not dependent on $p21^{Waf1/Cip1}$ (Deng et al. 1995).

Apoptosis is also being recognized as an important genetic mechanism in controlling cancer. Increasing the apoptotic threshold may be important for tumor growth because, in addition to causing proliferation, oncogene expression is often associated with increased programmed cell death (Evan et al. 1995). Additionally, an elevated apoptotic threshold contributes to radiation and chemotherapy resistance (Fisher 1994). p53 is also able to mediate apoptosis. Loss of p53 prevents thymocytes from undergoing apoptosis after gamma irradiation (Clarke et al. 1993; Lowe et al. 1993b) and decreases the efficacy of chemotherapy in vitro (Lowe et al. 1993a) and in vivo (Lowe et al. 1994). Loss of p53-mediated apoptosis also potentially contributes to tumorigenesis in conjunction with the loss of tumor suppressor genes such as *rb* (Haffner and Oren 1995) or the gain of oncogenes such as c-*myc* (Evan et al. 1995).

The inappropriate expression of antiapoptosis genes including members of the *bcl-2* family is another way to raise the apoptotic threshold of cancer cells (Hockenbery 1995). Overexpression of either Bcl-2 or the related protein Bcl-x_L can protect tumor cells from a wide variety of apoptotic stimuli and confers a multidrug resistance phenotype (Miyashita and Reed 1993; Dole et al. 1994; Minn et al. 1995). Recent evidence shows that Bcl-x_L can be highly expressed in both primary tumors and tumor cell lines (Dole et al. 1995; Schlaifer et al. 1995).

One function of cell cycle checkpoints is to prevent the expansion of cells with unrepaired genetic damage. In theory, mutations in any of numerous genes involved in a checkpoint pathway could result in accumulation of damaged cells. These include genes involved in sensing the damage, causing cell cycle arrest, initiating repair, or inducing apoptosis. Whether most cell cycle checkpoint controls are simple linear pathways or involve several independent pathways remains unclear. In a linear pathway, apoptosis may require cell cycle arrest, and simply disrupting the arrest mechanism may prevent death and allow expansion of damaged cells. Alternatively, if arrest and apoptosis are controlled independently, disrupting cell cycle arrest would still allow damaged cells to undergo apoptosis. Independent control of cell cycle arrest and apoptosis predicts that the expansion of cells with abnormalities would occur only if both pathways are perturbed, a prediction that is in accord with a multihit model of carcinogenesis. In the work presented here, we address these issues in the context of a cell cycle checkpoint that is responsive to mitotic spindle damage. Damage induced by agents that disrupt the mitotic spindle initiates a p53-dependent cell cycle arrest and causes apoptosis in a manner that is p53-independent and inhibitable by Bcl-x_L.

Results

Cells expressing Bcl-x_L have an increased propensity to become polyploid

Cells transfected with *bcl-x_L*, an antiapoptosis gene, have an increased propensity to become tetraploid after passage in cell culture when compared with cells transfected with a control vector. This was first noticed when the DNA content of murine FL5.12 cells transfected with *bcl-x_L* was measured during continuous passage in vitro. Using starting diploid clones, these cells often became tetraploid after only 2–3 weeks of culture.

These initial observations prompted us to further explore the relationship between Bcl-x_L expression and mechanisms involved in the control of ploidy. To assess whether Bcl-x_L enhanced the rate of spontaneous tetraploidization, FL5.12 cells were transfected with either a Bcl-x_L expression vector (FL5-Bcl-x_L) or a Neo control vector (FL5-Neo). These bulk transfected populations were then cloned by limiting dilution, and after expansion, the percentage of tetraploid clones was examined. After limiting dilution cloning, 30.2% of the expanded FL5-Bcl-x_L clones were tetraploid, compared with 4.2% of the expanded FL5-Neo clones (Table 1). This result suggests that Bcl-x_L expression is able to enhance the rate of spontaneous tetraploidization.

One way cells can become tetraploid is through disruption of the mitotic spindle and the failure of checkpoint controls to either arrest or repair the cells. To determine whether Bcl-x_L influenced the fidelity of a mitotic spindle checkpoint, we treated FL5-Neo and FL5-Bcl-x_L cells with nocodazole, a drug which disrupts the mitotic spindle by inhibiting microtubule polymerization. As seen in Figure 1, both FL5-Neo and FL5-Bcl-x_L cells arrested with a predominantly 4N DNA content after 24 hr of nocodazole exposure. This implies that Bcl-x_L does not affect the initial ability of checkpoint controls to arrest cells in M phase in response to mitotic spindle disruption. During the arrest, FL5-Neo cells rapidly lost viability in the presence of nocodazole. By 72 hr, <10% of FL5-Neo cells were viable, and of those viable cells 15% had escaped the cell cycle arrest to give rise to cells with a greater than 4N DNA content. In contrast, cells expressing Bcl-x_L were ~75% viable after 72 hr of nocodazole treatment and 40% of those cells had a

Table 1. *Spontaneous tetraploidization in cells expressing Bcl-x_L*

Cell type	Number of clones analyzed	Number tetraploid	Percent tetraploid
FL5-Neo	48	2	4.2
FL5-Bcl-x_L	76	23	30.2[a]

FL5.12 cells were transfected with either a Bcl-x_L expression vector (FL5 Bcl-x_L) or an empty Neo control vector (FL5-Neo). After selection, the bulk transfectants were cloned by limiting dilution. Clones were expanded and processed for DNA content analysis by flow cytometry.
[a] $P < 0.01$.

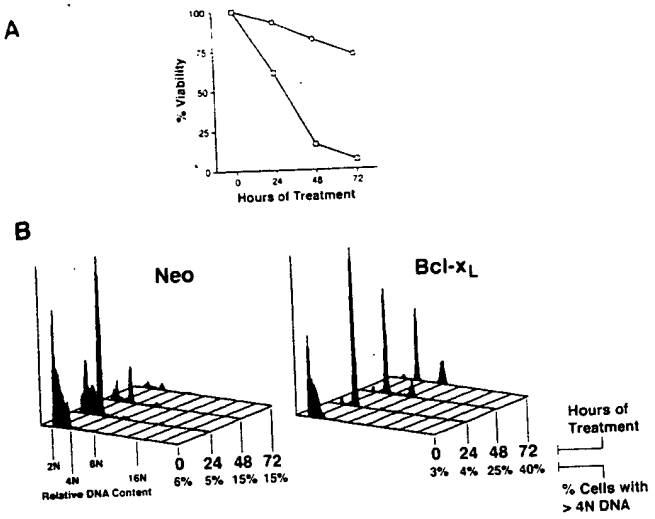

Figure 1. Bcl-x_L expression promotes the accumulation of polyploid cells after mitotic spindle damage. FL5.12 cells were stably transfected with the pSFFV-Neo expression vector with a Bcl-x_L cDNA insert (Bcl-x_L) (○) and an empty expression vector as a control (Neo) (□). Cells were treated with nocodazole for the indicated times. (*A*) At each time, cells were harvested and viability was quantitated by determining the percentage of subdiploid cells. (*B*) Cells were also processed for cell cycle analysis by flow cytometry of propidium iodide-stained cells. Shown are three-dimensional representations of overlaid DNA histograms. The x-axis corresponds to relative DNA content, as marked on the left graph. The z-axis represents hr of nocodazole treatment, as marked, and below these markings is the percentage of cells with a >4N DNA content. These data are representative of at least three independent experiments.

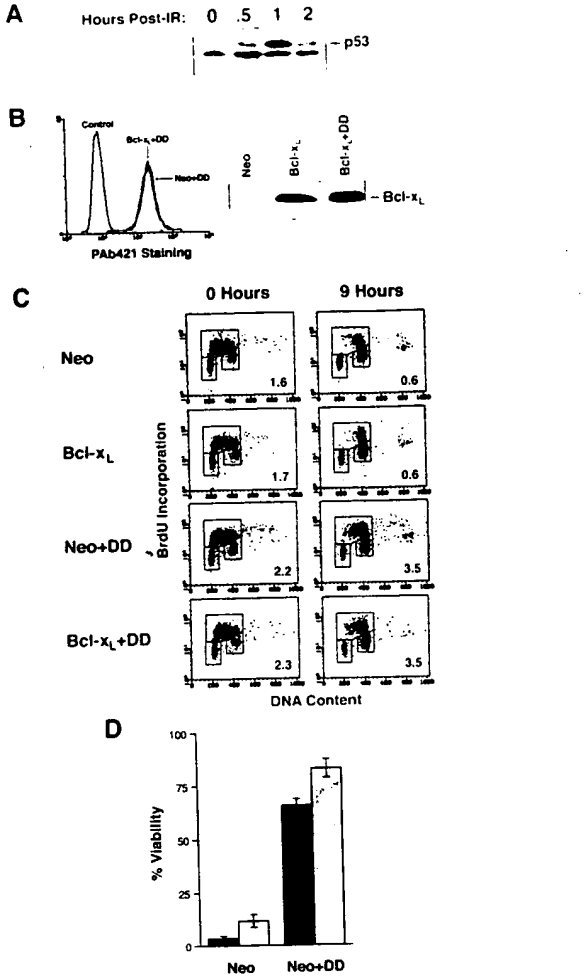

Figure 2. FL5.12 cells have functional p53 and a dominant negative p53 protein is able to abrogate both p53-dependent cell cycle arrest and p53-dependent apoptosis. (*A*) FL5-Neo cells were gamma irradiated at 5 Gy. At the indicated times postirradiation, cell lysates were made and analyzed by immunoblotting for p53. The position of p53 is indicated. The lower band seen on the blot is the result of nonspecific hybridization of the antibody. (*B*) FL5.12 cells were stably cotransfected with a Bcl-x_L expression vector and a DD expression vector (Bcl-x_L + DD) or an empty expression vector and a DD expression vector (Neo + DD). Clones were derived by limiting dilution. (*Left*) Expression levels of DD for two representative clones determined by flow cytometry of cells intracellularly stained using PAb421, an anti-p53 antibody that recognizes DD and endogenous p53. (*Right*) Immunoblot demonstrating expression levels for Bcl-x_L. (*C*) The indicated cells were gamma irradiated at 5 Gy and pulsed with BrdU at 0 and 9 hr postirradiation. Two-color cell cycle analysis using flow cytometry is presented with BrdU incorporation on the *y*-axis and propidium iodide DNA staining on the *x*-axis. Gates are drawn around the G_1, S, and G_2/M cell cycle populations. The *bottom left* gate is G_1; the *top* gate is S; and the *bottom right* gate is G_2/M. The number in the *lower right-hand* corner of each graph is the ratio of the percentage of cells in S to the percentage of cells in G_1. (*D*) The survival of FL5-Neo (Neo) and FL5-Neo + DD (Neo + DD) cells following treatment with either 1 μg/ml of etoposide (dark gray bars) or by irradiating with 5 Gy gamma radiation (light gray bars) was assayed as described in Materials and Methods. Shown is cell viability at 18 hr calculated as a percentage of an untreated control (means±standard deviations, $n = 4$).

greater than 4N DNA content. These experiments yielded similar results when done with various doses of nocodazole or vincristine (data not shown). Additionally, when nocodazole or vincristine was removed from FL5-Bcl-x_L cells at 48 and 72 hr of treatment, cells reinitiated exponential growth and the majority of the recovered cells were tetraploid. In contrast, the recovered FL5-Neo cells remained mainly diploid (data not shown).

FL5.12 Cells have functional p53

Because it has been reported previously that cells mutated or null for p53 have elevated rates of polyploidy and aneuploidy, the p53 status of FL5.12 cells was investigated. The best characterized role for p53 is in the G_1 arrest following DNA damage (Kastan et al. 1992; Kuerbitz et al. 1992). Thus, FL5-Neo and FL5-Bcl-x_L cells were irradiated with 5 Gy gamma radiation and analyzed for p53 induction and p53-dependent G_1 arrest. FL5.12 cells rapidly and transiently induced p53 protein after irradiation (Figure 2A). p53 protein levels peaked between 30 min and 2 hr and returned to basal levels shortly thereafter. When an asynchronous population of either FL5-Neo or FL5-Bcl-x_L cells was irradiated, cell cycle analysis by bromodeoxyuridine (BrdU) incorporation and DNA staining demonstrated that at 9 hr postir-

radiation both FL5-Neo and FL5-Bcl-x_L cells showed a distinct population of cells arrested in G_1 (Figure 2C). Furthermore, the ratio of the percentage of cells in S phase to the percentage of cells in G_1 phase decreased from 1.6 to 0.6 in FL5-Neo cells and from 1.7 to 0.6 in FL5-Bcl-x_L cells.

To further confirm the presence of functional p53 in FL5.12 cells, we wished to show that the G_1 arrest phenotype was p53-dependent. For this purpose, a dominant negative p53 miniprotein (DD) that comprises the last 89 amino acids of wild-type murine p53 was used (Shaulian et al. 1992). DD oligomerizes with endogenous p53 and inhibits p53 from binding to its DNA consensus site. FL5.12 cells were cotransfected with either a DD expression vector and a Bcl-x_L expression vector or a DD expression vector and a Neo control vector to create the stable cell lines FL5-Bcl-x_L + DD and FL5-Neo + DD, respectively. Clones of each cell line were screened for expression of DD by flow cytometry of cells intracellularly stained with PAb421, an anti-p53 antibody that recognizes both DD and the endogenous p53 stabilized by DD. FL5-Bcl-x_L + DD and FL5-Neo + DD clones that stained similarly with PAb421 were chosen. Additionally, the FL5-Bcl-x_L + DD clones expressed similar levels of Bcl-x_L compared with the FL5-Bcl-x_L cells. Several clones were characterized, but shown here are representative clones of FL5-Neo + DD and FL5-Bcl-x_L + DD (Figure 2B). As seen in Figure 2C, DD effectively abrogated the DNA damage-induced G_1 arrest in both Neo and Bcl-x_L backgrounds, as indicated by the increase in the S to G_1 ratio 9 hr postirradiation.

Because p53 has also been shown to mediate apoptosis in response to DNA damage, the ability of FL5.12 cells to undergo p53-dependent apoptosis after either irradiation or treatment with etoposide was examined. As seen in Figure 2D, FL5-Neo cells rapidly died after either etoposide treatment or irradiation. Stable transfection of the DD minigene was able to inhibit cell death under these conditions. Thus, the p53 expressed by FL5.12 cells is capable of inducing G_1 cell cycle arrest and promoting apoptosis in response to DNA damage.

p53 is induced in cells after mitotic spindle damage

Knowing that FL5.12 cells express functional p53 and that p53 has been implicated in G_2/M checkpoint controls, we determined whether p53 was induced after treatment with nocodazole. FL5-Bcl-x_L cells were treated with nocodazole for 72 hr, and p53 expression was analyzed by immunoblotting (Figure 3A). p53 was induced and peaked between 8 and 48 hr of treatment. By 72 hr, p53 levels declined despite the continuous presence of nocodazole. p53 induction was similar in FL5-Neo cells (data not shown).

As a test for p53 function after nocodazole treatment, FL5-Bcl-x_L cells were transfected with a CAT reporter construct that contained p53-specific DNA binding sites upstream of the promoter. Figure 3B demonstrates that p53 transactivated the reporter, and that this transactivation was induced more than threefold by nocodazole

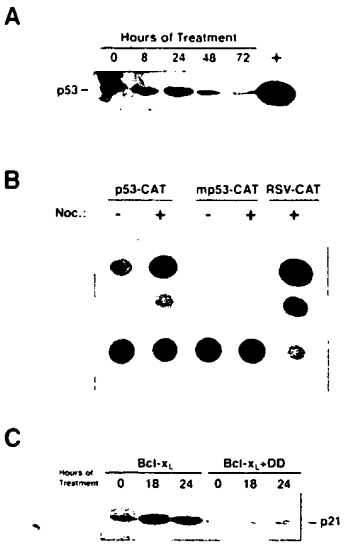

Figure 3. p53 is induced and able to transactivate gene expression after mitotic spindle damage. (*A*) FL5-Bcl-x_L cells were cultured with nocodazole for the indicated times. At each time, cell lysates were made and analyzed by immunoblotting for p53. (+) Positive control lane for p53. (*B*) FL5-Bcl-x_L cells were transfected with CAT reporter constructs and either left in media alone (−) or treated with nocodazole (Noc.) 6 hr after transfection (+). Cells were harvested for CAT assay at 48 hr posttransfection. Reporter constructs consisted of a basal promoter and the CAT gene either downstream of p53-specific DNA binding sites (p53–CAT), mutant p53 DNA binding sites (mp53–CAT), or the RSV LTR (RSV–CAT). Equal transfection efficiencies of p53–CAT and mp53–CAT transfected cells were determined by CD20 surface staining after cotransfection with a CD20 reporter construct. These data are representative of two independent experiments. (*C*) FL5-Bcl-x_L cells and FL5-Bcl-x_L + DD cells were treated with nocodazole for the indicated times. At each time, cell lysates were made and analyzed by immunoblotting for $p21^{Waf1/Cip1}$.

treatment. Little to no reporter activity was detected in cells transfected with a CAT reporter construct containing mutated p53 DNA binding sites. In addition, $p21^{Waf1/Cip1}$, a direct transcriptional target for p53, was also induced at the protein level by nocodazole treatment (Fig. 3C). Induction of $p21^{Waf1/Cip1}$ after nocodazole treatment is dependent on p53, as no induction was seen in cells transfected with DD.

Abrogation of p53 function and expression of Bcl-x_L cooperatively allow cells with mitotic spindle damage to continue cell cycle progression

The induction of p53 expression after nocodazole treatment suggests that p53 may function in a checkpoint control that prevents cell cycle progression and/or causes apoptosis in cells with a disrupted mitotic spindle. To test this, FL5-Neo + DD and FL5-Neo cells were treated with nocodazole, and cell viabilities and DNA histograms were determined over the course of 72 hr. Expression of DD had only a marginal effect on nocodazole-induced cell death because both FL5-Neo and FL5-

Neo + DD cells died at similar rates over a treatment course of 3 days (Figure 4A).

Despite marginal differences in viability, DD-expressing cells displayed a dramatically different cell cycle profile compared with FL5-Neo cells. In contrast to FL5-Neo cells, which predominantly remained arrested with a 4N DNA content after 72 hr of nocodazole exposure, FL5-Neo + DD cells continued progressing through the cell cycle despite the presence of mitotic spindle damage (Figure 4B). Between 24 and 48 hr, the majority of surviving FL5-Neo + DD cells had a DNA content between 4N and 8N, and at 72 hr, a significant fraction had a >8N DNA content. At the end of 72 hr, 68% of the surviving FL5-Neo + DD cells had a >4N DNA content compared with only 19% of the FL5-Neo cells. These data demonstrate that p53 is a necessary component of a checkpoint control that keeps cells with mitotic spindle damage from reinitiating DNA synthesis.

Because Bcl-x_L expression is able to enhance the accumulation of polyploid cells after mitotic spindle damage despite the induction of functional p53, and because introduction of DD only slightly influences viability after mitotic spindle damage, these results predict that after mitotic spindle damage the loss of p53 and the expression of Bcl-x_L might work in at least an additive fashion to further increase the percentage of cells with a >4N DNA content. To test this, FL5-Bcl-x_L + DD cells were also treated with nocodazole. Figure 4A shows that the viabilities of FL5-Bcl-x_L and FL5-Bcl-x_L + DD cells were similar. Both cell types were >75% viable after 72 hr of nocodazole exposure. However, whereas Bcl-x_L expression alone permitted a gradual increase in 8N cells during the 72-hr time course, Bcl-x_L expression combined with DD allowed rapid accumulation of 8N and then 16N cells. By 72 hr, 86% of FL5-Bcl-x_L + DD cells had a >4N DNA content, and of these cells, most had a >8N DNA content. In contrast, only 52% of FL5-Bcl-x_L cells had a >4N DNA content and few cells had a >8N DNA content. When compared with cells that express DD alone, the introduction of Bcl-x_L into DD-expressing cells enhanced cell viability and the percentage of cells that continued cell cycle progression after mitotic spindle damage (Figures 4A and 4B). The increase in the percentage of cells with a >4N DNA content was not a result of a higher level of DD in FL5-Bcl-x_L + DD cells compared with FL5-Neo + DD cells (Figure 2B). Thus, these data demonstrate that in cells with mitotic spindle damage, the inhibition of p53 function and the prevention of apoptosis through Bcl-x_L expression cooperate to overcome a checkpoint induced by mitotic spindle damage.

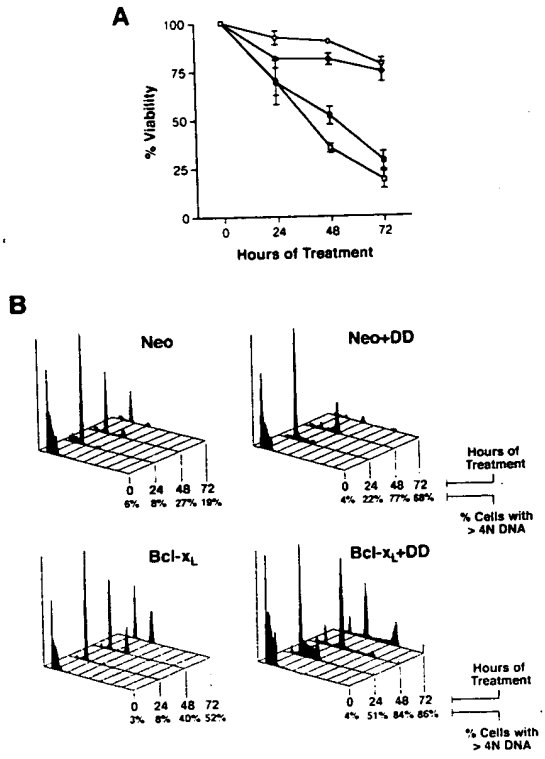

Figure 4. Expression of Bcl-x_L and abrogation of p53 function cooperatively allow accumulation and cell cycle progression of polyploid cells after mitotic spindle damage. (*A*) The indicated cells were treated with nocodazole for 72 hr. Every 24 hr, cell viability was determined by propidium iodide exclusion (means ±S.D., $n = 6$). (○) Bcl-x_L; (●) Bcl-x_L + DD; (□) Neo; (■) Neo + DD. (*B*) The indicated cells were treated with nocodazole for 72 hr. Every 24 hr, cells were harvested and processed for cell cycle analysis by flow cytometry of propidium iodide-stained cells as described in the legend for Fig. 1. These data are representative of at least three independent experiments.

Enforcing p53 levels in Bcl-x_L-expressing cells inhibits cell cycle progression after mitotic spindle damage

It has been demonstrated in many systems that blocking cell death with antiapoptosis genes does not prevent growth arrest (Hockenbery 1995). Therefore, we were interested in understanding why expression of an antiapoptosis gene like *bcl-x_L* resulted in the accumulation of polyploid cells in response to mitotic spindle damage.

The kinetics of p53 expression after nocodazole treatment indicated that p53 levels did not remain elevated during the entire 72 hr of treatment (Figure 3A). The 48 hr time point at which p53 levels began declining coincided with the time at which 4N cells began to accumulate in FL5-Bcl-x_L cultures (Figs. 1 and 4B). This suggests that a potential mechanism by which Bcl-x_L influences the ability of cells to remain arrested is by allowing cells to survive to a point after which p53 is downregulated, perhaps because of adaptation of the checkpoint pathway. Cells that are no longer able to maintain p53 normally would die, but when apoptosis is prevented by Bcl-x_L, these cells proceed to replicate their DNA. As a test of this model, we cotransfected FL5.12 cells with *bcl-x_L* and a temperature-sensitive *p53* (*tsp53*). For this mutant, incubation at the permissive temperature of 32°C leads to high-level expression of p53 in a wild-type conformation, resulting in G_1 arrest (Figure 5, cf. FL5-Bcl-x_L and FL5-Bcl-x_L + tsp53). To determine if maintaining high levels of wild-type p53 in cells expressing Bcl-x_L could inhibit cell cycle progression after mitotic

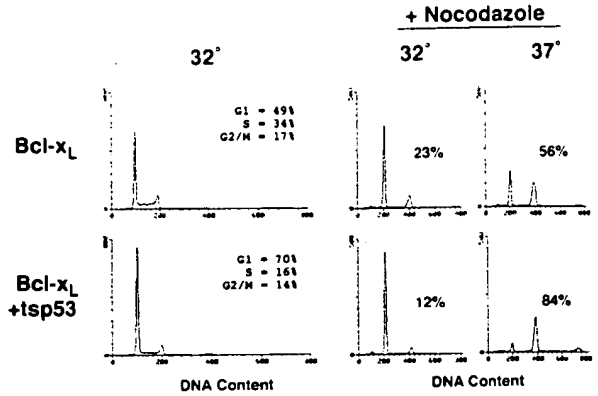

Figure 5. Enforced p53 expression inhibits the ability of Bcl-x_L to promote polyploidy after mitotic spindle damage. FL5.12 cells, stably cotransfected with *bcl-x_L* and a temperature-sensitive *p53* (*bcl-x_L* + *tsp53*) or transfected with *bcl-x_L* alone (*bcl-x_L*), were either treated with nocodazole for 72 hr or left untreated for 48 hr. One set of duplicate samples were maintained at 37°C and the other set was maintained at 32°C. Cells were then harvested for propidium iodide staining, followed by flow cytometry. The percentage of cells in G_1, S, and G_2/M is indicated in the *upper right* of the DNA histograms from the untreated samples. The percentage of cells with a >4N DNA content are shown for each histogram of the treated samples. These data are representative of three independent experiments performed with two different clones.

spindle damage, FL5-Bcl-x_L + tsp53 cells were treated with nocodazole and shifted to 32°C. As seen in Figure 5, enforced expression of a wild-type form of p53 in FL5-Bcl-x_L + tsp53 cells inhibited cell cycle progression after 72 hr of nocodazole treatment compared with FL5-Bcl-x_L cells. At the restrictive temperature of 37°C, the tsp53 is in a mutant conformation and acts as a dominant negative. Therefore, when compared with cells expressing Bcl-x_L alone, FL5-Bcl-x_L + tsp53 cells at 37°C had an increased percentage of cells with a >4N DNA content after nocodazole treatment, consistent with the data obtained from the DD transfectants. Thus, maintaining high p53 levels at later time points of nocodazole treatment is sufficient to antagonize the ability of Bcl-x_L to promote the accumulation of polyploid cells.

Mitotic spindle damage induces a transient M phase arrest that is not affected by either p53 or Bcl-x_L

The fact that the checkpoint control that is active after mitotic spindle damage is p53 dependent and arrests cells with a 4N DNA content suggests that p53 may be working to arrest cells in mitosis. To determine whether nocodazole-treated cells display a prolonged M-phase arrest, we analyzed three well-characterized M-phase markers: Cyclin B1 expression, MPM-2 expression, and the presence of condensed mitotic chromosomes. FL5-Neo and FL5-Bcl-x_L cells treated with nocodazole demonstrated high levels of Cyclin B1 expression at 8 hr, consistent with an accumulation of cells in M phase (Figure 6A). However, Cyclin B1 levels declined to near interphase levels by 24 hr, demonstrating that the majority of the cells did not remain arrested in mitosis. A Cdc2 immunoblot showed that Cdc2 did not undergo a similar decline in expression, arguing against a general decrease in protein synthesis.

MPM-2 is an epitope whose expression is restricted to M phase (Davis et al. 1983). Flow cytometry on nocodazole-treated cells intracellularly stained for MPM-2 was used to follow the percentage of cells that were in M phase at various times during nocodazole treatment. The left panels of Figure 6B show that at 12 hr, nearly 50% of the FL5-Neo cells were positive for MPM-2, demonstrating that an M-phase arrest did occur; however, the percentage of MPM-2 positive cells began to decline thereafter. By 24 hr of nocodazole treatment, the percentage of cells that were MPM-2 positive was only threefold higher than interphase levels. Thus, the decrease in MPM-2 reactive cells at 24 hr (and at later time points; data not shown), despite evidence of a prolonged p53-dependent cell cycle arrest by DNA staining, suggests

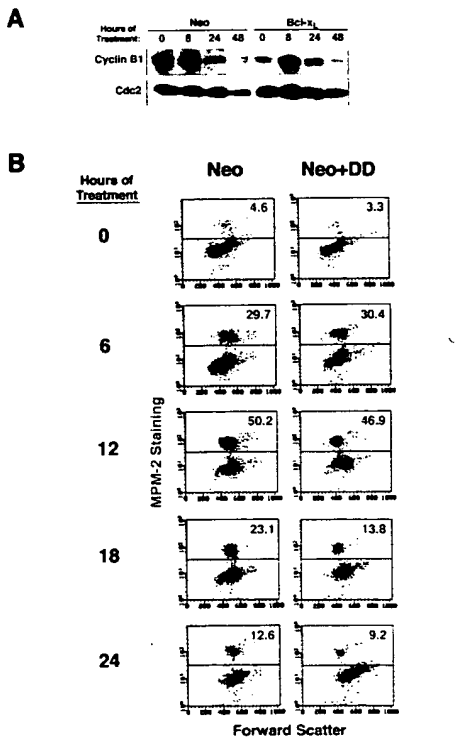

Figure 6. Mitotic spindle damage causes a transient arrest in mitosis as determined by the expression of mitotic proteins. FL5-Neo and FL5-Bcl-x_L cells were treated with nocodazole for the indicated times. (*A*) Cell lysates were made and analyzed by immunoblotting for Cyclin B1 and Cdc2. (*B*) FL5-Neo cells and FL5-Neo + DD cells were analyzed for the percentage of cells in mitosis by flow cytometry of MPM-2 stained cells. Results are plotted with MPM-2 fluorescence on the y-axis and forward scatter on the x-axis. The percentage of cells that are MPM-2 positive is indicated in the *upper right-hand* corner. For the 24 hr time point, a box is drawn that indicates the population of cells that demonstrate an increase in forward scatter. This population comprises 6.4% of the total FL5-Neo population and 22.7% of the total FL5-Neo + DD population. These data are representative of three independent experiments.

that p53 does not cause an extended arrest in mitosis. Consistent with this interpretation, a similar analysis on FL5-Neo + DD cells showed that the kinetics of MPM-2 reactivity was nearly identical to FL5-Neo cells (right panels of Fig. 6B). However, one notable difference is that at 24 hr the FL5-Neo + DD cells contained a large population that was MPM-2 negative and had an increase in cell size as indicated by an increase in forward light scatter (this population is boxed in Fig. 6B). This population likely reflects the failure of FL5-Neo + DD cells to undergo a p53-dependent cell cycle arrest that occurs after a transient M-phase arrest.

To confirm that MPM-2 staining accurately represents mitotic cells, nocodazole-treated cells were stained with both an anti-MPM-2 antibody and DAPI. Confocal microscopy demonstrated that in both FL5-Neo and FL5-Bcl-x_L cells, approximately half of the cells accumulated MPM-2 fluorescence at 16 hr of nocodazole treatment, which is consistent with the flow cytometry analysis (data not shown). These cells all exhibited condensed mitotic chromosomes, and almost all cells that were MPM-2 negative exhibited decondensed chromatin, demonstrating that MPM-2 reactivity and the presence of condensed mitotic chromosomes are nearly always coincidental. In FL5-Neo cells, condensed apoptotic nuclei were also seen. By 24 hr of nocodazole treatment, FL5-Bcl-x_L cells and FL5-Neo cells predominantly exhibited interphase chromatin and were negative for MPM-2.

In response to mitotic spindle damage p53 is not induced in mitosis but during a subsequent growth phase where it mediates cell cycle arrest

Thus far, we have shown that p53 is induced after mitotic spindle damage and its function is important in keeping the damaged cells arrested with a 4N DNA content. However, it would seem that the cells arrested with a 4N DNA content are not necessarily arrested in mitosis. Arrest in mitosis is short and uninfluenced by p53. This suggests that the induction of p53 might occur after cells are released from M-phase arrest. For this reason, nocodazole-treated cells were intracellularly stained with antibodies against both p53 and MPM-2 to test directly whether mitotic cells expressed the induced p53 protein. Figure 7A shows that p53 and MPM-2 staining were mutually exclusive. At 12 hr, MPM-2 staining peaked at 45%, just when p53 staining became detectable. Between 12 and 24 hr, there was a ~37% decrease in MPM-2 positive cells, in contrast to the 27% gain in p53 positive cells. The loss in the percentage of MPM-2 positive cells seen from 12 to 24 hr can be approximately accounted for by the gain in the percentage of p53 positive cells. At no time during the analysis was there a significant percentage of cells expressing both proteins. These data suggest that in response to mitotic spindle damage, p53 is induced after a transient mitotic arrest.

Because the nocodazole-induced M-phase arrest is transient and does not involve p53, we were interested in knowing the cell cycle phase that cells proceed to after M-phase arrest. Based on kinetics, this cell cycle phase is

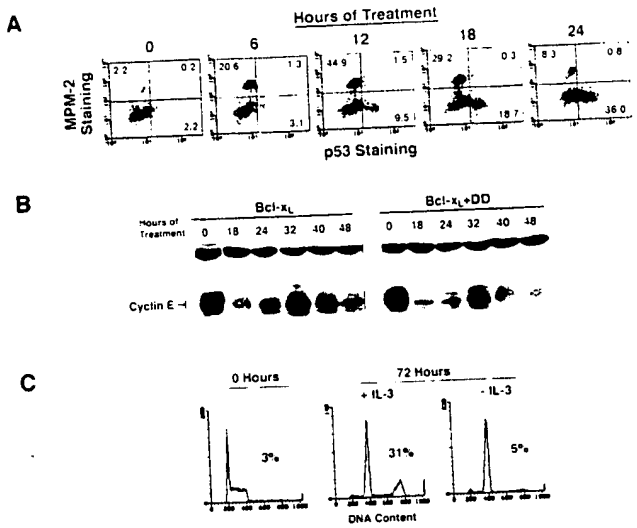

Figure 7. p53 induced after mitotic spindle damage is not expressed in cells arrested in mitosis but instead expressed in a subsequent G_1-like phase. FL5-Bcl-x_L cells were treated with nocodazole for the indicated times. (*A*) These cells were intracellularly stained for both MPM-2 and p53 expression and were analyzed by flow cytometry. MPM-2 fluorescence is on the y-axis and p53 fluorescence is on the x-axis. Quadrants are shown and the percentage of cells in the single-positive populations and the double-positive population is given. (*B*) FL5-Bcl-x_L cells and FL5-Bcl-x_L + DD cells were treated with nocodazole for the indicated times. At each time point, cell lysates were made and analyzed by immunoblotting for Cyclin E. The band at the top of the gel is nonspecific and serves as a loading control. (*C*) At 9 hr after addition of nocodazole, IL-3 was removed from the medium by washing and resuspending the cells in IL-3-free medium containing nocodazole. After 72 hr, cells were harvested and processed for cell cycle analysis by flow cytometry of propidium iodide-stained cells. The percentage of cells with a >4N DNA content is shown. No major differences in cell survival of FL5-Bcl-x_L cells treated in the presence or absence of IL-3 were observed. These data are representative of two independent experiments.

presumably where p53 is induced and mediates cell cycle arrest. The most likely situation is that the transiently arrested cells reset to G_1. To test this, the expression pattern of Cyclin E, a late G_1 cyclin, during nocodazole treatment of FL5-Bcl-x_L cells and FL5-Bcl-x_L + DD cells was analyzed. As seen in Figure 7B, in both FL5-Bcl-x_L cells and FL5-Bcl-x_L + DD cells, nocodazole treatment caused an initial decrease in Cyclin E expression as cells transiently arrested in M phase. However, in both populations of cells, Cyclin E began to reaccumulate after 24 hr of nocodazole treatment. In FL5-Bcl-x_L cells, once Cyclin E reaccumulated its expression was maintained for the rest of the culture period. In contrast, in FL5-Bcl-x_L + DD cells, once reaccumulated, Cyclin E again declined as cells began to resynthesize DNA. These data suggest that cells with mitotic spindle damage undergo a p53-dependent arrest in a state similar to late G_1.

As an independent confirmation that cells with mitotic spindle damage reset to G_1, we took advantage of

the fact that FL5.12 cells are dependent on IL-3 for G_1 cell cycle progression. As seen in Figure 7C, when IL-3 was removed from the media at 9 hr of nocodazole treatment FL5-Bcl-x_L cells did not go on to replicate their DNA. Because IL-3 is necessary for the cells to pass the G_1 restriction point, its requirement for generating cells with a >4N DNA content after mitotic spindle damage further supports that passage through a growth factor-dependent G_1-like phase occurs after the transient mitotic arrest.

Discussion

In this study, we show that mitotic spindle damage activates a checkpoint control that prevents DNA replication of damaged cells by causing p53-dependent cell cycle arrest and p53-independent apoptosis. If cells are prevented from undergoing apoptosis by expression of Bcl-x_L, we find that this promotes the accumulation of polyploid cells. Bcl-x_L does not seem to override the checkpoint induced by mitotic spindle damage but rather allows cells to survive until the p53-dependent arrest pathway either becomes exhausted or undergoes adaptation. Once the p53-dependent checkpoint decays, Bcl-x_L-protected cells replicate their DNA, despite having failed to properly execute the previous M phase. When p53 expression is enforced, resulting in continuously high levels of p53, DNA replication is inhibited. Further evidence that apoptosis is an important mechanism used to prevent polyploidy is the observation that cells that overexpress Bcl-x_L have higher rates of spontaneous tetraploidization.

The finding that p53 is a component of a checkpoint following mitotic spindle damage is consistent with previous reports (Cross et al. 1995). We find that p53 functions to keep cells with spindle damage arrested with a 4N DNA content. The introduction of DD, a dominant negative p53 miniprotein, abrogates the cell cycle arrest observed following mitotic spindle damage. These cells go on to become 8N and then 16N during the 72 hr of nocodazole treatment. During the 72 hr time course, 16N cells are not seen in cells that overexpress Bcl-x_L alone, emphasizing the differences in the way DD and Bcl-x_L function. With Bcl-x_L, cells are rescued from apoptosis and survive long enough to escape cell cycle arrest; however, these cells likely stop at the same checkpoint in the next cell cycle. In contrast, cells with DD lack the p53-mediated arrest altogether and are able to proceed through multiple rounds of DNA replication. However, these cells still lose viability at a rate comparable to wild-type cells.

The inability of DD to prevent apoptosis after mitotic spindle damage suggests that FL5.12 cells undergo cell death via p53-independent mechanisms. DD is able to inactivate p53-mediated apoptosis as demonstrated by experiments analyzing cell death after irradiation and etoposide treatment. Nevertheless, because we have used Bcl-x_L overexpression to prevent apoptosis in our studies and Bcl-x_L overexpression can inhibit both p53-dependent and p53-independent apoptosis, we cannot exclude an additional role for p53-dependent apoptosis in preventing the development of polyploid cells following mitotic spindle damage.

Many reports have suggested that arrest and apoptosis are downstream effects dependent on p53 and important in endowing p53 with tumor-suppressing properties (Cox and Lane 1995; Haffner and Oren 1995). Under circumstances where p53 mediates cell death, cooperation between loss of p53 and overexpression of antiapoptosis genes would not be expected. However, our data suggest that under circumstances where damaged cells undergo p53-independent cell death and p53-dependent cell cycle arrest, the expression of antiapoptosis genes can cooperate with the loss of p53 to enhance the accumulation of genetically damaged cells. Following mitotic spindle damage, p53-dependent growth arrest and p53-independent apoptosis can form a partly redundant checkpoint control system to abort genetically aberrant cells. Cells suffering mitotic spindle damage that are blocked from apoptosis can still cease or dramatically slow proliferation as a result of the arrest pathway. Conversely, cells suffering mitotic spindle damage that are prevented from undergoing growth arrest can still die as a result of the cell death pathway. Elimination of both pathways can cooperatively enhance the ability of cells with mitotic spindle damage to accumulate and progress through the cell cycle.

Recent data have suggested that p53 has a role in G_2 and/or M phase of the cell cycle. p53-null fibroblasts rapidly become polyploid and aneuploid during cell passage (Harvey et al. 1993) or after treatment with a mitotic spindle poison (Cross et al. 1995). Erythroid cell lines from p53 knockout mice are stably diploid but are susceptible to polyploidization (Metz et al. 1995). p53 has been shown to be phosphorylated by G_2/M cyclins, resulting in altered DNA binding specificity (Wang and Prives 1995). p53 expression from an inducible promoter is able to arrest cells in G_2/M (Agarwal et al. 1995). However, despite these observations that seem to support a role for p53 in G_2/M, we fail to observe any evidence for such a role for p53 after mitotic spindle damage.

Our data suggest that in murine cells, M phase-specific checkpoint controls that monitor mitotic spindles, as suggested by studies in yeast (Hoyt et al. 1991; Li and Murray 1991) and *Xenopus* (Minshull et al. 1994) and checkpoints that monitor kinetochores (Li and Nicklas 1995; Rieder et al. 1995) may only lead to a transient mitotic arrest. These data are consistent with previous findings (Kung et al. 1990). However, in addition, we show that this transient M-phase arrest does not involve p53. Rather, after the transient M-phase arrest, cells default to what appears to be a G_1-like phase in which the cells are MPM-2 negative, low in Cyclin B1, high in Cyclin E, and have interphase chromatin. It is at this point that p53 is induced and mediates growth arrest. After mitotic spindle damage, p53 may function in a pathway that senses the consequences of an abortive mitosis. An abortive mitosis may induce p53 due to DNA damage or topological structures caused by the failure to properly segregate sister chromatids. Alternatively, because p53

has been shown to influence centrosome duplication (Fukasawa et al. 1996), the presence of more than one centrosome in a G_1 cell due to mitotic failure may also lead to p53 induction. Thus, true mitotic checkpoints can function to monitor events within M phase to assure proper anaphase, whereas p53 can function subsequently to prevent cells that have failed M phase from reinitiating DNA replication. Figure 8 presents a model that summarizes our findings.

The disruption of genes involved in cell cycle checkpoint controls has long been recognized as one way cells can accumulate karyotypic abnormalities. However, checkpoint controls that simply lead to growth arrest may not be enough to ensure faithful cell division. Our data demonstrate that cell death pathways can also play an important role in preventing the accumulation of genetically abnormal cells. One reason for this may be that in the presence of constant stimuli, checkpoint pathways, like other signal transduction pathways, can undergo adaptation and lose activity (Sandell and Zakian 1993). Apoptosis may provide a mechanism to abort cells before adaptation occurs.

Materials and methods

Cell culture and cell transfections

The murine prolymphocytic IL-3-dependent cell line, FL5.12 was maintained as described previously (Boise et al. 1993). To create FL5-Bcl-x_L or FL5-Neo cell lines, transfection with either pSFFV-Bcl-x_L or pSFFV-Neo (Boise et al. 1993) was performed using 10 μg of plasmid, electroporated into 1×10^7 cells at 960 μF and 250 V. Neomycin-resistant cells were selected with 1 mg/ml G418. Single cell clones from the bulk transfection were derived by limiting dilution cloning. Clones were screened for Bcl-x_L expression by immunoblotting with 2A1, a mouse monoclonal antibody to Bcl-x_L (see below). To create FL5-Neo + DD, FL5-Bcl-x_L + DD, or FL5-Bcl-x_L + tsp53 cell lines, FL5.12 cells were cotransfected with either pCMVDD (Shaulian et al. 1992) or pLTRp53cGval135 (Yin et al. 1992) and either pSFFV-Bcl-x_L or pSFFV-Neo. Clones containing DD were screened by flow cytometry of cells intracellularly stained with PAb421, and clones containing tsp53 were screened by immunoblotting with PAb240. Several clones from all cell lines were used in experiments and were found to give similar results.

For drug treatments, cells were resuspended in medium without G418 at a concentration of 5×10^5 cells/ml, along with nocodazole (Sigma). Various doses of nocodazole were tested from 0.01 to 0.6 μg/ml; however, 0.1 μg/ml was generally chosen for most experiments. Cell death of FL5-Neo and FL5-Neo + DD cells in response to etoposide and irradiation was determined essentially as described previously (Canman et al. 1995). In brief, cells were washed three times and resuspended in medium without IL-3. Cells were then either irradiated with 5 Gy gamma radiation or treated with 1 μg/ml etoposide. Viability was determined at 18 hr as a percentage of an untreated control.

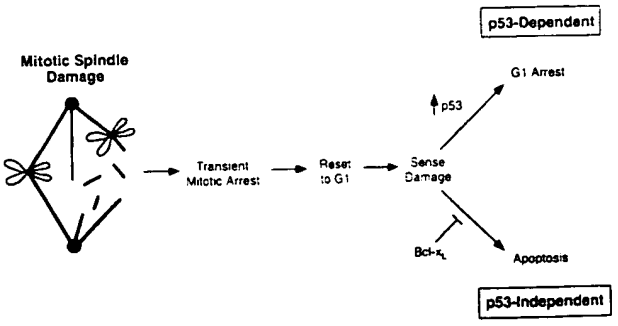

Figure 8. Proposed model for the cellular response to mitotic spindle damage. See text for details.

Cell viability and cell cycle analysis

Cell viability was determined by propidium iodide exclusion, as described previously (Minn et al. 1995). The percent viability was calculated as a percentage of either the viability at 0 hr or the viability of an untreated control. Cell cycle analysis by DNA staining alone was assayed by staining fixed cells with 0.01 mg/ml of propidium iodide. Cells were assayed by flow cytometry and the analysis was gated to exclude subdiploid cells and cell doublets. For cell cycle statistics, data was quantitated with CellFit software (Becton Dickinson) using the RFIT analysis mode. For cell cycle analysis by DNA staining and BrdU incorporation, 1×10^6 cells were pulsed for 30 min with 25 μM of BrdU (Boehringer Mannheim), harvested, and fixed with ethanol. Fixed cells were then washed and incubated in 1 ml of 2.5 M HCl + 0.1% Triton X-100 in PBS for 25 min at room temperature and then washed twice with 4 ml of neutralization/wash solution (0.5% Tween-20 in PBS). The cells were resuspended in 100 μl of antibody staining solution (50% fetal calf serum + 0.01% sodium azide in PBS) along with 4 μl of FITC-conjugated anti-BrdU antibody (Boehringer Mannheim) and incubated at room temperature in the dark for 30 min. Cells were washed twice with PBS and resuspended in 0.5 ml of PBS. Ten micrograms of propidium iodide were added. Samples were then analyzed by flow cytometry.

Immunoblotting

Protein lysates were made by lysing cells in RIPA (150 mM NaCl, 1% NP-40, 0.5% DOC, 0.1% SDS, and 50 mM Tris at pH 7.5) supplemented with 8 μg/ml aprotinin, 2 μg/ml leupeptin, and 170 μg/ml PMSF. Western blots were prepared as described previously (Minn et al. 1995) and blocked with blotto (5% nonfat milk and 0.05–0.2% Tween-20) for 1 hr at room temperature. The blot was then probed with either a 1:10000 dilution of 2A1 (mouse monoclonal anti-Bcl-x_L antibody) (Boise et al. 1995), 1 μg/ml of PAb240 (mouse monoclonal anti-p53 antibody, Santa Cruz), 1 μg/ml of a mouse monoclonal anti-Cyclin B1 antibody (Pharmingen), 1 μg/ml of a mouse monoclonal anti-Cdc2 antibody (#sc-54, Santa Cruz), 0.5 μg/ml of a rabbit polyclonal anti-p21 antibody (#sc-397, Santa Cruz), or 0.5 μg/ml of a rabbit polyclonal anti-Cyclin E antibody (#sc-481, Santa Cruz) for 1 hr at room temperature in blotto. The blot was washed and developed with the ECL system (Amersham).

Intracellular staining for flow cytometry

For intracellular staining, 1×10^6 cells were fixed with 1% paraformaldehyde in PBS for 10 min at room temperature. Cells were then washed in wash solution (0.03% saponin in PBS) and resuspended in 100 μl of staining solution (0.3% saponin and 20% goat serum in PBS) along with 1 μg of PAb421 (Oncogene Science) and/or 0.5 μl of a mouse monoclonal anti-MPM-2 antibody (Upstate Biotechnology) for 30 min at 4°C. Cells were then washed twice with wash solution and resuspended in 100 μl of staining solution without goat serum. For p53 staining or

MPM-2 staining alone, a 1:50 dilution of a FITC-conjugated anti-mouse IgG antibody (Sigma) was used. For p53 and MPM-2 double-staining, a 1:50 dilution of each of a FITC-conjugated anti-mouse IgG2a (Caltag) and a PE-conjugated anti-mouse IgG1 (Caltag) was used. Staining using the secondary antibodies was done for 30 min at 4°C. Cells were then washed twice with wash solution and resuspended in FACS buffer (0.1% sodium azide and 1% BSA in PBS). Cells were then analyzed by flow cytometry.

Chloramphenicol acetyltransferase assay

For CAT assays, cells were grown to 5×10^5 cell/ml and 1×10^7 cells were electroporated with 10 μg of either pPG_{13}-CAT (containing p53 DNA binding sites) or pMG_{15}-CAT (containing mutated p53 DNA binding sites) (Kern et al. 1992) along with 10 μg of pCMVCD20 (Van den Heuvel and Harlow 1993). After 6 hr, 0.1 μg/ml of nocodazole was added to two-thirds of the cells. At 48 hr, cells were stained for CD20 expression using a FITC-conjugated anti-CD20 antibody (Becton Dickinson) and analyzed by flow cytometry for equal transfection efficiencies. Cells were also harvested at 48 hr, washed with PBS, and resuspended in 100 μl of 0.25 M Tris (pH 7.8). Cells were lysed by three rounds of freezeing and thawing, and cellular debris was cleared by centrifugation at 14,000g for 5 min at 4°C. Protein concentration was quantitated by Bradford protein assay (Bio-Rad). Seventy micrograms of acetyl CoA and 1 μCi of ^{14}C-chloramphenicol were added to 50 μg of protein in 140 μl of 1M Tris (pH 7.8). The sample was then incubated for 2 hr at 37°C. After ethyl acetate extraction, the organic layer was lyophilized for 15 min, resuspended in 30 μl of ethyl acetate, and spotted on a thin-layer chromatography plate. After separation, the plate was air-dried and exposed to film.

Acknowledgments

The authors would like to thank Drs. Moshe Oren and Ed Harlow for their generous donation of plasmids; Drs. Steve Kron, Nissam Hay, and Tim McKeithan for thoughtful discussions and review of the manuscript; and Therese Conway for editorial assistance. This work was supported in part by research grant PO1 AI35294 from the National Institutes of Health. L.H.B. was supported by a fellowship from the Leukemia Society of America.

The publication costs of this article were defrayed in part by payment of page charges. This article must therefore be hereby marked "advertisement" in accordance with 18 USC section 1734 solely to indicate this fact.

References

Agarwal, M.L., A. Agarwal, W.R. Taylor, and G.R. Stark. 1995. p53 controls both the G2/M and the G1 cell cycle checkpoints and mediates reversible growth arrest in human fibroblasts. *Proc. Natl. Acad. Sci.* **92:** 8493–8497.

Boise, L.H., M. Gonzalez-Garcia, C.E. Postema, L. Ding, T. Lindsten, L.A. Turka, X. Mao, G. Nunez, and C.B. Thompson. 1993. *bcl-x*, a *bcl-2*-related gene that functions as a dominant regulator of apoptotic cell death. *Cell* **74:** 597–608.

Boise, L.H., A.J. Minn, P.J. Noel, C.H. June, M.A. Accavitti, T. Lindsten, and C.B. Thompson. 1995. CD28 costimulation can promote T cell survival by enhancing the expression of Bcl-x_L. *Immunity* **3:** 87–98.

Canman, C.E., T.M. Gilmer, S.B. Coutts, and M.B. Kastan. 1995. Growth factor modulation of p53-mediated growth arrest versus apoptosis. *Genes & Dev.* **9:** 600–611.

Clarke, A.R., C.A. Purdie, D.J. Harrison, R.G. Morris, C.C. Bird, M.L. Hooper, and A.H. Wyllie. 1993. Thymocyte apoptosis induced by p53-dependent and independent pathways. *Nature* **362:** 849–852.

Cox, L.S. and D.P. Lane. 1995. Tumour suppressors, kinases and clamps: How p53 regulates the cell cycle in response to DNA damage. *Bioessays* **17:** 501–508.

Cross, S.M., C.A. Sanchez, C.A. Morgan, M.K. Schimke, S. Ramel, R.L. Idzerda, W.H. Raskind, and B.J. Reid. 1995. A p53-dependent mouse spindle checkpoint. *Science* **267:** 1353–1356.

Davis, F.M., T.Y. Tsao, S.K. Fowler, and P.N. Rao. 1983. Monoclonal antibodies to mitotic cells. *Proc. Natl. Acad. Sci.* **80:** 2926–2930.

Deng, C., P. Zhang, J.W. Harper, S.J. Elledge, and P. Leder. 1995. Mice lacking p21CIP1/WAF1 undergo normal development, but are defective in G1 checkpoint control. *Cell* **82:** 675–684.

Dole, M., G. Nunez, A.K. Merchant, J. Maybaum, C.K. Rode, C.A. Bloch, and V.P. Castle. 1994. Bcl-2 inhibits chemotherapy-induced apoptosis in neuroblastoma. *Cancer Res.* **54:** 3253–3259.

Dole, M.G., R. Jasty, M.J. Cooper, C.B. Thompson, G. Nunez, and V.P. Castle. 1995. Bcl-x_L is expressed in neuroblastoma cells and modulates chemotherapy-induced apoptosis. *Cancer Res.* **55:** 2576–2582.

El-Deiry, W.S., T. Tokino, V.E. Velculescu, D.B. Levy, R. Parsons, J.M. Trent, D. Lin, W.E. Mercer, K.W. Kinzler, and B. Vogelstein. 1993. *WAF1*, a potential mediator of p53 tumor suppression. *Cell* **75:** 817–825.

Evan, G.I., L. Brown, M. Whyte, and E. Harrington. 1995. Apoptosis and the cell cycle. *Curr. Opin. Cell Biol.* **7:** 825–834.

Fisher, D.E. 1994. Apoptosis in cancer therapy: Crossing the threshold. *Cell* **78:** 539–542.

Fukasawa, K., T. Choi, R. Kuriyama, S. Rulong, and G.F. Vande Woude. 1996. Abnormal centrosome amplification in the absence of p53. *Science* **271:** 1744–1747.

Haffner, R. and M. Oren. 1995. Biochemical properties and biological effects of p53. *Curr. Opin. Genet. Dev.* **5:** 84–90.

Harper, J.W., G.R. Adami, N. Wei, K. Keyomarsi, and S.J. Elledge. 1993. The p21 Cdk-interacting protein Cip1 is a potent inhibitor of G1 cyclin-dependent kinases. *Cell* **75:** 805–816.

Hartwell, L.H. and M.B. Kastan. 1994. Cell cycle control and cancer. *Science* **266:** 1821–1828.

Harvey, M., A.T. Sands, R.S. Weiss, M.E. Hegi, R.W. Wiseman, P. Pantazis, B.C. Giovanella, M.A. Tainsky, A. Bradley, and L.A. Donehower. 1993. In vitro growth characteristics of embryo fibroblasts isolated from p53-deficient mice. *Oncogene* **8:** 2457–2467.

Hockenbery, D.M. 1995. *bcl-2*, a novel regulator of cell death. *BioEssays* **17:** 631–638.

Hollstein, M., D. Sidransky, B. Vogelstein, and C.C. Harris. 1991. p53 mutations in human cancers. *Science* **253:** 49–53.

Hoyt, M.A., L. Totis, and B.T. Roberts. 1991. S. cerevisiae genes required for cell cycle arrest in response to loss of microtubule function. *Cell* **66:** 507–517.

Kastan, M.B., Q. Zhan, W.S. El-Deiry, F. Carrier, T. Jacks, W.V. Walsh, B.S. Plunkett, B. Vogelstein, and A.J. Fornace Jr. 1992. A mammalian cell cycle checkpoint pathway utilizing p53 and GADD45 is defective in ataxia-telangiectasia. *Cell* **71:** 587–597.

Kern, S.E., J.A. Pietenpol, S. Thiagalingam, A. Seymour, K.W.

Kinzler, and B. Vogelstein. 1992. Oncogenic forms of p53 inhibit p53-regulated gene expression. *Science* **256:** 827–830.

Kuerbitz, S.J., B.S. Plunkett, W.V. Walsh, and M.B. Kastan. 1992. Wild-type p53 is a cell cycle checkpoint determinant following irradiation. *Proc. Natl. Acad. Sci.* **89:** 7491–7495.

Kung, A.L., S.W. Sherwood, and R.T. Schimke. 1990. Cell line-specific differences in the control of cell cycle progression in the absence of mitosis. *Proc. Natl. Acad. Sci.* **87:** 9553–9557.

Li, R. and A.W. Murray. 1991. Feedback control of mitosis in budding yeast. *Cell* **66:** 519–531.

Li, X. and R.B. Nicklas. 1995. Mitotic forces control a cell-cycle checkpoint. *Nature* **373:** 630–632.

Lowe, S.W., H.E. Ruley, T. Jacks, and D.E. Housman. 1993a. p53-dependent apoptosis modulates the cytotoxicity of anticancer agents. *Cell* **74:** 957–967.

Lowe, S.W., E.M. Schmitt, S.W. Smith, B.A. Osborne, and T. Jacks. 1993b. p53 is required for radiation-induced apoptosis in mouse thymocytes. *Nature* **362:** 847–849.

Lowe, S.W., S. Bodis, A. McClatchey, L. Remington, H.E. Ruley, D.E. Fisher, D.E. Housman, and T. Jacks. 1994. p53 status and the efficacy of cancer therapy in vivo. *Science* **266:** 807–810.

Metz, T., A.W. Harris, and J.M. Adams. 1995. Absence of p53 allows direct immortalization of hematopoietic cells by the myc and raf oncogenes. *Cell* **82:** 29–36.

Minn, A.J., C.M. Rudin, L.H. Boise, and C.B. Thompson. 1995. Expression of Bcl-x_L can confer a multidrug resistance phenotype. *Blood* **86:** 1903–1910.

Minshull, J., H. Sun, N.K. Tonks, and A.W. Murray. 1994. A MAP kinase-dependent spindle assembly checkpoint in Xenopus egg extracts. *Cell* **79:** 475–486.

Miyashita, T. and J.C. Reed. 1993. Bcl-2 oncoprotein blocks chemotherapy-induced apoptosis in a human leukemia cell line. *Blood* **81:** 151–157.

Murray, A.W. 1994. Cell cycle checkpoints. *Curr. Opin. Cell Biol.* **6:** 872–876.

———. 1995. The genetics of cell cycle checkpoints. *Curr. Opin. Genet. Dev.* **5:** 5–11.

Rieder, C.L., R.W. Cole, A. Khodjakov, and G. Sluder. 1995. The checkpoint delaying anaphase in response to chromosome monoorientation is mediated by an inhibitory signal produced by unattached kinetochores. *J. Cell Biol.* **130:** 941–948.

Sandell, L.L. and V.A. Zakian. 1993. Loss of a yeast telomere: Arrest, recovery, and chromosome loss. *Cell* **75:** 729–739.

Schlaifer, D., M. March, S. Krajewski, G. Laurent, J. Pris, G. Delsol, J.C. Reed, and P. Brousset. 1995. High expression of the bcl-x gene in Reed-Sternberg cells of Hodgkin's disease. *Blood* **85:** 2671–2674.

Shaulian, E., A. Zauberman, D. Ginsberg, and M. Oren. 1992. Identification of a minimal transforming domain of p53: Negative dominance through abrogation of sequence-specific DNA binding. *Mol. Cell. Biol.* **12:** 5581–5592.

Smith, M.L., I.T. Chen, Q. Zhan, I. Bae, C.Y. Chen, T.M. Gilmer, M.B. Kastan, P.M. O'Connor, and A.J. Fornace Jr. 1994. Interaction of the p53-regulated protein Gadd45 with proliferating cell nuclear antigen. *Science* **266:** 1376–1380.

Van den Heuvel, S. and E. Harlow. 1993. Distinct roles for cyclin-dependent kinases in cell cycle control. *Science* **262:** 2050–2054.

Wang, Y. and C. Prives. 1995. Increased and altered DNA binding of human p53 by S and G2/M but not G1 cyclin-dependent kinases. *Nature* **376:** 88–91.

Yin, Y., M.A. Tainsky, F.Z. Bischoff, L.C. Strong, and G.M. Wahl. 1992. Wild-type p53 restores cell cycle control and inhibits gene amplification in cells with mutant p53 alleles. *Cell* **70:** 937–948.

STIC-ILL

From: Canella, Karen
Sent: Sunday, February 03, 2002 9:00 PM
To: STIC-ILL
Subject: ill order 09/815,340

Art Unit 1642 Location 8E12(mail)

Telephone Number 308-8362

Application Number 09/815,340

1. Trends in Cell biology, 2001 Jan, 11(1):18-21
2. Clinical Cancer Research, 2000 Aug, 6(8):3215-3221
3. Mutation Research, 1997 Apr 29, 375(2):157-165
4. american Journal of Hematology, 1985 Mar, 18(3):243-249.
5. PNAS, 1989 Apr, 86(7):2276-2280
6. Genes and Development, 1996 Oct 15, 10(20):2621-2631
7. Cancer, 1975 Jun, 35(6):1664-1677
8. Mutation Research, 1978, 57(3): 313-324
9. Environ Mutagen, 1981, 3(1):53-64
10. Nucleic Acids Research, 2001 Mar 15, 29(6):1300-1307
11. Oncogene:
    1998 Oct 29, 17(17):2187-2193
    2000 Jan 20, 19(3):403-409
12. Molecular endocrinology, 1999 Jan, 13(1):156-166
13. Gene, 1999 Nov 29, 240(2):317-324
14. Science, 1999 Jul 16, 285(5426)418-422
15. Biochemistry and Molecular biology international, 1999 May, 47(5):891-897
16. Journal of Clinical Endocrinology and Metabolism, 1999 Mar, 84(3):1149-1152
17. Journal of biological chemistry:
    1999 Jan 29, 274(5):3151-3158
    2000 Nov 24, 275(47):36502-36505 ***
18. Gene 2000 May 2, 248(1-2):41-50
19. Molecular endocrinology, 2000 Aug, 14(8):1137-1146
20. Cancer Letters, 2001 Feb 10, 163(1):131-139
21. Brain Pathology, 2001 Jul, 11(3):328-341

Pituitary Tumor Transforming Gene (PTTG) Regulates Placental JEG-3 Cell Division and Survival: Evidence from Live Cell Imaging

Run Yu, Song-Guang Ren, Gregory A. Horwitz, Zhiyong Wang, and Shlomo Melmed

Division of Endocrinology
Cedars-Sinai Research Institute-UCLA School of Medicine
Los Angeles, California 90048

The pituitary transforming gene, PTTG, is abundantly expressed in endocrine neoplasms. PTTG has recently been recognized as a mammalian securin based on its biochemical homology to Pds1p. PTTG expression and intracellular localization were therefore studied during the cell cycle in human placental JEG-3 cells. PTTG mRNA and protein expressions were low at the G_1/S border, gradually increased during S phase, and peaked at G_2/M, but PTTG levels were attenuated as cells entered G_1. In interphase cells, wild-type PTTG, an epitope-tagged PTTG, and a PTTG-EGFP conjugate all localized to both the nucleus and cytoplasm, but in mitotic cells, PTTG was not observed in the chromosome region. PTTG-EGFP colocalized with mitotic spindles in early mitosis and was degraded in anaphase. Intracellular fates of PTTG-EGFP and a conjugate of EGFP and a mutant inactivated PTTG devoid of an SH3-binding domain were observed by real-time visualization of the EGFP conjugates in live cells. The same cells were continuously observed as they progressed from G_1/S border to S, G_2/M, and G_1. Most cells (67%) expressing PTTG-EGFP died by apoptosis, and few cells (4%) expressing PTTG-EGFP divided, whereas those expressing mutant PTTG-EGFP divided. PTTG-EGFP, as well as the mutant PTTG-EGFP, disappeared after cells divided. The results show that PTTG expression and localization are cell cycle-dependent and demonstrate that PTTG regulates endocrine tumor cell division and survival. (Molecular Endocrinology 14: 1137–1146, 2000)

INTRODUCTION

Pituitary tumor transforming gene (PTTG) was identified in rat pituitary tumor cells by differential mRNA display (1). Human PTTG (2, 3) is highly expressed in pituitary tumors (4, 5) and other neoplasms (3, 6, 7). Levels of PTTG expression positively correlate with pituitary tumor invasiveness (4) and are induced by estrogen (5). The mechanism of PTTG action is not clear. PTTG up-regulates basic fibroblast growth factor secretion (2) and transactivates DNA transcription (Refs. 3 and 8 and Horwitz, G. A., Z. Wong, X. Zhang, and S. Melmed, unpublished). Recently, PTTG protein has been recognized as a mammalian securin protein that maintains binding of sister chromatids during mitosis (10). At the end of metaphase, securin is degraded by an anaphasepromoting complex, releasing tonic inhibition of separin, which in turn mediates degradation of cohesins, the proteins that hold sister chromatids together. Overexpression of a nondegradable PTTG disrupts sister chromatid separation (10).

Since PTTG was identified, its cellular characteristics have not been studied. To address the mechanism of PTTG action, we studied PTTG expression and intracellular localization during the cell cycle in human placental JEG-3 cells, which are among the few available human endocrine cells in culture. The effects of PTTG expression on the cell cycle were also addressed. JEG-3 cells secrete hCG both basally and in response to a variety of stimulants (11–13). Our results show that PTTG expression and localization are cell cycle dependent and demonstrate that PTTG regulates placental tumor cell division and survival.

0888-8809/00/$3.00/0
Molecular Endocrinology 14(8): 1137–1146

RESULTS

Cell Cycle-Dependent PTTG Expression

Human placental JEG-3 cells express PTTG (Fig. 1). After JEG-3 cells were synchronized at the G_1/S border with double thymidine block and then released, they gradually entered S, G_2/M, and G_1 over 15 h (Fig. 1A). JEG-3 cells were also synchronized at the G_1/S border and at G_2/M by treating with aphidicolin and nocodazole, respectively (Fig. 1A). PTTG mRNA expression was low at the G_1/S border achieved by double thymidine block or by incubation with aphidicolin (Fig. 1B). When cells were released, PTTG mRNA

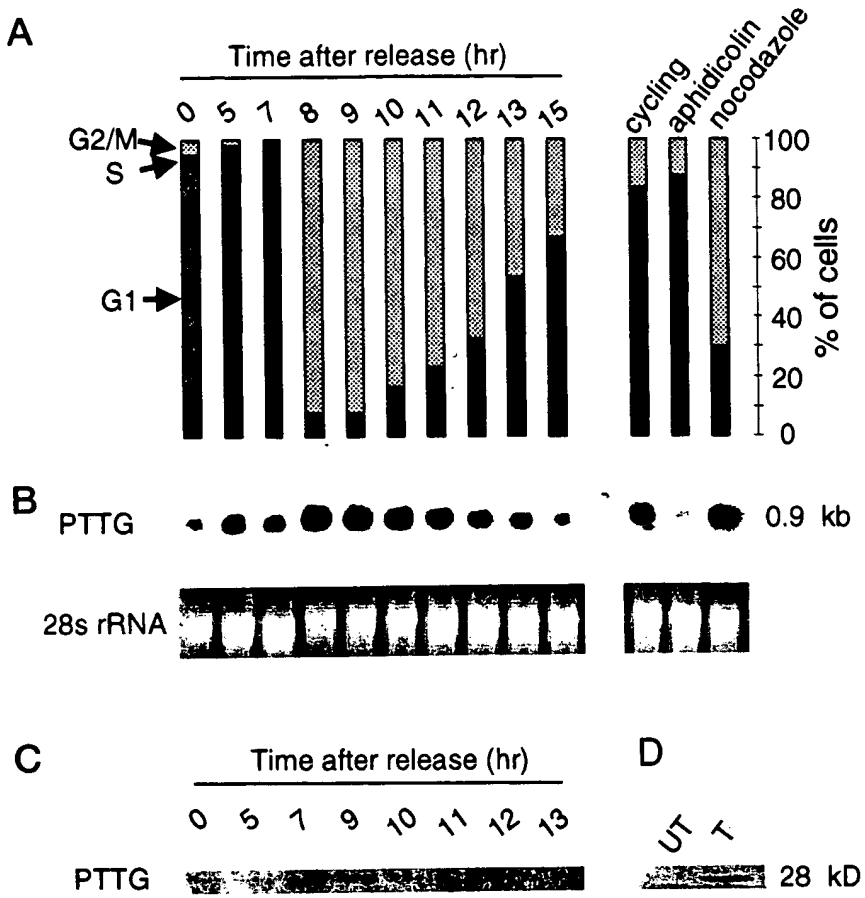

Fig. 1. Cell-Cycle Dependent Expression of PTTG

JEG-3 cells were synchronized at G_1/S border by double thymidine block and then released. JEG-3 cells were also blocked at the G_1/S border by aphidicolin, or at G_2/M by nocodazole. A, Phase components measured by flow cytometry after release from double thymidine block, or after treatments with aphidicolin or nocodazole. B, Corresponding PTTG mRNA measured by Northern blotting. Equal amounts of total RNA (10 μg) were loaded in each lane. C, PTTG protein after release from double thymidine block measured by Western blotting using a rabbit antiserum against PTTG. Equal amounts of protein (150 μg) were loaded in each lane. D, JEG-3 cells were transiently transfected with a pCIneo plasmid encoding PTTG and endogenous and overexpressed PTTG in cycling JEG-3 cells were shown in Western blot stained with rabbit anti-PTTG. UT, Untransfected, and T, transfected with PTTG. Experiments were repeated two to three times with similar results.

increased through the S phase and plateaued at G_2/M (2.0 ± 0.3-fold over G_1/S). Cells synchronized by nocodazole also expressed higher mRNA levels than did cycling cells. PTTG protein expression followed a similar cycle-dependent course (Fig. 1C). PTTG protein levels assessed by Western blotting were very low in cells at the G_1/S border, increased through S phase, and peaked at G_2/M (2.4 ± 0.6-fold over G_1/S). When cells divided, PTTG protein levels again decreased.

Localization of PTTG Protein in Interphase and Mitosis

Endogenous PTTG protein expression was low in cycling JEG-3 cells (Fig. 1D), and no significant results were obtained after immunofluorescent staining of those cells with rabbit anti-PTTG serum. To study PTTG localization, JEG-3 cells were transfected with plasmids encoding wild-type PTTG, a FLAG epitope-tagged PTTG (PTTG-FLAG), or a conjugated PTTG and EGFP protein (PTTG-EGFP). Intracellular localization of wild-type PTTG was followed by immunofluorescent staining using a rabbit anti-PTTG serum. No significant staining was found when transfected cells were stained with preimmune serum or when untransfected cells were stained with antiserum. Localization of FLAG-tagged PTTG was revealed with immunofluorescent staining using the M2 monoclonal antibody. Again, no significant immunoreactivity was observed when transfected cells were stained with an irrelevant monoclonal antibody or when untransfected cells were stained with the M2 antibody. The PTTG-EGFP conjugate was directly visualized after fixing. JEG-3 cells were also stained with Hoechst 33258 to delineate nuclear structures. In cycling JEG-3 cells, localizations of the three PTTG protein constructs were similar. During interphase, wild-type PTTG protein (Fig. 2a) and the tagged PTTG proteins (Fig. 2, b and

c) were evident throughout the cell, but PTTG was more concentrated in the nucleus than in the cytoplasm. Both the PTTG signals as well as DNA appeared distinct from the nucleoli. In some cells, PTTG protein also localized on the plasma membrane (found in <5% of transfected cells) (Fig. 2c). Localization of PTTG protein constructs was similar regardless of their respective expression level. Similar results were obtained when PTTG-EGFP was expressed in a variety of other cell lines including 3T3 murine fibroblast, GH3 and AtT20 rat pituitary tumor, SKOV-3 human ovarian cancer, MCF-7 human breast cancer, and COS-7 monkey kidney cells (data not shown).

Localization of PTTG-EGFP in cycling cells, most of which were in interphase, was confirmed by cell fractionation (Fig. 3). JEG-3 cells were transfected with plasmids encoding EGFP alone or PTTG-EGFP. EGFP and PTTG-EGFP were determined in cytosolic and nuclear fractions by Western blotting. EGFP was detected predominantly in the cytosol while PTTG-EGFP localized mostly in cell nuclei. The cytosolic fraction of cells expressing PTTG-EGFP contained two discrete EGFP antibody-reactive proteins in addition to EGFP, probably due to proteolysis of PTTG-EGFP. The purity of the cytosolic and nuclear fractions was confirmed by Western blot using cytosolic marker protein tubulin and nuclear marker protein lamin. No similar visualizing attempts were made on mitotic cells because they do not exhibit defined nuclei.

In metaphase cells evidenced by aligned chromosomes and characteristic spindles, wild-type PTTG (Fig. 4a) and PTTG-FLAG (Fig. 4b) were not visible in the chromosome region but remained elsewhere. Costaining of PTTG-FLAG and spindles was not at-

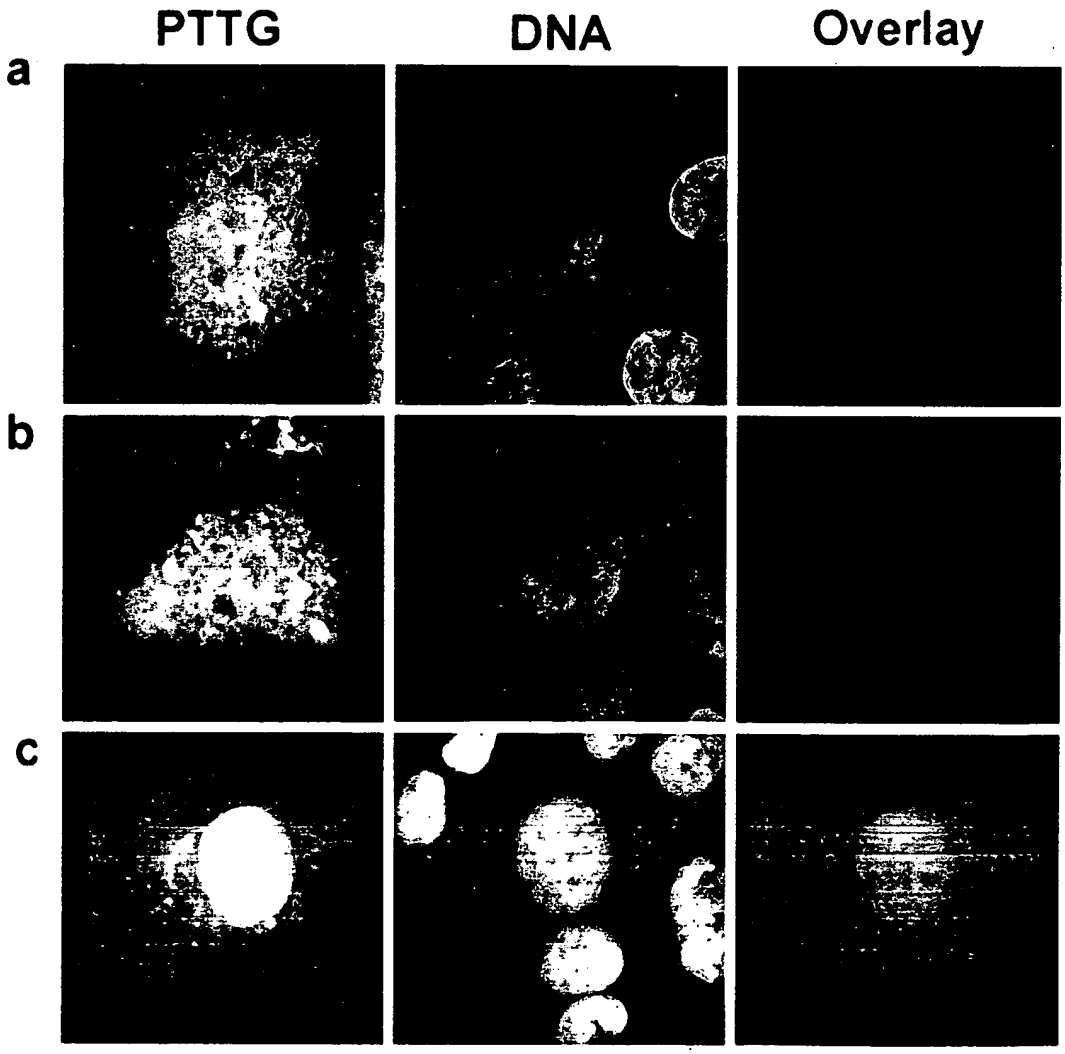

Fig. 2. Localization of PTTG in Interphase

JEG-3 cells were transfected with plasmids encoding PTTG (a), PTTG-FLAG (b), or PTTG-EGFP (c). PTTG or PTTG-FLAG was visualized by immunofluorescent staining, and PTTG-EGFP was visualized directly (*left*). Cells were also stained with Hoechst 33258 (*middle*) to highlight the nuclei and chromosomes and to determine the cell cycle. The images of cells expressing PTTG, PTTG-FLAG, or PTTG-EGFP were overlaid with images of cells stained with Hoechst (*right*). *Green*, PTTG or PTTG-EGFP; *red*: PTTG-FLAG; and *blue*, DNA.

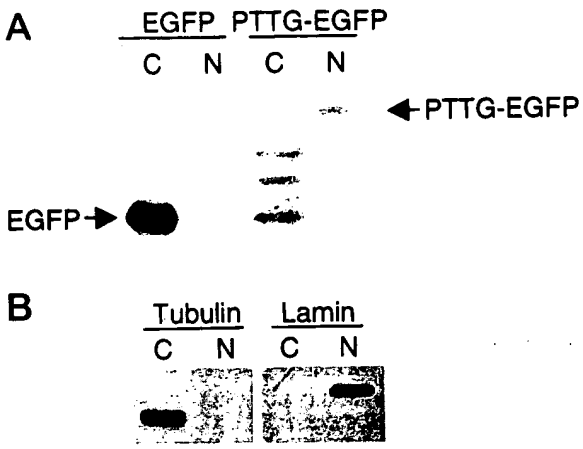

Fig. 3. Localization of PTTG-EGFP Determined by Cell Fractionation

JEG-3 cells were transfected with plasmids encoding EGFP only or PTTG-EGFP. A, Cytosolic (C) and nuclear (N) fractions were collected and EGFP or PTTG-EGFP in each fraction was examined by Western blotting using antibody against EGFP. B, The purity of the cytosolic and nuclear fractions was verified with antibodies to tubulin and nuclear lamin.

tempted because antibodies to both of them were of mouse origin. In these experiments, PTTG-EGFP transfection efficiency was highest and facilitated sufficient numbers of mitotic cells expressing PTTG-EGFP available for subsequent following (Fig. 5). Mitotic spindles were visualized by utilizing antibodies to tubulin. Although PTTG-EGFP was well visualized from prophase to metaphase, it was distinct from chromosomes (Fig. 5, a–c). PTTG-EGFP colocalized with microtubule asters in prophase and prometaphase (Fig. 5, a and b). During anaphase, PTTG-EGFP aggregated into distinct granules suggesting a proteasomal degradation process (Fig. 5d). No cells in telophase were found to express PTTG-EGFP.

Observation of PTTG-EGFP in Live, Synchronized Cells

To follow the fate of PTTG more closely and to study cellular effects of overexpressing PTTG, JEG-3 cells were transfected with plasmids encoding EGFP alone, PTTG-EGFP, and a mutant PTTG-EGFP. This mutant PTTG is mutated in the SH3-binding region (P163A, P170L, P172A, and P173L) and is devoid of transforming activity (2). Transfected cells were synchronized at the G_1/S border and released into normal cell cycle, and the same group of live cells were observed every 1–3 h before and after release (Figs. 6 and 7). Thus, EGFP, PTTG-EGFP, and mutant PTTG-EGFP were visualized in a real-time manner in live single cells for up to 14 h. EGFP alone was evenly distributed throughout the cells. PTTG-EGFP and mutant PTTG-EGFP were both evident largely in the nuclei, suggesting that the SH3-binding domain was not responsible for the nuclear localization. In cells expressing EGFP alone, EGFP remained intact during and after mitosis; however, in cells expressing wild-type or the mutant PTTG-EGFP, EGFP fluorescence was dissipated immediately after mitosis in daughter cells (Fig. 6). The daughter cells were viable because they showed normal morphology hours after mitosis.

Surprisingly, most cells (31/46, 67%) expressing wild-type PTTG-EGFP died shortly after cells were released from G_1/S block (Figs. 7–9). TUNEL staining of PTTG-EGFP-expressing dead cells showed that they were apoptotic (Fig. 8). In comparison, only 44% (27/61, $P < 0.05$) of cells expressing EGFP alone died randomly instead of early after release from block (Fig. 9). This background cell death may be the result of double thymidine block. About 30% (5/16, fewer cells were observed due to low transfection efficiency) of cells expressing mutant PTTG-EGFP died early after cells entered S phase. No cells expressing EGFP alone demonstrated EGFP degradation, indicating that EGFP itself is stable (Fig. 9). Some cells expressing PTTG-EGFP (6/46) or the mutant PTTG-EGFP (2/16) lost EGFP fluorescence while alive during interphase (Fig. 7), suggesting that both the wild-type and mutant PTTGs are also degraded in interphase. Only 4% of cells (2/46) expressing wild-type PTTG-EGFP eventually divided (Fig. 9), and mitosis was delayed when compared with cells expressing EGFP only, in which 8 of 61 (13%) divided. On the contrary, more cells (7/16, 44%) expressing mutant PTTG-EGFP divided and mitosis appeared to occur slightly earlier than in cells expressing EGFP (Fig. 9).

DISCUSSION

In this report, we characterize the cellular properties of PTTG in a human placental JEG-3 tumor cell line. JEG-3 cells express endogenous PTTG, making them a suitable human endocrine cell model for PTTG study. We first demonstrated that, in cell populations, expressions of PTTG mRNA and protein were both highly dependent on the cell cycle, highest at the G_2/M but decreased in the subsequent G_1 phase. At the single-cell level, intracellular PTTG imaging showed that PTTG was degraded in anaphase, and daughter cells express little PTTG. Degradation of PTTG protein upon cell division probably occurs by a proteosomal mechanism as suggested by the PTTG morphology during anaphase. PTTG contains a D-box, which is required for ubiquitin-mediated PTTG proteolysis (10). This cell cycle-dependent PTTG expression is consistent with that of a securin (10, 14–16). The human (17), rat (18), and mouse (19) PTTG promoters contain a conserved region that harbors several motifs such as CCAAT, which confer cell cycle-dependent expression (20). Thus, the mechanism of cell cycle-dependent PTTG mRNA expression probably lies at the transcriptional level. Interestingly, PTTG has also been shown to be serine phosphorylated during mitosis (16).

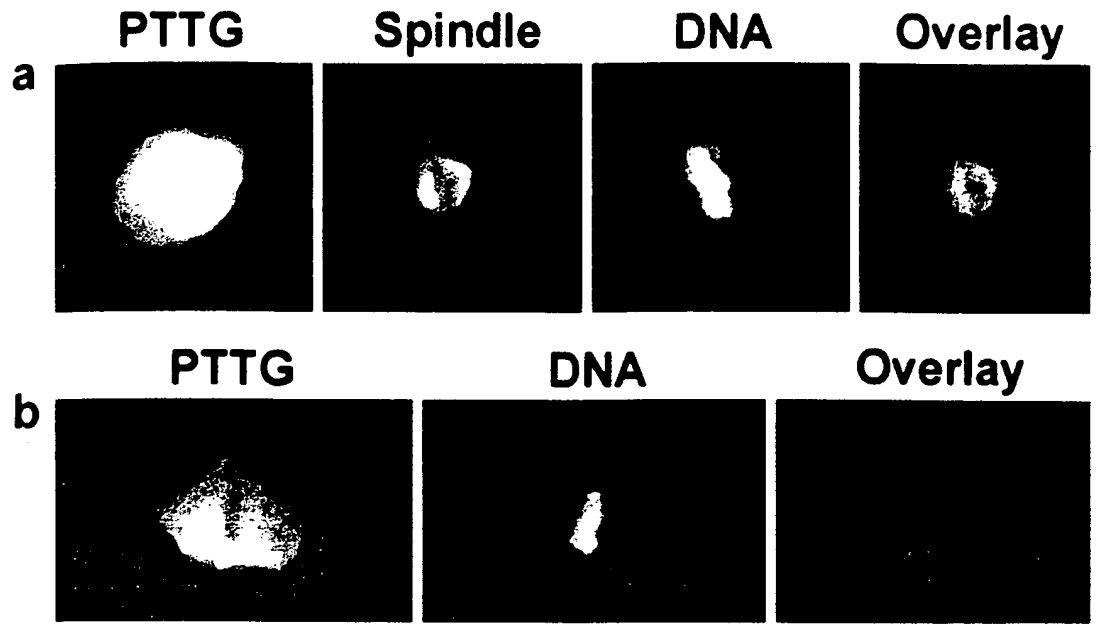

Fig. 4. Localization of PTTG in Mitosis

JEG-3 cells were transfected with plasmids encoding PTTG (a), or PTTG-FLAG (b). PTTG or PTTG-FLAG was visualized by immunofluorescent staining (PTTG). Cells were stained with Hoechst 33258 to highlight the mitotic nuclei (DNA). Wild-type PTTG-transfected cells were also stained with antibodies to tubulin (spindle). a, Images of PTTG, DNA, and mitotic spindle were overlaid. *Green*, PTTG; *red*, mitotic spindles; and *blue*, DNA. b, Images of PTTG-FLAG and DNA were overlaid. *Red*, PTTG-FLAG; and *blue*, DNA (looks *purple* because of some mixing with *red*).

We have also detailed the subcellular localization of PTTG during interphase and in different phases of mitosis. The subcellular localization of PTTG is similar to that of budding yeast securin Pds1 (14) and fission yeast securin Cut2 (15). Intracellular PTTG localization was predominantly nuclear in interphase with significant expression in the cytoplasm, but localized to mitotic spindles during early mitosis. Binding of securin to mitotic spindles is important for normal anaphase (21). We recognize that our imaging results depend on overexpressing PTTG proteins since endogenous PTTG protein level is low in JEG-3 cells. It is unlikely, however, that the observed localization of PTTG is due to overexpression, because erroneous localization as a result of overexpression usually occurs in the endoplasmic reticulum and the Golgi apparatus, organelles in which PTTG was not seen. Furthermore, similar results were derived from imaging of three different PTTG protein constructs as well as from cell fractionation experiments. The dual intracellular localization of PTTG is consistent with PTTG functions. As a securin (10), PTTG is required in the nucleus to regulate sister chromatid binding, and PTTG binds to a ribosomal protein DnaJ, which presumably is situated in the cytoplasm (22). Based on these lines of evidence, it appears that the results shown here faithfully describe the physiological subcellular localization of PTTG protein. It is not clear how PTTG is targeted to the nucleus. Although PTTG does not have an obvious nuclear localization signal, its small size (apparent mobility ~28 kDa) may permit it to enter the nucleus. Apparently, PTTG is not excluded from the nucleus because PTTG-EGFP is also predominantly nuclear. Our results are in contrast to previous reports suggesting that immunoreactive PTTG is localized predominantly in the cytoplasm (3, 4, 7). Although this difference may be due to different cell and tissue preparations used in these studies, we have now shown similar subcellular localization of PTTG-EGFP in eight different cell lines.

Functionally, PTTG overexpression inhibited mitosis as few cells overexpressing PTTG divided and cell division appeared delayed. The inhibitory effect of PTTG on mitosis is expected of a securin because the cell requires more time to degrade overexpressed PTTG before anaphase. In contrast to yeast cells that survive without sister chromatid separation (15), most human placental cells overexpressing PTTG died by apoptosis. Overexpressing PTTG may cause general cell cycle disruption or may induce transcription of apoptosis-promoting genes. It is well documented that cell cycle disruption may cause apoptosis (23). Our results are consistent with those of Uhlmann *et al.* (24) who showed that cells expressing an uncleavable form of a cohesin subunit die. Apoptosis induced by PTTG and the fewer and delayed mitoses provide an explanation for the finding that overexpressing PTTG inhibits cell proliferation (1).

This study again highlights the functional importance of the SH3-binding domain in the C terminus of PTTG protein. Mutant PTTG lacking an SH3-binding domain is devoid of transforming activity (2, and

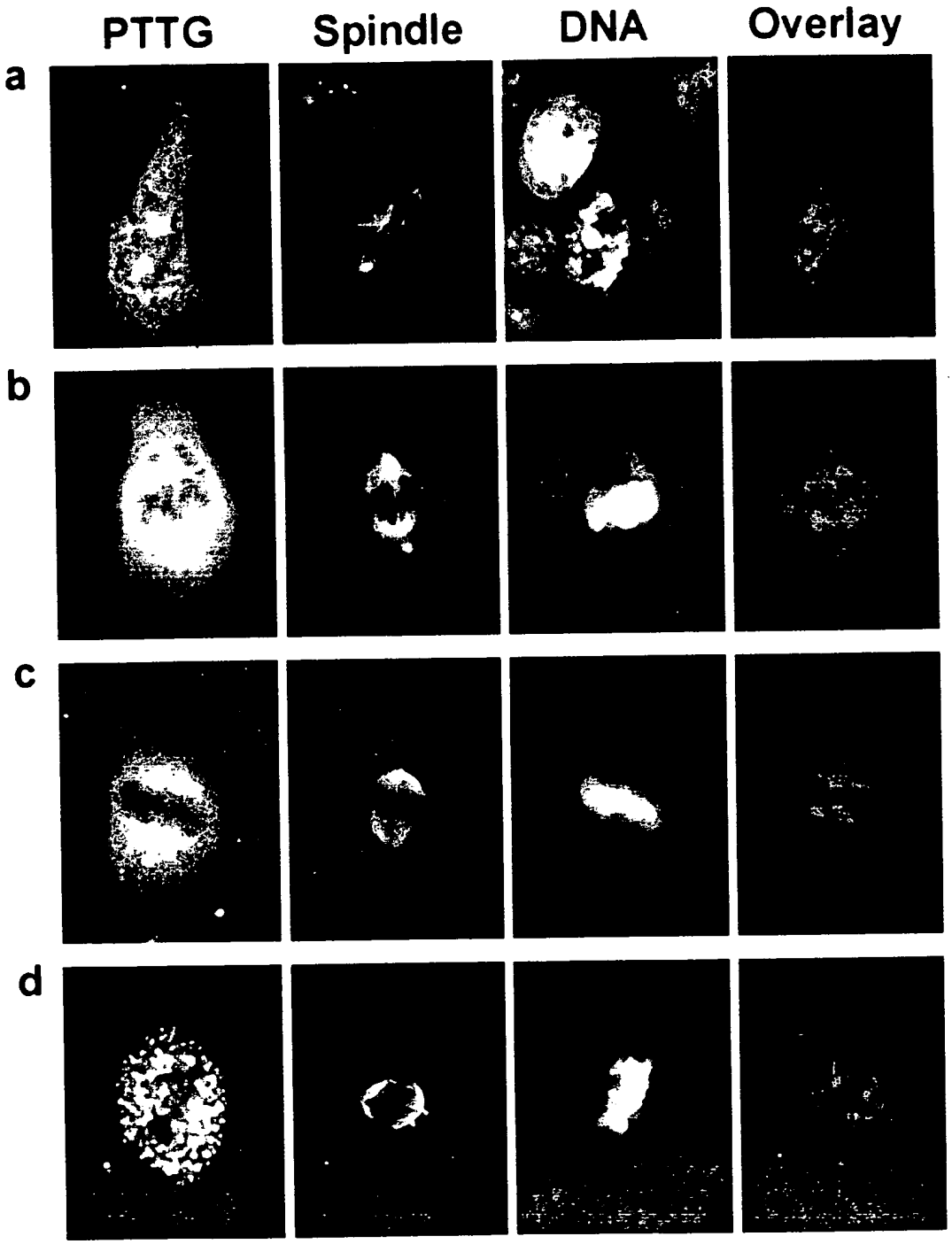

Fig. 5. Localization of PTTG-EGFP in Mitosis

JEG-3 cells were transfected with plasmids encoding PTTG-EGFP. PTTG-EGFP was visualized directly (*left*). Mitotic spindles were visualized by immunofluorescent staining of tubulin (*middle left*). Cells were stained with Hoechst 33258 to highlight the stage in mitosis (*middle right*). Images of PTTG-EGFP, mitotic spindle, and chromosome were overlaid (*right*). *Green*, PTTG-EGFP; *red*, mitotic spindles; and *blue*, DNA. *Orange* or *yellow* indicates where *green* and *red* colocalized. a, Prophase; b, prometaphase; c, metaphase; and d, anaphase.

Horwitz, G. A., Z. Wang, X. Zhang, and S. Melmed, unpublished), suggesting that critical interactions between PTTG and proteins containing SH3 domains are responsible for PTTG function. Our results suggest that the SH3-binding domain is not important for nuclear or cytosolic localization because the localization of this mutant PTTG was similar to that of wild-type PTTG. Since mutant PTTG facilitated mitosis as evidenced by more frequent and earlier mitosis, probably due to easier separation of sister chromatids, the SH3-

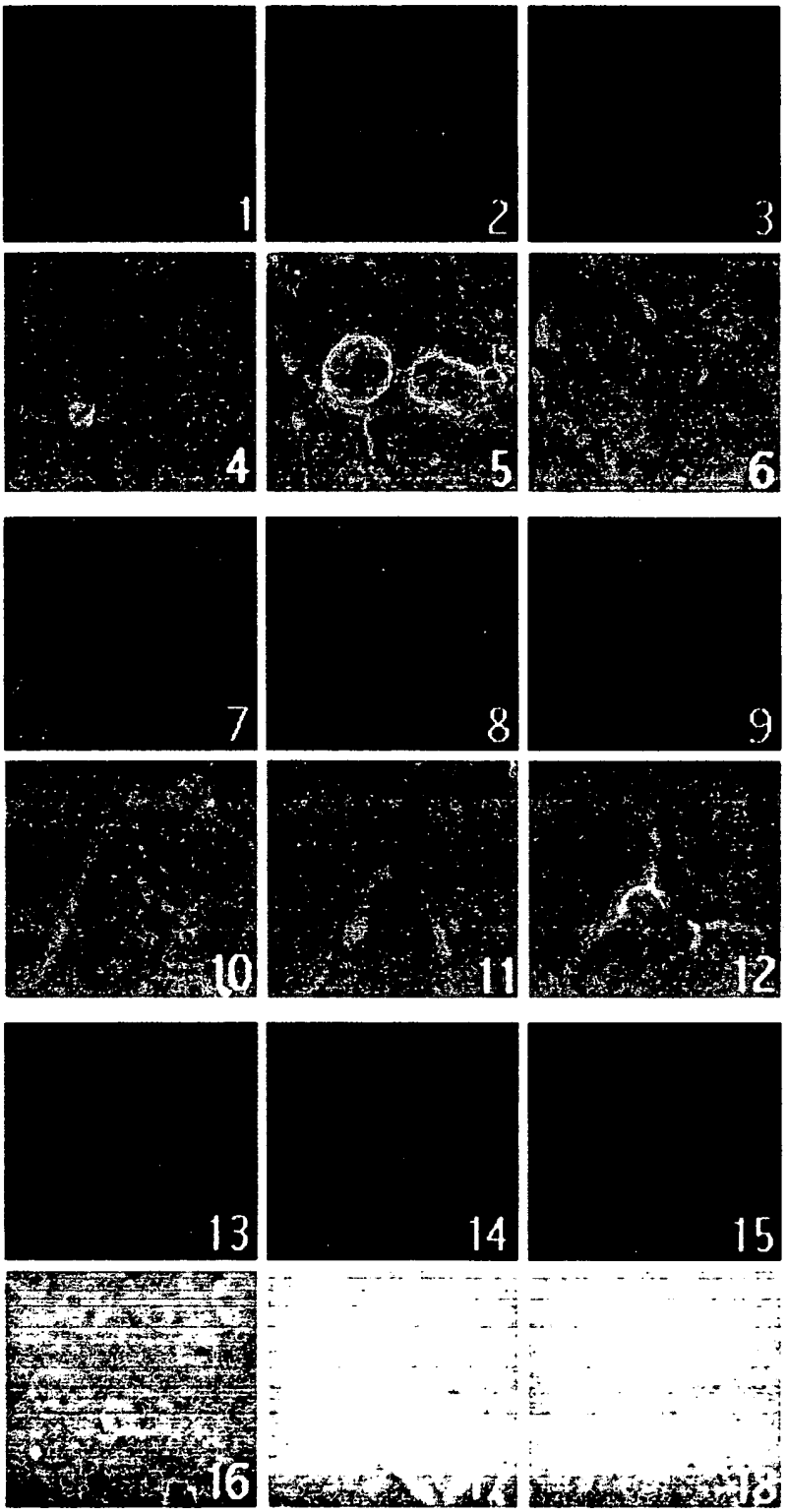

Fig. 6. Observation of Mitosis of Synchronized, Live Cells

JEG-3 cells were transiently transfected with plasmids encoding EGFP only (panels 1–6), PTTG-EGFP (panels 7–12), or the mutant PTTG-EGFP (panels 13–18). JEG-3 cells were synchronized at the G_1/S border by double thymidine block and then released. Live cells were observed every 1–3 h for 14 h after release. Cells that divided were shown before (panels 1 and 4; 7 and 10; 13 and 16), during (panels 2 and 5; 8 and 11; 14 and 17), and after mitosis (panels 3 and 6; 9 and 12; 15 and 18). Fluorescent (panels 1–3, 7–9, 13–15) and the corresponding brightfield (panels 4–6, 10–12, 16–18) images were both shown.

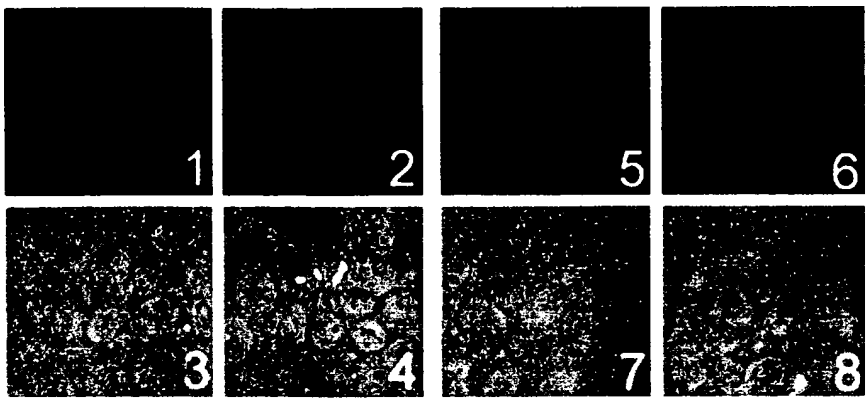

Fig. 7. Cell Death and Degradation of PTTG-EGFP

JEG-3 cells were transiently transfected with plasmids encoding PTTG-EGFP. JEG-3 cells were synchronized at the G_1/S border by double thymidine block and then released. Live cells were observed every 1–3 h for 14 h after release. Shown on the *left* (panels 1–4) are the same cells before (panels 1 and 3) and 2 h after (panels 2 and 4) release from block. One of the two cells expressing PTTG-EGFP died after release. Shown on the *right* (panels 5–8) are the same cells 4 h (5 and 7) and 7 h (6 and 8) after release. Two of the three cells expressing PTTG-EGFP degraded PTTG-EGFP. Fluorescent (panels 1, 2, 5, and 6) and the corresponding brightfield (panels 3, 4, 7, and 8) images were both shown.

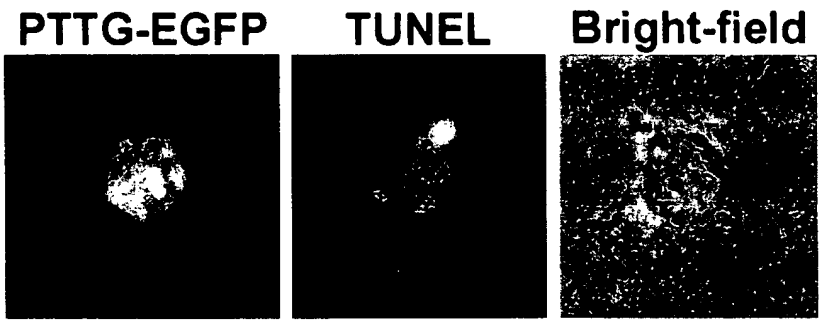

Fig. 8. Apoptosis of PTTG-EGFP-Expressing Cells

JEG-3 cells transiently expressing PTTG-EGFP were synchronized at the G_1/S border by double thymidine block then released. Cells were fixed 3.5 h after release and apoptotic cells were identified with a TUNEL staining kit using rhodamine-labeled UTP as substrate. Shown is one PTTG-EGFP expressing cell that is also positive for TUNEL staining.

binding domain may also be important for the securin function of PTTG.

Several lines of evidence from our study strongly indicate that PTTG is a securin in JEG-3 cells. Based on the securin function of PTTG, we propose that chromosomal instability and induction of aneuploidy may be a mechanism of PTTG action. By keeping sister chromatids held abnormally tight, overexpression of PTTG may enable daughter cells to either gain or lose one or more chromosomes. In both cases, the daughter cell may become tumorous.

MATERIALS AND METHODS

Cell Synchronization

Human placental choriocarcinoma JEG-3 cells were grown in DMEM plus 10% FBS. JEG-3 cells were grown to half-confluency, treated with 2 mM thymidine overnight, and were grown in normal medium for 10 h. When required, cells were transfected using FuGene (Roche Molecular Biochemicals, Indianapolis, IN) during this growth, and again treated with 2 mM thymidine overnight. At this stage, cells were blocked at the G_1/S border. Cells were released from the block by growing in normal medium supplemented with 10 μM deoxycytidine, and cell cycle progression was confirmed by fluorescence-activated cell sorting. Cells were also synchronized at the G_1/S border by incubating with aphidicolin (Calbiochem, La Jolla, CA, 2 μg/ml) for 12 h, and at G_2/M by incubating with nocodazole (Calbiochem, 150 ng/ml) for 16 h.

Plasmids and Transfection

Wild-type human PTTG and an SH3-binding domain-mutated PTTG (2) from a pCIneo vector were subcloned into an *Eco*RI/*Bam*HI site in a pEGFPN3 vector (CLONTECH Laboratories, Inc. Palo Alto, CA). Wild-type PTTG was also subcloned into an EcoI/*Xho*I site in a pCMVtag4 vector (Stratagene, La Jolla, CA). In both cases, EGFP and the FLAG epitope were fused in frame to the PTTG C terminus and the fusion proteins were termed PTTG-EGFP and PTTG-FLAG, respectively. Cells were transfected with FuGene (Roche Molecular Biochemicals), and plasmid-FuGene complex was directly added to cells grown in normal medium.

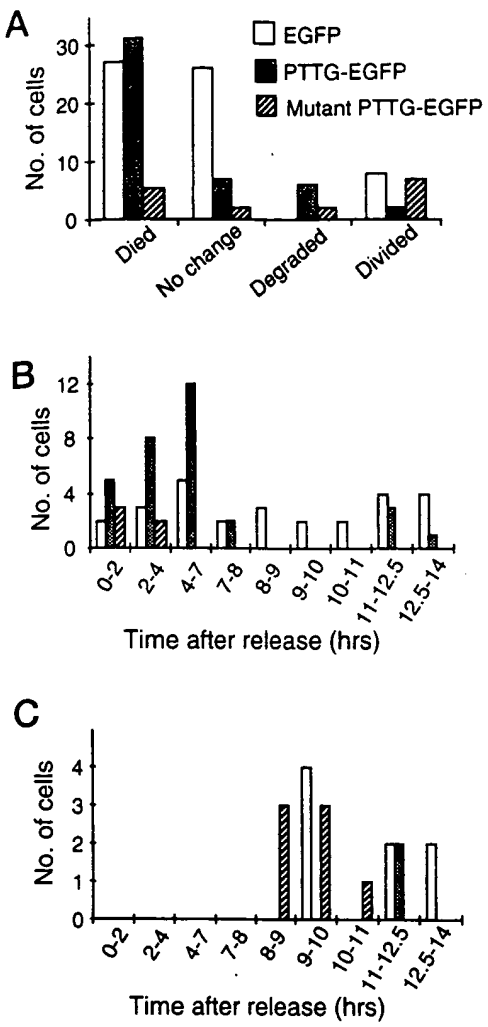

Fig. 9. Effects of PTTG on Cell Survival and Division

JEG-3 cells were transiently transfected with plasmids encoding EGFP, PTTG-EGFP, or the mutant PTTG-EGFP. JEG-3 cells were synchronized at G_1/S border by double thymidine block then released. Live cells were observed every 1 to 3 h for 14 h after release. A, Total number of cells that died, remained unchanged, degraded EGFP or EGFP conjugates, or divided during this 14 h. B, Number of cells that died over each observation. C, Number of cells that divided over each observation. Number of cells observed: 61 for EGFP, 46 for PTTG-EGFP, and 16 for the mutant PTTG-EGFP.

Preparation of Rabbit Antibody to PTTG

Polypeptide, PLKOKOPSFSAKKM-TEKTVKA (80–100 in human PTTG protein), was used to generate rabbit antiserum against human PTTG protein. This antiserum recognized purified PTTG protein. The antiserum and an anti-EGFP antibody detected the same PTTG-EGFP band (~55 kDa) by Western blot. The antiserum recognized a predominant 28-kDa protein in lysates of cells overexpressing PTTG.

Northern Blot Analysis

Total RNA from treated JEG-3 cells was extracted using Trizol Reagent (Life Technologies, Inc., Gaithersburg, MD) according to manufacturer's protocol. Isolated RNA was precipitated, washed, and denatured as described previously (2). Separated RNA was transferred to Hybond-N nylon membrane (Amersham International, Buckinghamshire, UK). The membrane was cross-linked and prehybridized at 68 C, and hybridized with approximately 10^7 cpm ^{32}P-labeled human PTTG cDNA in the presence of 100 μg/ml salmon sperm DNA (Stratagene). The entire human PTTG cDNA coding region was labeled with [α-^{32}P]dCTP using RadPrime Labeling Kit (Life Technologies, Inc.) according to manufacturer's protocol. Blots were then exposed to x-ray film (Eastman Kodak Co., Rochester, NY). A predominant 0.9-kb band was recognized by this probe as was previously shown (2).

Cell Fractionation

JEG-3 cells were trypsinized and incubated in TM buffer (10 mM Tris, 2 mM $MgCl_2$, pH 7.4) containing 500 nM phenylmethylsulfonyl fluoride for 10 min on ice. Triton × 100 (0.5% final concentration) was added and cells were incubated for a further 5 min on ice. Cell suspension was passed through a 22-gauge needle eight times and centrifuged at 800 × g at 4 C for 10 min. The pellet nuclear fraction was examined with microscopy for purity. Antibodies to α tubulin and nuclear lamin B (Calbiochem) were used in Western blot to verify the purity of cytosolic and nuclear fractions.

Western Blotting

Cells were lysed in SDS-PAGE sample buffer (100 μl per 35-mm dish). Cell lysate (2 to 20 μl) was run on 10% SDS PAGE, and proteins were transferred to polyvinylidene fluoride membrane and incubated with rabbit antiserum for PTTG (1:1,000) or monoclonal EGFP antibody (CLONTECH Laboratories, Inc. 1:1,000) at 4 C overnight followed by incubation with peroxidase-linked secondary antibody (Amersham Pharmacia Biotech, Arlington Heights, IL; 1:5,000). Blots were visualized with ECL (enhanced chemiluminescence) reagents (Amersham Pharmacia Biotech).

Immunofluorescent Staining

JEG-3 cells were rinsed with PBS, fixed with 4% paraformaldehyde in PBS, and permeabilized with blocking buffer (PBS with 5% FBS and 0.6% Tween 20). Primary antibody, rabbit polyclonal anti-PTTG, or mouse M2 monoclonal anti-FLAG (Stratagene), was added at 1:1,000 in the blocking buffer and incubated for 2 h. Cells were washed and incubated with fluorescein isothiocyanate-labeled swine anti-rabbit IgG (DAKO Corp. A/S, Glostrup, Denmark) or TRITC-labeled goat antimouse IgG (Molecular Probes, Inc., Eugene, OR) (1:500) for 30 min. Cells were finally stained with Hoechst 33258 (Molecular Probes, Inc., 1:10,000) for 5 min. Mitotic spindles were stained with a monoclonal tubulin antibody (Calbiochem). Samples were washed and kept in mowiol-based mounting medium. Cells expressing EGFP conjugate were fixed and stained with Hoechst 33258 and directly visualized. Apoptotic cells were identified with a TUNEL staining kit using rhodamine-labeled UTP as substrate (Roche Molecular Biochemicals). Staining was carried out according to the manufacturer's recommended protocol. Apoptotic cells were visualized with rhodamine filters.

Fluorescence Microscopy

Live or immunochemically stained cells were visualized on a TE200 inverted epifluorescence microscope (Nikon, Melville, NY) equipped with relevant fluorescence filters. Digital images were acquired by a SPOT CCD camera (Diagnostic Instruments, Sterling Heights, MI) and analyzed by ImagePro

software (Media Cybernetics, Bothell, WA). Serial observation of live cells was achieved by growing cells in a gridded flask and directly visualized with a 10× lens and an extra long working distance 40× lens. Several hundred cells were observed in each of the two to seven staining experiments and representative cells were depicted in the figures.

Acknowledgments

Received March 15, 2000. Revision received April 20, 2000. Accepted April 26, 2000.

Address requests for reprints to: Shlomo Melmed, Academic Affairs, Cedars-Sinai Medical Center, 8700 Beverly Boulevard, Los Angeles, California 90048. E-mail: melmed@csmc.edu.

Supported by NIH Grant CA-75979 and the Doris Factor Molecular Endocrinology Laboratory.

REFERENCES

1. Pei L, Melmed S 1997 Isolation and characterization of a pituitary tumor-transforming gene (PTTG). Mol Endocrinol 11:433–441
2. Zhang X, Horwitz GA, Prezant TR, Valentini A, Nakashima M, Bronstein MD, Melmed S 1999 Structure, expression, and function of human pituitary tumor-transforming gene (PTTG). Mol Endocrinol 13:156–166
3. Dominguez A, Ramos-Morales F, Romero F, Rios RM, Dreyfus F, Tortolero M, Pintor-Toro JA 1998 hpttg, A human homologue of rat pttg, is overexpressed in hematopoietic neoplasms. Evidence for a transcriptional activation function of hPTTG. Oncogene 17:2187–2193
4. Zhang X, Horwitz GA, Heaney AP, Nakashima M, Prezant TR, Bronstein MD, Melmed S 1999 Pituitary tumor transforming gene (PTTG) expression in pituitary adenomas. J Clin Endocrinol Metab 84:761–767
5. Heaney AP, Horwitz GA, Wang Z, Singson R, Melmed S 1999 Early involvement of estrogen-induced pituitary tumor transforming gene and fibroblast growth factor expression in prolactinoma pathogenesis. Nat Med 5:1317–1321
6. Heaney AP, Singson R, McCabe CJ, Nelson V, Nakashima M, Melmed S 2000 Pituitary tumor transforming gene in colorectal tumors. Lancet 355:712–715
7. Saez C, Japon MA, Ramos-Morales F, Romero F, Segura DI, Tortolero M, Pintor-Toro JA 1999 hpttg Is overexpressed in pituitary adenomas and other primary epithelial neoplasias. Oncogene 18:5473–5476
8. Wang Z, Melmed S 2000 Pituitary tumor transforming gene (PTTG) transactivating, transforming activity. J Biol Chem 275:7459–7461
9. Deleted in proof
10. Zou H, McGarry TJ, Bernal T, Kirschner MW 1999 Identification of a vertebrate sister-chromatid separation inhibitor involved in transformation and tumorigenesis. Science 285:418–422
11. Lieblich JM, Weintraub BD, Krauth GH, Kohler PO, Rabson AS Rosen SW 1976 Ectopic and eutopic secretion of chorionic gonadotropin and its subunits *in vitro*: comparison of clonal strains from carcinomas of lung and placenta. J Natl Cancer Inst 56:911–917
12. Jameson JL, Jaffe RC, Gleason SL, Habener JF 1986 Transcriptional regulation of chorionic gonadotropin α- and β-subunit gene expression by 8-bromo-adenosine 3′,5′-monophosphate. Endocrinology 119:2560–2567
13. Ren SG, Braunstein GD 1991 Insulin stimulates synthesis and release of human chorionic gonadotropin by choriocarcinoma cell lines. Endocrinology 128:1623–1629
14. Cohen-Fix O, Peters JM, Kirschner MW, Koshland D 1996 Anaphase initiation in Saccharomyces cerevisiae is controlled by the APC-dependent degradation of the anaphase inhibitor Pds1p. Genes Dev 10:3081–3093
15. Funabiki H, Yamano H, Kumada K, Nagao K, Hunt T, Yanagida M 1996 Cut2 proteolysis required for sister-chromatid separation in fission yeast. Nature 381: 438–441
16. Ramos-Morales F, Dominguez A, Romero F, Luna R, Multon MC, Pintor-Toro JA, Tortolero M 2000 Cell cycle regulated expression, phosphorylation of **hpttg** proto-oncogene product. Oncogene 19:403–409
17. Kakar SS 1999 Molecular cloning, genomic organization, and identification of the promoter for the human pituitary tumor transforming gene (PTTG). Gene 240:317–324
18. Pei L 1998 Genomic organization and identification of an enhancer element containing binding sites for multiple proteins in rat pituitary tumor-transforming gene. J Biol Chem 273:5219–5225
19. Wang Z, Melmed S 2000 Characterization of the murine pituitary tumor transforming gene (PTTG), its promoter. Endocrinology 141:763–771
20. Mantovani R 1998 A survey of 178 NF-Y binding CCAAT boxes. Nucleic Acids Res 26:1135–1143
21. Kumada K, Nakamura T, Nagao K, Funabiki H, Nakagawa T, Yanagida M 1998 Cut1 is loaded onto the spindle by binding to Cut2 and promotes anaphase spindle movement upon Cut2 proteolysis. Curr Biol 8:633–641
22. Pei L 1999 Pituitary tumor-transforming gene protein associates with ribosomal protein S10 and a novel human homologue of DnaJ in testicular cells. J Biol Chem 274:3151–3158
23. King KL, Cidlowski JA 1998 Cell cycle regulation and apoptosis. Annu Rev Physiol 60:601–617
24. Uhlmann F, Lottspeich F, Nasmyth K 1999 Sister-chromatid separation at anaphase onset is promoted by cleavage of the cohesin subunit Scc1. Nature 400:37–42

STIC-ILL · · NOS

QP 620 .N8

381364

From: Canella, Karen
Sent: Sunday, February 03, 2002 9:00 PM
To: STIC-ILL
Subject: ill order 09/815,340

5788724

Art Unit 1642 Location 8E12(mail)

Telephone Number 308-8362

Application Number 09/815,340

1. Trends in Cell biology, 2001 Jan, 11(1):18-21
2. Clinical Cancer Research, 2000 Aug, 6(8):3215-3221
3. Mutation Research, 1997 Apr 29, 375(2):157-165
4. american Journal of Hematology, 1985 Mar, 18(3):243-249.
5. PNAS, 1989 Apr, 86(7):2276-2280
6. Genes and Development, 1996 Oct 15, 10(20):2621-2631
7. Cancer, 1975 Jun, 35(6):1664-1677
8. Mutation Research, 1978, 57(3): 313-324
9. Environ Mutagen, 1981, 3(1):53-64
10. Nucleic Acids Research, 2001 Mar 15, 29(6):1300-1307
11. Oncogene:
    1998 Oct 29, 17(17):2187-2193
    2000 Jan 20, 19(3):403-409
12. Molecular endocrinology, 1999 Jan, 13(1):156-166
13. Gene, 1999 Nov 29, 240(2):317-324
14. Science, 1999 Jul 16, 285(5426)418-422
15. Biochemistry and Molecular biology international, 1999 May, 47(5):891-897
16. Journal of Clinical Endocrinology and Metabolism, 1999 Mar, 84(3):1149-1152
17. Journal of biological chemistry:
    1999 Jan 29, 274(5):3151-3158
    2000 Nov 24, 275(47):36502-36505 ***
18. Gene 2000 May 2, 248(1-2):41-50
19. Molecular endocrinology, 2000 Aug, 14(8):1137-1146
20. Cancer Letters, 2001 Feb 10, 163(1):131-139
21. Brain Pathology, 2001 Jul, 11(3):328-341

1238996

1300–1307 Nucleic Acids Research, 2001, Vol. 29, No. 6

Human securin, hPTTG, is associated with Ku heterodimer, the regulatory subunit of the DNA-dependent protein kinase

Francisco Romero[1,*], Marie-Christine Multon[2], Francisco Ramos-Morales[1], África Domínguez[1], Juan A. Bernal[1,3], José A. Pintor-Toro[3] and María Tortolero[1]

[1]Departamento de Microbiología, Facultad de Biología, Universidad de Sevilla, Apdo. 1095, 41080-Sevilla, Spain, [2]Rhône-Poulenc Rorer, CRVA-Pasteur Building, 13 quai J. Guesde, 94403 Vitry-sur-Seine, France and [3]Instituto de Recursos Naturales y Agrobiología, Apdo. 1052, 41080-Sevilla, Spain

Received December 5, 2000; Revised and Accepted January 29, 2001

ABSTRACT

We have previously isolated the *hpttg* proto-oncogene, which is expressed in normal tissues containing proliferating cells and in several kinds of tumors. In fact, expression of hPTTG correlates with cell proliferation in a cell cycle-dependent manner. Recently it was reported that PTTG is a vertebrate analog of the yeast securins Pds1 and Cut2, which are involved in sister chromatid separation. Here we show that hPTTG binds to Ku, the regulatory subunit of the DNA-dependent protein kinase (DNA-PK). hPTTG and Ku associate both *in vitro* and *in vivo* and the DNA-PK catalytic subunit phosphorylates hPTTG *in vitro*. Furthermore, DNA double-strand breaks prevent hPTTG–Ku association and disrupt the hPTTG–Ku complexes, indicating that genome damaging events, which result in the induction of pathways that activate DNA repair mechanisms and halt cell cycle progression, might inhibit hPTTG–Ku interaction *in vivo*. We propose that hPTTG might connect DNA damage-response pathways with sister chromatid separation, delaying the onset of mitosis while DNA repair occurs.

INTRODUCTION

The pituitary tumor-transforming gene (*pttg*) was first isolated from clonal rat GH_4 pituitary tumor cells by differential display (1), but no homology with known protein sequences or common functional motifs was found. However, overexpression of *pttg* in NIH 3T3 fibroblasts showed that it induces cell transformation *in vitro*, and injection of these transfected cells into athymic nude mice resulted in tumor formation in all animals (1). The *pttg*-transfected NIH 3T3 cells also stimulated expression and secretion of basic fibroblast growth factor, a human pituitary tumor growth-regulating factor (2). Nevertheless, we found that the human counterpart of PTTG, hPTTG (which was firstly isolated by us; 3), is also expressed in other non-pituitary tumors. Samples from patients with leukemia, lymphoma or myelodysplastic diseases (3), as well as adenocarcinomas of mammary and pulmonary origins (4) showed strong *hpttg* expression. Our further studies demonstrate a correlation between *hpttg* expression and cell proliferation (5). The hPTTG protein level is up-regulated in rapidly proliferating cells, is down-regulated in response to serum starvation or cell confluence and is regulated in a cell cycle-dependent manner peaking in mitosis. In addition, hPTTG is phosphorylated by CDC2 during mitosis.

hPTTG is a protein of 202 residues partially localized in the nucleus that has a basic N-terminal portion and an acidic C-terminal portion (3). It has several putative SH3-binding sites (3) and a conserved motif localized in the N-terminal portion matches the destruction box (D-box) shared by many anaphase-promoting complex or cyclosome (APC/C) substrates (6). Recently, PTTG has been shown to be involved in sister chromatid separation (7). Precise coordination of multiple cell cycle events is required to ensure proper mitosis. Chromosome cohesion must be maintained until all chromosomes are attached to opposite poles of the mitotic spindle and aligned at the metaphase plate. At the onset of anaphase, the activity of separins contributes to the release of cohesins from chromosomes, allowing for the segregation of sister chromatids to opposite spindle poles. Separin activity is blocked by binding to a class of proteins known as securins, whose destruction at the metaphase-to-anaphase transition is triggered by the APC/C (8–12). PTTG has been identified as a vertebrate securin on the basis of its biochemical analogy to the Pds1 protein of budding yeast and the Cut2 protein of fission yeast (7). The vertebrate securins share extensive sequence similarity with each other but show no sequence similarity to either of their yeast counterparts. Nevertheless, as was previously reported in yeast, expression of a stable *Xenopus* securin mutant protein blocks sister chromatid separation (7). hPTTG bound to a putative human separin homolog of yeast separins Esp1 and Cut1, and was degraded by proteolysis mediated by APC/C in a D-box-dependent manner. The finding that a vertebrate securin has tumorigenic activity is somewhat anticipated because chromosome missegregation has been predicted to be a major source of genetic instability, with profound consequences for cancer (13). On the basis of its function, the simplest explanation is

*To whom correspondence should be addressed. Tel: +34 9545 57119; Fax: +34 9545 57830; Email: frport@cica.es

that tumor formation is the result of aneuploidy caused by defects in the sister chromatid separation (7,14).

To further understand the role of hPTTG in sister chromatid separation and tumorigenesis, we searched for proteins able to bind to hPTTG using the yeast two-hybrid approach (15). This *in vivo* strategy was employed to provide a physiological environment in which to detect potential interactions involving hPTTG, and in this paper we demonstrate that hPTTG physically associates with Ku-70.

The Ku-70 protein associates with Ku-80 to form a heterodimeric complex (16,17), and together with the ~470 kDa catalytic subunit, DNA-PKcs, form the DNA-dependent protein kinase (DNA-PK) (18). This enzyme is involved in repairing DNA double-strand breaks (DSBs) caused, for example, by physiological oxidation reactions, V(D)J recombination, ionizing radiation and certain chemotherapeutic drugs. Ku heterodimer binds to DNA ends and other types of discontinuity in double-stranded DNA (19). Ku itself is probably involved in stabilizing broken DNA ends, bringing them together and preparing them for ligation (20). Ku also recruits DNA-PKcs to DNA DSBs, activating its kinase function (21).

Our results demonstrate that hPTTG specifically interacts with Ku-70, which forms a complex with the Ku-70/Ku-80 heterodimer in intact cells, and that DNA-PKcs phosphorylates hPTTG *in vitro*. In addition, we show that hPTTG–Ku-70 association is prevented by DNA DSBs. The implications of these results, as well as a model of the regulation of hPTTG–Ku-70 interaction, are discussed.

MATERIALS AND METHODS

Plasmids and cloning

Wild-type *hpttg* (coding for 202 residues) and the subclones *hpttg-ES* (residues 1–188), *hpttg-EA* (residues 1–163), *hpttg-EXb* (residues 1–124) and *hpttg-XbXh* (residues 123–202), were cloned inframe with *gal4-DB* (DNA-binding) in the yeast pGBT9 vector (22) to yield pGBT9-hPTTG, pGBT9-hPTTG-ES, pGBT9-hPTTG-EA, pGBT9-hPTTG-EXb and pGBT9-hPTTG-XbXh, respectively. Plasmids pGBT-SNF1 and pGAD-SNF4 (22), carrying unrelated proteins, were used as controls for the two-hydrid screen.

hpttg, *hpttg-EA* and *hpttg-HXh* (residues 87–202) were cloned in frame with a *6His*-tag in the bacterial pRSET-A vector (Invitrogen). The hPTTG-EXb subclone, previously fused to glutathione-*S*-transferase (GST) in pGEX4T2 (3), was also used in the *in vitro* experiments. Plasmids pRSET-S6 (6His-ribosomal protein S6; Romero,F. and Tortolero,M. unpublished results), pRSET-RIIα (23), pRSET-ΔGMAP (residues 618–803) (24) and pGEX (Pharmacia) were used as controls of the *in vitro* experiments.

Library screening

Saccharomyces cerevisiae strain Hf7c (*MATa trp1-901 leu2-3,112 his3-200 ura3-52 lys-801 ade2-101 canr gal4-542 gal80-538 LYS2::GAL1-HIS3 URA3::Gal4 binding site-CYC1-lacZ*) was grown at 30°C in YPD medium containing 1% yeast extract, 2% polypeptone and 2% glucose, and sequentially transformed with pGBT9-hPTTG-EA and a Jurkat cell oligo-dT cDNA library (25). Double transformants were plated on yeast drop-out medium lacking Trp, Leu and His (26). They were grown for 5 days at 30°C and then colonies were patched on the same medium and replica-plated on Whatman 40 filters to test for β-galactosidase activity (27). Positive clones were rescued and tested for specificity by retransformation into Hf7c either with pGBT9-hPTTG-EA or with extraneous targets (pGBT-SNF1 or pGBT9) (22). pGAD-Raf (28), pGAD-Sos1 (29), pGAD-hnRNP C (30), pGAD-hnRNP K (Romero,F., Ramos-Morales,F. and Tortolero,M., unpublished results), pGAD-Csk (31), pGAD-Lck (31), pGAD-Sumo (provided by Dr A. Germani, INSERM, Paris, France), pGAD-hPTTG (3) and pGAD-FcγRII(ID) (Romero,F., unpublished results) were also used to test the specificity of hPTTG interactions.

Sequence analysis

Sequences of cDNA inserts from positive clones of the two-hybrid screening were performed on both strands with an automatic sequencer (Pharmacia) using the Sanger dideoxy-termination method (32). Sequence comparisons were done with the BLAST 2.0 program (33).

Cell culture and lysis

HL-60 and Jurkat cells were grown in RPMI 1640 medium and Cos and HeLa cells in Dulbecco's modified Eagle's medium (BioWhittaker), supplemented with 10% heat-inactivated fetal calf serum (Gibco BRL), 2 mM L-glutamine, 100 U/ml penicillin and 100 µg/ml streptomycin (BioWhittaker), in a 5% CO_2 humidified atmosphere at 37°C. Cell lysis was performed with 5×10^7–10^8 cells/ml at 4°C in 150 mM NaCl, 10 mM Tris–HCl (pH 7.5), 1% Nonidet P-40 (NP-40), 10% glycerol, 1 mM Na-vanadate, 20 mM Na-pyrophosphate, 5 mM Na-fluoride, 1% aprotinin, 1 mM phenylmethylsulfonyl fluoride (PMSF), 1 µg/ml pepstatin and 1 µg/ml leupeptin for 20 min. The extract was centrifuged at 20 000 *g* for 20 min and the supernatant frozen in liquid nitrogen and stored at –80°C.

Induction of differentiation in HL-60 cells

HL-60 cells were diluted to 2×10^5 cells per ml and 40 ng/ml phorbol 12-myristate 13-acetate (PMA) or the vehicle dimethyl sulfoxide (DMSO) added. Cells were grown under standard conditions in bacteriological Petri plates for 24–48 h. We took attached cells to be differentiated cells, since attachment is an indicator of macrophage phenotype (34). As control cells we used untreated or DMSO-treated cells.

Electrophoresis and western blot analysis

Proteins were separated by SDS–PAGE and gels were electroblotted onto nitrocellulose membranes and probed with the different antibodies. Peroxidase-coupled anti-rabbit IgG from donkey and anti-mouse IgG from sheep were from Amersham. Immunoreactive bands were visualized using an enhanced chemiluminescence western blotting system (Amersham) according to the manufacturer's protocol.

Antibodies

Anti-hPTTG polyclonal antibody was produced by us (3), N3H10 (anti-Ku-70), 111 (anti-Ku-80) and 162 (anti-dimer Ku-70/Ku-80) monoclonal antibodies were provided by Dr W.H.Reeves (University of North Carolina) (35), and anti-Gal4-BD was from Clontech.

Affinity chromatography

Expression of the 6His fusion proteins was induced in *Escherichia coli* BL21 (DE3) by addition of 1 mM isopropyl-β-D-thiogalactoside (IPTG) and the fusion proteins isolated from bacterial lysates with Talon resin (Clontech). Cellular lysates (10^6–10^7 cells) were incubated for 2 h with fusion proteins (100–500 ng) bound to Talon resin. Resin was washed six times in lysis buffer and proteins eluted into SDS sample buffer at 95°C for 5 min and subjected to SDS–PAGE.

When indicated, fusion proteins were eluted from resin with 50 mM EDTA and dialyzed against 50 mM $NaHCO_3$ and 150 mM NaCl pH 7.5.

To study the effect of DNA DSBs, lysates from Cos or HL-60 cells were preincubated for 30 min at 4°C with sonicated salmon sperm DNA, pUC18 or pGBT9, supercoiled or digested with *Eco*RI at 100–200 μg/ml, and used for the *in vitro* experiments. In some experiments, DNA was added to hPTTG/Ku-70 complexes previously bound to Talon resin.

GST fusion proteins were produced and purified as described (3).

Co-immunoprecipitation experiments

Cellular lysates from HL-60 cells ($1.5–3 \times 10^7$) were incubated with preimmune serum for 30 min and protein A–Sepharose beads (Pharmacia Biotech Inc.) for 1 h at 4°C. After centrifugation, beads were discarded and supernatants incubated for 3 h with polyclonal anti-hPTTG or preimmune serum, followed by protein A–Sepharose beads for 1 h. Beads were washed six times with lysis buffer and bound proteins were dissolved into SDS sample buffer at 95°C for 5 min and subjected to SDS–PAGE.

In vitro kinase assays

Phosphorylation of hPTTG by DNA-PK. Purified DNA-PKcs–Ku complex (Promega) was incubated with eluted 6His-hPTTG (or derivative subclones) in the presence or absence of sonicated DNA (10 μg/ml) and with [γ-^{32}P]ATP and DNA-PK kinase buffer (12.5 mM HEPES pH 7.5, 25 mM KCl, 6.5 mM $MgCl_2$, 0.2 mM unlabeled ATP, 1 mM spermidine, 10% glycerol, 0.05% NP-40 and 0.5 mM DTT) for 15 min at 30°C. Reactions were terminated by adding 4× SDS sample buffer, and proteins analyzed by SDS–PAGE and autoradiography.

Phosphorylation of hPTTG by anti-dimer Ku-70/Ku-80 immunoprecipitates. HL-60 or HeLa cells were washed once with PBS and frozen. The cell pellets were later thawed and sonicated at 2×10^7 cells/ml in 50 mM NaCl-free Tris–HCl pH 7.5, 2 mM EDTA, 0.3% NP-40, 1 mM Na-vanadate, 20 mM Na-pyrophosphate, 5 mM Na-fluoride, 1% aprotinin, 1 mM PMSF, 1 μg/ml pepstatin and 1 μg/ml leupeptin, and the extracts were cleared twice by centrifugation at 13000 *g* for 15 min followed by immunoprecipitation with mAb 162. After incubation with protein A–Sepharose beads, the beads were washed three times with NET-NP-40 buffer (150 mM NaCl, 2 mM EDTA, 50 mM Tris–HCl pH 7.5 and 0.3% NP-40) and once with kinase buffer and stored at –80°C. *In vitro* kinase assays were performed as indicated above.

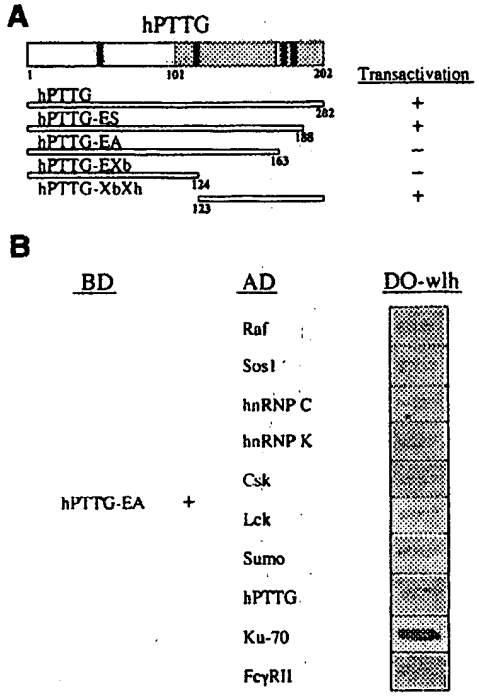

Figure 1. Interaction of Ku-70 with hPTTG using the two-hybrid system. (**A**) Schematic representation of hPTTG and study of the transcriptional activity of several hPTTG subclones. hPTTG protein can be divided into a basic N-terminal portion (residues 1–101) and an acidic C-terminal portion (residues 102–202). The four Pro-X-X-Pro motifs (black bars), putative binding sites for SH3-containing proteins and the CDC2 phosphorylation site (white bar) are also indicated. Several fragments of *hpttg* were subcloned in pGBT9 and their transactivation activity tested in Hf7c reporter strain. +, Growth in the absence of histidine and with or without 5 mM of 3-amino-1,2,4-triazole. –, Absence of growth in the same medium. (**B**) hPTTG associates specifically with Ku-70. Hf7c reporter strain was cotransformed with the indicated plasmids. The interaction between the two-hybrid proteins is indicated by growth in the absence of histidine (DO-wlh) (dark grey patch). BD, fusion with the DNA BD of Gal4. AD, fusion of the activation domain of Gal4.

RESULTS

Isolation of proteins interacting with hPTTG

We recently isolated *hpttg* cDNA, which codes for a protein highly expressed in proliferating cells and is involved in sister chromatid separation and tumorigenesis (1,3,7). To elucidate the molecular mechanisms that involve hPTTG in these cellular functions, we searched for proteins that interact with hPTTG using the yeast two-hybrid system with Gal4 recognition sites regulating expression of both *His3* and *LacZ* (22). Because full-length hPTTG fused to the DNA-binding domain (BD) of Gal4 in pGBT9 had shown a strong transactivation activity in yeast (3), we subcloned several fragments of *hpttg* in pGBT9 to find the longest without this transcriptional activity. As shown in Figure 1A, strain Hf7c transformed with pGBT9-hPTTG-EA was not able to grow in selective medium, although this fusion protein was well produced in yeast as detected by western blot with anti-Gal4-BD antibody (data not shown). This strain was retransformed with a Jurkat cell oligo-dT cDNA library constructed in pGAD1318 (25) to find clones

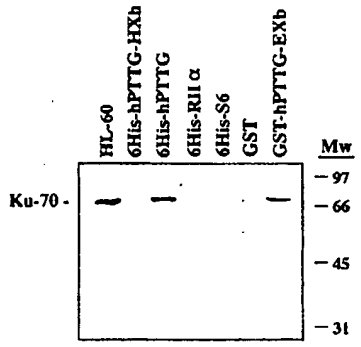

Figure 2. hPTTG interacts with Ku-70 *in vitro*. Expression of the 6His and GST fusion proteins was induced by addition of IPTG. Proteins were purified from bacterial lysates on Talon resin or glutathione–agarose beads. Fusion proteins were incubated with NP-40 extracts from HL-60 cells (5×10^6) and their associations with Ku-70 were determined by immunoblotting with anti-Ku-70 (N3H10) antibody. HL-60, extract from 5×10^5 HL-60 cells. Mw, molecular weights expressed in kDa. These interactions were detected with different amounts of fusion proteins (between 100 and 500 ng).

able to grow in the absence of histidine. We screened about one million clones and we found a positive clone that specifically interacts with hPTTG-EA. The nucleotide sequence showed that this clone codes for Ku-70 (residues 291–609). This protein forms a heterodimeric complex with Ku-80, which is the DNA-binding component of DNA-PK. This enzyme is involved in DNA repair and V(D)J recombination (36). Furthermore, the specificity of hPTTG/Ku-70 interaction was illustrated by the lack of reporter gene activation when hPTTG-EA association was assayed with cytosolic proteins (Raf or Sos1), protein kinases (Lck or Csk), nuclear proteins (hnRNP C or hnRNP K), the intracellular domain of a receptor (FcγRII), a ubiquitin-related protein (Sumo) or itself (Fig. 1B). Therefore, by using the two-hybrid system, we show that hPTTG interacts with Ku-70.

hPTTG interacts with Ku-70 from cellular extracts

To validate the results obtained with the yeast two-hybrid system, the interaction of hPTTG with Ku-70 was studied by *in vitro* binding experiments. Full-length *hpttg* and *hpttg-HXh* were cloned in frame with a *6His*-tag in pRSET-A and purified from bacterial lysates by affinity chromatography on Talon resin. Lysates from HL-60 cells were incubated with the resin bound to 6His fusion proteins, the resin was washed and the eluted proteins resolved on gels and immunoblotted with an anti-Ku-70 monoclonal antibody. Figure 2 clearly shows that the Ku-70 protein from cellular extracts interacts with 6His-hPTTG, whereas there is no interaction with 6His-hPTTG-HXh or with irrelevant fusion proteins (6His-S6, 6His-RIIα or GST). Similar results were obtained with lysates from Jurkat, Cos and HeLa cells (data not shown). These results indicate that hPTTG and Ku-70 also interact *in vitro*. Furthermore, the finding that 6His-hPTTG-HXh, which lacks the 86 N-terminal residues of hPTTG, no longer interacted with Ku-70 suggests that the N-terminal portion of hPTTG is responsible for the association with Ku-70. In fact, the GST-hPTTG-EXb fusion protein, containing the N-terminal moiety of hPTTG, was able to interact with Ku-70 (Fig. 2).

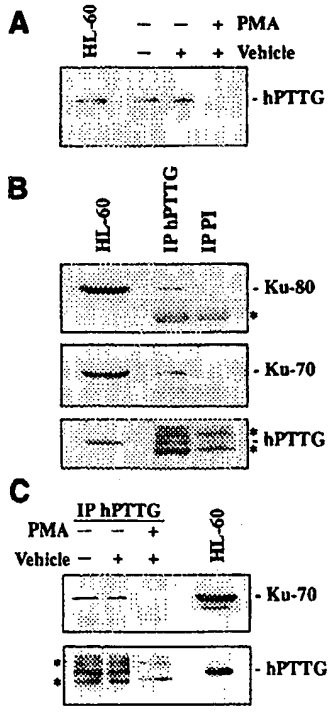

Figure 3. Binding of hPTTG to Ku-70 in intact cells. (**A**) Expression of hPTTG in differentiated and undifferentiated HL-60 cells. Equal amounts of total extracts from HL-60 cells treated with PMA (40 ng/ml), with the vehicle DMSO or untreated, were separated by SDS–PAGE, transferred to nitrocellulose filters and incubated with anti-hPTTG. HL-60, extract from 10^6 HL-60 cells. (**B**) Co-immunoprecipitation of hPTTG with Ku-70 and Ku-80 in undifferentiated HL-60 cells. Anti-hPTTG and preimmune (PI) sera were used to immunoprecipitate from NP-40 extracts of HL-60 cells (3×10^7 cells each). Complexes were resolved by SDS–PAGE, transferred to nitrocellulose filters and incubated with anti-Ku-70, anti-Ku-80 and anti-hPTTG. HL-60, extract from 10^6 HL-60 cells. (**C**) Study of the relevance of the hPTTG–Ku-70 interaction. Anti-hPTTG was used to immunoprecipitate from extracts of HL-60 cells (3×10^7) treated with PMA (40 ng/ml), the vehicle DMSO or untreated. Nitrocellulose filters were incubated with anti-Ku-70 and anti-hPTTG. HL-60, extract from 10^6 HL-60 cells. Asterisks indicate the IgG heavy and light chains.

hPTTG and Ku-70 form a complex in intact cells

hpttg is expressed in tissues that contain highly proliferating cells, and, in fact, we can establish a correlation between *hpttg* expression and cell proliferation (5). For this reason, we used the HL-60 cell line as an appropriate experimental model to study the *in vivo* protein complexes involving hPTTG. These cells respond to specific chemical stimuli by acquiring either a granulocyte- (37), monocyte- or macrophage-like phenotype (34). The acquisition of mature phenotypes can be demonstrated by a variety of differentiation markers and leads to growth arrest. As shown in Figure 3A, hPTTG protein is absent in HL-60 cells treated with PMA, which induces a macrophage-like differentiation. Therefore, we have a good model to examine the relevance of the hPTTG interactions.

Stable transfection of NIH 3T3 cells with *pttg* cDNA causes anchorage-independent transformation *in vitro* and induces *in vivo* tumor formation when transfectants are injected into athymic mice (1). This suggests that misregulation of chromatid separation may contribute to generation of malignant tumors (7). In this way, inactivation of the *ku-70* gene also leads to a propensity for malignant transformation (58). *ku-70*$^{-/-}$ mice develop T cell lymphomas and karyotyping analyses on cultured cells derived from primary T cell lymphomas reveal multiple chromosomal abnormalities (monosomies, trisomies, duplications, etc.). This might be explained *in vivo*, at least in part, in terms of an increased rate of sister chromatid exchange, but we cannot eliminate the possibility that defects in sister chromatid separation also play a role. Therefore, both defective regulation of hPTTG and inactivation of the *ku-70* gene facilitate neoplastic growth.

To summarize, our studies show that the human securin/hPTTG is associated with the DNA-dependent protein kinase both *in vitro* and *in vivo* and that it is phosphorylated by DNA-PKcs. Our data also demonstrate that DNA DSBs prevent hPTTG–Ku-70 association. Together, these observations suggest that hPTTG might connect the DNA damage–response pathway with sister chromatid separation.

ACKNOWLEDGEMENTS

This work was supported by grants from Ministerio de Educación y Cultura (MEC) of Spain (SAF99-0125-C03-01), from DGUI of the Junta de Andalucía and from Rhône-Poulenc Rorer (Paris, France). F.R. was supported by post-doctoral fellowships from the EU and Spanish MEC.

REFERENCES

1. Pei,L. and Melmed,S. (1997) Isolation and characterization of a pituitary tumor-transforming gene (PTTG). *Mol. Endocrinol.*, **11**, 433–441.
2. Zhang,X., Horwitz,G.A., Prezant,T.R., Valentini,A., Nakashima,M., Bronstein,M.D. and Melmed,S. (1999) Structure, expression and function of human pituitary tumor-transforming gene (PTTG). *Mol. Endocrinol.*, **13**, 156–166.
3. Dominguez,A., Ramos-Morales,F., Romero,F., Rios,R.M., Dreyfus,F., Tortolero,M. and Pintor-Toro,J.A. (1998) hpttg, a human homologue of rat pttg, is overexpressed in hematopoietic neoplasms. Evidence for a transcriptional activation function of hPTTG. *Oncogene*, **17**, 2187–2193.
4. Saez,C., Japon,M.A., Ramos-Morales,F., Romero,F., Segura,D.I., Tortolero,M. and Pintor-Toro,J.A. (1999) hpttg is over-expressed in pituitary adenomas and other primary epithelial neoplasias. *Oncogene*, **18**, 5473–5476.
5. Ramos-Morales,F., Dominguez,A., Romero,F., Luna,R., Multon,M.C., Pintor-Toro,J.A. and Tortolero,M. (2000) Cell cycle regulated expression and phosphorylation of hpttg proto-oncogene product. *Oncogene*, **19**, 403–409.
6. King,R.W., Glotzer,M. and Kirschner,M.W. (1996) Mutagenic analysis of the destruction signal of mitotic cyclins and structural characterization of ubiquitinated intermediates. *Mol. Biol. Cell*, **7**, 1343–1357.
7. Zou,H., McGarry,T.J., Bernal,T. and Kirschner,M.W. (1999) Identification of a vertebrate sister-chromatid separation inhibitor involved in transformation and tumorigenesis. *Science*, **285**, 418–422.
8. Biggins,S. and Murray,A.W. (1999) Sister chromatid cohesion in mitosis. *Curr. Opin. Genet. Dev.*, **9**, 230–236.
9. Morgan,D.O. (1999) Regulation of the APC and the exit from mitosis. *Nature Cell. Biol.*, **1**, E47–E53.
10. Nasmyth,K. (1999) Separating sister chromatids. *Trends Biochem. Sci.*, **24**, 98–104.
11. Zachariae,W. (1999) Progression into and out of mitosis. *Curr. Opin. Cell. Biol.*, **11**, 708–716.
12. Zachariae,W. and Nasmyth,K. (1999) Whose end is destruction: cell division and the anaphase-promoting complex. *Genes Dev.*, **13**, 2039–2058.
13. Lengauer,C., Kinzler,K.W. and Vogelstein,B. (1998) Genetic instabilities in human cancers. *Nature*, **396**, 643–649.
14. Orr-Weaver,T.L. (1999) The difficulty in separating sisters. *Science*, **285**, 344–345.
15. Fields,S. and Song,O. (1989) A novel genetic system to detect protein–protein interactions. *Nature*, **340**, 245–246.
16. Koike,M., Awaji,T., Kataoka,M., Tsujimoto,G., Kartasova,T., Koike,A. and Shiomi,T. (1999) Differential subcellular localization of DNA-dependent protein kinase components Ku and DNA-PKcs during mitosis. *J. Cell Sci.*, **112**, 4031–4039.
17. Wu,X. and Lieber,M.R. (1996) Protein–protein and protein–DNA interaction regions within the DNA end-binding protein Ku70-Ku86. *Mol. Cell. Biol.*, **16**, 5186–5193.
18. Jin,S. and Weaver,D.T. (1997) Double-strand break repair by Ku70 requires heterodimerization with Ku80 and DNA binding functions. *EMBO J.*, **16**, 6874–6885.
19. Blier,P.R., Griffith,A.J., Craft,J. and Hardin,J.A. (1993) Binding of Ku protein to DNA. Measurement of affinity for ends and demonstration of binding to nicks. *J. Biol. Chem.*, **268**, 7594–7601.
20. Ramsden,D.A. and Gellert,M. (1998) Ku protein stimulates DNA end joining by mammalian DNA ligases: a direct role for Ku in repair of DNA double-strand breaks. *EMBO J.*, **17**, 609–614.
21. Gottlieb,T.M. and Jackson,S.P. (1993) The DNA-dependent protein kinase: requirement for DNA ends and association with Ku antigen. *Cell*, **72**, 131–142.
22. Chien,C.T., Bartel,P.L., Sternglanz,R. and Field,S. (1991) The two-hybrid system: a method to identify and clone genes for proteins that interact with a protein of interest. *Proc. Natl Acad. Sci. USA*, **88**, 9578–9582.
23. Martin,M.E., Hidalgo,J., Vega,F.M. and Velasco,A. (1999) Trimeric G proteins modulate the dynamic interaction of PKAII with the Golgi complex. *J. Cell Sci.*, **112**, 3869–3878.
24. Infante,C., Ramos-Morales,F., Fedriani,C., Bornens,M. and Rios,R.M. (1999) GMAP-210, A *cis*-Golgi network-associated protein, is a minus end microtubule-binding protein. *J. Cell Biol.*, **145**, 83–98.
25. Romero,F., Dargemont,C., Pozo,F., Reeves,W.H., Camonis,J., Gisselbrecht,S. and Fischer,S. (1996) p95vav associates with the nuclear protein Ku-70. *Mol. Cell. Biol.*, **16**, 37–44.
26. Sherman,F., Fink,G.R. and Hicks,J.B. (1986) *Methods in Yeast Genetics*. Cold Spring Harbor Laboratory Press, Cold Spring Harbor, NY.
27. Breeden,L. and Nasmyth,K. (1985) Regulation of the yeast HO gene. *Quant. Biol.*, **50**, 643–650.
28. van Aelst,L., Barr,M., Marcus,S., Polverino,A. and Wigler,M. (1993) Complex formation between RAS and RAF and other protein kinases. *Proc. Natl Acad. Sci. USA*, **90**, 6213–6217.
29. Chardin,P., Camonis,J.H., Gale,N.W., van Aelst,L., Schlessinger,J., Wigler,M.H. and Bar-Sagi,D. (1993) Human Sos1: a guanine nucleotide exchange factor for Ras that binds to Grb2. *Science*, **260**, 1338–1343.
30. Romero,F., Germani,A., Puvion,E., Camonis,J., Varin-Blank,N., Gisselbrecht,S. and Fischer,S. (1998) Vav binding to heterogeneous nuclear ribonucleoprotein (hnRNP) C. Evidence for Vav-hnRNP interactions in an RNA-dependent manner. *J. Biol. Chem.*, **273**, 5923–5931.
31. Bougeret,C., Delaunay,T., Romero,F., Jullien,P., Sabe,H., Hanafusa,H., Benarous,R. and Fischer,S. (1996) Detection of a physical and functional interaction between Csk and Lck which involves the SH2 domain of Csk and is mediated by autophosphorylation of Lck on tyrosine 394. *J. Biol. Chem.*, **271**, 7465–7472.
32. Sanger,F., Nicklen,S. and Coulson,A.R. (1977) DNA sequencing with chain-terminating inhibitors. *Proc. Natl Acad. Sci. USA*, **74**, 5463–5467.
33. Gish,W. and States,D.J. (1993) Identification of protein coding regions by database similarity search. *Nature Genet.*, **3**, 266–272.
34. Murao,S., Gemmell,M.A., Callaham,M.F., Anderson,N.L. and Huberman,E. (1983) Control of macrophage cell differentiation in human promyelocytic HL-60 leukemia cells by 1,25-dihydroxyvitamin D3 and phorbol-12-myristate-13-acetate. *Cancer Res.*, **43**, 4989–4996.
35. Reeves,W.H., Satoh,M., Wang,J. and Ajmani,A.K. (1994) In van Venrooij,W.J. and Maini,R.N. (eds), *Manual of Biological Markers of Disease*. Kluwer Academic Publishers, Dordrecht, The Netherlands, pp. 1–22.
36. Smith,G.C. and Jackson,S.P. (1999) The DNA-dependent protein kinase. *Genes Dev.*, **13**, 916–934.

37. Collins,S.J., Bodner,A., Ting,R. and Gallo,R.C. (1980) Induction of morphological and functional differentiation of human promyelocytic leukemia cells (HL-60) by componuds which induce differentiation of murine leukemia cells. *Int. J. Cancer*, **25**, 213–218.
38. Zernik-Kobak,M., Vasunia,K., Connelly,M., Anderson,C.W. and Dixon,K. (1997) Sites of UV-induced phosphorylation of the p34 subunit of replication protein A from HeLa cells. *J. Biol. Chem.*, **272**, 23896–23904.
39. Watanabe,F., Teraoka,H., Iijima,S., Mimori,T. and Tsukada,K. (1994) Molecular properties, substrate specificity and regulation of DNA-dependent protein kinase from Raji Burkitt's lymphoma cells. *Biochim. Biophys. Acta*, **1223**, 255–260.
40. Pines,J. (1999) Four-dimensional control of the cell cycle. *Nature Cell Biol.*, **1**, E73–E79.
41. Holloway,S.L., Glotzer,M., King,R.W. and Murray,A.W. (1993) Anaphase is initiated by proteolysis rather than by the inactivation of maturation-promoting factor. *Cell*, **73**, 1393–1402.
42. Nigg,E.A., Blangy,A. and Lane,H.A. (1996) Dynamic changes in nuclear architecture during mitosis: on the role of protein phosphorylation in spindle assembly and chromosome segregation. *Exp. Cell Res.*, **229**, 174–180.
43. Cohen-Fix,O., Peters,J.M., Kirschner,M.W. and Koshland,D. (1996) Anaphase initiation in *Saccharomyces cerevisiae* is controlled by the APC-dependent degradation of the anaphase inhibitor Pds1p. *Genes Dev.*, **10**, 3081–3093.
44. Funabiki,H., Yamano,H., Kumada,K., Nagao,K., Hunt,T. and Yanagida,M. (1996) Cut2 proteolysis required for sister-chromatid seperation in fission yeast. *Nature*, **381**, 438–441.
45. Toth,A., Ciosk,R., Uhlmann,F., Galova,M., Schleiffer,A. and Nasmyth,K. (1999) Yeast cohesin complex requires a conserved protein, Eco1p(Ctf7), to establish cohesion between sister chromatids during DNA replication. *Genes Dev.*, **13**, 320–333.
46. Waizenegger,I.C., Hauf,S., Meinke,A. and Peters,J.M. (2000) Two distinct pathways remove mammalian cohesin from chromosome arms in prophase and from centromeres in anaphase. *Cell*, **103**, 399–410.
47. Featherstone,C. and Jackson,S.P. (1999) DNA double-strand break repair. *Curr. Biol.*, **9**, R759–R761.
48. Lieber,M.R. (1999) The biochemistry and biological significance of nonhomologous DNA end joining: an essential repair process in multicellular eukaryotes. *Genes Cells*, **4**, 77–85.
49. Cohen-Fix,O. and Koshland,D. (1997) The anaphase inhibitor of *Saccharomyces cerevisiae* Pds1p is a target of the DNA damage checkpoint pathway. *Proc. Natl Acad. Sci. USA*, **94**, 14361–14366.
50. Bentley,N.J. and Carr,A.M. (1997) DNA structure-dependent checkpoints in model systems. *Biol. Chem.*, **378**, 1267–1274.
51. Kumada,K., Nakamura,T., Nagao,K., Funabiki,H., Nakagawa,T. and Yanagida,M. (1998) Cut1 is loaded onto the spindle by binding to Cut2 and promotes anaphase spindle movement upon Cut2 proteolysis. *Curr. Biol.*, **8**, 633–641.
52. Nagase,T., Seki,N., Ishikawa,K., Tanaka,A. and Nomura,N. (1996) Prediction of the coding sequences of unidentified human genes. V. The coding sequences of 40 new genes (KIAA0161-KIAA0200) deduced by analysis of cDNA clones from human cell line KG-1. *DNA Res.*, **3**, 17–24.
53. Funabiki,H., Kumada,K. and Yanagida,M. (1996) Fission yeast Cut1 and Cut2 are essential for sister chromatid separation, concentrate along the metaphase spindle and form large complexes. *EMBO J.*, **15**, 6617–6628.
54. West,R.B., Yaneva,M. and Lieber,M.R. (1998) Productive and nonproductive complexes of Ku and DNA-dependent protein kinase at DNA termini. *Mol. Cell. Biol.*, **18**, 5908–5920.
55. Kirk,K.E., Harmon,B.P., Reichardt,I.K., Sedat,J.W. and Blackburn,E.H. (1997) Block in anaphase chromosome separation caused by a telomerase template mutation. *Science*, **275**, 1478–1481.
56. Bailey,S.M., Meyne,J., Chen,D.J., Kurimasa,A., Li,G.C., Lehnert,B.E. and Goodwin,E.H. (1999) DNA double-strand break repair proteins are required to cap the ends of mammalian chromosomes. *Proc. Natl Acad. Sci. USA*, **96**, 14899–14904.
57. Boulton,S.J. and Jackson,S.P. (1998) Components of the Ku-dependent non-homologous end-joining pathway are involved in telomeric length maintenance and telomeric silencing. *EMBO J.*, **17**, 1819–1828.
58. Li,G.C., Ouyang,H., Li,X., Nagasawa,H., Little,J.B., Chen,D.J., Ling,C.C., Fuks,Z. and Cordon-Cardo,C. (1998) Ku70: a candidate tumor suppressor gene for murine T cell lymphoma. *Mol. Cell*, **2**, 1–8.

STIC-ILL Vol IV

From: Canella, Karen
Sent: Sunday, February 03, 2002 9:00 PM
To: STIC-ILL
Subject: ill order 09/815,340

381360

Art Unit 1642 Location 8E12(mail)

Telephone Number 308-8362

5788790

Application Number 09/815,340

1. Trends in Cell biology, 2001 Jan, 11(1):18-21
2. Clinical Cancer Research, 2000 Aug, 6(8):3215-3221
3. Mutation Research, 1997 Apr 29, 375(2):157-165
4. american Journal of Hematology, 1985 Mar, 18(3):243-249.
5. PNAS, 1989 Apr, 86(7):2276-2280
6. Genes and Development, 1996 Oct 15, 10(20):2621-2631
7. Cancer, 1975 Jun, 35(6):1664-1677
8. Mutation Research, 1978, 57(3): 313-324
9. Environ Mutagen, 1981, 3(1):53-64
10. Nucleic Acids Research, 2001 Mar 15, 29(6):1300-1307
11. Oncogene:
    1998 Oct 29, 17(17):2187-2193
    2000 Jan 20, 19(3):403-409
12. Molecular endocrinology, 1999 Jan, 13(1):156-166
13. Gene, 1999 Nov 29, 240(2):317-324
14. Science, 1999 Jul 16, 285(5426)418-422
15. Biochemistry and Molecular biology international, 1999 May, 47(5):891-897
16. Journal of Clinical Endocrinology and Metabolism, 1999 Mar, 84(3):1149-1152
17. Journal of biological chemistry:
    1999 Jan 29, 274(5):3151-3158
    2000 Nov 24, 275(47):36502-36505 ***
18. Gene 2000 May 2, 248(1-2):41-50
19. Molecular endocrinology, 2000 Aug, 14(8):1137-1146
20. Cancer Letters, 2001 Feb 10, 163(1):131-139
21. Brain Pathology, 2001 Jul, 11(3):328-341

2058155

American Journal of Hematology 18:243–249 (1985)

Treatment of the Blastic Transformation of Chronic Granulocytic Leukemia Using High Dose BCNU Chemotherapy and Cryopreserved Autologous Peripheral Blood Stem Cells

Daniel D. Karp, Leroy M. Parker, Neil Binder, Ramana Tantravahi, Brian R. Smith, Thomas J. Ervin, and George P. Canellos

Dana Farber Cancer Institute and Brigham and Women's Hospital, Harvard Medical School, Boston

Seven nonsplenectomized patients with blastic CGL have received high dose BCNU chemotherapy followed by cryopreserved peripheral blood stem cells (PBSC). The PBSC obtained at diagnosis were stored in the vapor phase of liquid nitrogen in 10% dimethyl sulfoxide for 11–46 months prior to use. Patients received 2.9×10^8 (1.9–7.8) thawed washed mononuclear cells/kg over 30 minutes with minimal morbidity. One patient was not rendered pancytopenic and died with blastic leukemia at 4 months. One patient, previously treated with daily busulfan, died of progressive hepatic failure 2 months after high dose BCNU. Restoration of the chronic phase of CGL was observed in the remaining five patients. Peripheral blood counts returned to normal ranges after a median of 19 days. Median survival for all patients is 11 months. Cytogenetic studies revealed elimination of acquired aneuploid cell lines in four of seven patients with persistence of Ph^1. We conclude that: 1) frozen PBSC retain their viability for up to 4 years after cryopreservation and 2) the use of autologous PBSC following ablative chemotherapy may be associated with both symptomatic and karyotypic improvement in patients with blastic CGL.

Key words: chronic granulocytic leukemia, treatment, blastic phase, autologous stem cells, cryopreservation

INTRODUCTION

Autologous bone marrow infusion has been shown to shorten the duration of myelosuppression induced by high doses of certain chemotherapeutic agents and total body irradiation [1]. Goldman et al have demonstrated that large numbers of peripheral blood mononuclear cells, collected and cryopreserved during the chronic phase of chronic granulocytic leukemia (CGL), can reduce the duration of myelosuppression from chemoradiotherapy for blast transformation and restore the chronic phase of the

Received for publication February 7, 1984; accepted July 19, 1984.

This work was supported by NIH Grant No. PO1-CA19589 and a Junior Faculty Clinical Fellowship of the American Cancer Society #JFCF 614 (D.D.K.).

Address reprint requests to Daniel D. Karp, M.D., Director of Clinical Hematology, Boston V.A. Medical Center, 150 South Huntington Avenue, Jamaica Plain, MA 02130.

disease [2–5]. Previous investigation has shown that the alkylating agents as a group are all capable of inhibiting hematopoietic stem cell proliferation, but bischloroethylnitrosourea (BCNU) was especially effective in suppressing spleen colony units in mice [6]. High doses of BCNU followed by cryopreserved or nonfrozen bone marrow infusion have been used in the treatment of solid tumors in man [7–9]. We now report our experience in the treatment of seven patients in the blastic phase of CGL who received BCNU-based combination chemotherapy followed by infusion of cryopreserved autologous peripheral blood mononuclear cells.

PATIENTS AND METHODS

All patients had CGL with a single Ph^1 chromosome at the time of diagnosis. Patient characteristics are shown in Table I. There were four males and three females. They ranged in age from 15 to 62 (median age 47 years). Leukapheresis was carried out at the time of diagnosis or two weeks after chemotherapy was discontinued. The goal of leukapheresis was the collection of 1×10^{11} peripheral blood nucleated cells per patient. This number could easily be obtained in a single 3-hour session if the total WBC was greater than 100,000/μl and was chosen because it allowed for two or more courses of treatment at cell doses approaching 1×10^9 cells per kilogram, a range shown by Goldman et al to be effective [10]. The median number collected, using the IBM 2997 or Haemonetics Model 30 Cell Separators was 1.3×10^{11} and ranged from 0.5 to 2.0×10^{11}.

The technique for cryopreservation is a modification of that previously described for bone marrow [11, 12]. Cells were transferred (in the range of 2.0–5.0 $\times$ 10^8/ml) to polyolefin bags (Ucar 2030-2) in a medium consisting of 20–50% autologous plasma, Hank's basic salt solution, and 10% dimethylsulfoxide (DMSO). After stabilizing at 4°C, they were then frozen at −1°C per minute to −40°C in a Planer controlled-rate freezer (Polaron Instruments, Doylestown, PA) and then manually dropped to −80°C before being transferred to the vapor phase of liquid nitrogen. The median time of storage (in limited access cryogenic refrigerators) was 23 months and ranged from 9 to 46 months.

TABLE I. Patient Characteristics and Outcome

Patient I.D.	Number of months to blast crisis from diagnosis	Karyotypes pre- and post treatment		Return to chronic phase	Survival (mo.) from initial transplant
		Pre-RX	Post-RX		
1. 56 M[a]	18	Ph1/iso17	Ph1/iso17	+	14
2. 62 M[b]	9	47 Ph1 +C	46 Ph1	−	4
3. 57 F	46	Ph1/iso17	46 Ph1	+	11
4. 54 M[b]	29	45 Ph1 GQ-	45 Ph1 GQ-	Toxic death	2
5. 39 F	18	46 Ph1 XQ-	46 Ph1	+	16
6. 15 F	21	Double Ph1, trisomy 21	Mosaic 46 Ph1, double Ph1, trisomy 21,	+	10
7. 50 M	23	42–45 Ph1	46 Ph1	+	13

[a]Patient treated with cyclophosphamide, Ara-C, vincristine, and prednisone prior to high-dose BCNU.
[b]High-dose BCNU only, due to previous extensive therapy.

Blast transformation was defined as the appearance of 30% blasts in the peripheral blood or bone marrow [13]. All patients suffered from painful splenomegaly, fever, as well as requiring transfusions of red cells and/or platelets. At the time of blast transformation all patients had acquired a new chromosomal abnormality in addition to the Ph1 [Table I]. Six patients had myeloblastic transformations. One patient had a lymphoblastic transformation resistant to vincristine and prednisone.

Chemotherapy in four patients consisted of a 4-day continuous infusion of cytosine arabinoside (200 mg/M^2 per day) followed on a day 5 by BCNU 900 mg/M^2. The BCNU was given through a Hickman central venous catheter. Two patients (#2 and 4) who had been heavily pretreated received only BCNU, at a dose of 1,200 mg/M^2. Patient #1 received an initial preparative regimen of cyclophosphamide, ara-c, vincristine, and prednisone (COAP) and upon relapse 6 months later received high dose-BCNU only, at a dose of 1,200mg/M^2, achieving a successful result after both regimens.

Forty-eight hours after BCNU infusion, an aliquot of the cryopreserved cells was thawed in the laboratory by immersion in a 40°C water bath. The cells were immediately diluted in a step-wise fashion with 3 volumes containing 200-300 units per milliliter of bovine pancreatic deoxyribonuclease I (DN-100-Sigma Chemicals, St. Louis, MO) to prevent cell clumping [12]. After centrifugation, the cells were resuspended in a final medium also containing the enzyme. The final product resulted in a patient dose of 2.9×10^8 mononuclear cells/kg (1.9–7.8). This was placed in a standard polyethylene blood transfusion bag and infused within 1 hour through a standard recipient set. The infusion time was approximately 30 minutes.

During myelosuppression, supportive therapy using prophylactic platelet transfusions and antibiotics was identical to that of patients undergoing induction therapy for acute leukemia. Bone marrow aspirates were performed on a weekly basis following stem cell infusion. Bone marrow karyotyping was repeated after patients demonstrated evidence of bone marrow recovery. Complete response was defined as clinical disappearance of the Philadelphia chromosome as well as attainment of a normal hemogram. Partial response was defined as elimination of transfusion dependence, improvement in symptoms, and hematologic reversion to the chronic phase of CGL.

Upon discharge from the hospital, patients were followed without maintenance therapy until the onset of hematologic or symptomatic relapse. At the time of reappearance of blast crisis, patients went off protocol.

RESULTS

Response

No patient achieved a normal karyotype. Six of the seven patients developed marrow hypocellularity and pancytopenia with a white count of less than 200 cells/μl. Five of the six patients achieved a partial response with disappearance of circulating blasts and bone marrow aspirates/biopsies demonstrating fewer than 5% blasts and a pattern consistent with the chronic phase of CGL. All five had resolution of the symptoms of blast transformation as well. Four of these patients reverted to their original karyotype demonstrating only a single Ph^1 chromosome. The median duration of the second chronic phase after a single course of treatment was four months and ranged from 2 to 7 months. Therapy during the second chronic phase varied but was

not required in four patients for 3 months. Upon relapse, a second successful induction with autologous infusion was achieved in three of six patients, ranging from 4 to 7 months, and a third successful induction in one of two patients, lasting 4 months. Chemotherapy for these second attempts was variable and included high-dose Ara-C, high-dose cyclophosphamide, or Ara-C plus VM-26.

Toxicity

The stem cell infusions were accompanied by mild to moderate chills and fever in two of the seven patients and were easily managed with antipyretics. Nausea and vomiting following BCNU ranged from mild to severe in all patients despite trilafon and nembutal. Mild to moderate hypotension and headache occurred in all patients during BCNU infusion, which was managed by slowing or temporarily discontinuing the BCNU infusion. Patient #4, who was treated with single-agent BCNU, died of hepatic failure 2 months following BCNU. This patient had received daily oral busulphan for 2 years prior to referral and had no history of liver disease or alcohol use. Post mortem examination showed hepatic veno-occlusive disease and necrosis. The remaining patients had no pulmonary, hepatic, renal, or central nervous sytem toxicity which could be ascribed to BCNU. The median nadir of the white blood cell count was less than 100/μl and ranged from less than 100 to 2,000/μl. The median nadir of the platelet count was 5,000/μl and ranged from under 1,000 to 16,000/μl. Recovery with platelet count greater than 100,000/μl and white blood count greater than 1,000/μl occurred on day 19 and ranged from 12 to 25 days following stem cell infusion. Total hospitalization for the five responding patients averaged less than 1 month. Figure 1 shows blood counts at entry into the study and 2 months following stem cell infusion. The white blood count went from a median of 58,000 to 9,000/μl (2,500–25,000). The hematocrit rose from a median of 26% to 34% and the platelet count remained the same or rose in all patients going from a median of 88,000 to 450,000/μl.

Survival

Survival for all seven patients treated (measured from the onset of the protocol) was 11 months and ranged from 2 to 16 months. Measured from original CGL diagnosis, total survival was median of 34 months and ranged from 15 to 57 months in this small group. Median survival for the five responders from the onset of treatment protocol was 13 months (range, 10 to 16 months).

DISCUSSION

Seventy percent of patients with CGL undergo blastic transformation within 3 years of their diagnosis [13]. Coventional chemotherapeutic results for blastic phase have been disappointing [14–20]. In a study by the CALGB [21] using hydroxyurea, 6MP, prednisone, with or without vincristine and/or daunorubicin, a "complete response" occurred in 12% with partial responses in another 22%. A more recent report from the Baltimore Cancer Research Center and the Hospital de Clinicas, Montevideo, Uruguay, using a 5-day regimen of 5-azacytidine plus etoposide, produced one complete and 15 partial responses in 27 untreated blast crisis patients with myeloid phenotype [29]. In both the above studies median survival for *responders* was less than 8 months. Clearly, newer approaches are needed in this setting [30].

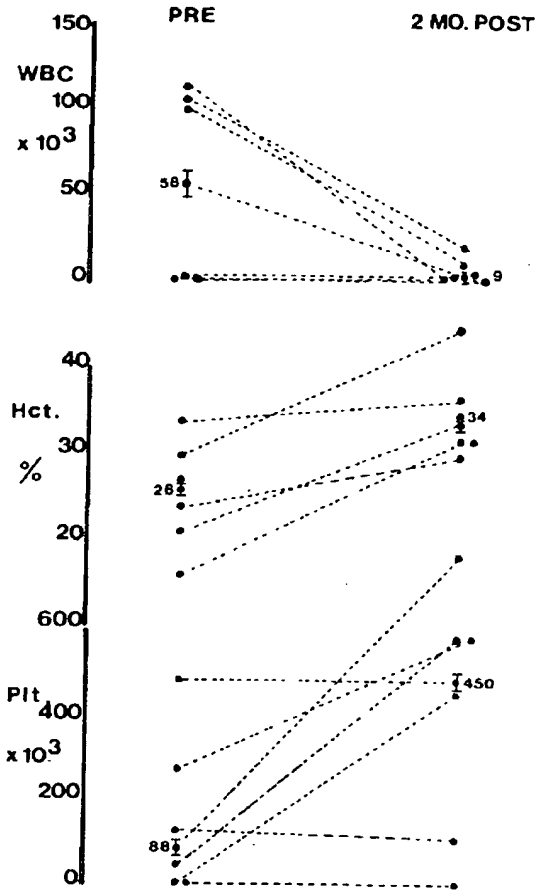

Fig. 1. Blood counts of seven patients at entry into the study and 2 months following stem cell infusion. Median value is shown in bars.

Using high-dose BCNU with or without Ara-C, we produced profound pancytopenia in six of the seven patients treated. Five of seven patients had a partial response with marked symptomatic improvement. The BCNU dose of 1200 mg/M^2 was less than that which routinely causes serious nonhematologic toxicity [9] and was associated with acceptable side effects. Had autologous cells not been used, prolonged BCNU myelosuppression would have been anticipated. The median time to recovery of 19 days supports the efficacy of the cryopreserved peripheral blood stem cells. Duration of hospital stay as well as blood support requirements and cost compare favorably to many "coventional" aggressive chemotherapy regimens for blast crisis.

The elimination of new chromosomal markers of blastic crisis in four of the five responders is of biological interest and is consistent with the clinical improvement in these patients. The median duration of remission in responding patients was 28 weeks—confirming the work of Goldman et al [5]. Secondary responses were also observed in three of six attempts. Overall, the median survival for all seven patients after the onset of blast crisis was 11 months. A series of induction courses using other agents and supplemented by autologous peripheral blood stem cells could potentially lead to more prolonged control of the late phase of the disease.

Isologous and allogeneic transplantation have curative potential when used during the chronic phase of CML [25–28] and often supercede peripheral blood infusion. Therefore, the ultimate usefulness of this therapy remains unclear, and the outcomes in our patients may need to be compared to results of even *unrelated* matched donor grafting. On the other hand, for those CGL patients without a compatible donor or who, because of age or other factors, may not be physiologically able to sustain an allograft, this technique of autologous reconstitution appears to offer an important option.

REFERENCES

1. Deisseroth A, Abrams RA: The role of autologous stem cell reconstitution in the intensive therapy for resistant neoplasm. Cancer Treat Rep 63:461–471, 1979.
2. Goldman JM, Catovsky D, Galton DAG: Reversal of blast cell crisis in CGL by transfusion of stored autologous buffy-coat cells: Lancet 437–438, 1978.
3. Goldman JM, Catovsky D, Goolden AWG, Johnson SA, Galton DAG: Buffy coat autografts for patients with chronic granulocytic leukemia in transformation. Blut 42:149–155, 1981.
4. Goldman JM, Johnson SA, Catovsky D, Wareham NJ, Galton DAG: Autografting for chronic granulocytic leukemia. N Engl J Med 305:700, 1981.
5. Goldman JM, Kearney L, Pittman S, Baughan A, Worsley A, Catovsky D, Geary C, Samson D, Gordon-Smith EC, Dalton DAG: Haematopoietic stem cell grafting for chronic granulocytic leukaemia: Clinical results and cytogenetic findings. Exp Hematol 10 (Suppl): 76–78, 1982.
6. Preisler HD, Henderson ES: Effect of cytosine arabinoside and 1,3-Bis (2-chloroethyl)-1-nitrosourea on hematopoietic precursors in the mouse. J Natl Cancer Inst 47:971–977, 1971.
7. Hochberg FH, Parker LM, Takvorian R, Canellos GP, Zervas N: High-dose BCNU with autologous bone marrow rescue for recurrent glioblastoma multiforme. J Neurosurg 54:455–460, 1981.
8. Spitzer G, Dicke KA, Verma DS, Zander A, McCredie KB: High-dose BCNU therapy with autologous bone marrow infusion: Preliminary observations. Cancer Treat Rep 63:1257–1264, 1979.
9. Herzig GP, Phillips GL, Herzig RH, Fay JW, Weiner RL, Wolff SN, Lazarus HM: Intensive (1,3-bis (chloroethyl)-1-nitrosourea, (BCNU) and autologous bone marrow transplantation for refractory malignancy. In Nitrosoureas: Prestayko AW, Crooke ST, Baker LH, et al (eds): "Nitrosoureas: Current Status and New Developments." Academic Press, 1981, pp 337–341.
10. Goldman JM, Thing KH, Park DS, Spiers ASD, Lowenthal RM, Rootu T: Collection, cryopreservation and subsequent viability of haematopoietic stem cells intended for treatment of chronic granulocytic leukaemia in blast cell transformation. Br J Haematol 40:185–195, 1978.
11. Parker LM, Binder N, Gelman R, Richman CM, Weiner RS, Yankee RA: Prolonged cryopreservation of human bone marrow. Transplantation 31:454–457, 1981.
12. Parker LM, Karp DD, Ervin TJ, Canellos GP: Modifications of techniques for storage and reinfusion of chronic granulocytic leukemia (CGL) peripheral blood stem cells (PBSC). Proc Am Assoc Cancer Res 22:172, 1981.
13. Rosenthal S, Canellos GP, DeVita VT, Gralnick HR: Characteristics of blast crisis in chronic granulocytic leukemia. Blood 49:705–714, 1977.
14. Foley HF, Bennett JM, Carbone PP: Combination chemotherapy in accelerated phase of chronic granulocytic leukemia. Arch Intern Med 123:166–170, 1969.
15. Canellos GP, DeVita VT, Whang-Peng J, Carbone PP: Hematologic and cytogenetic remission of blastic transformation in chronic granulocytic leukemia. Blood 38:671–679, 1971.
16. Marmont AH, Damasio EE: The treatment of terminal metamorphosis of chronic granulocytic leukaemia with corticosteroids and vincristine. Acta Haematol (Basel) 50:1–8, 1973.
17. Hayes DM, Ellison RR, Glidewell O, Holland JF, Silver RT: Chemotherapy for the terminal phase of chronic myelocytic leukemia. Cancer Chemother Rep:4 (Part 2):233–247, 1974.
18. Spiers ADS, Costello C, Catovsky D, Galton DAG, Goldman JM: Chronic granulocytic leukaemia: Multiple drug chemotherapy for acute transformation. Br Med J 3:77–80, 1974.
19. Vallejos CS, Trujillo JM, Cork A, Budey GP, McCredie KB, Freireich EJ: Blastic crisis in chronic granulocytic leukemia: Experience in 39 patients. Cancer 34:1806–1812, 1974.

20. Peterson LC, Bloomfield CD, Brunning RD: Blast crisis as an initial or terminal manifestation of chronic myeloid leukemia. Am J Med 60:209–220, 1976.
21. Coleman M, Silver RT, Pajak TF, Cavalli F, Rai KR, Kostinas JE, Glidewell O, Holland JF: Combination chemotherapy for terminal phase chronic granulocytic leukemia: Cancer and leukemia Group B studies. Blood 55:29–36, 1980.
22. Canellos GP: The Treatment of chronic granulocytic leukaemia. Clin Haematol 6:113–128, 1977.
23. Buckner CD, Clift RA, Fefer A, Neiman PE, Storb R, Thomas ED: Treatment of blastic transformation of chronic granulocytic leukemia by high dose cyclophosphamide, total body irradiation and infusion of cryopreserved autologous marrow. Exp Hematol 2:138–146, 1974.
24. Goldman JM, Lu D-P: New approaches in chronic granulocytic leukemia—origin, prognosis, and treatment. Semin Hematol:XIX, No4, Oct 1982, p 241.
25. Fefer A, Cheever MA, Greenberg PD, Applebaum FR, Boyd CN, Buckner CD, Kaplan HG, Ramberg R, Sanders JE, Storb R, Thomas ED: Treatment of chronic granulocytic leukemia with chemoradiotherapy and transplantation of marrow from identical twins. N Engl J Med 306:63–68, 1982.
26. Doney KC, Buckner CD, Sale GE, Ramberg R, Boyd C, Thomas ED: Treatment of chronic granulocytic leukemia by chemotherapy, total body irradiation and allogeneic bone marrow transplantation. Exp Hematol 6:738–747, 1978.
27. Doney KC, Buckner CD, Thomas ED, Sanders J, Clift RA, Hansen JA, Sale GE, Singer J, Storb R: Allogeneic bone marrow transplantation for chronic granulocytic leukemia. Exp Hematol 9:966–971, 1981.
28. Clift RA, Buckner CD, Thomas ED, Doney K, Fefer A, Neiman PE, Singer J, Sanders J, Stewart P, Sullivan KM, Deeg J, Storb R: The treatment of chronic granulocytic leukaemia in chronic phase by allogeneic marrow transplantation. Lancet 2(8299):621-623, 1982.
29. Schiffer CA, DeBellis R, Kasdorf H, Wiernik PH: Treatment of the blast crisis of chronic myelogenous leukemia with 5-Azacytidine and VP16-213. Cancer Treat Rep 66:267–271, 1982.
30. Wiernik, PH: The current status of therapy for and prevention of blast crisis of chronic myelocytic leukemia. J Clin Oncol, Vol 2, No 4 (April) 1984.

STIC-ILL

@0415.A1B52

From: Canella, Karen
Sent: Sunday, February 03, 2002 9:00 PM
To: STIC-ILL
Subject: ill order 09/815,340

Art Unit 1642 Location 8E12(mail)

Telephone Number 308-8362

Application Number 09/815,340

1. Trends in Cell biology, 2001 Jan, 11(1):18-21
2. Clinical Cancer Research, 2000 Aug, 6(8):3215-3221
3. Mutation Research, 1997 Apr 29, 375(2):157-165
4. american Journal of Hematology, 1985 Mar, 18(3):243-249.
5. PNAS, 1989 Apr, 86(7):2276-2280
6. Genes and Development, 1996 Oct 15, 10(20):2621-2631
7. Cancer, 1975 Jun, 35(6):1664-1677
8. Mutation Research, 1978, 57(3): 313-324
9. Environ Mutagen, 1981, 3(1):53-64
10. Nucleic Acids Research, 2001 Mar 15, 29(6):1300-1307
11. Oncogene:
    1998 Oct 29, 17(17):2187-2193
    2000 Jan 20, 19(3):403-409
12. Molecular endocrinology, 1999 Jan, 13(1):156-166
13. Gene, 1999 Nov 29, 240(2):317-324
14. Science, 1999 Jul 16, 285(5426)418-422
15. Biochemistry and Molecular biology international, 1999 May, 47(5):891-897
16. Journal of Clinical Endocrinology and Metabolism, 1999 Mar, 84(3):1149-1152
17. Journal of biological chemistry:
    1999 Jan 29, 274(5):3151-3158
    2000 Nov 24, 275(47):36502-36505 ***
18. Gene 2000 May 2, 248(1-2):41-50
19. Molecular endocrinology, 2000 Aug, 14(8):1137-1146
20. Cancer Letters, 2001 Feb 10, 163(1):131-139
21. Brain Pathology, 2001 Jul, 11(3):328-341

Vol. 47, No. 5, May 1999 BIOCHEMISTRY and MOLECULAR BIOLOGY INTERNATIONAL
pages 891-897

CLONING AND EXPRESSION OF HUMAN cDNA ENCODING HUMAN HOMOLOGUE OF PITUITARY TUMOR TRANSFORMING GENE

In Ae Lee[1], Changkeun Seong[2] and In Seong Choe[1]*

[1]*Molecular and Cellular Biology Research Group, Korea Research Institute of Bioscience and Biotechnology, Yoosung, P. O. Box 115, Taejon 305-600, Korea*
[2]*Department of Food Science and Technology, Chungnam National University, Taejon 305-764, Korea*

*To whom correspondence should be addressed: Korea Research Institute of Bioscience and Biotechnology, P. O. Box 115, Yoosung, Taejon 305-600, Korea. Tel: 82-42-860-4180; Fax: 82-42-860-4593; E-mail: choemcbg@kribb4680.kribb.re.kr

Summary: Recently, a potent transforming gene which was exclusively expressed in rat pituitary tumor but not in normal pituitary had been isolated and named as pituitary tumor transforming gene (PTTG). A cDNA clone encoding human homologue of rat PTTG was isolated from human fetal liver cDNA library. It contained an open reading frame of 603 base pairs predicting a protein composed of 201 amino acids with a calculated molecular weight of 26 kDa. The deduced protein showed about 85% homology (78% identity, 7% favored substitution) with the rat PTTG. Northern blot analysis showed that the cDNA hybridized to 1.0 kb mRNA species which was expressed in fetal liver and several cancer cell lines. These results suggest that the presence of the human homologue of rat PTTG gene may not be restricted to pituitary tumor.

Key Words: human PTTG homologue, cDNA cloning, mRNA expression

INTRODUCTION

Pituitary tumors are mostly benign hormone-secreting or nonfunctioning adenomas arising from a monoclonal expansion of a genetically mutated cell (1-3). They may hyper-secrete highly differentiated protein products such as prolactin (PRL), growth hormone (GH), adenocorticotropic hormone (ACTH), α-subunit of the gonadotrophin, and thyroid-stimulating hormone (TSH) (4). Recent applications of genetic analysis to pituitary tumors have allowed the elucidation of important molecular pathogenic mechanisms responsible for both sporadic and hereditary pituitary tumorigenesis. Point mutations of Ras oncogene (5, 6), loss of heterozygosity near the Rb locus on chromosome 13 (7, 8, 9), and loss of heterozygosity near MEN1 or basic fibroblast growth factor (bFGF) on chromosome 11 (10, 11) have been implicated in some pituitary tumors. But, the mechanism that causes pituitary cell transformation remains largely unknown. Recently, a potent transforming gene which was exclusively expressed in pituitary tumor but not in normal pituitary was isolated from rat, and named as pituitary tumor transforming gene (PTTG). This gene was expressed in rat testis and human fetal liver at low levels. Over-expression of this gene in mouse 3T3 fibroblasts showed that PTTG inhibited cell

1039-9712/99 $12.00 + 0.00

proliferation and induced cell transformation *in vitro*. Injection of transfected 3T3 cells into athymic nude mice resulted in tumor formation within 3 weeks in all animals tested (12).

To study the function of PTTG in the human system, it is important to obtain human cDNA clones harboring the full open reading frame (ORF) of the homologous gene. Here, we report the cloning and sequencing of the cDNA clone containing the full ORF of the human homologue of rat PTTG from human fetal liver tissue and named it as hPTTG. The expression of hPTTG messages in various human cell lines was also studied.

MATERIALS AND METHODS

Construction of human fetal liver cDNA libraries

cDNA libraries were constructed from the liver tissue of a 26 week old human fetus (Korean) using a Marathon cDNA amplification kit (Clonetech, California, USA). Total RNA was prepared by the acid guanidium-thiocyanate-phenol-chloroform extraction method described by Chomczynski and Sacchi (13). Poly-A^+ RNA isolated by oligo-dT cellulose column chromotography was converted to cDNA using the method described by Sambrook *et al.* (14) and ligated with a specific adaptor supplied by the manufacturer. The Marathon cDNA libraries from fetal liver were used directly as the templates for the polymerase chain reaction (PCR).

Screening of full length hPTTG cDNA clones

The hPTTG gene specific primer I (5'-ACCTGCCTGAAGAGCACCAGAT-3') and primer II (5'-GGAGAGGGCATCTTCACAGGTG-3') were synthesized and used for 5'- or 3'-rapid amplification of cDNA ends (RACE) (15). The Marathon cDNA library constructed from human fetal liver was used as a template for RACE. Thirty cycles of 5'-RACE reactions were performed using the following temperature profile ; denaturation (94℃ for 30sec), primer annealing (60℃ for 30sec) and primer extension (68℃ for 2min). PCR products were directly cloned into pCR2.1 vector using TA cloning kit (Invitrogen, Carlsbad, CA, U.S.A.). Recombinant DNA technology was performed following the methods described by Sambrook *et al.* (14).

DNA sequencing

Plasmid DNA was purified by an alkaline method (14) and affinity chromatography using a Wizard minipreps DNA purification system (Promega, Madison, WI, U.S.A.). Sequences were determined by the chain termination method (16) using a Sequenase kit Version 2.0 (USB, Cleveland, Ohio, U.S.A.) and [α -35S] dATP (Amersham, Buckinghamshire, U.K.).

Northern blot analysis

Total RNA preparations isolated from human fetal liver or hepatoma cell line HepG2 were resolved by formaldehyde gel electrophoresis and transferred to Hybond $^{(+)}$ nylon membrane (Boehringer Mannheim, Ottweiler, Germany) by capillary transfer method. The transferred RNAs was cross-linked by UV crosslinker (Spectroline, 나라?) and baked at 80℃ for 1 hour. Multiple Tissue Northern (MTN) blot membrane containing 2μg each of poly $(A)^+$ RNA from several human tissues (Clontech) was also used. The cDNA probe for the human homologue of PTTG was ^{32}P-labelled by the random priming method (17) employing Klenow enzyme and hexanucleotide mixture. The blot was hybridized with the probe at 65°C for 1 hr in an express hybridization solution (Clontech), and washed to a final stringency of 0.1 x SSC and 0.1% SDS at 50°C for 20min. The blots were subsequently hybridized with the glyceraldehyde 3-phosphate dehydrogenase(GAPDH) as the probe to correlate the RNA contents on each lane.

RESULTS AND DISCUSSIONS

Isolation of human PTTG homologue

A λ-ZAP cDNA library constructed from the liver tissue of human fetus was analyzed by single-pass sequencing and database search of the determined partial sequence for the similarity with the genes reported previously (18). Among the cDNA clones analyzed, a clone S28D02 showed 78% homology with the nucleotide sequence of rat PTTG. On the basis of the information from the partial cDNA sequence of the clone S28D02, the hPTTG gene specific primer I and II were synthesized and used for 5'- and 3'- rapid amplification of cDNA ends (RACE). The Marathon cDNA library constructed from human fetal liver was used as a template for RACE. PCR products with approximate size of 0.5 and 0.3kb were isolated and cloned into pCR2.1 vector and designated as clone S28 II-22 and S28 I-13. S28 II-22 was digested with Apa I, and re-ligated with 0.3kb ApaI-ApaI fragment isolated from S28 I-13. The ligation mixture was transformed into *E. coli* strain DH5 α and the transformants were analyzed by restriction mapping and DNA sequencing. The resulting recombinant plasmid containing the full ORF of hPTTG was named as clone S28D02-F13.

Sequence of human PTTG gene

The nucleotide sequence of the clone S28D02-F13, GenBank accession number AF062649, is shown in Fig. 1. The cDNA is 733 bp long and contains an ORF encoding 201 amino acids with a deduced molecular mass of 26 kDa. This ORF is presumed to start from the first AUG codon at position 72 found in the crucial context for efficient translation of eukaryotic mRNA (CC(A/G)CCAUGG) (19). The cDNA clone contains in-frame UGA stop codon 9 nucleotides upstream of the AUG. BLAST search of databases reveals that this clone has about 81% homology in nucleotide sequence with rat PTTG (20). We named this cDNA clone as human PTTG. The alignment of amino acid sequences in Fig. 2 shows that the amino acid sequence of the hPTTG exhibits 85% homology with the rat PTTG (78% identity, 7% favored substitutions). The high level of conservation between rat and human PTTG proteins might suggest the functional significance of the gene in both species. The amino acid sequence of the hPTTG between amino acid 32-66 demonstrated 41 to 59% homology with the proteins reported elsewhere (Table 1). Among the homologous proteins shown in Table 1, there were several nuclear proteins such as herpesvirus EBNA-3A and histone H1, and transmembrane proteins such as CNG-4 and F1 ATPase β–subunit. Above features of the hPTTG might be a clue for the estimation of its function.

```
CAGGAGTGCGCCGCGTCCGTTCACCGCGGCCTCAGATGAATGCGGCTGTTAAGACCTGCA    60
ATAATCCAGAATGGCTACTCTGATCTTTGTTGATAAGGAAAATGAAGAACCAGGCACCCG   120
        M  A  T  L  I  F  V  D  K  E  N  E  E  P  G  T  R      (17)

TGTGGTTGCTAAGGATGGGCTGAAGCTGGGGTCTGGACCTTCAATCAAAGCCTTAGATGG   180
 V  V  A  K  D  G  L  K  L  G  S  G  P  S  I  K  A  L  D  G    (37)

GAGATCTCAAGTTTCAACACCACGTTTTGGCAAAACGTTCGGTGCCCCAGCCTTACCTAA   240
 R  S  Q  V  S  T  P  R  F  G  K  T  F  G  A  P  A  L  P  K    (57)

AGCTAGCAGAAAGGCTTTGGGAACTGTCAACAGAGTTACAGAAAAGCCTGTTAAGTCCAA   300
 A  S  R  K  A  L  G  T  V  N  R  V  T  E  K  P  V  K  S  K    (77)

GGGACCCCTCCAATCAAAACAGCCCACGCTTTGTGCCAAAAAGATAACTGAGAAGAGTGT   360
 G  P  L  Q  S  K  Q  P  T  L  C  A  K  K  I  T  E  K  S  V    (97)

TAAGTCAAAAGGCTCTGTTCCTGCCTCAGATGATGCCTATCCAGAAATAGAAAAATTCTT   420
 K  S  K  G  S  V  P  A  S  D  D  A  Y  P  E  I  E  K  F  F    (117)

TCCCTTCAATCCTCTAGACTTTGAGAGTTTTGACCTGCCTGAAGAGCACCAGATTGCGCA   480
 P  F  N  P  L  D  F  E  S  F  D  L  P  E  E  H  Q  I  A  H    (137)

CCTCCCCTTGAGTGGAGTGCCTCTCATGATCCTTGACGAGGAGAGAGAGCTTGAAAAGCT   540
 L  P  L  S  G  V  P  L  M  I  L  D  E  E  R  E  L  E  K  L    (157)

GTTTCAGCTGGGCCCCCCTTCACCTGTGAAGATGCCCTTTCCACCATGGGAATCCGATCT   600
 F  Q  L  G  P  P  S  P  V  K  M  P  F  P  P  W  E  S  D  L    (177)

GTTGCAGTCTCCTTCAAGCATTCTGTCGACCCTGGATGTTGAATTGCCACCTGTTTGGTG   660
 L  Q  S  P  S  S  I  L  S  T  L  D  V  E  L  P  P  V  W  C    (197)

TGAAATAGATATTTAAATTTTTTAGTGCTTCAGAGTTTGTGTGTATTTGTATTAATAAAG   720
 E  I  D  I  *                                                  (201)

CATTCTTTAACTGTAAAAAAAAAAAAAAAAAAAAAAAAAAAAAAAA                 766
```

Fig. 1. Nucleotide sequence of the cDNA clone for the human homologue of rat PTTG and its deduced amino acid sequence. The numbers at the right of each line denote the positions of the last nucleotide and amino acid. In-frame stop codons defining the 5' and 3' ends of the reading frame are indicated by an underline and an asterisk, respectively.

Table 1. The result of amino acid homology search of hPTTG subsequences with the proteins reported previously.

a.a. residue (length)	homology (identity)	homologous proteins
1 - 199 (199)	85% (78%)	rat PTTG
162 - 193 (32)	59% (46%)	bovine CNG-4
11 - 73 (63)	41% (30%)	human herpesvirus EBNA-3A
172 - 195 (24)	58% (45%)	human herpesvirus EBNA-3A
31 - 96 (66)	43% (28%)	Arabidopsis histone H1-1
34 - 83 (50)	46% (30%)	Kluyveromyces F1 ATPase subunit
52 - 115 (58)	40% (28%)	rabbit neurofilament H

Expression of human PTTG

It had been reported that rat PTTG had been expressed not only in pituitary tumor but also in testis among adult tissues and embryonic liver at low levels (12). To study the expression pattern of the hPTTG messages in various human cancer cell lines and fetal liver tissue, Northern blot analysis was performed using the cDNA sequence of hPTTG as a probe. When the presence of hPTTG messages in total RNA preparations isolated from fetal liver tissue and a hepatoma cell line, HepG2 was tested, 1.0 kb transcript was found in HepG2, but barely expressed in fetal liver (Fig. 3A). Analysis of a multiple tissue blot membrane of cancer cell lines (Clontech) with the same probe revealed that the 1.0 kb transcript of hPTTG was expressed in promyelocytic leukemia HL-60, HeLa cell S3, chronic myelogenous leukemia K-562, and colorectal adenocarcinoma SW480 (Fig. 3B). The hPTTG mRNA was expressed in several non-pituitary cancer cell lines as well as in pituitary tumor cells. These results suggest that the presence of the human homologue of rat PTTG might not be restricted to pituitary cells but also is diversified in other tumors. The cDNA sequence covering the entire ORF of hPTTG was subcloned into an expression vector pGEX4T1, and its recombinant protein was produced in *E. coli* (data not shown).

```
hPTTG   :  MATLIFVDKENEEPGTRVVAKDGLKLGSGPSIKALDGRSQVSTPRFGKTFGAPA  :  54
rPTTG   :  MATLIFVDKDNEEPGSRLASKDGLKLGSG--VKALDGKLQVSTPRVGKVFGAPG  :  52

hPTTG   :  LPKASRKALGTVNRVTEKPVKSKGPLQSKQPTLGAKKITEKSVKSKGSVPASDD  :  108
rPTTG   :  LPKASRKALGTVNRVTEKPVKSSKPLQSKQPTLSVKKITEKSTKTQGSAPAPDD  :  106

hPTTG   :  AYPEIEKFFPFNPLDFESFDLPEEHQIAHLPLSGVPLMILDEERELEKLFQLGP  :  162
rPTTG   :  AYPEIEKFFPFDPLDFESFDLPEEHQISLLPLNGVPLMILNEERGLEKLLHLDP  :  160

hPTTG   :  PSPVKMPFPPWESDLLQSPSSILSTLDVELPPVWCEIDI  :  201
rPTTG   :  PSPLQKPFLPWESDPLPSPPSALSALDVELPPVCYDADI  :  199
```

Fig. 2. Sequence alignment of the predicted human homologue (hPTTG) sequence with rat PTTG (rPTTG) sequence using the Pile-Up program of GCG package (21). Perfectly matched residues were denoted as dark boxes and well conserved ones were denoted as gray boxes.

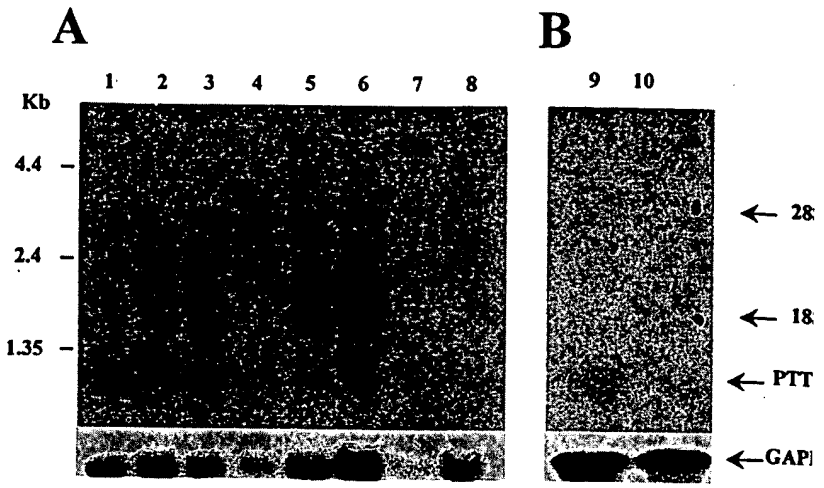

Fig. 3. Distribution of hPTTG mRNA in fetal liver tissue and various cancer cell lines **A.** A cancer cell line multiple tissue blot membrane (Clontech) was used. Lanes 1 to 8 contain in order, 2μg each of poly $(A)^+$ RNA from human cancer cell lines, promyelocytic leukemia HL-60 [1], HeLa cell S3 [2], chronic myelogenous leukemia K-562 [3], lymphoblastic leukemia MOLT-4 [4], Burkitt's lymphoma Raji [5], colorectal adenocarcinoma SW 480 [6], lung carcinoma A549 [7], and melanoma G361 [8]. Locations of size markers were indicated on the left. **B**. Total RNAs isolated from human fetal liver and human liver cancer cell line HepG2 were resolved by formaldehyde gel electrophoresis and transferred to a Hybond$^{(+)}$ nylon membrane by a capillary transfer method (14). Lanes 9 to 10 contain in order, 10μg each of total RNA from human liver cancer cell line HepG2 [9] and human fetal liver tissue [10]. Ribosomal RNAs (28S and 18S) were used as RNA size markers. The membrane blots were subsequently hybridized with the glyceraldehyde 3-phosphate dehydrogenase (GAPDH) probe to correlate the RNA contents on each lane.

Acknowledgements

This study was supported by a grant from Ministry of Science and Technology of Korea (HAN Project HS2070M). We are grateful to Drs. Y. Lee and J.W. Kim for their technical assistance and to Dr. D.Y. Yoon for his encouraging discussions.

Reference

1. Alexander, J.M., Biller, B.M.K., Bikkal, H., Zervas, N.T., Arnold, A., and Klibanski, A. (1990) J. Clin. Invest. 86: 336-340.
2. Herman, V., Fagin, J., Gonsky, R., Kovacs, K., and Melmed, S. (1990) J. Clin. Endocrinol. Metab. 71: 1427-1443.
3. Melmed, S. (1994) Endocrinol. Metab. Clin. North. Am. 23: 81-92.

4. Reichlin, S. (1991) Pathogenesis of pituitary tumors. *In* Faglia, G., Beck-Pecoz, P., Ambrosi, B, *et al.* (eds); Pituitary Adenomas; New Trends in Basic and Clinical Reserch. p. 113-121. Elsevier Science Publishers.
5. Karga, H.J., Alexander, J.M., Hedley-Whyte, E.T., Klibansky, A.., and Jameson, J.L. (1992) J. Clin. Endocrinol. Metab. 74: 914-919.
6. Pei, L., Melmed, M., Scheithauer, B., Kovacs, K., and Prager, D. (1994) J. Clin. Endocrinol. Metab. 78: 842-846.
7. Jacks, T., Fazelli, A., Schmitt, E., Bronson, R.T., Goodell, M., and Weinberg, R.A. (1992) Nature 359: 295-300.
8. Cryns, V.L., Alexander, J.M., Klibanski, A., and Arnold, A. (1993) J. Clin. Endocrinol. Metab. 77: 644-646.
9. Pei, L., Melmed, M., Scheithauer, B., Kovacs, K., Benetict, W.F., and Prager, D. (1995) Cancer Res. 55: 1613-1616.
10. Thakker, R.V., Pook, M.A., Wooding, C., *et al.* (1993) J. Clin. Invest. 91: 2815-2821.
11. Zimering, M.B., Katsumata, N., Sato, Y., *et al.* (1993) J. Clin. Endocrin. Metab. 76: 1182-1187.
12. Pei, L. and Melmed, M. (1997) Mol. ENDO 11 (4): 433-441.
13. Chomczynski, P., and Sacchi, N. (1987) Anal. Biochem. 162: 156-159.
14. Sambrook, J., Fritsch, E.F., and Maniatis, T. (1989) Molecular Cloning : A Laboratory Manual, 2nd Ed. Cold Spring Harber Lab. Cold Spring Harbor, NY
15. Chenchick, A., Moqadam, F., and Siebert, P. (1995) CLONETECHNIQUES X (1): 5-8.
16. Sanger, F., Nicklen, S., and Coulson, A.R. (1977) Proc. Natl. Acad. Sci. 74: 5463-467.
17. Feinberg, A.P., and Vogelstein, B. (1983) Anal. Biochem. 132: 6-13.
18. Kim, J.W., Song, J.C., Lee, I.A., Lee, Y., Nam, M.S., Hahn, Y., Chung, J.H., and Choe, I.S. (1995) Kor. J. Biochem. Mol. Biol. 28(5): 402-407.
19. Kozak, M. (1989) J. Cell. Biol. 108: 229-241.
20. Altschul, S.F., Gish, W., Miller, W., Eugene, W.M., and Lipman, D.J. (1990) J. Mol. Biol. 215: 403 - 410.
21. Higgins, D.G. and Sharp, P.M. (1988) Gene 73: 237-244.

STIC-ILL

Qp152.H152

From: Canella, Karen
Sent: Sunday, February 03, 2002 9:00 PM
To: STIC-ILL
Subject: ill order 09/815,340

Art Unit 1642 Location 8E12(mail)

Telephone Number 308-8362

Application Number 09/815,340

1. Trends in Cell biology, 2001 Jan, 11(1):18-21
2. Clinical Cancer Research, 2000 Aug, 6(8):3215-3221
3. Mutation Research, 1997 Apr 29, 375(2):157-165
4. american Journal of Hematology, 1985 Mar, 18(3):243-249.
5. PNAS, 1989 Apr, 86(7):2276-2280
6. Genes and Development, 1996 Oct 15, 10(20):2621-2631
7. Cancer, 1975 Jun, 35(6):1664-1677
8. Mutation Research, 1978, 57(3): 313-324
9. Environ Mutagen, 1981, 3(1):53-64
10. Nucleic Acids Research, 2001 Mar 15, 29(6):1300-1307
11. Oncogene:
    1998 Oct 29, 17(17):2187-2193
    2000 Jan 20, 19(3):403-409
12. Molecular endocrinology, 1999 Jan, 13(1):156-166
13. Gene, 1999 Nov 29, 240(2):317-324
14. Science, 1999 Jul 16, 285(5426)418-422
15. Biochemistry and Molecular biology international, 1999 May, 47(5):891-897
16. Journal of Clinical Endocrinology and Metabolism, 1999 Mar, 84(3):1149-1152
17. Journal of biological chemistry:
    1999 Jan 29, 274(5):3151-3158
    2000 Nov 24, 275(47):36502-36505 ***
18. Gene 2000 May 2, 248(1-2):41-50
19. Molecular endocrinology, 2000 Aug, 14(8):1137-1146
20. Cancer Letters, 2001 Feb 10, 163(1):131-139
21. Brain Pathology, 2001 Jul, 11(3):328-341

...nal Endocrinology & Metabolism
...by The Endocrine Society

Vol. 84, No. 3
Printed in U.S.A.

An Intronless Homolog of Human Proto-Oncogene *hPTTG* is Expressed in Pituitary Tumors: Evidence for *hPTTG* Family

TONI R. PREZANT, PINAR KADIOGLU AND SHLOMO MELMED
Division of Endocrinology and Metabolism, Cedars-Sinai Research Institute, University of California, Los Angeles, CA

ABSTRACT A novel proto-oncogene, *PTTG* (Pituitary Tumor Transforming Gene), was isolated in our laboratory by virtue of its increased expression in rat pituitary tumor cell lines. Cells which overexpress human or rat *PTTG* form tumors in athymic mice. *hPTTG* is highly expressed in cancer cell lines, pituitary adenomas and in normal testis, suggesting that hPTTG protein has different tissue-specific interactions in normal cells and in cancer. Alternatively, different *hPTTG* gene family members may be functional in normal development and in tumorigenesis. While mapping the chromosomal location of *hPTTG* to 5q33, we discovered a second gene, *hPTTG2*, which is intronless and maps to chromosome 4p12. Using gene-specific oligonucleotide hybridization in a PCR-ELISA assay, we determined that *hPTTG2* is expressed in both normal and tumorous pituitary. However, high levels of *hPTTG* mRNA in cancer cell lines are due to increased expression of *hPTTG1*. Thus, this family of proto-oncogenes appears to differentially participate in tumor-specific pathogenesis.

A novel proto-oncogene, *PTTG* was isolated in our laboratory (1, 2). NIH 3T3 cells transfected with wildtype *PTTG* cDNA are transformed *in vitro* and form tumors in athymic mice (1). The nucleotide sequence of *hPTTG* cDNA is 85% identical to rat *PTTG* cDNA and the encoded proteins are 89% similar. Sequence analysis of *hPTTG* cDNA in eight cancer cell lines revealed no activating mutations. Thus, wildtype *hPTTG* is a proto-oncogene, with its oncogenic potential dependent on its expression level.

The 609 bp open reading frame of *hPTTG* encodes a 202 amino acid protein with no other structurally similar proteins found in GenBank. However, two motifs of Pro-X-X-Pro in the carboxyl end could allow binding to SH3 domains, suggesting a role in intracellular signal transduction (3). These two SH3 binding motifs are necessary both for *hPTTG's* transforming ability and for *hPTTG*-mediated induction of the angiogenic basic fibroblast growth factor (4), which, like *hPTTG*, is increased in several tumors (2).

Although *hPTTG* mRNA is highly expressed in cancer cell lines and primary tumors, it has limited normal tissue expression (2, 5). The transcript is particularly abundant in testis and is also detectable in thymus, spleen and colon. *hPTTG* transcription appears to be developmentally regulated, with mRNA expressed in fetal but not adult liver. That high levels of *hPTTG* transcription occur without tumorigenesis suggests that other tissue-specific proteins and/or post-transcriptional events mediate the oncogenic potential of *hPTTG*. Alternatively, different members of an *hPTTG* gene family could be differentially expressed in cancer and in normal development.

The chromosomal location of *hPTTG* was determined by PCR analysis using a human-hamster radiation hybrid mapping panel, with primers from exons 4 and 5 of *hPTTG*. The 3.5 kb genomic DNA product was obtained only with DNAs from the mapping panel that contained the human chromosomal region 5q33. This location was confirmed by fluorescent *in situ* hybridization analysis using as probe a genomic DNA clone encompassing *hPTTG* (2).

During the course of these studies, several primer pairs were found to amplify PCR products of the sizes expected for a cDNA template, in addition to the expected intron-containing products. The cDNA-sized products were not due to PCR contamination, and the RH mapping panel results obtained for the intronless PCR product suggested a second locus, near the polymorphic marker D4S1581. Thus, *hPTTG* appears to have a closely related homolog on chromosome 4, which may contribute to the *hPTTG* mRNA signal detected in Northern blot analysis. In this study, we describe the preliminary characterization of *hPTTG2*, and determine the expression pattern of the two *hPTTG* genes in several normal tissues, pituitary tumors and cancer cell lines.

Materials and Methods

Nucleic acid preparation, tissues and cell lines

RNA and DNA were TRIZOL-extracted (Gibco, Gaithersburg, MD) from snap-frozen human tissues and pelleted culture cell lines, including: normal pituitary (Zoion Diagnostics, New York, NY), normal testis (#UMB95, Brain and Tissue Bank for Developmental Disorders, University of Maryland, Baltimore, MD), and the cell lines HeLa, HL-60, JEG3, MB231, SKOV3 and LL-24 (American Type Culture Collection, Manassas, VA). Multiple tissue cDNAs were from Clontech (Palo Alto, CA). Pituitary tumor samples were obtained according to institutional guidelines (6). DNAs were isolated from separate pieces of the above tissues, using DNAZOL (Gibco), and QIAamp tissue purification kit (QIAGEN, Valencia, CA). Hamster-human monochromo-somal DNAs (NA10114, human chromosome 5; NA10115, human chromosome 4) and Chinese hamster DNA (NA10658) were from Coriell Institute for Medical Research (Camden, NJ).

PCR and primers (Gibco)

Table 1. PCR primers

Primer	Sequence
34a	5' GGAGAACCAGGCACCCGTGTG
70a	5' CTGAAGCTGGGGTCTGGACCTTC
186a	5' GGCTTTGGGAACTGTC
314a	5' CTGCCTCAGATGATGCCTATCCAG
420F	5' CTTTGAGAGTTTTGACCTGCCTG
261b	5' GCTTGGCTGTTTTTGTTTGAGGGG
436b	5' GAGGCACTCCACTCAAGGGG
466b	5' CAAGCTCTCTCTCCTCGTCAAGG
601b	5' CTATGTCACAGCAAACAGGTGGC
604R	5' ACAGAATGCTTGAAGGAGACTGC

hPTTG was amplified from ~50 ng genomic DNA, with 1.75 U Expand High Fidelity enzyme (Boehringer Mannheim, Indianapolis, IN), 1 x reaction buffer, 1.5 mM $MgCl_2$, 0.2 mM dNTPs, and 300 nM each primer, in 35-40 cycles of: 94°C, 15 sec; 60°C, 30 sec; 68°C, 2.5 min.

Southern blot analysis of hPTTG1 and hPTTG2

*Eco*RI-digested DNAs (10 μg) were electrophoresed in 0.8% agarose and transferred to HybondN+ nylon membranes (Amersham, Arlington Heights, IL), and hybridized to random prime labelled (Gibco) 34a/261b cDNA product. 10^6 cpm/ml of probe was incubated in QUIK-Hyb hybridization buffer (Stratagene, La Jolla, CA), at 68°C. The stringent wash contained 0.2 x SSC, 0.1% SDS at 55°C.

Radiation hybrid mapping of hPTTG

The chromosomal location of *hPTTG* was determined by PCR analysis using the Stanford human-hamster G3 radiation hybrid (RH) mapping panel (Research Genetics, Huntsville, AL), with primers 314a/466b, from *hPTTG1* exons 4 and 5, respectively. In addition to the 3.5 kb product of *hPTTG1*, some PCR reactions produced an *hPTTG*-related 153 bp band, the results for which were separately submitted to the Stanford Human Genome Center website to determine linkage to previously mapped markers.

Sequence analysis

The *hPTTG2* genomic DNA was amplified with the 34a/601b primers, sequenced with α^{33}P-ddNTPs (ThermoSequenase, Amersham, Arlington Heights, IL), electrophoresed in 6% acrylamide/7M urea (National Diagnostics, Atlanta, GA) and subjected to autoradiography on BioMax MR film (Kodak).

PCR-ELISA

1 μg of total RNA was treated with amplification grade DNAse I (Gibco) and reverse transcribed using Superscript II (Gibco). Digoxigenin dUTP (PCR-ELISA kit, Boehringer Mannheim) was incorporated during PCR amplification, with 50 ng of first strand cDNA, primers 420F and 604R, in 35 cycles of: 93°C, 30 sec, 64°C, 30 sec, 72°C, 30 sec. After gel quantitation, approximately 50 ng RT-PCR product was hybridized in triplicate at 55°C, to the biotinylated gene-specific oligonucleotides: *hPTTG1* (5' CTTGACGAGGAGAGAGAG) or *hPTTG2* (5' CTTGATGAGGAGGGAGAG). The colorimetric results were quantitated in a Bio-Tek EL-311 microtiter plate reader. Two standard curves were prepared with purified PCR products (40, 10, 2, 0.5, 0.2 ng) and their homologous probes (i.e. Gene 1 with probe 1, Gene 2 with probe 2). Heterologous control hybridizations verified the assay. (-)RT-PCR controls were subtracted as background in the PCR-ELISAs. *hPTTG1* assays were diluted 1:10 to be in the linear range. As little as 0.2 ng of *hPTTG2* mRNA could be detected in the presence of 40 ng of *hPTTG1* mRNA. Results were subjected to weighted linear regression analysis. The intra-assay %CVs were 6.87 (43 ng *hPTTG1*) and 9.52 (0.87 ng *hPTTG2*). Inter-assay %CVs were 10.79 (10 ng *hPTTG1*) and 25.9 (0.5 ng *hPTTG2*). Data are expressed as *(hPTTG2/(hPTTG1 + hPTTG2)* x 100.

Dideoxy fingerprint screening

Two samples were screened by TA-cloning 34a/601b RT-PCR products into pCR2.1-TOPO (Invitrogen, Carlsbad, CA). 100 white colonies were screened by dideoxyfingerprinting (as in 6).

Results

Initial characterization of hPTTG2

Several primer pairs were found to amplify additional PCR products of the sizes expected for a cDNA template: 34a/466b = 433 bp; 34a/601b = 568 bp; 70a/466b = 397 bp; 70a/601b = 532 bp; 186a/436b = 251 bp; 314a/466b = 153 bp. The cDNA-sized products were not due to PCR contamination, as they were not produced in the water blank reaction nor with hamster genomic DNA as template. The 34a/601b and 314a/466b products were sequenced and found to be related to *hPTTG*.

Mapping the chromosomal location of hPTTG2

When the human-hamster G3 RH mapping panel was scored for the cDNA-sized product, it mapped to 4p12, a different location from *hPTTG1* with a LOD score of 13.7, at 7.68 cR from D4S1581. This chromosome 4 location was confirmed by PCR and Southern blot analyses, using monochromosomal human-hamster hybrid DNAs and human lymphocyte DNAs (6).

Figure 1 shows the PCR products obtained with primer pairs 34a/601b and 314a/466b. The human chromosome 4 amplification products (lanes 3 and 7) are the sizes expected for an intronless gene, and were sequenced to confirm relatedness to *hPTTG* (not shown).

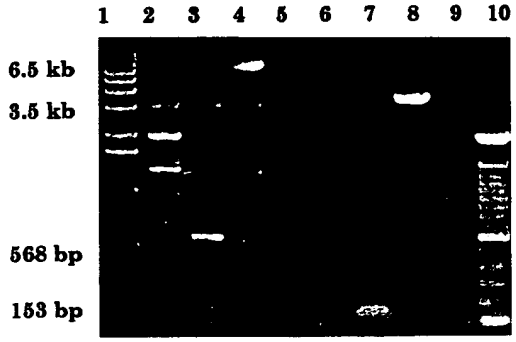

Figure 1. PCR of *hPTTG*. Genomic PCR with *hPTTG* primers 34a/601b (lanes 2-5), 314a/466b (lanes 6-9). Lanes: (2, 6) hamster DNA; (3, 7) hamster/human chr. 4; (4, 8) hamster/human chr. 5); (5, 9) water; (1, 10) DNA markers.

Southern blot hybridization (Figure 2) further confirmed the RH mapping panel results. The 5' half of *hPTTG* cDNA hybridizes to *Eco*RI fragments of ~2.5 kb (chromosome 5, lane 1) and ~7 kb (chromosome 4, lane 2). The hamster DNA (lane 3) does not hybridize to the human probe in these conditions. The two bands are not due to restriction fragment length polymorphisms, as both were found in human lymphocyte DNAs from 47 control individuals (lanes 4-6 show representative samples). Thus, *hPTTG1* appears to have a closely related homolog on chromosome 4, *hPTTG2*, which may contribute to the *hPTTG* mRNA signal detected in Northern blot analysis.

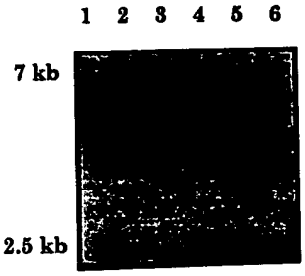

Figure 2. *hPTTG* Southern blot. *Eco*RI-digested DNAs hybridized with 5' half of *hPTTG* cDNA. Lanes: (1) hamster/human chr. 5; (2) hamster/human chr. 4; (3) hamster; (4-6) human lymphocyte DNAs.

Sequence homology of hPTTG1 and hPTTG2

The amplified genomic DNA containing *hPTTG2* (34a/601b primers) was sequenced. This analysis revealed 94% (462/489 bp) nucleotide homology to *hPTTG1* cDNA and 91% (138/152 amino acids) identity in the encoded open reading frames. The GenBank accession number is AF116538.

Quantitative analysis of hPTTG2 transcription

Since Northern blot analysis did not distinguish expression of the two *hPTTG* genes, we quantitated the relative ratios of expression by PCR-ELISA, detecting digoxigenin labelled RT-PCR products that anneal to biotinylated GSOs. In this assay, with 40-50 ng input cDNA, 0.2-5 ng of a minor product could be detected reliably. *hPTTG2* expression was also observed by an independent method, dideoxyfingerprint screening of cloned RT-PCR products.

RNAs from samples with normal *hPTTG2* sequence in all primer binding sites were used in the PCR-ELISA assay. These included normal human pituitary, brain, placenta, colon, ovary, spleen, thymus and testis, pituitary tumors, and a primary fibroblast cell line, LL-24, and five cancer cell lines. Since genomic DNA was not available for the multiple tissue

cDNAs, amplification used a 60°C annealing temperature, and cycle numbers were adjusted to obtain visible products. In addition, two pituitary tumors (T-29 and C-2) were assayed by ddF fingerprinting screening, with similar results.

Table 2. % *hPTTG2* Expression

Cells or Tissue	Description	% *hPTTG2* expression
Normal Tissues		
nl pit. B	normal pituitary	5.0
nl pit. C	normal pituitary	4.9, 6.5
pituitary	nl pituitary pool [18]	1.0
brain	MT pool [5]	1.6
placenta	MT pool [7]	2.1
colon	MT pool [11]	<1
ovary	MT pool [10]	1.6
spleen	MT pool [5]	5.3
thymus	MT pool [8]	<1
testis	MT pool [19]	<1
UMB95	normal testis	<1
Pituitary Tumors		
T-1	NF	<1
T-8	NF	<1
T-9	NF	<1
T-10	NF	2.5
T-75	NF	3.3
T-84	TSH	8.7
T-60	GH	8.5
T-62	GH	1.7
T-63	PRL	<1
T-77	PRL	4.9
T-46	ACTH	1.6
C-2	ACTH	8.5*
T-29	LH/FSH	2.1*
Cell Lines		
HeLa	cervical cancer	<1
HL-60	myeloid leukemia	<1
JEG3	choriocarcinoma	<1
MB231	breast cancer	1.1
SKOV3	ovarian cancer	1.7, <1
LL-24	primary fibroblast	<1

* assayed by dideoxy fingerprinting, [#] = number of individuals in the Multiple Tissue (MT) cDNA pool.

The results in Table 2 show that *hPTTG2* is expressed in normal pituitary, and has moderately elevated expression in some pituitary tumors. Although *hPTTG2* is not a silent pseudogene, it is a minor species even in pituitary, and is not the isoform of *hPTTG* that displays increased expression in cancer cell lines or normal testis.

Discussion

High levels of *hPTTG* mRNA are observed in cancer cells, and can lead to tumorigenesis in athymic mice (2). One hypothesis is that different members of an *hPTTG* gene family could be responsible for its normal and/or tumorigenic functions. Through PCR of genomic DNA, we identified an intronless homolog, *hPTTG2*, that maps to chromosome 4p12. The two *hPTTG* genes are highly conserved at both the nucleotide and amino acid levels, including the potential SH3 binding domains. We found that *hPTTG2* is expressed at low levels in normal pituitary and in some normal tissues. *hPTTG2* may be involved in pituitary tumorigenesis, since total *hPTTG* mRNA is generally increased in pituitary tumors (5), and we detected increased proportions of *hPTTG2* mRNA in three tumors. However, it is unlikely that *hPTTG2* contributes to tumorigenesis in general, since >99% of the *hPTTG* cDNA in cancer cell lines is *hPTTG1*. Recently, we also observed multiple (37) polymorphisms in a region of *hPTTG2* in thymus derived from a normal subject. This may suggest the existence of yet a third member of this family.

Gene-specific studies will unravel the roles of the respective hPTTG proteins.

Acknowledgements

This work was supported by NIH grant CA75979 and by the Doris Factor Molecular Endocrinology Laboratory.

References

1. Pei L and Melmed S 1997 Isolation and characterization of a pituitary tumor-transforming gene (PTTG). Mol Endocrinol 11: 433-441.
2. Zhang X, Horwitz GA, Prezant TR, Valentini A, Bronstein MD and Melmed S 1999 Structure, expression and function of human pituitary tumor transforming gene (PTTG). Mol Endocrinol 13: 156-166.
3. Pawson T 1995 Protein molecules and signalling network. Nature 373: 573-580.
4. Liotta LA, Steeg PS and Stetler-Stevenson WG 1991 Cancer metastasis and angiogenesis: an imbalance of positive and negative regulation. Cell 64: 327-336.
5. Zhang X, Horwitz GA, Heaney AP, et al. 1999 Pituitary tumor transforming gene (PTTG) expression in human pituitary adenomas. J Clin Endocrinol Metab, in press.
6. Prezant TR, Levine J and Melmed S 1998 Molecular characterization of the *men1* tumor suppressor gene in sporadic pituitary tumors. J Clin Endocrinol Metab 83: 1388-1391.

STIC-ILL

RC.261. A1 C15

From: Canella, Karen
Sent: Sunday, February 03, 2002 9:00 PM
To: STIC-ILL
Subject: ill order 09/815,340

Art Unit 1642 Location 8E12(mail)

Telephone Number 308-8362

Application Number 09/815,340

1. Trends in Cell biology, 2001 Jan, 11(1):18-21
2. Clinical Cancer Research, 2000 Aug, 6(8):3215-3221
3. Mutation Research, 1997 Apr 29, 375(2):157-165
4. american Journal of Hematology, 1985 Mar, 18(3):243-249.
5. PNAS, 1989 Apr, 86(7):2276-2280
6. Genes and Development, 1996 Oct 15, 10(20):2621-2631
7. Cancer, 1975 Jun, 35(6):1664-1677
8. Mutation Research, 1978, 57(3): 313-324
9. Environ Mutagen, 1981, 3(1):53-64
10. Nucleic Acids Research, 2001 Mar 15, 29(6):1300-1307
11. Oncogene:
    1998 Oct 29, 17(17):2187-2193
    2000 Jan 20, 19(3):403-409
12. Molecular endocrinology, 1999 Jan, 13(1):156-166
13. Gene, 1999 Nov 29, 240(2):317-324
14. Science, 1999 Jul 16, 285(5426)418-422
15. Biochemistry and Molecular biology international, 1999 May, 47(5):891-897
16. Journal of Clinical Endocrinology and Metabolism, 1999 Mar, 84(3):1149-1152
17. Journal of biological chemistry:
    1999 Jan 29, 274(5):3151-3158
    2000 Nov 24, 275(47):36502-36505 ***
18. Gene 2000 May 2, 248(1-2):41-50
19. Molecular endocrinology, 2000 Aug, 14(8):1137-1146
20. Cancer Letters, 2001 Feb 10, 163(1):131-139
21. Brain Pathology, 2001 Jul, 11(3):328-341

RADIOBIOLOGICAL STUDIES OF A HIGH-ENERGY MODULATED PROTON BEAM UTILIZING CULTURED MAMMALIAN CELLS

JAMES B. ROBERTSON, MS,*† JERRY R. WILLIAMS, DSc,† ROBERT A. SCHMIDT, MS,‡ JOHN B. LITTLE, MD,† DANIEL F. FLYNN, MS,† AND HERMAN D. SUIT, MD*

The modulated, 160-MeV proton beam produced by the Harvard Cyclotron has been examined in detail for its ability to kill mammalian cells as assayed by colony forming ability. Using two different cell exposure techniques, the characteristics of position and total dose in producing cell death in two aneuploid cell lines selected for their radiobiological relevance have been determined. The parameters which describe the survival curves after proton or ^{60}Co irradiation show no statistical differences, except on the distal portion of the final Bragg peak of the proton beam, where RBE increases to approximately 1.4. This increase in RBE results in extending the cell killing effect of the beam by approximately 2 mm. This effect may be of practical significance in the irradiation of tissue such as the pituitary where the position of the Bragg peak is of great importance. The overall killing efficiency ratio between the modulated high-energy proton beam and ^{60}Co γ rays was 1.00 ± .01 (standard error).

Cancer 35:1664–1677, 1975.

CLINICAL ADVANTAGES WHICH MIGHT OBtain from therapeutic applications of high-energy protons were first considered by Wilson.[51] Recently, Koehler and Preston[24] discussed advantages in dose distribution which can be achieved with modulated-energy proton beams. High-energy proton beams have been used clinically at several centers in the United States,[22,28] Sweden,[17] and the USSR.[16]

A clinical trial of proton radiation therapy is being planned which will utilize the 160-MeV Harvard Cyclotron.[42] The study will feature large fields and fractionated dose (180–200 rads per fraction), and a proton beam of broadly modulated energy. Based upon work by other groups, the RBE of such of a beam will be expected to approach closely 1.0. There is, however, a wide spread in reported RBE values for proton irradiation, as given in Table 1. Reported values that compare the RBE of protons in the plateau region with those in the Bragg peak region are tabulated in Table 2. At any given cross section within the modulated region of a particular proton beam, the flux of protons will be a composite of protons in the plateau region and protons in various positions on the Bragg peak. As this composition varies among beams from different sources, the RBE must be determined experimentally for each specific proton beam.

In preparation for our clinical study, the need for experimental determination of RBE values for the actual beams to be employed became clear. For this purpose, inactivation of mammalian cells in vitro was selected as the endpoint. RBE values have been determined by comparing D_0 and n values and cell survival at specified doses for proton and ^{60}Co irradiation. This paper describes the result of that work.

Presented at the 16th Annual Meeting of the American Society of Therapeutic Radiologists, Key Biscayne, Fl, October 30–November 3, 1974.

From the Laboratory of Radiobiology, Department of Physiology, Harvard University School of Public Health, and the Department of Radiation Medicine, Massachusetts General Hospital, Boston, MA, and The Harvard University Cyclotron, Cambridge, MA.

Supported by Grants CA-11751 and ES-00002 from the National Institutes of Health, RANN—GI—32991 from the National Science Foundation, and National Cancer Institute Grant No. CA13311.

* Department of Radiation Medicine, Massachusetts General Hospital.

† Laboratory of Radiobiology, Department of Physiology, Harvard University School of Public Health.

‡ Harvard University Cyclotron.

Address for reprints: James B. Robertson, MS, Laboratory of Radiobiology, Dept. of Physiology, Harvard University School of Public Health, 665 Huntington Avenue, Boston, MA 02115.

The authors wish to thank Dr. R. J. Schneider and Mr. A. M. Koehler of the Harvard University Cyclotron for their expert assistance and advice in these experiments.

Received for publication February 25, 1975.

TABLE 1. Reported RBE Values for High Energy Protons

Biological endpoint	Proton energy (MeV)	Dose rate (rads/min)	Reference radiation (MeV)	Dose rate (rads/min)	RBE	Reference
Mouse (whole body)						
LD_{50}[4]	730	–	.250	–	1.0	2
LD_{50}[8]	730	1000	.250	100	1.4 (MAD)	1
	730	100	.250	100	1.2 (MAD)	1
	730	100	.250	–	.96	3
	200	–	.250	–	.95, .98	3
	138	545	$^{60}Co_\gamma$	550	1.26 ± .06	13
	138	265	$^{60}Co_\gamma$	256	1.06 ± .05	13
	138	87	$^{60}Co_\gamma$	86	1.18 ± .07	13
LD_{50}[8]	157	250	.250	80	.77 ± .1	6
LD_{50}[12]	730	100, 1000	.250	20,100	.9 (MAD)*	1
	730	100, 1000	.100	100	1.2 (MAD)*	1
	730	100, 1000	.100	20	1.3 (MAD)*	1
	730	100	.250	–	.81	3
	200	–	.250	–	.81, .84	3
	138	545	$^{60}Co_\gamma$	550	1.02 ± .04	13
	138	265	$^{60}Co_\gamma$	256	.97 ± .05	13
	138	87	$^{60}Co_\gamma$	86	1.10 ± .04	13
LD_{50}[30]	2200	350	.250	112	.87 ± .05	20
	730	500–1000	.200	30	.75	49
	730	100	.250	–	.75	3
	730	–	.250	–	.7	2
	730	100, 1000	.250	20, 100	.8 (MAD)	1
	730	100, 1000	.100	20,100	1.2 (MAD)	1
	660	300–450	.180	–	.5→.6	26
	592	361	.250	80	.98	4
	440	40–80	.250	40	.72	33
	440	18	.125	18	.7 ± .2	7
	315	–	.180	–	~1	45
	200	–	.250	–	.75, .79	3
	138	545	$^{60}Co_\gamma$	550	1.06 ± .04	13
	138	265	$^{60}Co_\gamma$	256	.97 ± .05	13
	138	87	$^{60}Co_\gamma$	86	1.07 ± .04	13
	126	18–90	$^{60}Co_\gamma$	~18–90	.7	19
Mouse						
thymus weight loss	2200	350	.250	118 R/min.	1	31
	592	361	.250	80 R/min.	1.01 ± .1	4
	~90	(v. low)	.250	16 R/min.	2.08 ± .07	50
spleen weight loss	2200	350	.250	118 R/min.	1	31
	~90	(v. low)	.250	16 R/min.	1.75 ± .1	50
testes weight loss	592	361	.250	80	1.03 ± .1	4
median survival time	592	361	.250	80	1.06 ± .1	4
induction of dominant lethals	730	100	.250	–	~1	3
spermatogonial genesis	730	100	.250	–	~1	3
cataract formation	60	–	.300	–	1	15
Mouse (eye)						
chromosome aberrations	126	–	.180	–	0.67	30
Rat (whole body)						
LD_{50}[30]	660	300–450	.180	–	.6→.7	26
	510	18–90	$^{60}Co_\gamma$	~18–90	.75	19
	500	42→138	.180	5.1	.80 ± .05*	32
	500	42→138	$^{60}Co_\gamma$	4.3	.72 ± .04*	32
	240	18–90	$^{60}Co_\gamma$	~18–90	.73	19
	126	18–90	$^{60}Co_\gamma$	~18–90	.80	19
LD_{100}[30]	510	18–90	$^{60}Co_\gamma$	~18–90	.75	19
	240	18–90	$^{60}Co_\gamma$	~18–90	.79	19
	126	18–90	$^{60}Co_\gamma$	~18–90	.80	19

TABLE 1. *continued*

Biological endpoint	Proton energy (MeV)	Dose rate (rads/min)	Reference radiation (MeV)	Dose rate (rads/min)	RBE	Reference
Rat						
(rectum) histopathologic change	185	300–800	.220	340	.6–.7	39
(abdomen) weight loss and mortality	185	350	.220	400	.77 ± .18	40
Monkey (whole body)						
Macaca mulatta LD_{50}^{30}	730	1000	$^{60}Co_\gamma$	1000	1.3	52
	400	16	2.0	10.7	1.14 ± .07	12
	138	50–65	2.0	10.7	1.30 ± .09	11
hematologic changes and ^{59}Fe ferro-kinetics	400	16	2.0	10.7	1	12
	250	8.4	2.0	10.7	~1	14
	138	50–65	2.0	10.7	1	11
cardiovascular changes	400	55	$^{60}Co_\gamma$	100	1.0	25
	138	55	$^{60}Co_\gamma$	100	1.0	25
min. lethal dose LD_{50}^{30}	~200	14–20	$^{60}Co_\gamma$	–	.6 (ABD)	44
80% WBC depression	~200	14–20	$^{60}Co_\gamma$	–	1.0 (ABD)	44
Dog (whole body)						
LD_{50}^{30}	510	18–90	$^{60}Co_\gamma$	~18–90	1.15	19
	240	18–90	$^{60}Co_\gamma$	~18–90	1.15	19
	126	18–90	$^{60}Co_\gamma$	~18–90	1.0	19
Rabbit						
cataract formation	100	25	1.0	–	2.0	9
	100	25	1.0	–	2→2.4	10
	20	25	1.0	–	2.6→3	10
	20	25	1.0	–	2.6	9
skin damage	40	–	.220	–	.6–.7	38
tumor clinical response and histo-pathology	40	–	.220	–	~1	18
Mammal (whole body) mortality and organ damage	126–730	–	.200 (or ^{60}Co corrected to .200)	–	.82 ± .04	47
Vicia faba chromosome aberrations	170	–	.180	–	.70 ± .05 (AIR) .66 ± .05 (N_2)	27
E. coli K12 phage production	100	–	$^{60}Co_\gamma$	–	.85	34
Salmonella typhi TY2 reduction to 10% survival	152	8000	.250	80	1.0	5
	152	8000	$^{60}Co_\gamma$	–	1.0	5
Maize cytogenetic effects	2800	–	.250	500	4.4	37
Cultured cells						
HeLa survival	90	300	$^{137}Cs_\gamma$	78	.75 ± .06	48
CHO survival	90	300	$^{137}Cs_\gamma$	78	.68 ± .09	48
CHO abnormal metaphase	90	300	$^{137}Cs_\gamma$	78	.77	48
Ribonuclease G value	120	7000	$^{60}Co_\gamma$	7800	.91	41
Lysozyme G value	120	7000	$^{60}Co_\gamma$	7800	.92	41

* Calculated from the authors' data.

MAD = midline air dose; ABD = average body dose.

TABLE 2. Reported RBE Values of Protons in the Region of the Bragg Peak Relative to Plateau Protons

Biological endpoint	Maximum proton energy (MeV)*	Plateau reference energy (MeV)	Dose rate† (rads/min)	RBE‡ peak/plateau	Remarks	Reference
Allium cepa abnormal metaphase	185	170	40	1.2 ± 0.2	At peak and 2 mm before.	27
	185	170	15	$2.3^{+0.9}_{-0.6}$	Near the mean proton range, ~4mm H_2O after BP.	27
	185	170	1	8^{+24}_{-5}	~9mm H_2O after BP; dose ~2% of peak value.	27
Mouse bone marrow and tumor cells cell degeneration	180	~100	50–80 average	1.0	Degraded from 680 MeV; LET measured 0.7 to 2.3 kev/μ. Peak and about 2 cm after peak examined.	36
abnormal anaphase	180	~100	50–80 average	1.3		36
Cebus monkey brain lesion	160	~30–40 (~7 mm before Bragg peak)	200–7,000	1.1 – 1.4	RBE increases at end of range.	43
Chinese hamster Ovary cells cell survival	100	90 (20 r/min)	1,200	1.44 ± 0.08	Instantaneous dose rate about 10^9 rads/min.	48
	100	90 (20 r/min)	1,200	1.85 ± 0.15		48
Ribonuclease G value	160	120	7,000	0.96		41
			22,000	1.00		
Lysozyme G value	160	120	7,000	0.90		41
			22,000	0.85		

* The maximum energy is that of the accelerator employed, except in the case of the Dubna[36] beam where a magnetic channel allows momentum selection from the higher fixed energy. The ITEP[48] beam can be varied in maximum energy from 70 to 200 MeV.

† The plateau dose rates are the same as the Bragg peak rates unless otherwise noted.

‡ Note that some measurements refer to points on the descending slope of the peak, where the dose is falling off rapidly.

MATERIALS AND METHODS

Cultured Cells

The cells used for the majority of these experiments are an aneuploid line originally derived from a rat hepatoma and designated H4. They were obtained from Dr. A. H. Tashjian, Jr. at the Harvard School of Dental Medicine. The cells were maintained in Eagle's Minimum Essential Medium supplemented with nonessential amino acids, 50 U/ml of potassium penicillin, 50 mg/ml of streptomycin sulfate, 5% fetal calf serum, and 5% horse serum. Stock cultures were grown in 8-ounce glass prescription bottles (80-cm^2 growing surface area) at 37°C in a humified 5% CO_2, 95% air atmosphere. LICH cells, a human aneuploid cell originally derived from a liver explant,[8] were maintained as reported elsewhere.[29] These cells were used in some low-dose experiments.

In Technique I, cells were harvested from exponentially growing stock cultures 72 hours prior to irradiation, and plated at 2.5–5 × 10^5 cells per bottle. The cells were harvested 18 hours prior to irradiation, counted, and seeded into 250-ml plastic Falcon flasks at cell concentrations calculated to produce 100 to 200 survivors within the irradiation area. Special efforts were made to ensure an even distribution of attached cells. Response of H4 cells to irradiation is independent of plating densities up to 2 × 10^3 cells/cm^2; in the studies reported here, cells were plated at ≤ 1.2 × 10^3 cells/cm^2.

Two hours prior to irradiation, the flasks were completely filled with nutrient medium without serum, yielding a final serum concentration of

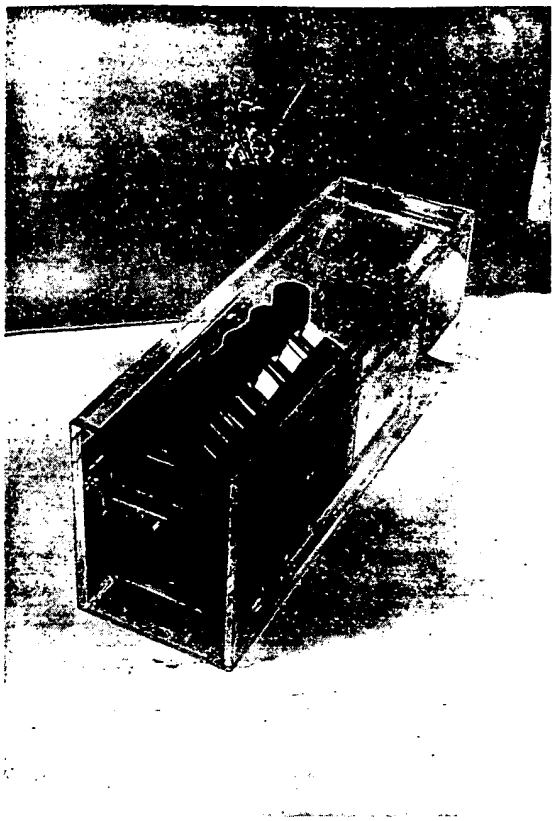

FIG. 1. Cell flask positioner. A water-tight box constructed of 1/4 inch lucite. The flasks may be positioned at any location. This apparatus was used for Technique I irradiations.

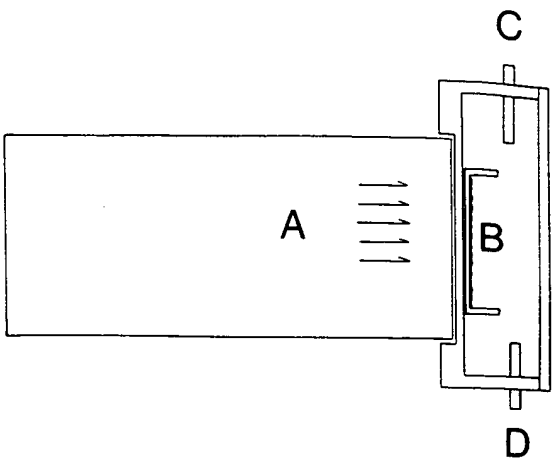

FIG. 2. The apparatus used for Technique II irradiations. The proton beam exits the telescoping water-filled sleeve (A) and strikes the cells attached to the petri dish (B). The atmosphere desired for the irradiation enters and exits through ports C and D.

2%. The flasks to be irradiated, as well as the controls, were transported by automobile to the irradiation site about 4 miles distant from the laboratory: there the cells were maintained in a 37°C water bath. Upon completion of the irradiation, the cells were returned to the laboratory, and the medium was decanted and replaced with 10 ml of fresh complete medium. The cells were then incubated for 7 days; colonies were then stained and scored. All colonies composed of 50 or more cells were counted as survivors.

In Technique II, cells were harvested from exponentially growing stock cultures, and plated at a concentration of 1×10^5 cells per (30-mm) petri dish. These cells were allowed to attach overnight, and were then transported to the irradiation site. Upon completion of irradiation, the petri dishes were returned to the laboratory and the cells were detached with trypsin, counted, and seeded in fresh medium in 100-mm petri dishes at concentrations calculated to produce 100–200 survivors. These cells were incubated for 10 to 14 days, stained, and scored.

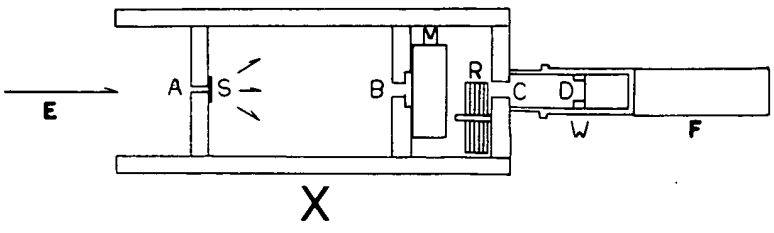

FIG. 3. Schematic view of cell irradiations: vertical cross-section along the beam axis. The beam emerges from the vacuum transport system at E and is focused at aperture A of the collimating device (X). After being scattered by a lead scatterer (S), the beam is further collimated by apertures B, C, and D. A telescoping water-filled sleeve (W) allows any portion of the depth-dose curve to be selected as the entrance dose to the cell flask positioner (F). Dose is monitored by an ionization chamber (M). The range modulator (R) is located just proximal to aperture C.

FIG. 4. Range modulator wheel. Plate I is open; all other plates are symmetrically opposed lucite blades mounted on a central motor-driven shaft. One revolution represents two modulation cycles.

Irradiation

Proton irradiations were carried out at the 160-MeV cyclotron at Harvard University, Cambridge, Massachusetts, at a dose rate of 160 to 250 rads/minute. ^{60}Co irradiations were performed on a teletherapy unit (Atomic Energy of Canada) at the Massachusetts General Hospital, Boston, at a dose rate of 20 to 73 rads/minute (see below).

The apparatus used to hold the culture flasks for Technique I is shown in Fig. 1. The lucite box is constructed to hold the plastic tissue culture flasks with the growing surfaces perpendicular to the beam of radiation; their positions along the beam axis are variable. Water at a constant temperature of 37°C circulated around the flasks. This technique permitted determination of survival at various points along the proton beam during a single irradiation. The apparatus used in Technique II is shown in Fig. 2. When this method was employed, the medium was aspirated from the dish just prior to irradiation, and immediately replaced upon completion of the irradiation. As can be seen in Fig. 2, the atmosphere overlying the cells may be readily controlled by this technique.

Cobalt-60 Dosimetry

All ^{60}Co data were generated using Technique I. The position of each flask was fixed, and the entire holder was aligned with the beam and centered such that the cell surface of the third flask was 55-cm from the source. The doses to the other flasks were then calculated, correcting for field size dependence, distance, and attenuation in the medium. The dose rate varied from 73 rads/minute to the first flask to 20 rads/minute to the fifth flask.

Proton Beam Configuration and Dosimetry

The 160-MeV proton beam of the Harvard synchrocyclotron was used in all proton irradiations. Two geometries were investigated: a small field (51-mm diameter) with 5-cm range modulation (see below), using standard collimating techniques, and a large field (25-cm diam-

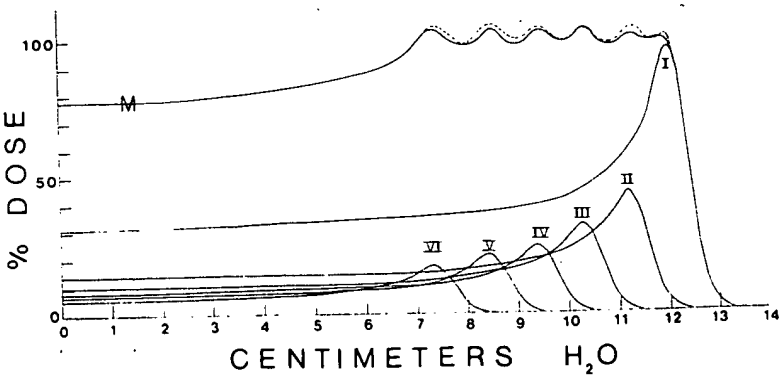

FIG. 5. Proton depth-dose employed in cell irradiations measured in a water phantom. The individual peaks (I–VI) contributing to the 5-cm broadened distribution correspond in position and height to the thickness and dwell angle of the range modulator plates, based on a measurement of the unmodulated Bragg peak for the same flux of protons as in the modulated case. The hatched curve is the summation of curve I through VI and compares well with the one experimentally measured (M).

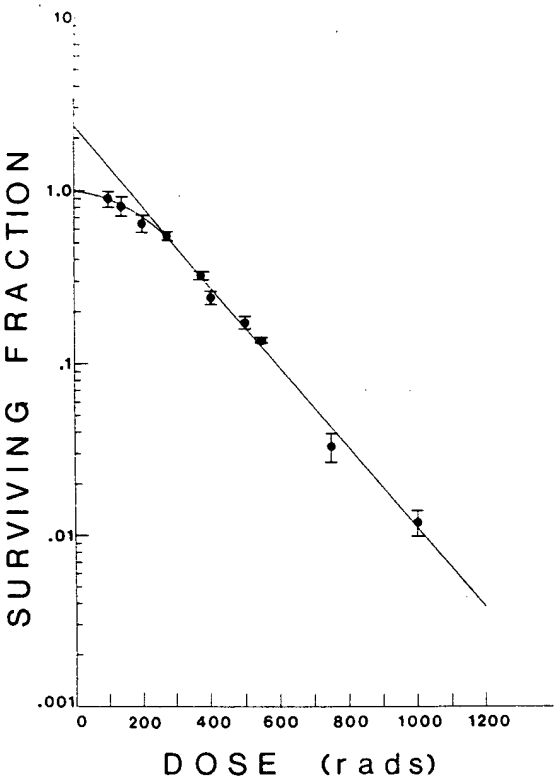

FIG. 6. Radiation survival curve for H4 cells irradiated with ^{60}Co γ rays. The D_0 was 185 rads, and the extrapolation number was 2.4. Line is the result of regression analysis of data at doses greater than 300 rads. Error bars represent one standard error.

eter) with 10-cm range modulation that has been used for fractionated therapy of cancer patients.[35] The two systems are analogous; only the former will be described here. All dose measurements were made with a miniature silicon diode. The diode was calibrated absolutely in rads against a Faraday cup which measures flux of protons of known energy in a standardized geometry.[23] The diode was then mounted on a micrometer stage at the position where the cells were located during irradiations. The dose distribution was mapped in a water phantom and normalized to the integrated output from a transmission ion chamber mounted in the collimator (M, X, Fig. 3) which acted as the dose monitor during the irradiations.

Proton Beam Shaping and Modulation

The beam was brought to a focus of about 1-cm diameter at the first of a series of four circular brass collimating apertures (Fig. 3), and then spread by a lead scatterer (9.52 g/cm^2, θ rms = 3.5°). The beam was then further collimated to the desired size, it could be adjusted in penetration depth by a water-filled adjustable telescope (W, Fig. 3) mounted after the defining aperture. The beam had some divergence at the target site and underwent a limited spreading due to multiple scattering as it penetrated. The uniformity across the beam was within 10% of the central intensity at all depths of penetration.

A rotating range modulator, as suggested by Wilson,[51] was used to alter the depth-dose characteristic of the beam, in order to achieve a flat distribution extending over 5 cm in water. The principle was that of varying the depth of penetration of the beam by interposing different thicknesses of absorber in its path, so that the result of integrating the temporally varying spatial distribution over long time periods (seconds) produced a broadened uniform axial distribution. The range modulator we constructed (Fig. 4) consisted of a stack of symmetrical lucite

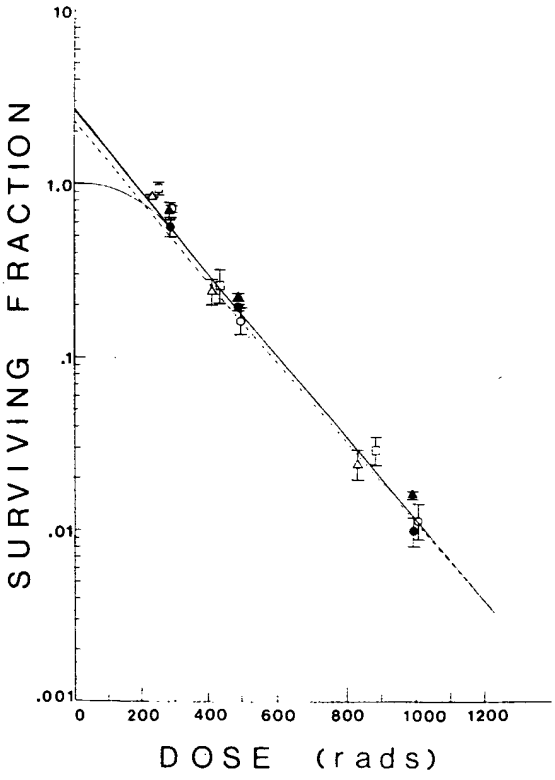

FIG. 7. Radiation survival curve for H4 cells irradiated with protons at various positions of the modulated proton beam. The D_0 was 184 rads, and the extrapolation number was 2.6. △, 2.2 cm (a); □, 4.1 cm (b); ▲, 6.2 cm (c); ●, 8.3 cm (d); ○, 8.9 cm (e). Letters represent positions as outlined on Fig. 8. Line is the result of regression analysis of data at doses greater than 300 rads. Broken line is the ^{60}Co survival curve. Error bars represent one standard error.

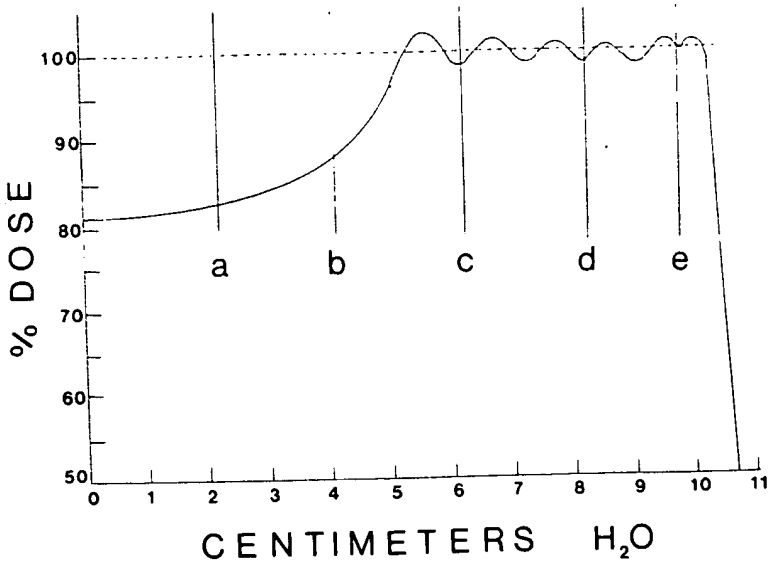

FIG. 8. Axial depth-dose profile. The locations used in proton irradiations for the results presented in Fig. 7. The apparent reduction in proton range presented here when compared with Fig. 5 is due to a fixed amount of water absorber proximal to the cell flask positioner.

plates, each with two opposing blades, mounted on a common motor-driven shaft (40 rpm, 1 ⅓ modulation cycles per second) and situated in the collimator immediately before aperture C (Fig. 3). The individual peaks obtained from the five plates and one open position were calculated from a measurement of the unmodulated Bragg peak and are plotted in Fig. 5, along with the experimentally measured depth-dose curve M. The principle of superposition of individual peaks has been described by Koehler and Preston,[24] and is verified by the dotted curve in Fig. 5, which is the summation of the dose distribution from all six peaks. The amplitudes of the peaks required were obtained by varying the dwell time of the beam at a particular depth sta-

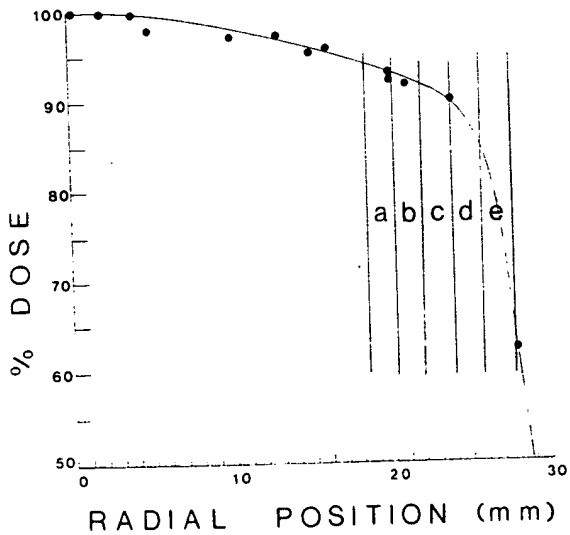

FIG. 9. Cross-section dose profile. The dose profile obtained by making a lateral scan of the modulated beam at 9.8 cm (point e, Fig. 8). The regions a, b, c, d, and e correspond to the annuli referred to in the text and in Fig. 11.

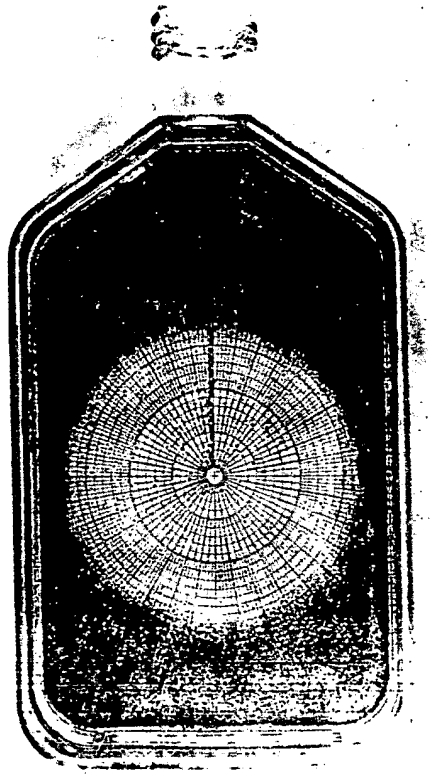

FIG. 10. An irradiated and stained flask that has been divided into annuli with polar graph paper.

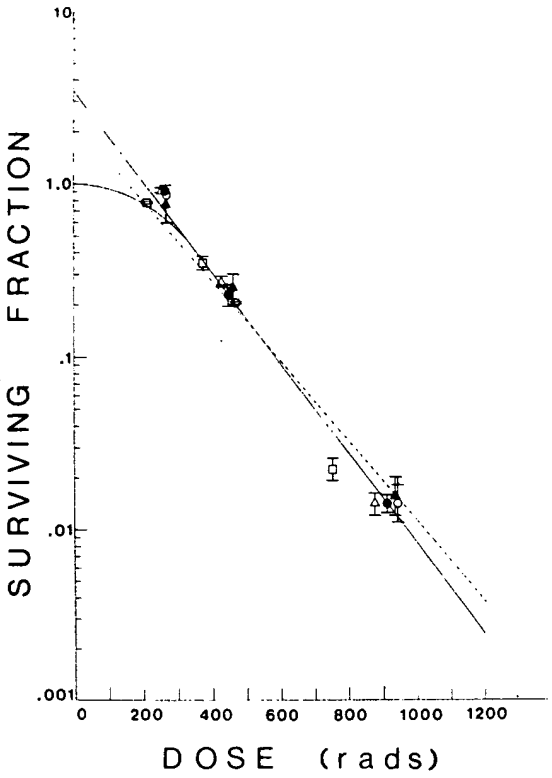

FIG. 11. Radiation survival curve for H4 cells irradiated with protons at various positions lateral to the beam central axis. The D_0 was 164 rads and the extrapolation number was 3.5. O, 94% (a); △, 93% (b), ●, 91% (c); ▲, 87% (d); □, 75% (e). The letters in brackets represent regions included as shown on Fig. 9. Line is the result of regression analysis of data at doses greater than 300 rads. Hatched line is ^{60}Co survival curve. Error bars represent one standard error.

tion, which is governed by the thickness of the plates. A full modulation cycle is represented by 180° rotation of the range modulation wheel; at the pulsed rate of the cyclotron output (≃200 pulses/second) the plate of smallest angle received an average of 11 pulses per modulation cycle. The time required for a typical dose of 200 rads was about 1 minute in this geometry, which could result in a local dose error of 1% due to an incomplete modulation cycle. Higher doses and longer irradiation times make this source of error negligible except for calibration purposes, where multiple readings and moderate dose rates improve reproducibility to ≃1%. The overall dosimetry error in absolute rads was estimated to be about 3%.

RESULTS

The results reported were all obtained using Technique I unless otherwise specified. The survival curve obtained for H4 cells with ^{60}Co γ rays is presented in Fig. 6. Figure 7 presents the results obtained with the modulated proton beam. The letters represent the various axial positions where the determinations were made. These positions are outlined in Fig. 8. The straight line portions of the survival curves were determined by a least-squares regression analysis of the survival data at doses greater than 300 rads. One can readily see that there is no significant difference in the survival curves obtained for the two different radiations used. The D_0 (inverse of the slope) for ^{60}Co and proton curves were 185 and 184 rads respectively. The extrapolation numbers were 2.4 for ^{60}Co and 2.6 for protons.

Jesseph et al.,[20] using higher-energy protons (2200 MeV), reported that laterally scattered protons might have a higher LET component. Such a component could lead to higher values of RBE at the perimeter of the modulated beam. The method used here easily lent itself to determining whether such an effect existed at lower

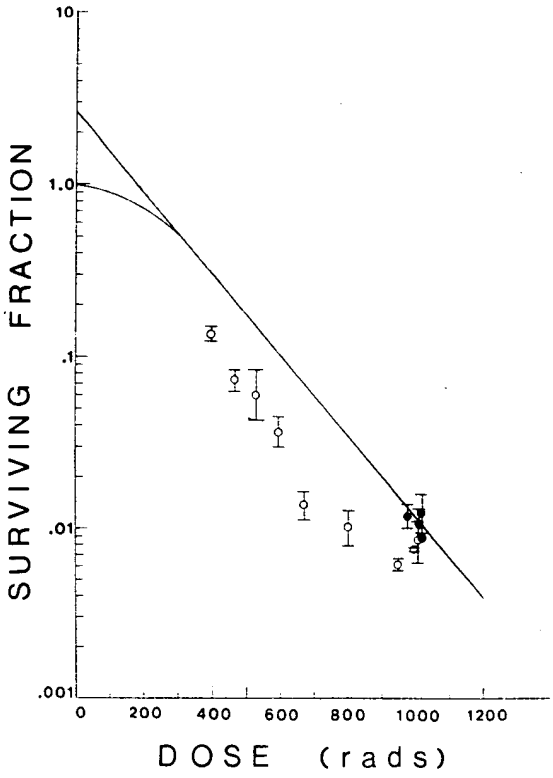

FIG. 12. Radiation survival at points distal to last maximum of modulated beam for H4 cells. Curve is that obtained for porton irradiations proximal to the last peak (Fig. 7). ●, points proximal to last peak, O, points distal to the last peak. Error bars represent one standard error.

energies. This was performed in the following manner: A lateral scan of the deposited dose at a given point was made. The dose profile obtained is presented in Fig. 9. With this information the irradiated area could be divided into annuli, the area of each annulus determined, and the number of cells plated into each annulus calculated. By counting the numbers of survivors within each annulus and using the dose delivered to the center of the annuli as the dose absorbed in each annulus, a survival curve was constructed. A typical flask irradiated and then divided into annuli with polar graph paper is shown in Fig. 10. The survival curve derived from data obtained in this manner is presented in Fig. 11, along with the curve obtained for axial positions. The slopes of the two curves obtained do not differ singificantly from each other ($.2 > p > .1$; t-test of slopes). However, at survival levels between .01 and .02 one can see an apparent trend toward increasing RBE as one proceeds laterally. Additional studies are planned to examine this effect. The sharpness of the beam prevented obtaining meaningful results on the periphery where the dose was less than 75% of the axial dose.

Figure 12 represents cell survival on the distal portion of the last maximum of the modulated beam. The survival curve is that of cells on the broadened peak; the data points correspond to cell survival as flasks are positioned sequentially at more distal regions of the beam, where the attenuation of the proton beam is reducing the absorbed dose. The closed circles represent survival at or proximal to the last maximum. The open circles represent survival at points distal to the last maximum. The fact that these points fall below the survival curve demonstrates that distal irradiation is more effective in killing cells. The RBE for each position can be calculated from these data, such calculations from several experiments are plotted in Fig. 13. In this figure, the RBE values obtained are plotted as a function of the distance from the center of the last Bragg peak. The open circles represent the data obtained with the unmodulated beam and Technique II, and the closed circles are the data obtained with the modulated beam and Technique I. Figure 14 shows the difference observed between the dose measured physically and that required to produce the survival levels observed at those positions (biological dose). One can see that the "biological" Bragg peak is extended about 2 mm beyond the physical peak.

Since most therapeutic treatments involve exposures of 200 to 300 rads, experiments were undertaken to measure the RBE of protons in this dose range. Measurements in this range are difficult, because survival changes are small compared to the variability in a single measurement. Figure 15 represents a composite of 102 survival measurements with H4 cells in this dose range. Here the surviving fraction was plotted on linear coordinates for doses from 100 to 300 rads, and least-squares regression performed. The hatched lines represent the 99% confidence interval for proton irradiations. The confidence interval for the proton irradiations is contained

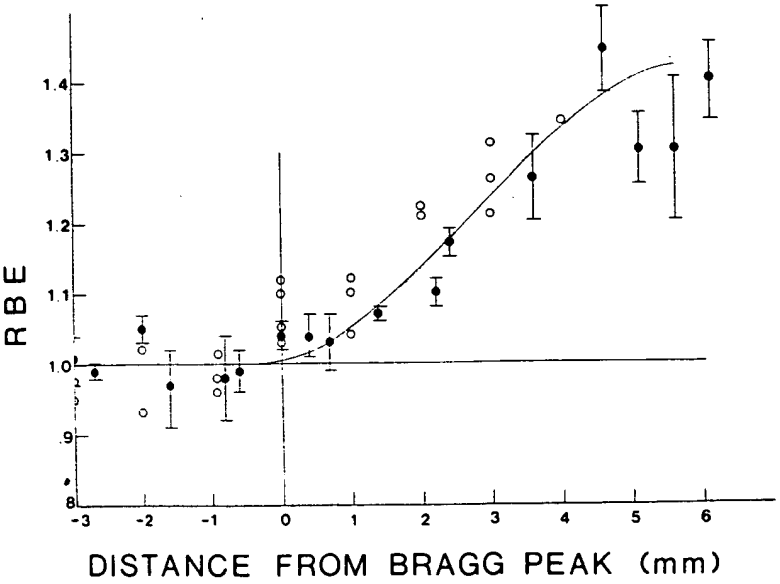

FIG. 13. RBE for H4 cell survival of protons with respect to ^{60}Co at various positions of the Bragg peak. Open circles represent results obtained with the unmodulated beam (peak I. Fig. 5) using Technique II. Closed circles represent results obtained with the modulated beam using Technique I. Error bars represent standard error. The curve was drawn by eye to demonstrate trend.

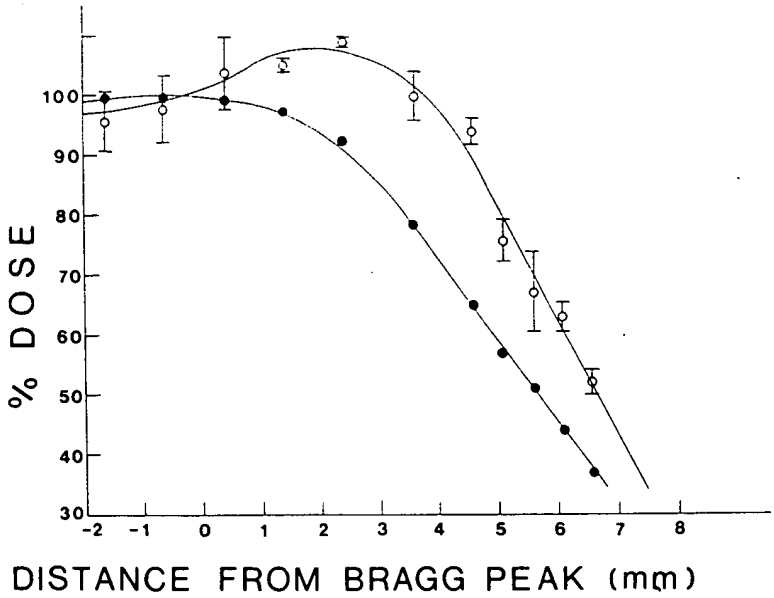

FIG. 14. Physical and biological Bragg peak. The closed circles represent the Bragg peak as determined by physical measurement. The open circles represent the "biological Bragg peak" (proximal dose required to produce observed survival levels of H4 cells). Error bars represent range of dose needed to produce one standard error in survival.

entirely within the corresponding interval for the ^{60}Co results. Similar results were obtained when LICH cells were used.

DISCUSSION

The average of a total of 78 determinations, at doses greater than 300 rads and proximal to the last Bragg peak, yielded an RBE of 1.00 ± .01 (standard error; standard deviation ± .08) for the proton beam. Analysis of 102 measurements indicated that the RBE at doses between 200 and 300 is also approximately 1.0. The effect of the increased RBE at the distal end of the last Bragg peak in the modulated beam was to extend the effect of the beam by approximately 2mm.

In an effort to evaluate what effect this extension of the Bragg peak would have within the modulated region of the beam, a calculation was done using the RBE values obtained at given distances from the last Bragg peak. In Fig. 16 the solid curve represents the beam calculated from physical considerations only. The hatched line represents the beam that is constructed if each millimeter segment of the modulated beam is

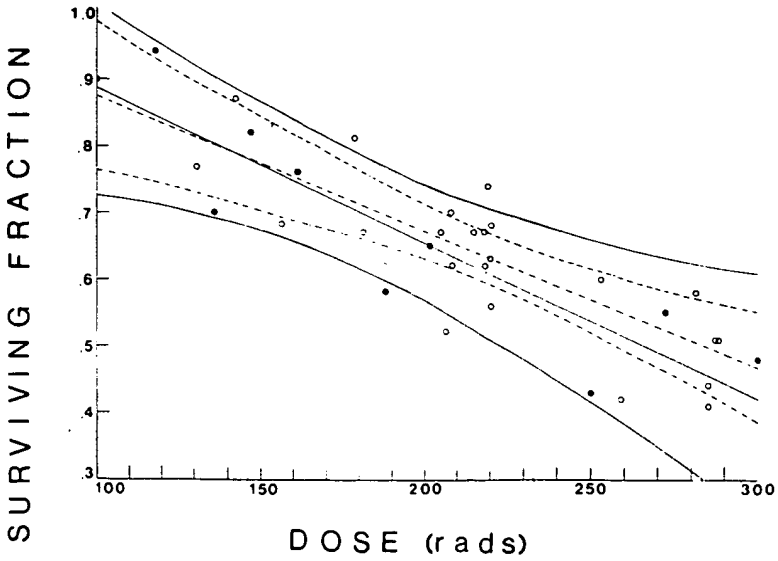

FIG. 15. Radiation survival at low doses of H4 cells. O, proton irradiation: ●, ^{60}Co γ-ray irradiation. Hatched lines represent regression analysis of proton data and 99% confidence interval for regression line. Solid lines represent regression analysis of ^{60}Co data and 99% confidence interval for regression line. Points represent mean survival value at the given doses.

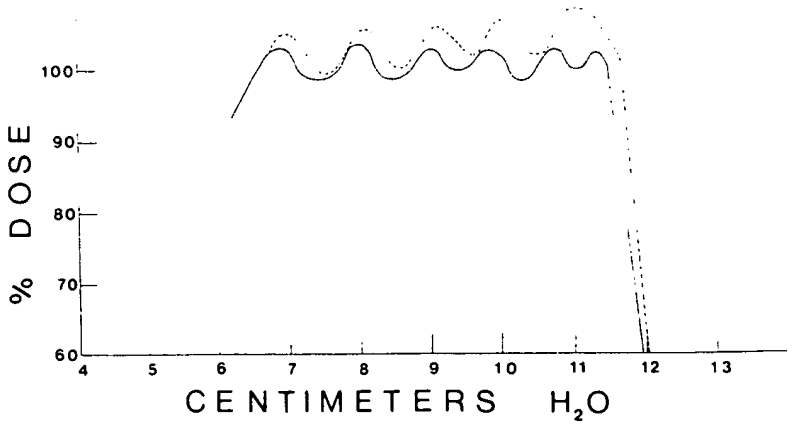

FIG. 16. The solid line represents the modulated beam calculated from physical considerations only. The broken line is the curve obtained if RBE corrections are made for individual peaks before summing them to obtain the modulated beam. Note abbreviated ordinate.

broken down into its fractional portion of individual beams and these are corrected for the RBE expected at that portion of the beam. By integrating the area under the two curves one can calculate that the increase in biologically effective dose for the RBE corrected beam would be 3% in the modulated region.

In simultaneous experiments, Todd,[46] using T-1 human kidney cells grown and irradiated on plastic cover slips, determined that the RBE of this beam was about 1.0 at all locations and at all doses examined. These findings are in agreement with ours.

Our results may explain the wide range of values reported for the RBE of the Bragg peak portion of the proton beam when compared to the plateau region. Jung[21] demonstrated that protons became more effective in inactivating ribonuclease as they decreased in energy. This was attributed to an increase in LET as the proton energy decreased below 0.1 MeV. Wainson et al.[48] reported no difference in RBE for plateau protons and those in the ascending curve, but found an RBE of 1.4 in the descending portion of the curve, using survival of Chinese hamster cells as the endpoint. These same authors reported an RBE of 1.9 for peak vs. plateau protons for the induction of chromosome aberrations in Chinese hamster cells. Other investigators have reported different values: Larsson et al.[27] found an RBE of 1.2 ± 0.2 for Bragg peak vs. plateau protons using chromosome aberrations in root tips of *Allium cepa* as the endpoint, and Sweet *et al.*[43] found an increasing RBE for brain lesions in cebus monkeys as one proceeded distally along the descending portion of the Bragg peak. On the other hand, Shmakova and Yarmoneko,[36] using mouse bone marrow and tumor cell degeneration, reported no difference in the effects of Bragg peak or plateau protons (RBE = 1.0). It would thus appear that the RBE of protons in the Bragg peak when compared to those in the plateau is a function of the endpoint chosen to measure the effect. The present findings would also indicate that it is a function of position on the Bragg peak, in accord with the findings of Larsson and Kihlman.[27]

In summary, our results suggest that no unexpected RBE effects are likely to be seen in therapeutic use of a modulated proton beam, and that the experience gained in clinical use of ^{60}Co γ rays should have direct application in treatment planning using a beam of modulated protons. One should, however, be aware of the biological extension of the peak in those applications where exact positioning of the end of the beam is required.

REFERENCES

1. Ashikawa, J. K., Sondhaus, C. A., Tobias, C. A., Greenfield, A. G., and Paschkes, V.: Difference in injury mode, dose-rate dependence and RBE of 730 MeV protons, 100 kVp X-rays and 250 kVp X-rays. *In* Biological Effects of Neutron and Proton Irradiations, vol. 1. Vienna, International Atomic Energy Agency, 1964; pp. 249-260.

2. Ashikawa, J. K., Sondhaus, C. A., Tobias, C. A., and Kayfetz, L. L.: Effects of high energy charged particles irradiation on mice—II. Factors influencing biological effectiveness of high energy charged particles. *Radiat. Res.* 25:173-174, 1965 (abstr.).

3. Ashikawa, J. K., Sondhaus, C. A., Tobias, C. A.,

Kayfetz, L. L., Stephens, S. O., and Donovan, M.: Acute effects of high-energy protons and alpha particles in mice. *Radiat. Res. [Suppl.]* 7:312–324, 1967.

4. Baarli, J., and Bonét-Maury, P.: Relative biological effectiveness of 592 MeV protons on mice. *Nature* 205:361–365, 1965.

5. Bonét-Maury, P., Baarli, J., Kahn, T., Dardenne, G., Frilley, M., and Deysine, A.: Determination on mice and other organisms of the RBE of high energy protons and electrons. *In* Biological Effects of Neutron and Proton Irradiations, vol. 1. Vienna, International Atomic Energy Agency, 1964; pp. 261–277 (French).

6. Bonét-Maury, P., Deysine, A., Frilley, M., and Stephan, C.: Efficacité biologique relative des protons de 157 MeV. *C. R. Acad. Sci. [D] (Paris)* 251:3087–3089, 1960.

7. Bradley, F. J., Watson, J. A., Doolittle, D. P., Brodsky, A., and Sutton, R. B.: RBE of 440 MeV proton radiation compared to 125 kVp X-rays for LD^{30}_{50} of mice. *Health Phys.* 10:71–73, 1964.

8. Chang, R. S.: Continuous subcultivation of epithelial-like cells from normal human tissues. *Proc. Soc. Exp. Biol. Med.* 87:440–443, 1954.

9. Cleary, S. F., Geeraets, W. J., Williams, R. C., Mueller, H. A., and Ham, W. T., Jr.: Lens changes in the rabbit from fractionated X-ray and proton irradiations. *Health Phys.* 24:269–276, 1973.

10. Cleary, S. F., Geeraets, W. J., Williams, R. C., Mueller, H. A., and Ham, W. T., Jr.: X-ray and proton induced lens changes in the rabbit. *Health Phys.* 24:453–459, 1972.

11. Dalrymple, G. V., Lindsay, I. R., Ghidoni, J. J., Hall, J. D., Mitchell, J. C., Kundel, H. L., and Morgan, I. L.: Some effects of 138 MeV protons on primates. *Radiat. Res.* 28:471–488, 1966.

12. Dalrymple, G. V., Lindsay, I. R., Ghidoni, J. J., Mitchell, J. C., and Morgan, I. L.: Some effects of 400 MeV protons on primates. *Radiat. Res.* 28:507–528, 1966.

13. Dalrymple, G. V., Lindsay, I. R., Hall, J. D., Mitchell, J. C., Ghidoni, J. J., Kundel, H. L., and Morgan, I. L.: The relative biological effectiveness of 138 MeV protons as compared to cobalt 60 gamma radiation. *Radiat. Res.* 28:489–506, 1966.

14. Dalrymple, G. V., Lindsay, I. R., Ghidoni, J. J., Mitchell, J. C., and Morgan, I. L.: An estimate of the biological effects of the space proton environment. *Radiat. Res.* 28:548–566, 1966.

15. Darden, E. B., Christenberry, K. W., Beauchamp, J. J., Bender, R. S., Jernigan, M. C., Conklin, J. W., and Upton, A. C.: Comparison of 60 MeV protons and 300 kVp X-rays for induction of lens opacities in R.F. mice. *Radiat. Res.* 43:598–612, 1970.

16. Dzhelepov, V. P., Goldin, L. L.: The use of existing heavy particle accelerators and the possibilities of creating new domestic ones for radiation therapy. Transl. 142 of JINR—P9—4560 Univ. Calif. Radiat. Lab., 1969.

17. Falkmer, S., Fors, B., Larsson, B., Lindell, A., Naeslund, J., and Sténson, S.: Pilot study on proton irradiation of human carcinoma. *Acta Radiol.* 58:33–51, 1962.

18. Falkmer, S., Larsson, B., and Sténson, S.: Effects of single dose proton irradiation of normal skin and VX2 carcinoma in rabbit ears—A comparative investigation with protons and roentgen rays. *Acta Radiol.* 52:217–234, 1959.

19. Grigoriev, Yu. G., Darenskia, N. G., Domshlak, M. M., Lebedinsky, A. V., Nefedov, Yu. G., and Rizov, N. I.: Characteristics of the biological effects and the RBE of high energy protons. *In* Biological Effects of Neutron and Proton Irradiations, vol. 1. Vienna, International Atomic Energy Agency, 1964; pp. 223–230 (Russian).

20. Jesseph, J. E., Moore, W. H., Straub, R. F., Tisljarlentulis, G. M., and Bond, V. P.: The RBE of 2.2 BeV protons for 30 day lethality in mice. *Radiat. Res.* 36:242–253, 1968.

21. Jung, H.: Inactivation of ribonuclease by elastic nuclear collisions. *Radiat. Res.[Suppl.]* 7:64–73, 1967.

22. Kjellberg, R. N., Sweet, W. H., Preston, W. M., and Koehler, A. M.: The Bragg peak of a proton beam in intracranial therapy of tumors. *Trans. Am. Neurol. Assoc.* 87:216–218, 1962.

23. Koehler, A. M.: Dosimetry of proton beams using small silicon diodes. *Radiat. Res. [Suppl.]* 7:53–63, 1967.

24. Koehler, A. M., and Preston, W. M.: Protons in radiation therapy—Comparative dose distributions for protons, photons, and electrons. *Radiology* 104:191–195, 1972.

25. Kundel, H. L.: The effects of high energy proton irradiation on the cardiovascular system of the Rhesus monkey. *Radiat. Res.* 28:529–537, 1966.

26. Kurlyandskaya, E. B., Avrunina, G. A., Ponosmaneva, V. L., Fedorous, V. I., Yanovskaya, B. I., and Yarmonenko, S. P.: Relative biological effectiveness (RBE) of 660 MeV protons. *Dokl. Akad. Nauk SSSR* 142:702–705, 1962 (Russian).

27. Larsson, B., and Kihlman, B.: Chromosome aberrations following irradiation with high energy protons and their secondary radiation—a study of dose distribution and biological efficiency using root-tips of *Vicia faba* and *Allium cepa*. *Int. J. Radiat. Biol.* 2:8–19, 1960.

28. Lawrence, J. H., Tobias, C. A., Born, J. L., Wang, C. C., and Linfoot, J. H.: Heavy-particle irradiation in neoplastic and neurologic disease. *J. Neurosurg.* 19:717–722, 1962.

29. Little, J. B.: Differential response of rapidly and slowly proliferating human cells to x-irradiation. *Radiology* 93:307–313, 1969.

30. Mastrukova, E. M., and Strijijowsky, A. D.: The biological action of 126 MeV protons on the mouse cornea epithelium. *In* Problems of Radiation Safety of the Space Flights. Moscow, Atomizdat, 1964; pp. 143–151 (Russian).

31. Montour, J. L., Straub, R. F., and Shellabarger, C. J.: The relative biological effectiveness of 2.2 GeV protons for thymus and splenic weight-loss in mice. *Int. J. Radiat. Biol.* 15:491–496, 1969.

32. Moskalev, Yu. I., Petrovich, I. K., Strelchova, V. N.: The biological effect of fast neutrons and high energy protons. *In* Biological Effects of Neutron and Proton Irradiations, vol. 1. Vienna, International Atomic Energy Agency, 1964; pp. 197–219 (Russian).

33. Oldfield, D., Doull, J., Plzak, V., Hasegawa, A., and Sandberg, A.: *USAF Radiation Laboratory Quarterly Report* 46:134–158, 1963.

34. Rybakov, N. I., Ryjov, I. I., Kolobov, A. V., and Kovalev, E. E.: RBE of 630 and 100 MeV protons measured by their action on lysogenic bacteria. *In* Biological Action of High Energy Protons. Moscow, Atomizdat, 1967; pp. 146–153 (Russian).

35. Schneider, R. J., Schmidt, R. A., and Koehler, A. M.: Physical preparations for cancer therapy at the Harvard Cyclotron Laboratory. *Bull. Am. Phys. Soc.* 19:31, 1974 (Abstr.).

36. Shmakova, N. L., and Yarmonenko, S. P.: Action of 180 MeV protons in different parts of the Bragg curve on the normal and neoplastic cells. *Med. Radiol. (Mosk.)* 15, No. 7:8–12, 1970 (Russian).

37. Smith, H. H.: Relative biological effectiveness of different types of ionizing radiations: cytogenetic effects in maize. *Radiat. Res.[Suppl.]* 7:190–195, 1967.

38. Sténson, S.: Högenergetiska protoners inverkan på VX2 tumörer på kanin. *Nord. Med.* 59:786, 1958.

39. Sténson, S.: Effects of proton and Roentgen radiation

on the rectum of the rat. *Acta Radiol. [Ther.](Stockh.)* 8:263–278, 1969.

40. Sténson, S.: Weight change and mortality of rats after abdominal porton and Roentgen irradiation. *Acta Radiol.[Ther.] (Stockh.)* 8:423–432, 1969.

41. Stratton, K.: Electron spin resonance studies on proton-irradiated ribonuclease and lysozyme. *Radiat. Res. [Suppl.]* 7:102–115, 1967.

42. Suit, H. D., Goitein, M., Tepper, J., Koehler, A. M., Schmidt, R. A., and Schneider, R.: Exploratory study of proton radiation therapy using large field techniques and fractionated dose schedules. *Cancer* 35:1646–1657, 1975.

43. Sweet, W. H., Kjellberg, R. N., Field, R. A., Koehler, A. M., and Preston, W. M.: Time intensity data in solar cosmic-ray events: biological data relevant to their effects in man. *Radiat. Res. [Suppl.]* 7:369–383, 1967.

44. Taketa, S. T., Castle, B. L., Howard, W. H., Conley, C. C., Haymaker, W., and Sondhaus, C. A.: Effects of acute exposure to high energy protons on primates. *Radiat. Res: [Suppl.]* 7:336–359, 1967.

45. Tobias, C. A., Anger, H. O., and Lawrence, J.H.: Radiological use of high energy deutrons and alpha particles. *Am. J. Roentgenol.* 67:1–27, 1952.

46. Todd, P.: Radiobiology with heavy charged particles directed at radiotherapy. *Eur. J. Cancer* 10:207–210, 1974.

47. Ueno, Y., and Grigoriev, Y. G.: The RBE of protons with energy greater than 126 MeV. *Br. J. Radiol.* 42:475, 1969.

48. Wainson, A. A., Lomanov, M., F., Shmakova, N. L., Blokhin, S. I., and Jarmonenko, S. P.: The RBE of accelerated protons in different parts of the Bragg curve. *Br. J. Radiol.* 45:525–529, 1972.

49. Wang, C. C., Lyman, J., and Tobias, C. A.: Relative biological effectiveness of 730-MeV proton particles for acute lethality of mice. *UCRL-10211*:43–49, 1962.

50. Warshaw, S. D., and Oldfield, D. G.: Pretherapeutic studies with the Chicago synchrocyclotron. *Am. J. Roentgenol.* 78:876–886, 1957.

51. Wilson, R. R.: Radiological use of fast protons. *Radiology* 47:487–491, 1946.

52. Zellmer, R., Culver, J., and Pickering, J. E.: Proton-irradiation effects in primates. *Radiat. Res. [Suppl.]* 7:325–329, 1967.

STIC-ILL

Q11.N26

From: Canella, Karen
Sent: Sunday, February 03, 2002 9:00 PM
To: STIC-ILL
Subject: ill order 09/815,340

Art Unit 1642 Location 8E12(mail)

Telephone Number 308-8362

Application Number 09/815,340

1. Trends in Cell biology, 2001 Jan, 11(1):18-21
2. Clinical Cancer Research, 2000 Aug, 6(8):3215-3221
3. Mutation Research, 1997 Apr 29, 375(2):157-165
4. american Journal of Hematology, 1985 Mar, 18(3):243-249.
5. PNAS, 1989 Apr, 86(7):2276-2280
6. Genes and Development, 1996 Oct 15, 10(20):2621-2631
7. Cancer, 1975 Jun, 35(6):1664-1677
8. Mutation Research, 1978, 57(3): 313-324
9. Environ Mutagen, 1981, 3(1):53-64
10. Nucleic Acids Research, 2001 Mar 15, 29(6):1300-1307
11. Oncogene:
    1998 Oct 29, 17(17):2187-2193
    2000 Jan 20, 19(3):403-409
12. Molecular endocrinology, 1999 Jan, 13(1):156-166
13. Gene, 1999 Nov 29, 240(2):317-324
14. Science, 1999 Jul 16, 285(5426)418-422
15. Biochemistry and Molecular biology international, 1999 May, 47(5):891-897
16. Journal of Clinical Endocrinology and Metabolism, 1999 Mar, 84(3):1149-1152
17. Journal of biological chemistry:
    1999 Jan 29, 274(5):3151-3158
    2000 Nov 24, 275(47):36502-36505 ***
18. Gene 2000 May 2, 248(1-2):41-50
19. Molecular endocrinology, 2000 Aug, 14(8):1137-1146
20. Cancer Letters, 2001 Feb 10, 163(1):131-139
21. Brain Pathology, 2001 Jul, 11(3):328-341

Proc. Natl. Acad. Sci. USA
Vol. 86, pp. 2276–2280, April 1989
Genetics

Lack of DNA homology in a pair of divergent chromosomes greatly sensitizes them to loss by DNA damage

MICHAEL A. RESNICK*, METTE SKAANILD†, AND TORSTEN NILSSON-TILLGREN†

*Yeast Genetics/Molecular Biology Group, Cellular and Genetic Toxicology Branch, National Institute of Environmental Health Sciences, Research Triangle Park, NC 27709; and †Institute of Genetics, University of Copenhagen, O.Farimagsgade 2A, DK-1353 Copenhagen K, Denmark

Communicated by Leland Hartwell, November 9, 1988

ABSTRACT **Chromosomal DNA is considered *a priori* to be a target for the induction of numerical (whole chromosome) aneuploidy in mitotic cells. If true, DNA repair would be expected to contribute to genome stability. One type of repair that appears to play an important role in the response of many organisms to DNA-damaging agents involves recombination. Using the yeast *Saccharomyces cerevisiae* containing a pair of DNA divergent (homoeologous) chromosomes, we have been able to determine the importance of recombinational repair of DNA damage in the maintenance of chromosome number. Specifically, the induction of aneuploidy by ionizing radiation has been examined in diploids that had one chromosome III replaced by a divergent chromosome from *Saccharomyces carlsbergensis*. The chromosomes are functionally equivalent but lack precise DNA homology over one-half their length. The absence of homology, and thus the opportunity for recombinational repair (presumably of DNA double-strand breaks) in the divergent chromosomes, results in high levels (5–10%) of aneuploidy for chromosome III at doses of radiation resulting in almost no killing. For homologous chromosomes, the frequency of loss is 20–50 times lower.**

Chromosomal segregation in mitotically growing cells is an accurate process with an error frequency that varies from approximately 10^{-2} to 10^{-4} per chromosome in human cells to as low as 10^{-5} in yeast (summarized in ref. 1). While much of the segregation apparatus is expected to be a target for aneuploidy induction, there is a paucity of information about processes leading to aneuploidy or the mechanisms of action by reported aneuploidogens (1). Evidence is generally lacking that chromosomal DNA is a target for the induction of numerical (whole chromosome) aneuploidy in mitotic cells.

In the yeast *Saccharomyces cerevisiae*, considerable progress has been made in the genetic characterization of the segregational apparatus and systems required for chromosome stability. Mutations include those affecting cell division cycle (2), repair and recombination (3, 4), specific and general chromosome stability (5, 6), the centromere (summarized in ref. 7), topoisomerase II (8), and α-tubulin (9). We are using the yeast *S. cerevisiae* to identify the components of the mitotic apparatus that are targets for aneuploidy induction as well as the processes that lead to aneuploidy (10).

Chromosomal DNA is a likely target for induction of numerical aneuploidy, and DNA repair would be expected to contribute to genome stability. Recombinational repair plays an important role in the response of many organisms to DNA damage. The repair of radiation-induced double-strand breaks (DSBs) is an efficient process in yeast, where it occurs through recombination (11, 12). In this paper, we address the role of recombinational repair in maintaining genomic stability following ionizing radiation exposure and the consequences when recombination is prevented due to lack of homology.

Radiation-induced aneuploidy has been examined in *S. cerevisiae* diploids that had one chromosome III replaced by a divergent chromosome from the related yeast *Saccharomyces carlsbergensis* (13). While the two chromosomes were functionally equivalent and exhibited the same gene order, the lack of precise DNA homology in half the length of a chromosome pair (ref. 13; see Fig. 1 and *Materials and Methods*) was expected to prevent recombinational repair processes in this region. The inability to repair ionizing radiation-induced DNA damage (presumably DSBs) in this region via recombination results in high levels of chromosome loss rather than chromosome deletions or malsegregation at nonlethal doses.

MATERIALS AND METHODS

Strains. Strains 230283BI-57 and 021281AI-6 are derived from the Cold Spring Harbor collection (Table 1). The his^- alleles in each diploid strain are complementing (i.e., HIS^+). Strains 300686C-2, 300686H-45, and 290986C-34U are *S. cerevisiae* haploids with chromosome III replaced by a divergent chromosome from *S. carlsbergensis* (13). The *his4* alleles in the *S. carlsbergensis* chromosomes were induced by ethyl methane sulfonate (T.N.-T., unpublished data). The alleles belong to the *HIS4A* and the *HIS4C* region (T.N.-T., unpublished data) based on complementation patterns with known *S. cerevisiae his4* alleles.

S. carlsbergensis chromosome III is functionally homologous to chromosome III of *S. cerevisiae* but genetic as well as molecular analyses indicate that the chromosome is composed of two different sections (13, 14) with the left part being divergent from and the right part homologous to the *S. cerevisiae* chromosome (see Fig. 1). No meiotic recombination occurs in the region from *HML* (near the left telomere) to *MAT*. This appears to result from nucleotide sequence differences in this region, as shown for four loci (*HML*, *HIS4*, *LEU2*, and *MAT* exhibit about 80–90% DNA homology; ref. 14). In the region to the right of *MAT*, the recombination levels are normal for the *MAT–THR4* interval and the molecular structure of *SUP61* and *HMR* appears identical to those of *S. cerevisiae* (14).

Noncomplementing heteroallelic diploids carrying one *S. carlsbergensis* allele and one *S. cerevisiae* allele exhibit spontaneous and ultraviolet light-induced mitotic recombination levels that are both 100–1000 times lower than in similar pure *S. cerevisiae* strains. Since recombination is greatly reduced, stable diploids with complementing heteroalleles can be constructed. The appearance of histidine auxotrophs in such diploids is likely to signal genetic events other than recombination.

Growth Conditions and Irradiation. Media and growth procedures have been described (15). Cells were grown in

The publication costs of this article were defrayed in part by page charge payment. This article must therefore be hereby marked "*advertisement*" in accordance with 18 U.S.C. §1734 solely to indicate this fact.

Abbreviation: DSB, double-strand break.

Table 1. Genotypes of strains

Strain	Chromosome	Genotype						
D-VG	(*S. cerevisiae*) 021281AI-6 / 300686C-2 (*S. carlsbergensis*)	*his4-15 leu2 MATa thr4* / *his4-S3 + MATα +*	*ade2* / +	+ / *ade1*	*cyh2* / +	*+ ura3* / *can1 +*	+ / *lys2*	+ / *ura4*
D-VGG	Same as D-VG except the strain is disomic for the *S. carlsbergensis* chromosome							
H-VV	021281AI-6 / 230283BI-57 (*S. cerevisiae*)	*his4-15 leu2 MATa thr4* / *his4-290 + MATα +*	*ade2* / +	*cyh2* / +	*ura3* / +	+ / *lys1*		
H-GG	(*S. carlsbergensis*) 300686H-45 / 290986C-34a (*S. carlsbergensis*)	*his4-S7 + MATa* / *his4-S3 + MATα*	*ade1* / +	*lys2* / +	*can1 +* / *+ ura3*			

histidineless medium for 2–3 days. Since ≈95% of the cells lacked buds, only 5% were in the S or G_2 phase of the cell cycle. Cells were washed with water, resuspended at 5×10^4 cells per ml, and irradiated at 0°C in a Shepherd Mark I ^{137}Cs irradiator (model 68-A) at a dose rate of 3.6 krad/min (1 rad = 0.01 Gy). Cells were diluted and plated to yeast extract/peptone/dextrose (YEPD) and grown at 30°C. Colonies were replicated to the appropriate medium to determine genotype.

Genetic Analysis. Standard tetrad analysis methods were used. To investigate whether strains expressing the *MAT***a** or *MATα* mating type were monosome or euploid for chromosome III, they were crossed to appropriately marked diploids. For isolates expressing the *S. carlsbergensis*-specific markers (*his4-S3* and *MATα*) the tester strain was a diploid monosomic for chromosome III (*his4-15 leu2 MAT***a** *thr4*). For isolates expressing the *S. cerevisiae* specific markers (*his4-15 leu2 MAT***a** and *thr4*) the tester strain carried two copies of the *S. carlsbergensis* chromosomes III (*his4-S3 MATα*). The resulting tetraploids were sporulated and dissected. Based on the mating characteristics of spore colonies from the tetrads and the segregation of the *his4* and *leu2* markers, it was possible to assess whether the original diploids were monosome or euploid. Because homologous chromosomes (*S. cerevisiae* or *S. carlsbergensis*; unpublished data) preferentially disjoin in meiosis and there is no recombination between the linked genes *HIS4*, *LEU2*, and *MAT*, this linkage group segregates in the first meiotic division.

Physical Analysis of Chromosomes. Chromosomes were separated according to size using pulse field gel electrophoresis methods (16).

RESULTS

Radiation-Induced Loss of Genetic Markers in Divergent vs. Homologous Pairs of Chromosome III. In yeast, the repair of radiation-induced DSBs, as well as other double-strand damage involves recombination (11, 12), and a reduction in homology would be expected to reduce repair. To examine the consequences of reducing the opportunity for recombination, we developed diploid strains in which all but 1 (chromosome III) of the 16 pairs of chromosomes are homologous. The remaining pair is divergent (i.e., homoeologous); one chromosome is derived from *S. carlsbergensis* and the other is from *S. cerevisiae*. Nearly half of the chromosome III pair exhibits no or greatly reduced recombination in both meiosis and mitosis (from *MAT* to the left telomere); a high level of DNA homology exists in the other half (Fig. 1; see *Materials and Methods*; ref. 13). The system we developed to detect possible damage-induced genetic changes was based on complementing mutations in the *HIS4* locus at different functional regions of the locus (19). Loss of an allele results in histidine auxotrophy and can be detected by replica-plating colonies that arise on rich medium to histidineless medium. At high levels of survival, this also allows sectored vs. whole colony events to be discriminated.

Exposure of the divergent chromosome III strain to nonlethal doses of radiation induced high frequencies of his^- colonies. After only 5 krad, the histidine auxotroph frequency was ≈3%, and this increased linearly to ≈20 krad (Table 2). The induction of his^- colonies was much lower in homologous strains. Over 95% of the his^- colonies derived from the divergent strain also expressed a mating-type allele. Nearly half were *MAT***a** and expressed *leu2* and *thr4*; the

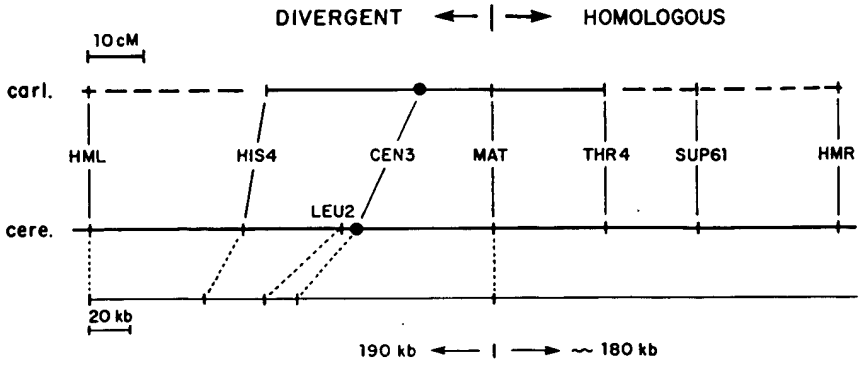

FIG. 1. The genetic maps of chromosome III from *S. carlsbergensis* (carl.) and *S. cerevisiae* (cere.; summarized from refs. 17 and 13, respectively); dashed line, unmapped region. Lower line, physical map of the *S. cerevisiae* chromosome (16, 18).

Table 2. Induction of aneuploidy in strains that are divergent (D-VG) or homologous (*S. cerevisiae*, H-VV; *S. carlsbergensis*, H-GG) for chromosome III

Homologous (H) or divergent (D) strain	Dose, krad	Total colonies	% his⁻*	% chromosome lost† α	% chromosome lost† a
H-VV	0	842[a]	<0.1	0	0
H-VV	0	1370[b]	<0.1	0	0
H-GG	0	1213[a]	<0.1	0	0
D-VG	0	454[a]	<0.2	0	0
	0	1088[b]	<0.1	0	0
D-VGG‡	0	1118	<0.1	0	0
D-VG	5	303[a]	2.7	1.7	1.0
D-VG	5	382[b]	3.5	1.1	2.4
H-VV	10	414[a]	0.5	0	0.2
H-VV	10	1620[b]	0.2	0	0.06
H-GG	10	1168	0.4	0	0
D-VG	10	321[a]	5.6	3.4	2.2
D-VG	10	650[b]	5.4	2.5	2.8
D-VGG‡	10	688	2.0	0	1.9
D-VG	15	424[b]	10.6	3.3	6.4
H-VV	20	429[a]	0.7	0.2	0.2
H-VV	20	2785[b]	1.1	0.18	0.29
H-GG	20	2597	1.0	0.19	0.16
D-VG	20	274[a]	9.9	6.6	2.9
D-VG	20	390[b]	8.0	2.1	5.4
D-VGG‡	20	382	3.7	0	3.4
D-VG	25	244[b]	11.1	7.0	4.1
H-VV	30	373[a]	1.1	0.3	0.6
H-VV	30	1047[b]	1.2	0.1	0.6
H-GG	30	1284	1.6	0.16	0.4
D-VG	30	328[a]	12.5	6.1	5.5
D-VG	30	397[b]	7.8	3.5	2.8
D-VGG‡	30	382			(4.0)
H-VV	40	287[a]	0	0	0
H-VV	40	1184[b]	1.6	0.17	0.68
H-GG	40	1148	1.4	0.26	0.43
D-VG	40	309	12.3	6.1	5.8
D-VG	40	252	15.5	7.5	6.4
D-VGG‡	40	380			(3.4)

Superscripts a and b indicate two experiments done on different days.

*Frequency of total colonies that require histidine for growth. In the controls (0 krad), no his⁻ colonies were detected.

†Frequency of total colonies that are due to loss of the *S. carlsbergensis* chromosome III and are, therefore, his⁻ leu⁻ *MAT***a** thr⁻ or due to loss of the *S. cerevisiae* chromosome III and are, therefore, his⁻ *MATα*.

‡Strain disomic for the *S. carlsbergensis* chromosome III. Results in parentheses correspond to the total frequency of his⁻ colonies. Based on results with 10 and 20 krad, most of these are likely to be due to loss of the *S. cerevisiae* chromosome.

other half expressed *MATα*. Since *HIS4* and *MAT* are located on either side of the centromere, the radiation efficiently induced aneuploidy and/or malsegregation of the *S. carlsbergensis* chromosome. As discussed below, the events are primarily due to chromosome loss. The lack of genetic markers on the *S. carlsbergensis* chromosome might render analysis of the remaining his⁻ colonies somewhat less accurate. However, the comparable frequency of his⁻ *MATα* and his⁻ leu⁻ *MAT***a** thr⁻ colonies (Table 2) suggests that events involving the *S. cerevisiae* chromosome occur with similar frequency (even when there is an additional copy of the *S. carlsbergensis* chromosome; see D-VGG in Table 2 and Fig. 3).

We conclude that low doses of ionizing radiation (Fig. 2) can be efficient inducers of chromosome loss. Few if any events could be explained by multiple reciprocal recombination events since the frequency of the his⁻ only category is low (histidine auxotrophs not expressing mating type; Table 3). Furthermore, the cells were predominantly (>95%) in the G_1 phase of the cell cycle when irradiated, which would preclude the detection of reciprocal exchange events.

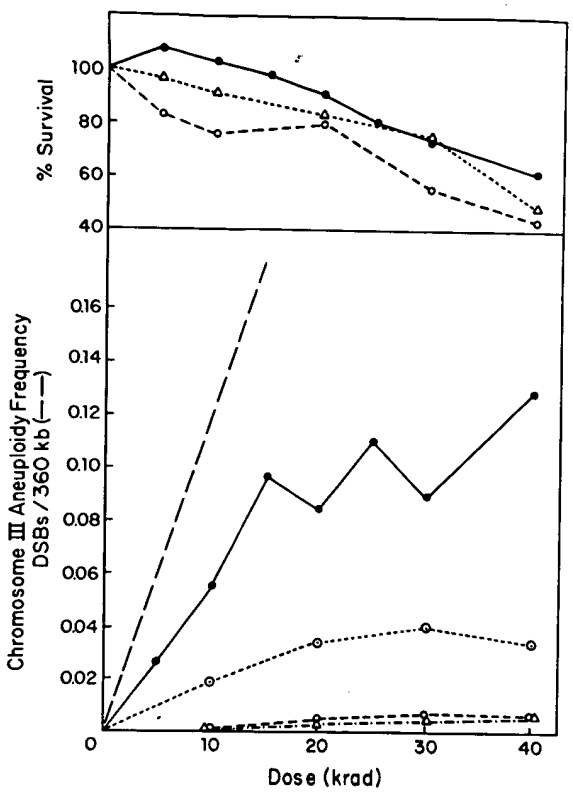

FIG. 2. The induction by ionizing radiation of chromosome III aneuploidy in strains that are divergent (●), homologous *S. cerevisiae* (○), or homologous *S. carlsbergensis* (△) for chromosome III. Also included are results with a trisomic chromosome III strain that has two copies of the *S. carlsbergensis* chromosome III and one copy of the *S. cerevisiae* III (◎). Presented is total aneuploidy for chromosome III based on the data in Table 1. The two results for the divergent experiment are averaged; the results for the homologous experiments are pooled between experiments (because of the small number of events). Also shown (– – –) is the expected induction of DSBs as a function of dose (12) in a 360-kb stretch of DNA (180 kb × 2); this corresponds to the divergent portion of the chromosomes.

Table 3. Expression of recessive markers in colonies from irradiated (10 and 20 krad) cells of divergent (D-VG) or homologous (H-VV or H-GG) strains

Strain	Dose, krad	Colonies examined	% his⁻ only	% thr⁻ only	% ade⁻ only
D-VG	10	971	0.1 (1)*	0.2 (2)	2.2
D-VG	20	664	0.2 (1)	0.8 (5)	4.3
H-VV	10	2034	0.1 (2)	0.2 (4)	2.1
H-VV	20	3214	0.6 (18)	0.2 (7)	3.8
H-GG	10	1168	0.4 (5)	—	1.2
H-GG	20	2597	0.6 (16)	—	1.4

Among the colonies arising from unirradiated cells (see Table 2), none expressed the recessive markers described in this table.

*Numbers in parentheses correspond to the number of colonies. The ade⁻ colonies were observed from a much larger sample and therefore the numbers of colonies are not presented. The divergent strain is +/*ade1* +/*ade2*; the H-VV strain is +/*ade2*; the H-GG strain is +/*ade1*. The distances to the centromere of the *ADE2* and *ADE1* genes are ≈65 and 5 centimorgans, respectively, which accounts for the differences in response between the H-VV and H-GG strains.

The chromosome III loss frequency in the homologous strains was 20–50 times lower than for the divergent strains (Fig. 2 and Table 2). Based on the data in Tables 2 and 3, the low level of *MAT***a** or *MAT*α histidine auxotrophs found in the homologous chromosome experiments could not be explained by recombination on both sides of the centromere. Thus, precise homology greatly reduces the potential for radiation-induced chromosome loss.

Mechanism of Chromosome Loss. The above results could have arisen by nondisjunction of a sister chromatid pair resulting in a monosomic and a trisomic daughter cell, nondisjunction of pairs of sister chromatids resulting in two daughter cells both euploid for chromosomes III, or chromosome loss so that the progeny would only be monosomic. If the first hypothesis were true, the colonies containing his$^-$ cells should be sectored (his$^-$/HIS$^+$). If the second hypothesis were true, the colonies would be entirely his$^-$ but they would be sectored for the associated mutations on chromosome III. Only 5% of the his$^-$ colonies showed evidence of his$^-$/HIS$^+$ sectors; the rest were whole his$^-$ colonies. The lack of sectoring is not due to a growth advantage by either his$^-$ or HIS$^+$ cells (unpublished results) or lethal sectoring, since nonlethal doses were used. We conclude that the radiation-induced appearance of his$^-$ colonies in the divergent strain is largely the result of chromosome loss in the G_1 cells.

Chromosome loss was examined further genetically and by karyotype analysis using pulse field gel electrophoresis methods to display chromosomes (16). Eleven his$^-$ leu$^-$ *MAT***a** thr$^-$ strains were crossed with a diploid that was carrying two copies of the *S. carlsbergensis* chromosome III found in strain 300686C-2. After meiosis, the tetrads contained two his$^-$ *MAT*α cells and two HIS$^+$ nonmaters (*his4-15* and *his4-S3* are complementing). Since all the cells were also LEU$^+$ and THR$^+$, the tested strains were monosomic for chromosome III, presumably from *S. cerevisiae*. This was confirmed by pulse field gel electrophoresis analysis (Fig. 3, lanes 6 and 7; unpublished data; the intensity of the chromosome III band was approximately half that of the chromosome VI band). Thus, when the *S. cerevisiae* chromosome is retained, the radiation-induced loss of a divergent chromosome results in monosomy.

When the *S. carlsbergensis* chromosome III is retained, the situation is somewhat different. Nine his$^-$ LEU$^+$ *MAT*α THR$^+$ isolates were tested genetically by crossing to a diploid monosomic for a his$^-$ *S. cerevisiae* chromosome III. Four produced tetrads containing only his$^-$ spores of either *MAT***a** or *MAT*α mating types and were monosomic for chromosome III. The remaining five strains were euploid for chromosome III since they yielded tetrads in which HIS$^+$/his$^-$ segregated 2:2 and the HIS$^+$ strains were nonmaters. Pulse field gel electrophoresis analysis confirmed euploidy for three strains in Fig. 3 (lanes 8–10). The intensity of the *S. carlsbergensis* chromosome III band approximately equals the intensity of the chromosome VI band (migrating slightly faster than chromosome III). It is possible that euploidy results as a consequence of a secondary event following loss of the *S. cerevisiae* chromosome and is selected during clonal outgrowth.

Induction of Other Genetic Events. Among the his$^-$ colonies arising from the divergent strains after low doses, nearly all were associated with the appearance of other genetic markers (Table 3). Of 358 his$^-$ colonies recovered from all doses in two experiments, all but 20 could be attributed to chromosome loss. Seven of the 20 were his$^-$ and 5 of these were examined with the pulse field gel electrophoresis system. Three appeared to contain a *S. cerevisiae* chromosome III with reduced mobility (one of these corresponds to lane 3 in Fig. 3). The other two did not exhibit chromosome rearrangements (lanes 2 and 4). The origin of the genetic change in these cells remains unknown; it is possible that a rare gene conversion may have occurred even though there is limited homology. Among the remaining 13 colonies, 7 could be explained by chromosome loss and associated recombination between *MAT* and *THR4*. One colony appears to have resulted from a break or recombinational event between *LEU2* and the centromere. The other 5 colonies remain unexplained.

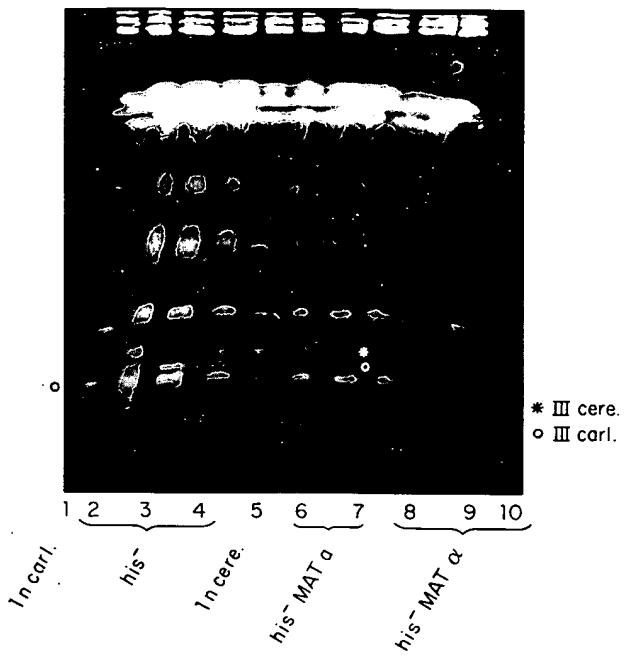

FIG. 3. Pulse field gel electrophoresis analysis of chromosomal DNA extracted from his$^-$ haploid parents and radiation-induced his$^-$ isolates of strain D-VG (divergent; see Table 1). Lanes: 1, haploid parent 300686C-2 (*S. carlsbergensis*); 5, haploid parent 021281AI-6 (*S. cerevisiae*); 2–4, his$^-$ (only) isolates from strain D-VG; 6 and 7, his$^-$ leu$^-$ *MAT***a** thr$^-$ isolates of strain D-VG; 8–10, his$^-$ *MAT*α isolates of strain D-VG. The chromosomes III of the diploid parent D-VG migrate as expected based on the haploid parents (data not shown). * and o, correspond to positions of chromosome III from *S. cerevisiae* and *S. carlsbergensis*, respectively.

While the total frequency of his$^-$ colonies was much lower in the homologous strains, the frequency of the "his$^-$ only" category among these colonies was much higher, presumably because of recombination. Somewhat comparable numbers of colonies that were only thr$^-$ occurred with both types of strains; they probably arose by recombination between the *MAT* and *THR4* loci.

Events on other chromosomes were similar between the various strains (ade$^-$, Table 3; ura$^-$, data not shown). Comparable levels of homozygosis would be expected to occur by recombinational repair between homologous chromosomes.

DISCUSSION

Recombination requires sufficient homology to enable productive DNA interactions. We showed (13) that some chromosomes or portions of chromosomes derived from *S. carlsbergensis* would not undergo meiotic recombination with their *S. cerevisiae* counterparts because of insufficient DNA homology (13, 14, 20, 21), although they were functionally homologous. The repair of ionizing radiation-induced DSBs requires recombination either between homologous chromosomes (in G_1 or G_2) or sister chromatids (in G_2; ref. 22; summarized in ref. 23). We have shown that the reduction of homology that results in loss of meiotic reciprocal recombination in one-half of chromosome III has a profound effect

on the recovery of this chromosome after irradiation of mitotic cells. More than 10% of the cells lose one or the other copy of chromosome III. Because loss in strains that are homologous for chromosome III is 20–50 times less frequent while the survival is comparable, we conclude that the absence of opportunity for chromosomal interactions due to limited homology prevents recombinational repair of DNA damage, which, in turn, leads to chromosome loss. The unrepaired damage does not lead to the deletion of portions of chromosomes although a few cases of chromosome alterations have been found (cf. Fig. 3, lane 3).

The lesions responsible for the radiation-induced aneuploidy are presumed to be DSBs; they require repair via a recombination mechanism. Approximately 25–50 DSBs (corresponding to 20–40 krad) are efficiently repaired in logarithmically growing diploid cells (12). DSBs induced in stationary (G_1) cells are repaired once the cells are incubated in fresh nutrient medium (24). The frequency of DSBs induced in the divergent regions of the two chromosomes has been estimated from the length of the region (Fig. 1) and the efficiency of DSB induction (12). As shown in Fig. 2, the DSB frequency is within a factor of 2 of the induced aneuploidy frequency at low doses. The "tailing off" in aneuploidy induction at higher doses could be due in part to DSBs being induced in both chromosomes in the divergent regions, resulting in lethality.

Thus unrepaired DSBs appear to have two biological consequences. In a *rad52* mutant lacking DSB repair, they have a dominant lethal effect (12, 25). The dominant lethal effect of DSBs in *rad52* mutants could result from an unresolved recombinational event between two chromosomes (as discussed in ref. 12). Consistent with this, *rad52* has been shown to be defective in an intermediate step in meiotic recombination (26). We propose a second genetic consequence for unrepaired DSBs—namely, the induction of chromosome loss, when recombination is prevented by a lack of homology. Possible reasons for the loss include degradation of the chromosome or inability to replicate the chromosomes in the absence of a telomere.

Previously, it was shown (3) that low radiation doses administered to a *rad52* diploid mutant caused a large increase in the already high spontaneous aneuploidy levels. The frequency of chromosome loss far exceeded that of DSBs and chromosome number approached near-haploid levels after several generations. The mechanism involved in the secondary aneuploidy is not understood, but it may be related to the generally poor growth of *rad52* mutants and the decrease in an essential nuclease (27, 28). We do not find evidence of aneuploidy for multiple chromosomes in our repair-proficient strains. Among the monosomic colonies for chromosome III, there was no increase in homozygosis for ade^-.

There are several inferences that can be derived from the present observations. (*i*) The consequences of damage in nonhomologous regions is only important in G_1 cells, since repair can occur between sister chromatids in G_2 (22). (*ii*) Given the efficiency of induction of aneuploidy, it may be possible to determine the size of the divergent region between two chromosomes using just one genetic marker; chromosome loss should be proportional to size. (*iii*) The mapping of genes to specific chromosomes would be greatly facilitated by divergent chromosomes. This approach may account for the ability to develop linkage maps in the yeast *Pichia pinus* (29). (*iv*) Other damage requiring recombinational repair may also lead to chromosome loss of divergent chromosomes. (*v*) It is possible that even in homologous chromosomes there may be small regions of relatively low homology. Damage induced in these regions would not be subject to recombinational repair and could therefore lead to aneuploidy. (*vi*) Our results may be relevant to observations with a human chromosome/CHO cell hybrid. Waldren *et al.* (30) demonstrated that low radiation doses efficiently induced inactivation of a gene associated with the human chromosome. An alternative explanation is that the radiation damage in the human chromosome induced chromosome loss, possibly due to lack of opportunity for interaction with a homologous chromosome.

We thank Jim Mason, Carl Barrett, and Craig Bennett for valuable comments on the manuscript.

1. Dellarco, V. L., Voytek, P. E. & Hollaender, A. (1985) *Aneuploidy, Etiology and Mechanisms* (Plenum, New York and London).
2. Hartwell, L. H. & Smith, D. (1985) *Genetics* **110**, 381–395.
3. Mortimer, R. K., Contopoulou, R. & Schild, D. (1981) *Proc. Natl. Acad. Sci. USA* **78**, 5778–5782.
4. Esposito, M. S., Maleas, D. T., Bjornstad, K. A. & Holbrook, L. L. (1986) *Curr. Genet.* **10**, 425–433.
5. Liras, P., McCusker, J., Mascioli, S. & Haber, J. E. (1978) *Genetics* **88**, 651–671.
6. Kouprina, N. Y., Pachina, O. B., Nikolaishwili, N. T., Tsouladze, A. M. & Larionov, V. L. (1988) *Yeast* **4**, 257–270.
7. Fitzgerald-Hayes, M. (1987) *Yeast* **3**, 187–200.
8. DiNardo, S., Voelkel, K. & Sternglanz, R. (1984) *Proc. Natl. Acad. Sci. USA* **81**, 2616–2620.
9. Schatz, P. J., Solomon, F. & Botstein, D. (1986) *Mol. Cell. Biol.* **6**, 3722–3733.
10. Resnick, M. A., Zimmermann, F. K., Fogel, S. & Bloom, K. (1989) *Mutat. Res.*, in press.
11. Resnick, M. A. (1976) *J. Theor. Biol.* **59**, 97–106.
12. Resnick, M. A. & Martin, P. (1976) *Mol. Gen. Genet.* **143**, 119–129.
13. Nilsson-Tillgren, T., Gjermansen, C., Kielland-Brandt, M. C., Petersen, J. G. L. & Holmberg, S. (1981) *Carlsberg Res. Commun.* **46**, 65–76.
14. Holmberg, S. (1982) *Carlsberg Res. Commun.* **47**, 233–244.
15. Resnick, M. A., Stasiewicz, S. & Game, J. C. (1983) *Genetics* **104**, 583–602.
16. Carle, G. F. & Olson, M. V. (1985) *Proc. Natl. Acad. Sci. USA* **82**, 3756–3760.
17. Mortimer, R. K. & Schild, D. (1985) *Microbiol. Rev.* **49**, 181–212.
18. Newlon, C. S., Green, R. P., Hardeman, K. J., Kim, K. E., Lipchitz, L. R., Palzkill, T. G., Synn, S. & Woody, S. T. (1986) in *Yeast Cell Biology*, ed. Hicks, J. (Liss, New York), pp. 211–223.
19. Fink, G. R. & Styles, C. A. (1974) *Genetics* **77**, 231–244.
20. Petersen, J. G. L., Nilsson-Tillgren, T., Kielland-Brandt, M. C., Gjermansen, C. & Holmberg, S. (1987) *Curr. Genet.* **12**, 167–174.
21. Nilsson-Tillgren, T., Gjermansen, C., Holmberg, S., Petersen, J. G. L. & Kielland-Brandt, M. C. (1986) *Carlsberg Res. Commun.* **51**, 309–326.
22. Brunborg, G., Resnick, M. A. & Williamson, D. H. (1980) *Radiat. Res.* **82**, 547–588.
23. Resnick, M. A. (1979) *Adv. Radiat. Biol.* **8**, 175–217.
24. Resnick, M. A. (1977) *Mutat. Res.* **42**, 131–145.
25. Ho, K. S. Y. & Mortimer, R. K. (1973) *Mutat. Res.* **20**, 45–51.
26. Resnick, M. A., Nitiss, J., Edwards, C. & Malone, R. E. (1986) *Genetics* **113**, 531–550.
27. Chow, T. Y.-K. & Resnick, M. A. (1988) *Mol. Gen. Genet.* **211**, 41–48.
28. Chow, T. Y.-K. & Resnick, M. A. (1987) *J. Biol. Chem.* **262**, 17659–17667.
29. Tolstoryukov, I. I., Efremov, B. D. & Bliznik, K. M. (1983) *Genetika* **19**, 897–902.
30. Waldren, C., Correll, L., Sognier, M. A. & Puck, T. T. (1986) *Proc. Natl. Acad. Sci. USA* **83**, 4839–4843.

STIC-ILL

Adonis 2A only

From: Canella, Karen
Sent: Sunday, February 03, 2002 9:00 PM
To: STIC-ILL
Subject: ill order 09/815,340

Art Unit 1642 Location 8E12(mail)

Telephone Number 308-8362

Application Number 09/815,340

1. Trends in Cell biology, 2001 Jan, 11(1):18-21
2. Clinical Cancer Research, 2000 Aug, 6(8):3215-3221
3. Mutation Research, 1997 Apr 29, 375(2):157-165
4. american Journal of Hematology, 1985 Mar, 18(3):243-249.
5. PNAS, 1989 Apr, 86(7):2276-2280
6. Genes and Development, 1996 Oct 15, 10(20):2621-2631
7. Cancer, 1975 Jun, 35(6):1664-1677
8. Mutation Research, 1978, 57(3): 313-324
9. Environ Mutagen, 1981, 3(1):53-64
10. Nucleic Acids Research, 2001 Mar 15, 29(6):1300-1307
11. Oncogene:
    1998 Oct 29, 17(17):2187-2193
    2000 Jan 20, 19(3):403-409
12. Molecular endocrinology, 1999 Jan, 13(1):156-166
13. Gene, 1999 Nov 29, 240(2):317-324
14. Science, 1999 Jul 16, 285(5426)418-422
15. Biochemistry and Molecular biology international, 1999 May, 47(5):891-897
16. Journal of Clinical Endocrinology and Metabolism, 1999 Mar, 84(3):1149-1152
17. Journal of biological chemistry:
    1999 Jan 29, 274(5):3151-3158
    2000 Nov 24, 275(47):36502-36505 ***
18. Gene 2000 May 2, 248(1-2):41-50
19. Molecular endocrinology, 2000 Aug, 14(8):1137-1146
20. Cancer Letters, 2001 Feb 10, 163(1):131-139
21. Brain Pathology, 2001 Jul, 11(3):328-341

Article title	Managing the centrosome numbers game: From chaos to stability in cancer cell division
Article identifier	0962892401000113
Authors	Brinkley_B_R
Journal title	Trends in Cell Biology
ISSN	0962-8924
Publisher	Elsevier Current Trends
Year of publication	2001
Volume	11
Issue	1
Supplement	0
Page range	18-21
Number of pages	4
User name	Adonis
Cost centre	
PCC	$20.00
Date and time	Tuesday, February 05, 2002 9:10:25 PM

Managing the centrosome numbers game: from chaos to stability in cancer cell division

Bill R. Brinkley

Aneuploid tumor cells can arise through multipolar mitosis caused by supernumerary centrosomes. Multipolar spindles, however, are antagonistic to cell viability. Thus, most cells derived from such an aberrant mitosis would be eliminated by apoptosis. A rare daughter cell, through chance acquisition of an appropriate chromosome complement and/or gene dosage, could survive and contribute to a clone of aneuploid tumor cells. Survival and perpetuation of the clone, however, requires an additional step – the resumption of mitotic stability through the assembly of a bipolar, not multipolar, spindle. Either selective inactivation of the extra centrosomes or their coalescence into two functional spindle poles corrects the problem of centrosome excess. Current data support coalescence as a mechanism for regulating the number of functional centrosomes in tumor cells.

Aneuploidy – the gain or loss of one or more chromosomes from a diploid genome – is the most frequent manifestation of genomic instability in human cancer cells[1]. Proposed over a century ago as the principal cause of cancer[2–4], the hypothesis was soon abandoned in favor of one based on somatic mutations[5], with aneuploidy being relegated to an epiphenomenon in oncogenesis[6]. Recently, the discovery of centrosome hypertrophy or amplification (i.e. more than the usual one to two centrosomes per cell) in cells of a variety of human tumors, and its direct correlation with aneuploidy[7–9], has added new fuel to an old debate and provided a rational mechanism for at least one pathway to aneuploidy in cancer cells. Thus, a condition that favors the overproduction of centrosomes could contribute directly to the initiation of chromosome imbalance, through the formation of multipolar spindles and aberrant mitosis. Most cell progeny derived from such a defective mitosis would very likely undergo apoptosis, but it is reasonable to speculate that a daughter cell, receiving the appropriate chromosome complement and gene dosage, could survive and contribute, via clonal selection, to a population of aneuploid tumor cells. The survivor, however, must overcome the condition of centrosome overproduction in order to divide efficiently.

Bill R. Brinkley
Dept of Molecular and Cellular Biology, Baylor College of Medicine, Houston, TX 77030, USA.
e-mail: brinkley@bcm.tmc.edu

Successful cell division requires stable and efficient mitosis, a condition that almost certainly favors bipolar over multipolar spindles. Although a multipolar spindle might give rise to the progenitor daughter cell, it is likely that the clone of cells derived from that daughter would regain mitotic stability through a process that favored the assembly of bipolar, not multipolar, spindles. This article will comment on how centrosome overproduction could initiate multipolar spindles and mitotic instability, causing cell transformation and aneuploidy, and how a surviving daughter cell might correct the centrosome burden and regain a bipolar spindle.

Centrosomes are microtubule-organizing centers

The dual and opposing nature of centrosomes in normal mitotic cells facilitates the assembly of a bipolar spindle and assures equal distribution of the replicated genome to each daughter cell. Moreover, this process provides each daughter with a single centrosome or microtubule-organizing center (MTOC) on which to rebuild a significant component of the cytoskeleton and reinitiate the next centrosome replication cycle. The regulatory mechanism (checkpoint) that assures that centrosomes divide once and only once in a given cell cycle[10] establishes a condition favoring a bipolar spindle assembly and mitotic stability. This process also assures the orderly passage of a single centrosome to each daughter cell in succeeding cell cycles.

Presumably, mutations or altered expression of genes controlling centrosome duplication could abrogate the checkpoint that assures a single round of centrosome replication, resulting in cells that assemble more than the usual pair of centrosomes. Alternative pathways for cellular acquisition of extra centrosomes are also feasible, as discussed later. The supernumerary centrosomes function as extra MTOCs and give rise to aberrant spindles assembled in response to three or more spindle poles. Multipolar spindles are antagonistic to cell viability and growth, resulting either in aborted mitoses or the production of daughter cells with a lethal genetic imbalance. The resulting mitotic chaos would most certainly lead to serious loss of viability and cell death in a normal cell population. It is conceivable, however, that some cells, perhaps one daughter cell, might survive the chaotic phase

... a condition that favors the overproduction of centrosomes could contribute directly to the initiation of chromosome imbalance

http://tcb.trends.com 0962-8924/01/$ – see front matter PII: S0962-8924(00)01872-9

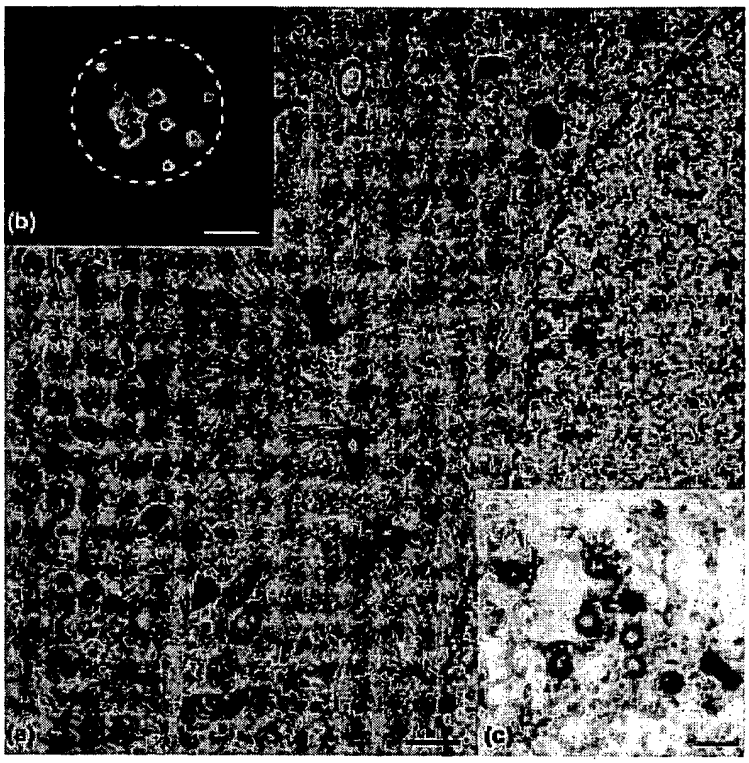

Fig. 1. Giant 'compound' centrosomes in mouse neuroblastoma cells N115. (a) Thin-section electron micrograph of a cell showing a large centrosome with numerous radiating microtubules near the nucleus. Bar, 1 μm. (b) Immunofluorescence preparation stained with human autoantibodies against centrosomes showing multiple centrosomes coalesced into one large microtubule-organizing center (MTOC; circle). Bar, 10 μm. (c) Electron micrograph showing numerous centrioles in the giant centrosome of a neuroblastoma cell. Bar, 1 μm.

and thrive by the chance acquisition of a chromosome complement and gene dosage favorable for neoplastic growth. It is well recognized that tumor cells are veritable 'mitotic machines' that thrive on their ability to divide continuously and successfully during the pervasive growth of neoplasia. Therefore, they not only benefit from a more favorable gene complement, but also apparently compensate for a perilous condition of centrosome overload that would normally produce multipolar spindles and cell death. It is unknown how cells tolerate a condition of supernumerary centrosomes, but achieving mitotic stability and survival requires a process whereby the surviving cell and its progeny regain a bipolar spindle in spite of the presence of extra centrosomes and MTOCs.

Molecular scenarios for the origin of supernumerary centrosomes

The centrosome cycle is initiated at the beginning of the G1 phase of the cell cycle, when each new daughter cell receives a single centrosome. Subsequently, when cells progress through S phase, the centrosome is duplicated such that two equal but opposing centrosomes can split apart and, at the end of G2, form opposite poles of the spindle. Closer examination by electron microscopy (EM) reveals that each centrosome contains a pair of centrioles surrounded by an electron-dense pericentriolar matrix, from which a polarized array of cytoplasmic microtubules is assembled. Although it is still uncertain what, if any, role centrioles play in centrosome function, they do undergo their own replication cycle, an event closely coupled to the ability of the centrosome to duplicate[11].

The accompanying cascade of regulatory molecules required for centrosome replication is poorly defined but has recently become an active research endeavor. Significant players in the centriole duplication cycle include a family of serine/threonine kinases identified as cyclin-dependent kinases (CDKs) and aurora Ipl-like kinases[12,13]. Mutational inactivation of the tumor-suppressor p53[14,15], along with overexpression of one or more kinases, such as breast-tumor-amplified kinase (BTAK/aurora 2)[16,17], appears to alter a checkpoint and initiate multiple rounds of centrosome replication within a single cell cycle. Extra centrosomes can also arise through other pathways, such as failure of cytokinesis, fusion of two or more cells, or through the fragmentation of one or both of the cell's centrosomes into smaller ectopic fragments that continue to function as MTOCs. Centrosome amplification has also been shown to result from the arrest of cells in S phase, uncoupling DNA replication from centrosome duplication[10]. Regardless of the mechanism of origin, mitotic chaos and cell death would probably ensue because of the presence of multiple MTOCs and too many spindle poles. Surviving cells would be selected based on their proliferative advantage and their ability to manage the burden of extra centrosomes in the cytoplasm. Very likely, survival would be a rare, but nevertheless a defining, event for establishing viable aneuploid cell progeny expressing a transformed phenotype. The resulting tumor would assemble mostly bipolar spindles in mitosis while maintaining and perpetuating an enlarged complement of centrosomes, centrioles and, possibly, acentriolar fragments. Indeed, such conditions have been reported in a variety of tumor cells *in vitro* and *in vivo* as discussed below.

Supernumerary centrosomes in established cell lines and human tumor cells

The earliest observation on centrosome abnormalities in tumor cell cultures came from EM and early immunofluorescence studies of neuroblastoma cells *in vitro*[18–20]. Using a newly discovered human autoimmune serum that specifically recognizes centrosomes, it was noted that N115 mouse neuroblastoma cells contained unusually large centrosomes containing as many as ten or more centrioles per centrosome (Fig. 1a–c). Yet during mitosis, the centrosomes were arranged into two large spindle poles at each end of the mitotic spindle. Similar observations were made by Sharp *et al.*[20], who

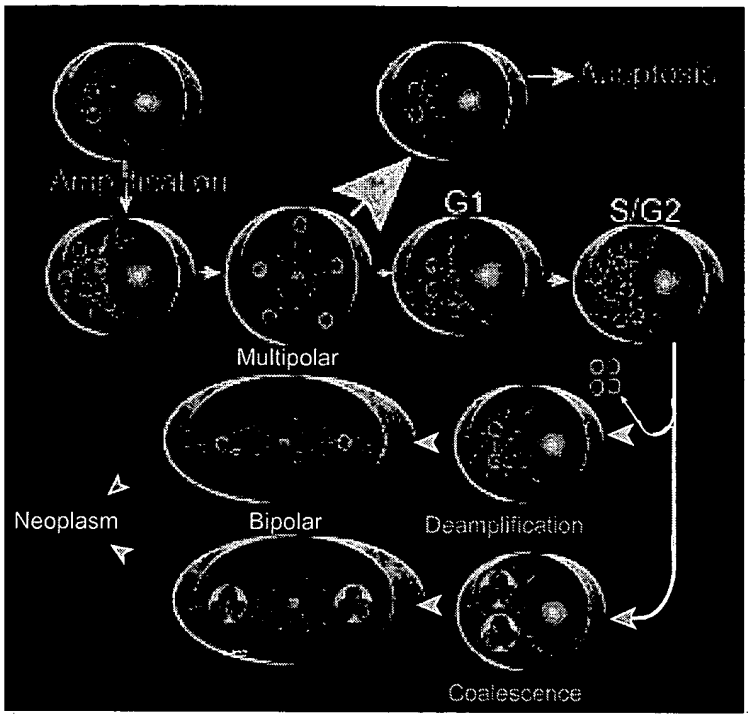

Fig. 2. Two possible scenarios for the control of centrosome amplification. Initially, centrosome amplification occurs by one of several pathways resulting in a cell with multiple centrosomes (red dots), each functioning as a site of microtubule (green) assembly. Multipolar spindles assemble in mitosis, resulting in daughter cells with genomic insufficiency owing to missegregation of chromosomes to multiple poles, a lethal condition leading to apoptosis (large arrow indicates fate of most daughter cells). A rare daughter cell might receive a favorable chromosome complement, resulting in survival and growth (small arrow). The surviving cell progresses through G1 phase, and the full centrosome complement is duplicated late in the S/G2 phase of the cycle. As cells enter mitosis, bipolar spindles with two functional spindle poles arise through either a process of deamplification, where all but one dominant pair of centrosomes are inactivated or discarded, or a process in which all of the centrosomes undergo coalescence, forming two functional microtubule-organizing centers (MTOCs). Current data from electron microscopy favor the latter scenario.

reported that 72% of differentiated mouse N18 neuroblastoma cells and 80% of N115 undifferentiated cells in culture contained three or more centrioles in each centrosome. Initially, this finding was postulated to be an anomaly of neuronal cells, but later it was concluded that it is a manifestation of centrosome amplification in cultured neuroblastoma cells (Fig. 1a–c). More recently, supernumerary centrosomes have been reported in a variety of different tumor cells *in vitro* and *in vivo*[7–9] and appear to be a consistent feature of aneuploid tumors[9].

Corralling maverick centrosomes

How do cells control extra centrosomes and maintain numerical order of MTOCs during interphase and mitosis? It is known that some normal diploid cells have the capacity to dispense with the centrioles and centrosomes or initiate centrosome assembly *de novo*, at various stages of their life cycles[21–23]. The embryos of the surf clam, *Spisula*, can selectively turn off the paternally derived centrosome and diminish its ability to nucleate microtubules[23]. Higher plant cells lack centrioles and distinct centrosomes even though they have functional MTOCs and assemble anastral spindles[24,25]. Mouse embryo cells complete up to 16 cell divisions without centrioles and then generate new centrioles *de novo* in subsequent cell divisions[21,22]. When the proteins that regulate centrosome structure and duplication are mutated or overproduced, replication checkpoints are violated, creating potentially new MTOCs and a crisis in microtubule management. It is likely that cells surviving this crisis do so by one of two strategies:

- by a process of 'deamplification' where all but two dominant centrosomes are inactivated and/or eliminated, thereby reverting to a more controlled capacity to assemble microtubules;
- through a process where supernumerary centrosomes are retained but coalesced into one or two 'compound' MTOCs.

Although the actual process is not yet well defined, most of the available experimental and observational data favor coalescence, as discussed below.

Figure 2 illustrates the process of deamplification, whereby a cell deactivates or discards most or all of its supernumerary centrosomes, returning the cell to a state where one or two dominant centrosomes become the principal MTOCs. As already mentioned, it is well established that some normal eukaryotic cells can actually discard centrioles and regain them *de novo* during their life cycles; there is, however, no experimental or observational evidence to support this pathway in tumor cells. Alternatively, the hypothesis of coalescence, or the formation of giant 'compound' centrosomes (Fig. 2), is supported by several reports[18–20,26,27]. The clustering of multiple centrosomes into one or two large aggregates reduces the number of individual MTOCs to a manageable one or two per cell. Salisbury *et al.*[27], noting the low frequency of abnormal mitosis in human breast cancer cells, concluded that multiple centrioles can remain linked together, functioning as one large centrosome in interphase and, presumably, as two centrosomes in mitosis.

Multipolar spindles persist in tumor cells and in other pathological tissues[26], but, as in normal tissues, they are probably selected against and removed by apoptosis unless they confer further selective advantage. In fact, karyotypic[28] as well as centrosomal changes continue to occur as tumors progress, leading, perhaps, to even further clonal expansion and ultimately conversion to relatively stable chromosome and centrosome complements, as shown recently for cells *in vitro*[29].

Concluding remarks

Aneuploidy is a common feature of most human cancers and probably represents an early and significant event in tumorigenesis. The discovery of centrosome amplification in most human cancer cells and its one-to-one correlation with aneuploidy

in colorectal tumors[9] suggest the following scenario for the initiation of a transformed cell focus within tissue.

- Extra centrosomes appear either through a mutation involving a component of the cell cycle checkpoint controlling centrosome duplication or other defects in the dividing cells that result in the acquisition of additional centrosomes.
- Subsequently, when cells enter mitosis, the supernumerary centrosomes initiate the assembly of a multipolar spindle that causes mitotic failure or malsegregation of the replicated chromosome complement, producing nonviable daughter cells that are removed by apoptosis.
- Out of such chaos, a rare daughter cell acquires, by chance, a chromosome complement and gene dosage that confers survival, a mutator phenotype and tumorigenesis.
- The surviving daughter cells retain mutations that cause and perpetuate centrosome hypertrophy, but are selected for their ability to suppress the centrosome overload by aggregating them into one or two MTOCs capable of assembling a bipolar spindle, a condition that favors mitotic stability and neoplastic growth.

Thus, the centrosome overload that causes aneuploidy through the formation of multipolar spindles must be quickly corralled and coalesced into a manageable number of MTOCs in order to assure mitotic stability and perpetuation of transformed daughter cells. The mitotic potential of the neoplastic outgrowth is such that it might even tolerate a higher than normal burden of multipolar divisions and, through this process, further shuffle the genome to produce additional karyotypic heterogeneity. Although numerical changes in chromosome complements can probably arise through alternative pathways involving other components of the mitotic apparatus[30], the discovery of centrosome hypertrophy in cancer cells resurrects and renews an old hypothesis for aneuploidy and cancer and presents a logical new direction for future cell research.

Acknowledgements
Thanks are extended to Ilia Ouspenski and Thea Goepfert for helpful discussions and critical reading of the manuscript, Frank Herbert for help with the illustrations, and Betty Ledlie and Michael Wise for editorial assistance. Supported by RO1 grant CA-41424 to B.R.B. and PO1 grant CA-64255 to Daniel Medina and by the National Cancer Institute, NIH.

References

1 Mitelman, F. (1994) Catalogue of Chromosome Aberrations in Cancer (Vol. 2), Wiley-Liss
2 von Hansemann, D. (1890) Ueber asymmetrische Zelltheilung in Epithelkrebsen und deren biologische Bedeutung. *Virchows Arch. Pathol. Anat.* 119, 299–326
3 Boveri, T. (1902) On multipolar mitosis as a means of analysis of the cell nucleus. Reprinted in 1964 in *Foundations of Experimental Biology* (Willier, B.H. and Oppenheimer, J.M., eds), pp. 74–97, Prentice-Hall
4 Boveri, T. (1914) *Zur Frage der Enstehung maligner Tumoren*, Fischer Verlag. English translation by M. Boveri reprinted (1929) as *The Origin of Malignant Tumors*, Williams & Wilkins
5 Tyzzer, E.E. (1916) Tumor immunity. *J. Cancer Res.* 1, 125–155
6 Nowell, P.C. (1976) The clonal evolution of tumor cell populations. *Science* 194, 23–28
7 Lingle, W.L. *et al.* (1998) Centrosome hypertrophy in human breast tumors: implications for genomic stability and cell polarity. *Proc. Natl. Acad. Sci. U. S. A.* 95, 2950–2955
8 Pihan, G.A. *et al.* (1998) Centrosome defects and genetic instability in malignant tumors. *Cancer Res.* 58, 3974–3985
9 Ghadimi, B.M. *et al.* (2000) Centrosome amplification and instability occurs exclusively in aneuploid, but not diploid colorectal cancer cell lines, and correlates with numerical aberrations. *Genes Chromosomes Cancer* 27, 183–190
10 Balczon, R. *et al.* (1995) Dissociation of centrosome replication events from DNA synthesis and mitotic division in hydroxyurea-arrested Chinese hamster ovary cells. *J. Cell Biol.* 130, 105–115
11 Sluder, G. and Rieder, C.L. (1985) Centriole number and the reproductive capacity of spindle poles. *J. Cell Biol.* 100, 887–896
12 Mussman, J.G. *et al.* (2000) Synergistic induction of centrosome hyperamplification by loss of p53 and cyclin E overexpression. *Oncogene* 19, 1635–1646
13 Goepfert, T.M. and Brinkley, B.R. (2000) The centrosome-associated aurora/Ipl kinase family. In *The Centrosome in Cell Replication and Early Development* (Vol. 49) (Palazzo, R. and Schatten, G., eds), pp. 331–342, Academic Press
14 Fukasawa, K. *et al.* (1996) Abnormal centrosome amplification in the absence of p53. *Science* 271, 1744–1747
15 Wang, X-J. *et al.* (1998) Expression of a p53 mutant in the epidermis of transgenic mice accelerates chemical carcinogenesis. *Oncogene* 17, 35–45
16 Zhou, H. *et al.* (1998) Tumor amplified kinase STK15/BTAK induces centrosome amplification, aneuploidy and transformation. *Nat. Genet.* 20, 189–193
17 Bischoff, J.R. (1998) A homologue of *Drosophila* aurora kinase is oncogenic and amplified in human colorectal cancers. *EMBO J.* 17, 3052–3065
18 Brinkley, B.R. *et al.* (1981) Tubulin assembly sites and the organization of cytoplasmic microtubules in cultured mammalian cells. *J. Cell Biol.* 90, 554–562
19 Ring, D. *et al.* (1982) Mitosis in a cell with multiple centrioles. *J. Cell Biol.* 94, 549–556
20 Sharp, G.A. *et al.* (1981) Ultrastructure of multiple microtubule initiation sites in mouse neuroblastoma cells. *J. Cell Sci.* 47, 1–24
21 Szollosi, D. (1972) Changes of some cell organelles during oogenesis in mammals. In *Oogenesis* (Biggers, J.D. and Schuetz, A.W., eds), pp. 47–64, US Government Printing Office
22 Calarco, P.G. (2000) Centrosome precursors in the acentriolar mouse oocyte. *Microsc. Res. Tech.* 49, 428–434
23 Wu, X. and Palazzo, R.E. (1999) Differential regulation of maternal vs. paternal centrosomes. *Proc. Natl. Acad. Sci. U. S. A.* 96, 1397–1402
24 Smirnova, E.A. and Bajer, A.S. (1992) Spindle poles in higher plant mitosis. *Cell Motil. Cytoskeleton* 23, 1–7
25 Lambert, A.M. (1993) Microtubule organizing centers in higher plants. *Curr. Opin. Cell Biol.* 5, 116–122
26 Lingle, W.L. and Salisbury, J.L. (1999) Altered centrosome structure is associated with abnormal mitosis in human breast tumors. *Am. J. Pathol.* 155, 1941–1951
27 Salisbury, J.L. *et al.* (1999) Microtubule nucleating capacity of centrosomes in tissue sections. *J. Histochem. Cytochem.* 47, 1265–1273
28 Aldaz, C.M. *et al.* (1996) Allelotypic and cytogenetic characterization of chemically induced mouse mammary tumors: high frequency of chromosome 4 loss of heterozygosity at advanced stages of progression. *Mol. Carcinog.* 17, 126–133
29 Chiba, S. *et al.* (2000) Genomic convergence and suppression of centrosome hyperamplification in primary 53 $^{-/-}$ cells in prolonged culture. *Exp. Cell Res.* 258, 310–321
30 Pihan, G.A. and Doxsey, S.J. (1999) The mitotic machinery as a source of genetic instability in cancer. *Cancer Biol.* 9, 289–302

FILE 'MEDLINE, BIOSIS, CANCERLIT, LIFESCI' ENTERED AT 18:56:44 ON 03 FEB 2002

```
L1            98 S SECURIN
L2            13 S HSEC
L3          1912 S H-SEC?
L4             3 S HSECURIN
L5            98 S L1 OR L4
L6            41 S L1 AND HUMAN
L7            41 S L6 OR L4
L8            20 DUP REM L7 (21 DUPLICATES REMOVED)
L9            28 S HPTTG
L10          147 S PTTG OR VSECURIN OR (PITUITARY(2W)TRANSFORM?(W)GENE)
L11           82 S L10(S)HUMAN
L12           86 S L11 OR L9
L13           85 S L12 AND PY<2002
L14           32 DUP REM L13 (53 DUPLICATES REMOVED)
L15         4724 S ANEUPLOID?(S)(TREAT? OR TARGET? OR DRUG?)
L16          517 S ANEUPLOID?(5A)(TREAT? OR TARGET? OR DRUG?)
L17         3676 S ANEUPLOID?(2W)CELL#
L18           88 S L17(S)(ELIMINAT? OR KILL?)
L19           46 DUP REM L18 (42 DUPLICATES REMOVED)

=> s aneuploid? or hyperploid?
L20       33101 ANEUPLOID? OR HYPERPLOID?

=> s target?(3a)l20
L21          22 TARGET?(3A) L20

=> s l21 (s)chemotherap?
L22           0 L21 (S) CHEMOTHERAP?

=> s l20(5a)chemotherap?
L23          95 L20(5A) CHEMOTHERAP?

=> s l23/ti
```

L8 ANSWER 17 OF 20 MEDLINE DUPLICATE 11
ACCESSION NUMBER: 2001034845 MEDLINE
DOCUMENT NUMBER: 20531877 PubMed ID: 11081627
TITLE: Two distinct pathways remove mammalian cohesin from chromosome arms in prophase and from centromeres in anaphase.
AUTHOR: Waizenegger I C; Hauf S; Meinke A; Peters J M
CORPORATE SOURCE: Research Institute of Molecular Pathology, Vienna, Austria.
SOURCE: CELL, (2000 Oct 27) 103 (3) 399-410.
Journal code: CQ4. ISSN: 0092-8674.
PUB. COUNTRY: United States
Journal; Article; (JOURNAL ARTICLE)
LANGUAGE: English
FILE SEGMENT: Priority Journals
ENTRY MONTH: 200011
ENTRY DATE: Entered STN: 20010322
Last Updated on STN: 20010322
Entered Medline: 20001130

AB In yeast, anaphase depends on cohesin cleavage. How anaphase is controlled in vertebrates is unknown because their cohesins dissociate from chromosomes before anaphase. We show that residual amounts of the cohesin SCC1 remain associated with **human** centromeres until the onset of anaphase when a similarly small amount of SCC1 is cleaved. In Xenopus extracts, SCC1 cleavage depends on the anaphase-promoting complex and separin. Separin immunoprecipitates are sufficient to cleave SCC1, indicating that separin is associated with a protease activity. Separin activation coincides with **securin** destruction and partial separin cleavage, suggesting that several mechanisms regulate separin activity. We propose that in vertebrates, a cleavage-independent pathway removes cohesin from chromosome arms during prophase, whereas a separin-dependent pathway cleaves centromeric cohesin at the metaphase-anaphase transition.

L8 ANSWER 16 OF 20 MEDLINE DUPLICATE 10
ACCESSION NUMBER: 2001074910 MEDLINE
DOCUMENT NUMBER: 20388582 PubMed ID: 10935539
TITLE: Pituitary tumor transforming gene (PTTG) regulates placental JEG-3 cell division and survival: evidence from live cell imaging.
AUTHOR: Yu R; Ren S G; Horwitz G A; Wang Z; Melmed S
CORPORATE SOURCE: Division of Endocrinology, Cedars-Sinai Research Institute-UCLA School of Medicine, Los Angeles, California 90048, USA.
CONTRACT NUMBER: CA-75979 (NCI)
SOURCE: MOLECULAR ENDOCRINOLOGY, (2000 Aug) 14 (8) 1137-46. Journal code: NGZ. ISSN: 0888-8809.
PUB. COUNTRY: United States
Journal; Article; (JOURNAL ARTICLE)
LANGUAGE: English
FILE SEGMENT: Priority Journals
ENTRY MONTH: 200101
ENTRY DATE: Entered STN: 20010322
Last Updated on STN: 20010322
Entered Medline: 20010104

AB The pituitary transforming gene, PTTG, is abundantly expressed in endocrine neoplasms. PTTG has recently been recognized as a mammalian **securin** based on its biochemical homology to Pds1p. PTTG expression and intracellular localization were therefore studied during the cell cycle in **human** placental JEG-3 cells. PTTG mRNA and protein expressions were low at the G1/S border, gradually increased during S phase, and peaked at G2/M, but PTTG levels were attenuated as cells entered G1. In interphase cells, wild-type PTTG, an epitope-tagged PTTG, and a PTTG-EGFP conjugate all localized to both the nucleus and cytoplasm, but in mitotic cells, PTTG was not observed in the chromosome region. PTTG-EGFP colocalized with mitotic spindles in early mitosis and was degraded in anaphase. Intracellular fates of PTTG-EGFP and a conjugate of EGFP and a mutant inactivated PTTG devoid of an SH3-binding domain were observed by real-time visualization of the EGFP conjugates in live cells. The same cells were continuously observed as they progressed from G1/S border to S, G2/M, and G1. Most cells (67%) expressing PTTG-EGFP died by apoptosis, and few cells (4%) expressing PTTG-EGFP divided, whereas those expressing mutant PTTG-EGFP divided. PTTG-EGFP, as well as the mutant PTTG-EGFP, disappeared after cells divided. The results show that PTTG expression and localization are cell cycle-dependent and demonstrate that PTTG regulates endocrine tumor cell division and survival.

L8 ANSWER 17 OF 20 MEDLINE DUPLICATE 11

L8 ANSWER 13 OF 20 BIOSIS COPYRIGHT 2002 BIOLOGICAL ABSTRACTS INC.
ACCESSION NUMBER: 2001:197840 BIOSIS
DOCUMENT NUMBER: PREV200100197840
TITLE: Two distinct pathways remove mammalian cohesin from chromosome arms in prophase and from centromeres in anaphase.
AUTHOR(S): Waizenegger, Irene C. (1); Hauf, Silke (1); Meinke, Andreas; Peters, Jan-Michael (1)
CORPORATE SOURCE: (1) Research Institute of Molecular Pathology, Dr. Bohr-Gasse 7, A-1030, Vienna: Waizenegger@nt.imp.univie.ac.at Austria
SOURCE: Cell Biology International, (2001) Vol. 25, No. 2, pp. A31.
print.
Meeting Info.: 12th European Cell Cycle Conference Tyrol, Austria February 10-14, 2001
ISSN: 1065-6995.
DOCUMENT TYPE: Conference
LANGUAGE: English
SUMMARY LANGUAGE: English

L8 ANSWER 14 OF 20 MEDLINE DUPLICATE 9

L8 ANSWER 11 OF 20 MEDLINE DUPLICATE 8
ACCESSION NUMBER: 2001277711 MEDLINE
DOCUMENT NUMBER: 21264234 PubMed ID: 11371342
TITLE: **Securin** is required for chromosomal stability in **human** cells.
AUTHOR: Jallepalli P V; Waizenegger I C; Bunz F; Langer S; Speicher
M R; Peters J M; Kinzler K W; Vogelstein B; Lengauer C
CORPORATE SOURCE: The Johns Hopkins Oncology Center, 1650 Orleans Street, Baltimore, MD 21231, USA.
CONTRACT NUMBER: CA 43460 (NCI)
CA 57345 (NCI)
CA 62924 (NCI)
GM 41690 (NIGMS)
SOURCE: CELL, (2001 May 18) 105 (4) 445-57.
Journal code: 0413066. ISSN: 0092-8674.
PUB. COUNTRY: United States
Journal; Article; (JOURNAL ARTICLE)
LANGUAGE: English
FILE SEGMENT: Priority Journals
ENTRY MONTH: 200107
ENTRY DATE: Entered STN: 20010709
Last Updated on STN: 20020125
Entered Medline: 20010705

AB Abnormalities of chromosome number are the most common genetic aberrations in cancer. The mechanisms regulating the fidelity of mitotic chromosome transmission in mammalian cells are therefore of great interest. Here we show that **human** cells without an **hSecurin** gene lose chromosomes at a high frequency. This loss was linked to abnormal anaphases during which cells underwent repetitive unsuccessful attempts to segregate their chromosomes. The abnormal mitoses were associated with biochemical defects in the activation of separin, the sister-separating protease, rendering it unable to cleave the cohesin subunit Scc1 efficiently. These results illuminate the function of mammalian **securin** and show that it is essential for the maintenance of euploidy.

L8 ANSWER 10 OF 20 MEDLINE
ACCESSION NUMBER: 2001699704 MEDLINE
DOCUMENT NUMBER: 21614485 PubMed ID: 11747808
TITLE: Dual inhibition of sister chromatid separation at metaphase.
AUTHOR: Stemmann O; Zou H; Gerber S A; Gygi S P; Kirschner M W
CORPORATE SOURCE: Department of Cell Biology, Harvard Medical School, Boston,
MA 02115, USA.
CONTRACT NUMBER: GM26875-17 (NIGMS)
GM39023-08 (NIGMS)
HG00041 (NHGRI)
SOURCE: CELL, (2001 Dec 14) 107 (6) 715-26.
Journal code: 0413066. ISSN: 0092-8674.
PUB. COUNTRY: United States
Journal; Article; (JOURNAL ARTICLE)
LANGUAGE: English
FILE SEGMENT: Priority Journals
ENTRY MONTH: 200201
ENTRY DATE: Entered STN: 20011219
Last Updated on STN: 20020125
Entered Medline: 20020117

AB Separation of sister chromatids in anaphase is mediated by separase, an endopeptidase that cleaves the chromosomal cohesin SCC1. Separase is inhibited by **securin**, which is degraded at the metaphase-anaphase transition. Using Xenopus egg extracts, we demonstrate that high CDC2 activity inhibits anaphase but not **securin** degradation. We show that separase is kept inactive under these conditions by a mechanism independent of binding to **securin**. Mutation of a single phosphorylation site on separase relieves the inhibition and rescues chromatid separation in extracts with high CDC2 activity. Using quantitative mass spectrometry, we show that, in intact cells, there is complete phosphorylation of this site in metaphase and significant dephosphorylation in anaphase. We propose that separase activation at the metaphase-anaphase transition requires the removal of both **securin** and an inhibitory phosphate.

L8 ANSWER 11 OF 20 MEDLINE DUPLICATE 8
ACCESSION NUMBER: 2001277711 MEDLINE

Human Genetics

The Molecular Revolution

Edwin H. McConkey

Department of Molecular, Cellular, and Developmental Biology
University of Colorado, Boulder

Jones and Bartlett Publishers
BOSTON LONDON

and under ordinary conditions of life, the sickle-cell allele is recessive to the wild-type allele of beta-globin; heterozygotes have normal health. However, under conditions of moderate oxygen deprivation, such as one encounters at high altitudes, heterozygotes may develop abdominal pain and bloody urine. If the heterozygote is observed at such a time, one would be obliged to conclude that the wild-type allele is only partially dominant.

There have been a few reports suggesting that when a sickle-cell heterozygote is subjected to extreme physiological exertion, as during an athletic contest, the exceptional demand for oxygen may lead to a sickle-cell crisis, occasionally with a fatal outcome. In such a case, the sickle-cell allele could be considered as a full dominant, but whether the presence of the heterozygous state was really the primary cause of the fatal or near-fatal response to stress, or whether sickling occurred *ex post facto* in the few reported cases, is a moot point.

When the blood of a sickle-cell heterozygote is examined by electrophoresis under appropriate conditions, two forms of hemoglobin can be identified; one contains wild-type beta-globin, while the other contains sickle-cell beta-globin. Alternatively, there is a restriction endonuclease that will cut the normal beta-globin gene, but will not cut the sickle-cell beta-globin allele at the site of the mutation. Both the protein assay and the nuclease assay reveal the sickle-cell allele as codominant with the normal allele.

Genetic Diseases Rarely Show Complete Dominance at the Phenotypic Level

Homozygotes for dominant genetic diseases are hard to find. That is not surprising, given the facts that affected heterozygotes are not numerous and that their abnormality often reduces the likelihood of their becoming parents. However, matings between heterozygotes for dominant genetic diseases occasionally occur, usually within an extended family. Unrelated heterozygotes may be brought together by the "misery loves company" phenomenon, known more formally as *assortative mating*. In either case, the potential for homozygous progeny exists. Pauli (1983) compiled data on a dozen dominant genetic diseases, where one or more matings between heterozygotes were known; some examples were achondroplasia, brachydactyly, and aniridia. In every case, one or more of the children were more severely affected than either of the parents; some of them died in infancy. Several other dominant genetic diseases not covered by Pauli, such as the Marfan Syndrome (Chemke et al., 1984), also showed exceptionally severe manifestations in putative homozygotes. Although there was no formal proof, either by linkage analysis or molecular analysis, that the severely affected offspring of these heterozygote-heterozygote matings were actually homozygous for the mutant allele, the assumption is unlikely to have been universally wrong.

Thus, for some years it appeared that complete dominance rarely or never applied to human genetic diseases. Then, in 1987, Wexler et al. reported on four homozygotes for Huntington Disease in the large Venezuelan kindred. These were found in a family of 14 children from a mating between relatives, both of whom were subsequently affected with the disease, and their genotypes were established by molecular analysis. The fascinating result of their study of this family was that the homozygotes were not more severely affected than their heterozygous sibs or other affected persons in the family. There was no apparent difference in the age of onset of symptoms, either. Here at last was the first well-documented case of a

of mutations in the same gene in different individuals. Some variable expressivity is caused by the fact that different mutant alleles have different effects on the expression of the same gene, but molecular explanations of most examples of variable expressivity are not yet available.

Genomic imprinting is a process whereby some genes are differentially inactivated during gametogenesis in the two sexes, so that their activity in the embryo depends upon the parent from which they were derived. The earliest manifestation of genomic imprinting is the requirement for one pronucleus from each parent; two female pronuclei or two male pronuclei will not allow normal development.

Many examples of genomic imprinting involving limited regions of specific chromosomes are known. It is believed that one phase of genomic imprinting is caused by methylation of DNA on cytosine residues, but the whole process is probably more complex.

REFERENCES

Becker, M. A., Meyer, L. J., Wood, A. W., and Seegmiller, J. E. 1973. Purine overproduction in man associated with increased PRPP synthetase activity. Science 179:1123–1126.

Brown, M. S. and Goldstein, J. L. 1986. A receptor-mediated pathway for cholesterol homeostasis. Science 232:34–47.

Chemke, J., Nisani, R., Feigl, A., et al., 1984. Homozygosity for autosomal dominant Marfan syndrome. J. Med. Genet. 21:173–177.

Friefelder, D. and Malouinski, G. M. 1993. Essentials of Molecular Biology, 2nd ed. Jones and Bartlett Publishers, Boston.

Frischer, L. E., Hagen, F. S., and Garber, R. L. 1986. An inversion that disrupts the *Antennapedia* gene causes abnormal structure and localization of RNAs. Cell 47:1017–1023.

Hall, J. G. 1990. Genomic imprinting: review and relevance to human diseases. Am. J. Hum. Genet. 46:857–873.

Holliday, R. and Pugh, J. E. 1975. DNA modification mechanisms and gene activity during development. Science 187:226–232.

Hollocher, H. and Place, A. R. 1987. Partial correction of structural defects in alcohol dehydrogenase through interallelic complementation in *Drosophila melanogaster*. Genetics 116:265–274.

Killian, J. M. and Kloepfer, H. W. 1979. Homozygous expression of a dominant gene for Charcot-Marie-Tooth neuropathy. Annals of Neurology 5:515–522.

Knoll, J., Nicholls, R., Magenis, R., Graham, J., Lalande, M., and Latt, S. 1989. Angelman and Prader-Willi syndromes share a common chromosome deletion but differ in parental origin of the deletion. Am. J. Med. Genet. 32:285–290.

Laird, C. D. 1990. Proposed genetic basis of Huntington's disease. Trends in Genetics 6:242–247.

Levitan, M. 1988. Textbook of human genetics, 3rd ed. Oxford University Press, New York.

Mange, A. P. and Mange, E. J. 1990. Genetics: human aspects, 2nd ed. Sinauer Associates, Sunderland, MA.

McKusick, V. A. 1991. The defect in Marfan syndrome. Nature 352:279–281.

Myers, R. H., Leavitt, J., et al. 1989. Homozygote for Huntington disease. Am. J. Hum. Genet. 45:615–618.

Neel, J. V. and Schull, W. J. 1954. Human Heredity. University of Chicago Press, Chicago, IL.

Pauli, R. M. 1983. Dominance and homozygosity in man. Am. J. Med. Genet. 16:455–458.

Pyeritz, R. E. 1989. Pleiotropy revisited: molecular explanations of a classic concept. Am. J. Med. Genet. 34:124–134.

Riggs, A. D. 1975. X inactivation, differentiation, and DNA methylation. Cytogenet. Cell Genet. 14:9–25.

Strong, L. C., Riccardi, V. M., Ferrell, R. E., and Sparkes, R. S. 1981. Familial retinoblastoma and chromosome 13 deletion transmitted via an insertional translocation. Science 213:1501–1503.

Surani, M. A. H., Barton, S. C., and Norris, M. L. 1984. Development of reconstituted mouse eggs suggests imprinting of the genome during gametogenesis. Nature 308:548–550.

Valentine, W. N., Paglia, D. E., Tartaglia, A. P., and Gilsanz, F. 1977. Hereditary hemolytic anemia with increased red cell adenosine deaminase activity (45-70 fold) and decreased ATP. Science 195:783–785.

Vogel, F. and Motulsky, A. G. 1979. Human genetics: problems and approaches. Springer-Verlag, Heidelberg.

Wexler, N. S., Young, A. B., Tanzi, R. E., et al. 1987. Homozygotes for Huntington's disease. Nature 326:194–197.

L25 ANSWER 16 OF 16 BIOTECHDS COPYRIGHT 2002 THOMSON DERWENT AND ISI
ACCESSION NUMBER: 1998-08045 BIOTECHDS
TITLE: New **pituitary** tumor **transforming** gene **protein** and related nucleic acid; recombinant **pituitary** tumor **transforming** gene **protein**, antisense oligonucleotide, DNA probe, DNA primer and non-human transgenic animal for use in cancer diagnosis, therapy, gene therapy, etc.
AUTHOR: Melmed S; Pei L
PATENT ASSIGNEE: Cedars-Sinai-Med.Cent.
LOCATION: Los Angeles, CA, USA.
PATENT INFO: WO 9822587 **28 May 1998**
APPLICATION INFO: WO 1997-US21463 21 Nov 1997
PRIORITY INFO: US 1996-31338 21 Nov 1996
DOCUMENT TYPE: Patent
LANGUAGE: English
OTHER SOURCE: WPI: 1998-312473 [27]
AN 1998-08045 BIOTECHDS
AB New, purified, isolated **pituitary** tumor **transforming** gene (PTTG) **protein** (I) expressed by pituitary tumor cells and binding antibodies specific for PTTG is claimed. Also claimed are: nucleic acid (II) encoding (I); vectors containing (II); host cells containing the vector; oligonucleotides of at least 15 nucleotides that hybridize to (II) under stringent conditions; antisense oligonucleotides that hybridize under stringent conditions with mRNA transcribed from (II); isolated antibodies; non-human transgenic animals containing at least 1 non-native sequence expressing a PPTG protein; and ss amplification DNA primers and DNA probes containing 10-150 nucleotides of (II). Cells are used to produce recombinant (I), which is useful as an immunogen for raising antibodies and in therapy. The oligonucleotide is preferably labeled and used to detect, isolate and quantify PPTG-encoding DNA or its transcripts. The antisense oligonucleotides are used to inhibit expression of human PPTG. (II) is useful in cancer gene therapy.
The transgenic animals are used as models for pituitary tumors. (44pp)

L39 ANSWER 1 OF 8 MEDLINE
ACCESSION NUMBER: 2000394766 MEDLINE
DOCUMENT NUMBER: 20312182 PubMed ID: 10855492
TITLE: Destruction of the **securin** Pds1p occurs at the onset of anaphase during both meiotic divisions in yeast.
AUTHOR: Salah S M; Nasmyth K
CORPORATE SOURCE: Vienna Biocenter, Institute of Biochemistry and Molecular Biology, Austria.
SOURCE: CHROMOSOMA, **(2000)** 109 (1-2) 27-34.
Journal code: 2985138R. ISSN: 0009-5915.
PUB. COUNTRY: GERMANY: Germany, Federal Republic of
Journal; Article; (JOURNAL ARTICLE)
LANGUAGE: English
FILE SEGMENT: Priority Journals
ENTRY MONTH: 200008
ENTRY DATE: Entered STN: 20000824
Last Updated on STN: 20000824
Entered Medline: 20000811

AB Sister chromatid cohesion is established during DNA replication and depends on a multiprotein complex called cohesin. At the onset of anaphase the cohesive structures that hold sisters together must be destroyed to allow segregation of sisters. In the budding yeast Saccharomyces cerevisiae loss of sister chromatid cohesion depends on a separating protein (separin) called Esp1. At the metaphase to anaphase transition, separin is activated by proteolysis of its inhibitory subunit (**securin**) called Pds1. This process is mediated by the anaphase promoting complex and an accessory protein Cdc20. In meiosis a single round of DNA replication is followed by two successive rounds of segregation. Thus loss of cohesion is spun out over two divisions. By studying the mechanisms that initiate anaphase in meiotic division we show that the yeast **securin** Pds1p is present in meiotic nuclei and is destroyed at the onset of each meiotic division. We also show that **securin** destruction depends on Cdc20p which accumulates within nuclei around the time of Pds1p's disappearance.

L25 ANSWER 9 OF 16 CAPLUS COPYRIGHT 2002 ACS
ACCESSION NUMBER: 2000:208584 CAPLUS
DOCUMENT NUMBER: 133:102972
TITLE: Pituitary tumor transforming gene (PTTG) transforming and transactivation activity
AUTHOR(S): Wang, Zhiyong; Melmed, Shlomo
CORPORATE SOURCE: Cedars-Sinai Research Institute, UCLA School of Medicine, Los Angeles, CA, 90048, USA
SOURCE: Journal of Biological Chemistry (**2000**), 275(11), 7459-7461
CODEN: JBCHA3; ISSN: 0021-9258
PUBLISHER: American Society for Biochemistry and Molecular Biology
DOCUMENT TYPE: Journal
LANGUAGE: English

AB Pituitary tumor transforming gene (PTTG) is a newly identified transforming gene, the functional mechanism of which is little understood.

Computational anal. reveals a C terminus rich in Glu and Pro, a known characteristic of transcriptional activation domains. The authors report here that murine PTTG indeed possesses transactivation ability, which correlates highly with its transforming properties. Pro139, Ser159, Pro157-Pro158-Ser159-Pro160 (PPXP motif), and Leu120-Asp121-Phe122-Asp123-

Leu124 were found to be important for transactivation. Mutation to Ala at

a key Pro139 residue not only disrupted the transactivation function but also resulted in the loss of transforming ability in NIH3T3 cells. A murine PTTG cDNA that encodes a variant C-terminal tail (Gly-Lys-Gly-Val-Arg-Ser-Asn-Gly-Cys-Lys-Asp-Leu-Val-Thr) was cloned. This novel PTTG is devoid of transactivation and transforming ability; deletion of its variant C-terminal tail restores both transactivation and transforming ability. These results show a high correlation between the transforming and transactivation functions of PTTG and also indicate that the novel PTTG variant may function as an endogenous competitor to wild-type PTTG.

REFERENCE COUNT: 14 THERE ARE 14 CITED REFERENCES AVAILABLE FOR THIS

L25 ANSWER 15 OF 16 CAPLUS COPYRIGHT 2002 ACS
ACCESSION NUMBER: 1999:24853 CAPLUS
DOCUMENT NUMBER: 130:233054
TITLE: Structure, expression, and function of human pituitary tumor- transforming gene (PTTG)
AUTHOR(S): Zhang, Xun; Horwitz, Gregory A.; Prezant, Toni R.; Valentini, Alberto; Nakashima, Masahiro; Bronstein, Marcello D.; Melmed, Shlomo
CORPORATE SOURCE: Cedars-Sinai Research Institute, UCLA School of Medicine, Los Angeles, CA, 90048, USA
SOURCE: Molecular Endocrinology (1999), 13(1), 156-166
CODEN: MOENEN; ISSN: 0888-8809
PUBLISHER: Endocrine Society
DOCUMENT TYPE: Journal
LANGUAGE: English

AB Despite advances in characterizing the pathophysiol. and genetics of pituitary tumors, mol. mechanisms of their pathogenesis are poorly understood. Recently, we isolated a transforming gene [pituitary tumor-transforming gene (PTTG)] from rat pituitary tumor cells. Here we describe the cloning of human PTTG, which is located on chromosome 5q33 and shares striking sequence homol. with its rat counterpart. Northern anal. revealed PTTG expression in normal adult testis, thymus, colon, small intestine, brain, lung, and fetal liver, but most abundant levels of PTTG mRNA were obsd. in several carcinoma cell lines. Stable transfection of NIH 3T3 cells with human PTTG cDNA caused anchorage-independent transformation in vitro and induced in vivo tumor formation when transfectants were injected into athymic mice. Overexpression of PTTG in transfected NIH 3T3 cells also stimulated expression and secretion of basic fibroblast growth factor, a human pituitary tumor growth-regulating factor. A proline-rich region, which contains two PXXP motifs for the SH3 domain-binding site, was detected in the PTTG protein sequence. When these proline residues were changed by site-directed mutagenesis, PTTG in vitro transforming and in vivo tumor-inducing activity, as well as stimulation of basic fibroblast growth factor, was abrogated. These results indicate that human PTTG, a novel oncogene, may function through SH3-mediated signal transduction pathways and activation of growth factor(s).

L17 ANSWER 6 OF 7 MEDLINE DUPLICATE 3
ACCESSION NUMBER: 1998148071 MEDLINE
DOCUMENT NUMBER: 98148071 PubMed ID: 9478977
TITLE: **Genomic** organization and identification of an enhancer element containing binding sites for multiple proteins in rat pituitary tumor-transforming gene.
AUTHOR: Pei L
CORPORATE SOURCE: Division of Endocrinology, Cedars-Sinai Research Institute,
UCLA School of Medicine, Los Angeles, California 90048, USA.. Pei@CSMC.edu
CONTRACT NUMBER: DK-02346 (NIDDK)
SOURCE: JOURNAL OF BIOLOGICAL CHEMISTRY, **(1998 Feb 27)** 273 (9) 5219-25.
Journal code: 2985121R. ISSN: 0021-9258.
PUB. COUNTRY: United States
Journal; Article; (JOURNAL ARTICLE)
LANGUAGE: English
FILE SEGMENT: Priority Journals
OTHER SOURCE: GENBANK-AF021802
ENTRY MONTH: 199803
ENTRY DATE: Entered STN: 19980407
Last Updated on STN: 19980407
Entered Medline: 19980325

AB The rat pituitary tumor transforming gene (**PTTG**) **genomic** structure was characterized in this study. Northern blot analysis showed that **PTTG** mRNA is highly expressed in testicular cell lines. Transfection of testicular cell lines with fusion constructs containing various portions of **PTTG** 5'-flanking sequences linked to luciferase showed that at least 745 base-pair (bp(s)) 5'-flanking sequences are required for **PTTG** transcriptional activation. DNaseI footprinting assays indicated that nuclear protein(s) from testicular cell lines interacts with **PTTG** 5'-flanking sequence between -509 and -624 bp, including two consensus Sp1 binding sites. Western and Southwestern blot analysis showed that three nuclear proteins in addition to Sp1 protein specifically interact with this DNA sequence and that two of these proteins are testicular cell-specific. Deletion of this 115-bp sequence from **PTTG** promoter resulted in complete loss of promoter function. Site-directed mutagenesis within the Sp1 consensus sequences indicated that the Sp1 binding sites are not critical components of the enhancer sequence for **PTTG** trancriptional activation in testicular cell lines. Finally, the 115-bp enhancer sequence was shown to be able to activate transcription from a heterologous promoter. These results suggest that **PTTG** transcriptional activation in testicular cell lines involves interactions of multiple nuclear factors with the **PTTG** 5' enhancer sequence.

L8 ANSWER 5 OF 9 MEDLINE DUPLICATE 2
ACCESSION NUMBER: 2000267846 MEDLINE
DOCUMENT NUMBER: 20267846 PubMed ID: 10806349
TITLE: Identification of the human **pituitary** tumor **transforming gene** (**hPTTG**) family: molecular structure, expression, and chromosomal localization.
AUTHOR: Chen L; Puri R; Lefkowitz E J; Kakar S S
CORPORATE SOURCE: Department of Physiology and Biophysics, University of Alabama at Birmingham, Birmingham, AL 35294, USA.
CONTRACT NUMBER: CA82511 (NCI)
SOURCE: GENE, **(2000 May 2)** 248 (1-2) 41-50.
Journal code: 7706761. ISSN: 0378-1119.
PUB. COUNTRY: Netherlands
Journal; Article; (JOURNAL ARTICLE)
LANGUAGE: English
FILE SEGMENT: Priority Journals
OTHER SOURCE: GENBANK-AF200719; GENBANK-AF200720
ENTRY MONTH: 200007
ENTRY DATE: Entered STN: 20000714
Last Updated on STN: 20000714
Entered Medline: 20000706

AB In an attempt to determine the mechanism of human tumorigenesis, we have searched for oncogenes and recently reported the molecular cloning of a potent oncogene (**hPTTG**) from human testis. **hPTTG** mRNA is expressed at high levels in various human tumors and tumor cell lines. Overexpression of **hPTTG** in the mouse fibroblast cell line (NIH 3T3) results in an increase in cell proliferation, induces cellular transformation in vitro, and promotes tumor formation in nude mice. The **hPTTG** gene isolated from the human **genomic** library consists of five exons and four introns and spans over 10kb. In the studies reported here, we further investigated the possibility of the presence of additional genes homologous to **hPTTG** in the human genome, which was first indicated by **Southern** blot analysis of the human **genomic** DNA and chromosomal mapping of the **hPTTG** gene using DNA from humanxhamster hybrid cell lines in PCR. Sequencing and restriction map analysis of the additional **genomic** clones identified two intronless genes homologous to **hPTTG**. This finding was confirmed by the chromosomal location of the second gene to chromosome 4p15.1 and the third gene to chromosome 8q13.1. Based on the similarity in sequences, we proposed that **hPTTG** be renamed hPTTG1 and the new genes be named hPTTG2 and hPTTG3. hPPTG2 was found to be 91% identical and hPPTG3 89% identical with hPPTG1 at the amino acid level. Northern blot and reverse transcriptase/polymerase chain reaction (RT/PCR) analyses of the mRNA from various human tissues revealed differential expression of the hPTTG2 and hPTTG3 genes in normal and tumor tissues, suggesting that these genes may be associated with tumorigenesis.

L8 ANSWER 4 OF 9 MEDLINE DUPLICATE 1
ACCESSION NUMBER: 2000171910 MEDLINE
DOCUMENT NUMBER: 20171910 PubMed ID: 10702375
TITLE: The control of mitosis.
AUTHOR: Hixon M L; Gualberto A
CORPORATE SOURCE: Division of Cardiovascular Research, Department of Medicine, St. Elizabeth's Medical Center, Boston, MA 02135,
USA.. mlhixon@opal.tufts.edu
SOURCE: FRONTIERS IN BIOSCIENCE, **(2000 Jan 1)** 5 D50-7.
Ref: 116
Journal code: 9702166. ISSN: 1093-4715.
PUB. COUNTRY: United States
Journal; Article; (JOURNAL ARTICLE)
General Review; (REVIEW)
(REVIEW, ACADEMIC)
LANGUAGE: English
FILE SEGMENT: Priority Journals
ENTRY MONTH: 200005
ENTRY DATE: Entered STN: 20000525
Last Updated on STN: 20000525
Entered Medline: 20000512

AB A precise coordination of multiple cell cycle events is required to ensure
proper mitosis. Chromosome cohesion must be maintained until all chromosomes are attached to opposite poles of the mitotic spindle and aligned at the metaphase plate. At the onset of anaphase, the activity of separins contributes to the release of cohesins from chromosomes, allowing
for the segregation of bivalents to opposite spindle poles. Separin activity is blocked by binding to a class of proteins known as **securins**, whose turnover at the metaphase-to-anaphase transition is triggered by the Anaphase Promoting Complex or cyclosome. The mitotic spindle cell cycle checkpoint coordinates the timing of these events and acts as input mechanism for DNA damage/stress pathways. Failure of this precise network leads to **genomic** instability and/or cell death.

L8 ANSWER 1 OF 9 CAPLUS COPYRIGHT 2002 ACS
ACCESSION NUMBER: 2001:749385 CAPLUS
DOCUMENT NUMBER: 136:321097
TITLE: Drosophila Separase is required for sister chromatid separation and binds to PIM and THR
AUTHOR(S): Jager, Hubert; Herzig, Alf; Lehner, Christian F.; Heidmann, Stefan
CORPORATE SOURCE: Department of Genetics, University of Bayreuth, Bayreuth, 95440, Germany
SOURCE: Genes & Development (**2001**), 15(19), 2572-2584
CODEN: GEDEEP; ISSN: 0890-9369
PUBLISHER: Cold Spring Harbor Laboratory Press
DOCUMENT TYPE: Journal
LANGUAGE: English
AB Drosophila PIM and THR are required for sister chromatid sepn. in mitosis and assoc. in vivo. Neither of these two proteins shares significant sequence similarity with known proteins. However, PIM has functional similarities with **securin** proteins. Like **securin**, PIM is degraded at the metaphase-to-anaphase transition and this degrdn. is required for sister chromatid sepn. **Securin** binds and inhibits separase, a conserved cysteine endoprotease. Proteolysis of **securin** at the metaphase-to-anaphase transition activates separase, which degrades a conserved cohesin subunit, thereby allowing sister chromatid sepn. To address whether PIM regulates separase activity or functions with THR in a distinct pathway, we have characterized a Drosophila separase homolog (SSE). SSE is an unusual member of the separase family. SSE is only about one-third the size of other separases and has a diverged endoprotease domain. However, our genetic analyses show that SSE is essential and required for sister chromatid sepn. during mitosis. Moreover, we show that SSE assocs. with both PIM and THR. Although our work shows that separase is required for sister chromatid sepn. in higher eukaryotes, in addn., it also indicates that the regulatory proteins have diverged to a surprising degree, particularly in Drosophila.
REFERENCE COUNT: 45 THERE ARE 45 CITED REFERENCES AVAILABLE FOR THIS

L13 ANSWER 2 OF 2 BIOSIS COPYRIGHT 2002 BIOLOGICAL ABSTRACTS INC.
ACCESSION NUMBER: 1999:297096 BIOSIS
DOCUMENT NUMBER: PREV199900297096
TITLE: New pituitary oncogenes.
AUTHOR(S): Melmed, Shlomo (1)
CORPORATE SOURCE: (1) Cedars-Sinai Research Institute, UCLA School of Medicine, Los Angeles, CA USA
SOURCE: Journal of Endocrinology, (March, 1999) Vol. 160, No. SUPPL., pp. S22.
Meeting Info.: 18th Joint Meeting of the British Endocrine Societies Bournemouth, England, UK April 12-15, 1999 British Endocrine Societies
. ISSN: 0022-0795.
DOCUMENT TYPE: Conference
LANGUAGE: English

L17 ANSWER 7 OF 7 CAPLUS COPYRIGHT 2002 ACS
ACCESSION NUMBER: 1999:150142 CAPLUS
DOCUMENT NUMBER: 131:54524
TITLE: Assignment of the human tumor transforming gene TUTR1 to chromosome band 5q35.1 by fluorescence in situ hybridization
AUTHOR(S): Kakar, S. S.
CORPORATE SOURCE: Department of Physiology and Biophysics, University of Alabama at Birmingham, Birmingham, AL, 35294-0005, USA
SOURCE: Cytogenetics and Cell Genetics (**1998**), 83(1-2), 93-95
CODEN: CGCGBR; ISSN: 0301-0171
PUBLISHER: S. Karger AG
DOCUMENT TYPE: Journal
LANGUAGE: English
AB We have recently clone the human tumor transforming gene (TUTR1, tumor transforming 1) from human testis. TUTR1 gene encodes a 202-amin acid protein that is extremely hydrophilic and that contains a proline-rich domain. In this study, using polymerase chain reaction (PCR) anal. of **genomic** DNA from human-hamster somatic cell hybrids, we localized TUTR1 to human chromosome 5. Fluorescence in situ hybridization anal. showed that the gene is located on human chromosome 5q35.1.
REFERENCE COUNT: 3 THERE ARE 3 CITED REFERENCES AVAILABLE FOR THIS RECORD. ALL CITATIONS AVAILABLE IN THE RE FORMAT

L17 ANSWER 4 OF 7 BIOSIS COPYRIGHT 2002 BIOLOGICAL ABSTRACTS INC.
ACCESSION NUMBER: 1999:111850 BIOSIS
DOCUMENT NUMBER: PREV199900111850
TITLE: Pituitary tumor-transforming gene protein associates with ribosomal protein S10 and a novel human homologue of DnaJ in testicular cells.
AUTHOR(S): Pei, Lin (1)
CORPORATE SOURCE: (1) Div. Endocrinol., Cedars-Sinai Med. Cent., 8700 Beverly Blvd., D-3066, Los Angeles, CA 90048 USA
SOURCE: Journal of Biological Chemistry, (**Jan. 29, 1999**) Vol. 274, No. 5, pp. 3151-3158. ISSN: 0021-9258.
DOCUMENT TYPE: Article
LANGUAGE: English

AB Pituitary tumor-transforming gene (**PTTG**) is a recently characterized proto-oncogene that is expressed specifically in adult testis. In this study, we have used in situ hybridization and developmental Northern blot assays to demonstrate that **PTTG** mRNA is expressed stage-specifically in spermatocytes and spermatids during rat spermatogenic cycle. We have used the yeast two-hybrid system to identify proteins that interact with **PTTG** in testicular cells. Two positive clones were characterized. One of the clones is the ribosomal protein S10, the other encodes a novel human DnaJ homologue designated HSJ2. Northern blot analysis showed that testis contains higher levels of HSJ2 mRNA than other tissues examined, and the expression pattern of HSJ2 mRNA in postnatal rat testis is similar to **PTTG**. S10 mRNA levels do not vary remarkably among different tissues and remains unchanged during testicular germ cell differentiation. In vitro binding assays demonstrated that both S10 and HSJ2 bind to **PTTG** specifically and that **PTTG** can be co-immunoprecipitated with S10 and HSJ2 from transfected cells. Moreover, the binding sites for both proteins were located within the C-terminal 75 amino acids of the **PTTG** protein. These results suggest that **PTTG** may play a role in spermatogenesis.

L17 ANSWER 2 OF 7 CANCERLIT
ACCESSION NUMBER: 2000166534 CANCERLIT
DOCUMENT NUMBER: 20166534
TITLE: Towards post-**genomic** investigation of colorectal cancer [comment].
COMMENT: Comment on: Lancet 2000 Feb 26;355(9205):716-9
AUTHOR: Midgley R; Kerr D
CORPORATE SOURCE: CRC Institute for Cancer Studies, University of Birmingham,
Edgbaston, UK.
SOURCE: LANCET, **(2000)**. Vol. 355, No. 9205, pp. 669-70.
Journal code: L0S. ISSN: 0140-6736.
DOCUMENT TYPE: Commentary
Journal; Article; (JOURNAL ARTICLE)
FILE SEGMENT: MEDL; L; Abridged Index Medicus Journals; Priority Journals; Cancer Journals
LANGUAGE: English
OTHER SOURCE: MEDLINE 20166534
ENTRY MONTH: 200004

L17 ANSWER 1 OF 7 MEDLINE
ACCESSION NUMBER: 2000166534 MEDLINE
DOCUMENT NUMBER: 20166534 PubMed ID: 10703794
TITLE: Towards post-**genomic** investigation of colorectal cancer.
COMMENT: Comment on: Lancet. 2000 Feb 26;355(9205):716-9
AUTHOR: Midgley R; Kerr D
CORPORATE SOURCE: CRC Institute for Cancer Studies, University of Birmingham,
Edgbaston, UK.
SOURCE: LANCET, **(2000 Feb 26)** 355 (9205) 669-70.
Journal code: 2985213R. ISSN: 0140-6736.
PUB. COUNTRY: ENGLAND: United Kingdom
Commentary
Journal; Article; (JOURNAL ARTICLE)
LANGUAGE: English
FILE SEGMENT: Abridged Index Medicus Journals; Priority Journals
ENTRY MONTH: 200003
ENTRY DATE: Entered STN: 20000327
Last Updated on STN: 20000327
Entered Medline: 20000316

As an example, to create a...Particularly, as described herein with respect to
Figure 3, within the networkMCI Interact framework for producing Java **applications** over the Internet, there is provided common objects and an infrastructure allowing secure communications between a client...

...traffic between the
web server and the dispatcher via DSA encry tion; and enabling the dispatcher to **validate** all pa0ets
6
destined to internal MCI servers to ensure that they are from an **authenticated** client, and that a particular client has permission to communicate with a s@ecific back-end server. To **make** this seamless for t e client the aforementioned set of common objects performs this messaging. In the...

...Figure 2 , the communication path from the client and the server is as follows.

The TFNM server **application** 840 registers remote objects with CORMI's CORemoteSessionServer (analogous to Java RMI's Registry service) and then...

...for connections. The TFNM client applet initiates communication by performing a log9n through COClientSession object. The COClientsession **creates** COSynchTransaction (an atomic unit of work based
...is behind
the outer firewall 25(b)) and interfacing with StarOE server 39. The dispatcher server 26 **validates** the client's authorization to logon (a process that involves contacting the StarOE service and **generating** a session keK with a :cookie@arltprocess). After validating t e client the dispa cher uses a...

...select a TFNM server and then opens
an HTTPS connection to an instance of the TFNM server **application** . On this server, the
CORemoteSessionServer **creates** a new session for this client and records the session key.

A reply to a logon is...the
Enti@,rprise. Particularly, in response to a user login, in the preferred embodiment, a TFNM server **application** is executed. From this **application** , the
8
TFNM server instantiates a Profile Manager Java object which is registered with CORMI and called...

...invoke further objects relating to the following: user profile, e.g., preferences, user security profiles,
@
e., for **tracking** customer entitlements7privileges including rights for creating or modifying specific TFNM routing plans or **generating** QUIK or IMPL orders; and, session management, i.e., objects which encapsulate the state and behavior associated...Particularly, as described herein with respect to
Figure 2, within the networkMCI Interact framework for producing Java **applications** over the Internetr there is provided common objects and an infrastructure allowing secure communications between a client...

...encrypting traffic between the web server and

the dispatcher via DSA cryption; and enabling the dispatcher to **validate** all packets destined to internal MCI servers to ensure that they are from an **authenticated** client, and that a particular client has permission to communicate with a specific back-end server. To **make** this seamless for the client, the set of Common objects performs this messaging. In the preferred embodiment...with a drop down menu (not shown) presenting a section of the order types which can be **created** via their Web Browser, e.g., CPN, Calling Card, Dialing Plan, and ID Code Set. When the...

...down menu of Figure 29(a), the user is presented with a web page 2725 displaying a **request** order window where the user may enter search criteria from which a user may select orders, or...

...may enter the following search criteria: an exact order number or partial order number in the "order **match** " field 2730; an order type, e.g., Calling Card, CPN, Dialing Plan, ID Code Set, or all...

...or default current user ID from the "user ID" field 2739; and, a set of order status **check** boxes 2740 which enables the user to choose an order status, e.g., not approved, approved, complete...gy a customer, is launched automatically when an alarm is detected. For example, if an alarm is **generated** regarding,a fiber outage that impacts a customer's toll free circuit, an option allows the user...

...number, service id, circuit id, and type of service, e.g., toll free or broadband. The TFNM **application** is t pically launched directly from an alarm view with t@e above parameters for finding the associated routing plan. User profile information needed b@ TFNM for **authentication** and entitlement verification efore actually proceeding with the alternate routing plan, are also passed as parameters to the TFNM **application** at the same time.

Performance metrics
The event monitor follows and conforms to general "networkMCI Interact" reporting...

Set	Items	Description
S1	22814	RESOURCE()LOCATOR? OR ADDRESS? OR URL OR URLS OR HYPERLINK? OR LINK? OR ANCHOR? OR PATH? OR NAMESPACE OR DOMAIN
S2	14669	IDENTIFY? OR DETECT? OR DETERMIN? OR RECOGNI? OR INTERROGAT? OR VERIF? OR JUDGE? OR AUTHENTICAT? OR VALIDAT?
S3	18013	INITIAL OR FIRST OR 1ST OR LEADING OR CARDINAL OR ORIGINAL OR PRIMARY
S4	32715	IMAGE? OR PHOTO? OR PICTURE? OR OBJECT? OR DOCUMENT?
S5	4699	(EDIT? OR MODIF? OR CHANG? OR REVIS? OR REVAMP? OR ALTER? OR UPDAT? OR REWORK? OR UP()(DATING OR DATE? ?) OR ADULTERAT? OR CORRUPT? OR TAMPER? OR MUTATE?)(2N)(VERSION? OR EDITION? OR RELEASE?)
S6	52293	OPERATION? OR FUNCTION? OR INSTRUCTION? OR EXECUTION? OR COMMAND? OR PROGRAM? OR ROUTINE?
S7	45788	GENERAT? OR REPRODUCE? OR CREAT? OR PRODUCE? OR MAKE
S8	265	(ACCESS OR AUTHENTICAT? OR VERIF? OR CERTIF? OR VALIDAT? OR AUTHORIZATION)(2N)(KEY OR KEYS)
S9	39628	ACCREDIT? OR VALIDATE? OR VERIFYING OR VERIFY? OR AUTHENTICAT? OR CONFIRM? OR ACTIVAT? OR TEST? OR INSPECT? OR ANALYS? OR ANALYZ? OR CHECK? OR MEASURE? OR TRACK? OR MATCH?
S10	46229	REQUEST? OR APPLY OR APPLYING OR PETITION? OR ASK OR ASKING OR APPLICATION? OR QUER? OR INQUIR? OR QUESTION? OR REQUISITION?
S11	0	S1 AND S2 AND (S3 (2N) S4) AND S5
S12	7	S1 AND S2 AND S3 AND S4 AND S5
S13	3	S12 AND S6
S14	0	S1 AND (S7 (3N) S8) AND S9 AND S10
S15	0	RESOURCE()LOCATOR? AND S7 AND S8
S16	4	S12 NOT PY>2001
S17	4	S16 NOT PD>20010801

File 256:SoftBase:Reviews,Companies&Prods. 82-2003/Nov

L8 ANSWER 8 OF 8 MEDLINE DUPLICATE 3
ACCESSION NUMBER: 84106535 MEDLINE
DOCUMENT NUMBER: 84106535 PubMed ID: 6692381
TITLE: Phase I study of aziridinylbenzoquinone (AZQ, NSC 182986) in children with cancer.
AUTHOR: Tan C T; Hancock C H; Mondora A; Hoffman N W
CONTRACT NUMBER: CA 29564 (NCI)
N01-CM 07463 (NCI)
SOURCE: CANCER RESEARCH, (1984 Feb) 44 (2) 831-5.
Journal code: CNF; 2984705R. ISSN: 0008-5472.
PUB. COUNTRY: United States
Journal; Article; (JOURNAL ARTICLE)
LANGUAGE: English
FILE SEGMENT: Priority Journals
ENTRY MONTH: 198403
ENTRY DATE: Entered STN: 19900319
Last Updated on STN: 19980206
Entered Medline: 19840301

AB Aziridinylbenzoquinone is a quinone compound capable of penetrating the central nervous system. It has demonstrated activity against both intracranial and i.p. murine tumors and **human tumor xenographs**. We have conducted a Phase I trial of aziridinylbenzoquinone in 60 children with advanced cancer who were refractory to conventional therapy. The drug was given by slow i.v. push on a daily schedule for 5 days every 3 to 4 weeks. The dose range explored included 6 dose levels, ranging from 6 to 12 mg/sq m daily for 5 days in patients with solid tumors and leukemia, and in patients with leukemia, 20, 25, and 30 mg/sq m daily for 5 days. Myelosuppression was the dose-limiting side effect. In patients with solid tumor the highest dose studied was 12 mg/sq m, and the median nadir white blood cell and platelet counts were 0.7 X 10(3) and 6.0 X 10(3)/microliter on Days 17 and 22, respectively. The median recovery day for white blood cells was 39. There may be some evidence of cumulative toxicity with prolonged thrombocytopenia. Other side effects were mild nausea, vomiting, and mucositis. Elevations in liver enzymes and bilirubin were transient and dose dependent, occurring 3 to 4 weeks after drug administration. Of the 34 children with solid tumors, 33 were evaluable for hematopoietic toxicity, 3 were early deaths, and 31 receiving a total of 55 courses were evaluable for therapeutic response. Partial responses lasting 3 weeks to 6 months were seen in the 4 patients with Hodgkin's disease, and in a child with a metastatic spinal cord ependymoma. Fifty-two courses were given to 9 patients with acute lymphocytic leukemia and 17 with acute nonlymphoblastic leukemia. Of the 15 patients with acute nonlymphoblastic leukemia treated at doses greater than or equal to 25 mg/sq m/day for 5 days there was one early death and there were 2 M1 (less than or equal to 5% blasts with normal cellularity), 3 M2A (6 to 15% blasts), and 2 M2B (16 to 39% blasts) bone marrow responses lasting 1 to 3.5 months. Aziridinylbenzoquinone demonstrated activity against acute nonlymphocytic leukemia with maximal tolerated doses of 30 mg/sq m daily for 5 days. Its effect in Hodgkin's disease is encouraging; however, further study will be required to determine its efficacy in central nervous system cancers.

Recommended doses for Phase II studies, using daily schedule for 5 days in children with solid tumors, is 9 mg/sq m, and in children with leukemia, it is 25 mg/sq m.

L8 ANSWER 5 OF 8 BIOSIS COPYRIGHT 2002 BIOLOGICAL ABSTRACTS INC.
ACCESSION NUMBER: 1992:404478 BIOSIS
DOCUMENT NUMBER: BR43:60353
TITLE: SEVERE COMBINED IMMUNODEFICIENT SCID MICE BEARING **HUMAN TUMOR XENOGRAPHS** ARE A USEFUL MODEL FOR EVALUATION OF CHEMOTHERAPEUTIC REGIMENS.
AUTHOR(S): SHORTALL M; SENTZ D; MACAULEY C; AISNER D; BILELLO J; EISEMAN J L
CORPORATE SOURCE: UNIV. M. D. CANCER CENT., BALTIMORE, MD. 21201.
SOURCE: 83RD ANNUAL MEETING OF THE AMERICAN ASSOCIATION FOR CANCER RESEARCH, SAN DIEGO, CALIFORNIA, USA, MAY 20-23, 1992.
PROC
AM ASSOC CANCER RES ANNU MEET, (1992) 33 (0), 558.
CODEN: PAMREA.
DOCUMENT TYPE: Conference
FILE SEGMENT: BR; OLD
LANGUAGE: English

Dual inhibition of sister chromatid separation at metaphase.

Stemmann O, Zou H, Gerber SA, Gygi SP, Kirschner MW.

Cell. 2001 Dec 14;107(6):715-26.

Department of Cell Biology, Harvard Medical School, Boston, MA 02115, USA.

Separation of sister chromatids in anaphase is mediated by separase, an endopeptidase that cleaves the chromosomal cohesin SCC1. Separase is inhibited by securin, which is degraded at the metaphase-anaphase transition. Using Xenopus egg extracts, we demonstrate that high CDC2 activity inhibits anaphase but not securin degradation. We show that separase is kept inactive under these conditions by a mechanism independent of binding to securin. Mutation of a single phosphorylation site on separase relieves the inhibition and rescues chromatid separation in extracts with high CDC2 activity. Using quantitative mass spectrometry, we show that, in intact cells, there is complete phosphorylation of this site in metaphase and significant dephosphorylation in anaphase. We propose that separase activation at the metaphase-anaphase transition requires the removal of both securin and an inhibitory phosphate.

MeSH Terms:

- Anaphase/physiology
- Animal
- Cell Cycle Proteins/antagonists & inhibitors
- Cell Cycle Proteins/genetics
- Cell Cycle Proteins/*metabolism
- Chromatids/*metabolism
- Cyclin B/genetics

- Cyclin B/metabolism
- Hela Cells
- Human
- Metaphase/*physiology
- Oocytes/physiology
- Peptide Mapping
- Phosphorylation
- Protein p34cdc2/genetics
- Protein p34cdc2/*metabolism
- Spectrum Analysis, Mass
- Support, Non-U.S. Gov't
- Support, U.S. Gov't, P.H.S.
- Xenopus laevis

Substances:

- 0 (Cell Cycle Proteins)
- 0 (Cyclin B)
- 0 (Protein p34cdc2)
- 0 (SCC1 protein)
- 0 (cyclin B1)
- 0 (separin)

Grant Support:

- GM26875-17/GM/NIGMS
- GM39023-08/GM/NIGMS
- HG00041/HG/NHGRI

PMID: 11747808 [PubMed - indexed for MEDLINE]
From PubMed

L8 ANSWER 15 OF 20 BIOSIS COPYRIGHT 2002 BIOLOGICAL ABSTRACTS INC.
ACCESSION NUMBER: 2000:347397 BIOSIS
DOCUMENT NUMBER: PREV200000347397
TITLE: Splitting the chromosome: Cutting the ties that bind sister chromatids.
AUTHOR(S): Nasmyth, Kim (1); Peters, Jan-Michael; Uhlmann, Frank
CORPORATE SOURCE: (1) Research Institute of Molecular Pathology (IMP), Dr. Bohr-Gasse 7, A-1030, Vienna Austria
SOURCE: Science (Washington D C), (26 May, 2000) Vol. 288, No. 5470, pp. 1379-1384. print.
ISSN: 0036-8075.
DOCUMENT TYPE: General Review
LANGUAGE: English
SUMMARY LANGUAGE: English
AB In eukaryotic cells, sister DNA molecules remain physically connected from their production at S phase until their separation during anaphase. This cohesion is essential for the separation of sister chromatids to opposite poles of the cell at mitosis. It also permits chromosome segregation to take place long after duplication has been completed. Recent work has identified a multisubunit complex called cohesin that is essential for connecting sisters. Proteolytic cleavage of one of cohesin's subunits may trigger sister separation at the onset of anaphase.

L8 ANSWER 18 OF 20 MEDLINE
ACCESSION NUMBER: 2000171910 MEDLINE
DOCUMENT NUMBER: 20171910 PubMed ID: 10702375
TITLE: The control of mitosis.
AUTHOR: Hixon M L; Gualberto A
CORPORATE SOURCE: Division of Cardiovascular Research, Department of Medicine, St. Elizabeth's Medical Center, Boston, MA 02135, USA.. mlhixon@opal.tufts.edu
SOURCE: FRONTIERS IN BIOSCIENCE, (2000 Jan 1) 5 D50-7. Ref: 116
Journal code: CUE; 9702166. ISSN: 1093-4715.
PUB. COUNTRY: United States
Journal; Article; (JOURNAL ARTICLE)
General Review; (REVIEW)
(REVIEW, ACADEMIC)
LANGUAGE: English
FILE SEGMENT: Priority Journals
ENTRY MONTH: 200005
ENTRY DATE: Entered STN: 20000525
Last Updated on STN: 20000525
Entered Medline: 20000512

AB A precise coordination of multiple cell cycle events is required to ensure proper mitosis. Chromosome cohesion must be maintained until all chromosomes are attached to opposite poles of the mitotic spindle and aligned at the metaphase plate. At the onset of anaphase, the activity of separins contributes to the release of cohesins from chromosomes, allowing for the segregation of bivalents to opposite spindle poles. Separin activity is blocked by binding to a class of proteins known as **securins**, whose turnover at the metaphase-to-anaphase transition is triggered by the Anaphase Promoting Complex or cyclosome. The mitotic spindle cell cycle checkpoint coordinates the timing of these events and acts as input mechanism for DNA damage/stress pathways. Failure of this precise network leads to genomic instability and/or cell death.

L8 ANSWER 20 OF 20 MEDLINE DUPLICATE 13
ACCESSION NUMBER: 1999340303 MEDLINE
DOCUMENT NUMBER: 99340303 PubMed ID: 10411507
TITLE: Identification of a vertebrate sister-chromatid separation inhibitor involved in transformation and tumorigenesis.
COMMENT: Comment in: Science. 1999 Jul 16;285(5426):344-5
AUTHOR: Zou H; McGarry T J; Bernal T; Kirschner M W
CORPORATE SOURCE: Department of Cell Biology, Harvard Medical School, 240 Longwood Avenue, Boston, MA 02115, USA.
CONTRACT NUMBER: GM26875 (NIGMS)
SOURCE: SCIENCE, (1999 Jul 16) 285 (5426) 418-22.
Journal code: UJ7; 0404511. ISSN: 0036-8075.
PUB. COUNTRY: United States
Journal; Article; (JOURNAL ARTICLE)
LANGUAGE: English
FILE SEGMENT: Priority Journals
OTHER SOURCE: GENBANK-AF220426
ENTRY MONTH: 199908
ENTRY DATE: Entered STN: 19990816
Last Updated on STN: 19990816
Entered Medline: 19990804

AB A vertebrate **securin** (vSecurin) was identified on the basis of its biochemical analogy to the Pds1p protein of budding yeast and the Cut2p protein of fission yeast. The vSecurin protein bound to a vertebrate homolog of yeast separins Esp1p and Cut1p and was degraded by proteolysis mediated by an anaphase-promoting complex in a manner dependent on a destruction motif. Furthermore, expression of a stable Xenopus **securin** mutant protein blocked sister-chromatid separation but did not block the embryonic cell cycle. The vSecurin proteins share extensive sequence similarity with each other but show no sequence similarity to either of their yeast counterparts. **Human securin** is identical to the product of the gene called pituitary tumor-transforming gene (PTTG), which is overexpressed in some tumors and exhibits transforming activity in NIH 3T3 cells. The oncogenic nature of increased expression of vSecurin may result from chromosome gain or loss, produced by errors in chromatid separation.

L19 ANSWER 3 OF 46 MEDLINE DUPLICATE 1
ACCESSION NUMBER: 2001133543 MEDLINE
DOCUMENT NUMBER: 21066759 PubMed ID: 11146294
TITLE: Managing the centrosome numbers game: from chaos to stability in cancer cell division.
AUTHOR: Brinkley B R
CORPORATE SOURCE: Dept of Molecular and Cellular Biology, Baylor College of Medicine, 77030, Houston, TX, USA.
SOURCE: TRENDS IN CELL BIOLOGY, (2001 Jan) 11 (1) 18-21. Ref: 30
Journal code: C5K; 9200566. ISSN: 0962-8924.
PUB. COUNTRY: England: United Kingdom
Journal; Article; (JOURNAL ARTICLE)
General Review; (REVIEW)
(REVIEW, TUTORIAL)
LANGUAGE: English
FILE SEGMENT: Priority Journals
ENTRY MONTH: 200103
ENTRY DATE: Entered STN: 20010404
Last Updated on STN: 20010404
Entered Medline: 20010301

AB **Aneuploid** tumor **cells** can arise through multipolar mitosis caused by supernumerary centrosomes. Multipolar spindles, however, are antagonistic to cell viability. Thus, most cells derived from such an aberrant mitosis would be **eliminated** by apoptosis. A rare daughter cell, through chance acquisition of an appropriate chromosome complement and/or gene dosage, could survive and contribute to a clone of **aneuploid** tumor **cells**. Survival and perpetuation of the clone, however, requires an additional step - the resumption of mitotic stability through the assembly of a bipolar, not multipolar, spindle. Either selective inactivation of the extra centrosomes or their coalescence into two functional spindle poles corrects the problem of centrosome excess. Current data support coalescence as a mechanism for regulating the number of functional centrosomes in tumor cells.

L19 ANSWER 4 OF 46 MEDLINE DUPLICATE 2

L8 ANSWER 9 OF 20 MEDLINE DUPLICATE 7
ACCESSION NUMBER: 2001205082 MEDLINE
DOCUMENT NUMBER: 21099256 PubMed ID: 11179223
TITLE: **Securin** degradation is mediated by fzy and fzr, and is required for complete chromatid separation but not for cytokinesis.
AUTHOR: Zur A; Brandeis M
CORPORATE SOURCE: Department of Genetics, Silberman Institute of Life Sciences, The Hebrew University of Jerusalem, Jerusalem 91904, Israel.
SOURCE: EMBO JOURNAL, (2001 Feb 15) 20 (4) 792-801.
Journal code: EMB; 8208664. ISSN: 0261-4189.
PUB. COUNTRY: England: United Kingdom
Journal; Article; (JOURNAL ARTICLE)
LANGUAGE: English
FILE SEGMENT: Priority Journals
ENTRY MONTH: 200104
ENTRY DATE: Entered STN: 20010417
Last Updated on STN: 20010417
Entered Medline: 20010412

AB We have studied the ubiquitination and degradation patterns of the **human securin**/PTTG protein. We show that, in contrast to budding yeast pds1, **securin** degradation is catalyzed by both fzy (fizzy/cdc20) and fzr (fizzy-related/cdh1/hct1). Both fzy and fzr also induce the APC/C to ubiquitinate **securin** in vitro. **Securin** degradation is mediated by an RXXL destruction box and a KEN box, and is inhibited only when both sequences are mutated. Interestingly, the non-degradable **securin** mutant is also partially ubiquitinated by fzy and fzr in vitro. Expressing the non-degradable **securin** mutant in cells frequently resulted in incomplete chromatid separation and gave rise to daughter cells connected by a thin chromatin fiber, presumably of chromosomes that failed to split completely. Strikingly, the mutant **securin** did not prevent the majority of sister chromatids from separating completely, nor did it prevent mitotic cyclin degradation and cytokinesis. This phenotype, reminiscent of the fission yeast cut (cells untimely torn) phenotype, is reported here for the first time in mammals.

L8 ANSWER 10 OF 20 MEDLINE
ACCESSION NUMBER: 2001699704 MEDLINE

L19 ANSWER 4 OF 46 MEDLINE DUPLICATE 2
ACCESSION NUMBER: 2001060144 MEDLINE
DOCUMENT NUMBER: 20410773 PubMed ID: 10955806
TITLE: Alteration of DNA ploidy status and cell proliferation induced by preoperative radiotherapy is a prognostic factor in rectal cancer.
AUTHOR: Lammering G; Taher M M; Gruenagel H H; Borchard F; Porschen R
CORPORATE SOURCE: Department of Radiation Oncology, Medical College of Virginia, Virginia Commonwealth University, Richmond 23298, USA.
SOURCE: CLINICAL CANCER RESEARCH, (2000 Aug) 6 (8) 3215-21. Journal code: C2H. ISSN: 1078-0432.
PUB. COUNTRY: United States
(CLINICAL TRIAL)
Journal; Article; (JOURNAL ARTICLE)
LANGUAGE: English
FILE SEGMENT: Priority Journals
ENTRY MONTH: 200012
ENTRY DATE: Entered STN: 20010322
Last Updated on STN: 20010322
Entered Medline: 20001228

AB To identify predictors of prognosis after preoperative radiotherapy, DNA ploidy and cell proliferation were investigated in 116 patients with rectal cancer. For flow cytometry, a nuclear suspension was prepared by pepsin digestion of paraffin samples of biopsies taken before preoperative radiotherapy (15 x 2 Gy) and also of the resected rectal tumors after radiotherapy. The median follow-up period was 6 years. The proportion of tumor necrosis was evaluated in histological sections before and after irradiation. There was a significant decrease (74 to 48%) in aneuploid tumors after radiation. Of 86 patients with aneuploid biopsies, 28 revealed no reduction in the proportion of **aneuploid** tumor **cells** [group AN(=/increase)], and 58 showed a reduction (mean 48.9%) or complete **elimination** of **aneuploid** tumor **cells** [group AN(decrease/psi)]. The incidence of local or distal failure was significantly reduced in the group AN(decrease/psi) (7.8%/20%), compared with the group AN (=/increase) (27%/54%) and the group of constant diploid tumors (n = 22; 13.6%/31.8 %; P = 0.034). There was a trend of decreased recurrence rate in diploid tumors with a reduced fraction of cells in S-phase after radiotherapy. Survival was significantly increased in group AN(decrease/psi) (P < 0.0001). In a multivariate regression analysis, variables of independent prognostic significance were increased proportion of necrosis after irradiation and DNA ploidy group and the postoperative tumor stage. These results suggest that alterations in tumor DNA ploidy and cell proliferation induced by preoperative radiotherapy might help to identify patients likely to benefit from preoperative radiation in rectal cancer.

L19 ANSWER 5 OF 46 BIOSIS COPYRIGHT 2002 BIOLOGICAL ABSTRACTS INC.

L19 ANSWER 11 OF 46 MEDLINE DUPLICATE 8
ACCESSION NUMBER: 97346306 MEDLINE
DOCUMENT NUMBER: 97346306 PubMed ID: 9202726
TITLE: Detection of subpopulations resistant to DNA-damaging agents in spheroids and murine tumours.
AUTHOR: Olive P L; Banath J P; Durand R E
CORPORATE SOURCE: Medical Biophysics Department, British Columbia Cancer Research Centre, Vancouver, Canada.. olive@unixg.ubc.ca
CONTRACT NUMBER: CA-37879 (NCI)
SOURCE: MUTATION RESEARCH, (1997 Apr 29) 375 (2) 157-65. Journal code: NNA; 0400763. ISSN: 0027-5107.
PUB. COUNTRY: Netherlands
Journal; Article; (JOURNAL ARTICLE)
LANGUAGE: English
FILE SEGMENT: Priority Journals
ENTRY MONTH: 199707
ENTRY DATE: Entered STN: 19970724
Last Updated on STN: 19970724
Entered Medline: 19970717

AB Chinese hamster V79 monolayers, V79 spheroids, and SCCVII murine tumours were examined for DNA damage using the alkaline comet assay and for cell **killing** by measuring clonogenicity following a 1-h exposure to doxorubicin, N-methyl-N'-nitro-N-nitrosoguanidine (MNNG), 4-nitroquinoline-N-oxide (4-NQO), etoposide, or 3-amino-1,2,4-benzotriazine-1,4-dioxide (tirapazamine). Greater heterogeneity in DNA damage was evident in spheroids compared to monolayers exposed to these drugs, and cell survival was correlated with the fraction of cells which lacked sufficient DNA damage following treatment with tirapazamine or doxorubicin. Cell sorting experiments verified that subpopulations of cells resistant to DNA damage were also more resistant to cell **killing**. Significant heterogeneity was observed in cells from SCCVII tumours exposed to tirapazamine and etoposide, and comet DNA content was used to independently assess DNA damage to **aneuploid** tumour **cells** and diploid host cells. These results suggest that, for some drugs, the comet assay may be an effective method of identifying drug-resistant cells in solid tumours.

L19 ANSWER 12 OF 46 MEDLINE DUPLICATE 9
ACCESSION NUMBER: 97050924 MEDLINE

L19 ANSWER 30 OF 46 MEDLINE DUPLICATE 22
ACCESSION NUMBER: 85145798 MEDLINE
DOCUMENT NUMBER: 85145798 PubMed ID: 2858155
TITLE: Treatment of the blastic transformation of chronic granulocytic leukemia using high dose BCNU chemotherapy and cryopreserved autologous peripheral blood stem cells.
AUTHOR: Karp D D; Parker L M; Binder N; Tantravahi R; Smith B R; Ervin T J; Canellos G P
CONTRACT NUMBER: PO1-CA19589 (NCI)
SOURCE: AMERICAN JOURNAL OF HEMATOLOGY, (1985 Mar) 18 (3) 243-9. Journal code: 3H4; 7610369. ISSN: 0361-8609.
PUB. COUNTRY: United States
Journal; Article; (JOURNAL ARTICLE)
LANGUAGE: English
FILE SEGMENT: Priority Journals
ENTRY MONTH: 198504
ENTRY DATE: Entered STN: 19900320
Last Updated on STN: 19970203
Entered Medline: 19850404

AB Seven nonsplenectomized patients with blastic CGL have received high dose BCNU chemotherapy followed by cryopreserved peripheral blood stem cells (PBSC). The PBSC obtained at diagnosis were stored in the vapor phase of liquid nitrogen in 10% dimethyl sulfoxide for 11-46 months prior to use. Patients received 2.9 X 10(8) (1.9-7.8) thawed washed mononuclear cells/kg over 30 minutes with minimal morbidity. One patient was not rendered pancytopenic and died with blastic leukemia at 4 months. One patient, previously treated with daily busulfan, died of progressive hepatic failure 2 months after high dose BCNU. Restoration of the chronic phase of CGL was observed in the remaining five patients. Peripheral blood counts returned to normal ranges after a median of 19 days. Median survival for all patients is 11 months. Cytogenetic studies revealed **elimination** of acquired **aneuploid cell** lines in four of seven patients with persistence of Ph1. We conclude that: 1) frozen PBSC retain their viability for up to 4 years after cryopreservation and 2) the use of autologous PBSC following ablative chemotherapy may be associated with both symptomatic and karyotypic improvement in patients with blastic CGL.

L19 ANSWER 31 OF 46 BIOSIS COPYRIGHT 2002 BIOLOGICAL ABSTRACTS INC.
ACCESSION NUMBER: 1986:152037 BIOSIS

L19 ANSWER 21 OF 46 MEDLINE DUPLICATE 16
ACCESSION NUMBER: 89184609 MEDLINE
DOCUMENT NUMBER: 89184609 PubMed ID: 2928332
TITLE: Lack of DNA homology in a pair of divergent chromosomes greatly sensitizes them to loss by DNA damage.
AUTHOR: Resnick M A; Skaanild M; Nilsson-Tillgren T
CORPORATE SOURCE: Yeast Genetics/Molecular Biology Group, National Institute of Environmental Health Sciences, Research Triangle Park, NC 27709.
SOURCE: PROCEEDINGS OF THE NATIONAL ACADEMY OF SCIENCES OF THE UNITED STATES OF AMERICA, (1989 Apr) 86 (7) 2276-80. Journal code: PV3; 7505876. ISSN: 0027-8424.
PUB. COUNTRY: United States
Journal; Article; (JOURNAL ARTICLE)
LANGUAGE: English
FILE SEGMENT: Priority Journals
ENTRY MONTH: 198905
ENTRY DATE: Entered STN: 19900306
Last Updated on STN: 19900306
Entered Medline: 19890505

AB Chromosomal DNA is considered a priori to be a target for the induction of numerical (whole chromosome) **aneuploidy** in mitotic **cells**. If true, DNA repair would be expected to contribute to genome stability.

One type of repair that appears to play an important role in the response of many organisms to DNA-damaging agents involves recombination. Using the yeast Saccharomyces cerevisiae containing a pair of DNA divergent (homoeologous) chromosomes, we have been able to determine the importance of recombinational repair of DNA damage in the maintenance of chromosome number. Specifically, the induction of aneuploidy by ionizing radiation has been examined in diploids that had one chromosome III replaced by a divergent chromosome from Saccharomyces carlsbergensis. The chromosomes are functionally equivalent but lack precise DNA homology over one-half their length. The absence of homology, and thus the opportunity for recombinational repair (presumably of DNA double-strand breaks) in the divergent chromosomes, results in high levels (5-10%) of aneuploidy for chromosome III at doses of radiation resulting in almost no **killing**. For homologous chromosomes, the frequency of loss is 20-50 times lower.

L19 ANSWER 12 OF 46 MEDLINE DUPLICATE 9
ACCESSION NUMBER: 97050924 MEDLINE
DOCUMENT NUMBER: 97050924 PubMed ID: 8895663
TITLE: Expression of Bcl-xL and loss of p53 can cooperate to overcome a cell cycle checkpoint induced by mitotic spindle damage.
AUTHOR: Minn A J; Boise L H; Thompson C B
CORPORATE SOURCE: Gwen Knapp Center for Lupus and Immunology Research, The University of Chicago, Illinois 60637, USA.
CONTRACT NUMBER: PO1 AI35294 (NIAID)
SOURCE: GENES AND DEVELOPMENT, (1996 Oct 15) 10 (20) 2621-31. Journal code: FN3; 8711660. ISSN: 0890-9369.
PUB. COUNTRY: United States
Journal; Article; (JOURNAL ARTICLE)
LANGUAGE: English
FILE SEGMENT: Priority Journals
ENTRY MONTH: 199701
ENTRY DATE: Entered STN: 19970128
Last Updated on STN: 19970128
Entered Medline: 19970102

AB During somatic cell division, faithful chromosomal segregation must follow DNA replication to prevent aneuploidy or polyploidy. Damage to the mitotic spindle is one potential mechanism that interferes with chromosomal segregation. The accumulation of **aneuploid** or polyploid **cells** resulting from a disrupted mitotic spindle is presumably prevented by cell cycle checkpoint controls. In the course of studying cells that overexpress the apoptosis-inhibiting protein Bcl-xL, we found that these cells have an increased rate of spontaneous tetraploidization, suggesting that apoptosis may play an important role in **eliminating** cells that fail to complete mitosis properly. When cells expressing Bcl-xL are treated with mitotic spindle inhibitors, a significant percentage reinitiate DNA replication and become polyploid. Nevertheless, the majority of cells expressing Bcl-xL undergo a prolonged p53-dependent cell cycle arrest following mitotic spindle damage. Unexpectedly, p53 expression is not induced in mitosis, nor does it influence M-phase arrest. Instead, cells with mitotic spindle damage only transiently arrest in M phase, and despite failing to complete mitosis, appear to proceed to G1. During this subsequent growth factor-dependent phase, p53 is induced and mediates cell cycle arrest. In cells that do not overexpress Bcl-xL, **elimination** of the p53-dependent growth arrest with a dominant negative mutant also results in polyploidy after mitotic spindle damage, but under these conditions most cells die by apoptosis. Expression of Bcl-xL and abrogation of p53 cooperate to allow rapid and progressive polyploidization following mitotic spindle damage. Our results suggest that suppression of apoptosis by bcl-2-related genes and loss of p53 function can act cooperatively to contribute to genetic instability.

L19 ANSWER 13 OF 46 MEDLINE DUPLICATE 10

L19 ANSWER 45 OF 46 MEDLINE DUPLICATE 27
ACCESSION NUMBER: 75207132 MEDLINE
DOCUMENT NUMBER: 75207132 PubMed ID: 807318
TITLE: Radiobiological studies of a high-energy modulated proton beam utilizing cultured mammalian cells.
AUTHOR: Robertson J B; Williams J R; Schmidt R A; Little J B; Flynn D F; Suit H D
SOURCE: CANCER, (1975 Jun) 35 (6) 1664-77.
Journal code: CLZ; 0374236. ISSN: 0008-543X.
PUB. COUNTRY: United States
Journal; Article; (JOURNAL ARTICLE)
LANGUAGE: English
FILE SEGMENT: Abridged Index Medicus Journals; Priority Journals
ENTRY MONTH: 197511
ENTRY DATE: Entered STN: 19900310
Last Updated on STN: 19900310
Entered Medline: 19751108

AB The modulated, 160-MeV proton beam produced by the Harvard Cyclotron has been examined in detail for its ability to **kill** mammalian cells as assayed by colony forming ability. Using two different cell exposure techniques, the characteristics of position and total dose in producing cell death in two **aneuploid cell** lines selected for their radiobiological relevance have been determined...

L19 ANSWER 46 OF 46 BIOSIS

L19 ANSWER 43 OF 46 CANCERLIT
ACCESSION NUMBER: 78706814 CANCERLIT
DOCUMENT NUMBER: 78706814
TITLE: CHROMOSOME ABERRATIONS INDUCED BY MONOMERIC ACRYLAMIDE IN BONE MARROW AND GERM CELLS OF MICE.
AUTHOR: Shiraishi Y
CORPORATE SOURCE: Dept. Anatomy, Kochi Medical Univ., Nangoku City, Kochi 781-51, Japan.
SOURCE: Mutat Res, (1978). Vol. 57, No. 3, pp. 313-324. ISSN: 0027-5107.
DOCUMENT TYPE: Journal; Article; (JOURNAL ARTICLE)
FILE SEGMENT: CARC
LANGUAGE: English
ENTRY MONTH: 197810

AB The chromosomes of the marrow, spermatogonia, and primary spermatocytes of male DDY mice were examined quantitatively after the mice were treated with acrylamide (AA) po (500 ppm of diet for 1, 2, or 3 wk) or ip (single dose of 100, 150, or 200 mg/kg). Samples were taken at various times after treatment. A comparatively high frequency of chromatid exchanges and breaks was induced in the spermatogonia of the 3-wk po mice only (19% vs 2.4% in controls). However, the frequency of chromosome aberrations was not increased appreciably in the marrow cells of any of the mice. The number of mitotic cells was reduced significantly in the spermatogonia of all treated mice, especially 12 and 24 hr after the ip injections. Thus, it was not possible to examine the acute cytogenetic effects of AA on spermatogonia. The frequency of **aneuploid** and polyploid **cells** increased with time after treatment in both the marrow and spermatogonia cells. AA induced a significant number of chain quadrivalents, ring quadrivalents, fragments, and univalents in the primary spermatocytes, especially in ip mice. There was no noticeable increase in the sister chromatid exchange frequency over control levels in the marrow and spermatogonia cells. AA also reduced the testis wt significantly, which suggests that there is a correlation between AA-induced chromosome aberrations and cell **killing**. The findings of a high frequency of rearrangements and univalents in the primary spermatocytes is significant, but it is not known whether these aberrations are transmitted to the next generation. (21 Refs)

L19 ANSWER 44 OF 46 CANCERLIT

L19 ANSWER 39 OF 46 CANCERLIT
ACCESSION NUMBER: 82606459 CANCERLIT
DOCUMENT NUMBER: 82606459
TITLE: ISOLATION AND PARTIAL CHARACTERIZATION OF MUTAGEN-SENSITIVE
AND DNA REPAIR MUTANTS OF CHINESE HAMSTER FIBROBLASTS.
AUTHOR: Schultz R A; Trosko J E; Chang C C
CORPORATE SOURCE: (c/o Trosko) Dept. Pediatrics and Human Development, Coll. Human Medicine, Michigan State Univ., East Lansing, MI, 48824.
SOURCE: Environ Mutagen, (1981). Vol. 3, No. 1, pp. 53-64.
DOCUMENT TYPE: Journal; Article; (JOURNAL ARTICLE)
FILE SEGMENT: ICDB
LANGUAGE: English
ENTRY MONTH: 198204

AB Isolation and partial characterization of several mutants of Chinese hamster cells, which are affected in their ability to repair DNA damage or
in their sensitivity to radiation or chemical mutations, are discussed. Cells of a subclone of the V79 **aneuploid cell** line were mutagenized by combined treatment with 5-bromodeoxyuridine and blacklight, followed by UV irradiation. 3H-thymidine was incorporated in repair-proficient cells at high temperature (38.5 C) following UV damage. Cells were held in the cold (4.0 C) to induce radioactive thymidine **killing**. Repair-deficient and UV-sensitive cells which had survived and formed colonies at low temperature (34.0 C) were tested for recovery. Seventy-two surviving colonies were isolated from 2 x 10(7) cells plated for selection. Four colonies were selected for extensive study. Colony UVs-7 was slightly more sensitive to UV, but not sensitive to x-rays or N-acetoxy-2-acetylaminofluorene (NAc-AAF); this mutant exhibited a highly reduced level of unscheduled DNA synthesis (UDS), as compared to the parental line. UVs-40 and UVs-44 line colonies were sensitive to UV, x-ray, N-methyl-N-nitro-N-nitrosoguanidine, and NAc-AAF, but exhibited normal UDS. Line UVr-23 had enhanced UDS, was resistant to UV, but exhibited no difference in sensitivity to x-ray or NAc-AAF. These four mutants are all stable, and may be useful for the study of mammalian DNA repair processes and mechanisms of mutagenesis. (38 Refs)

L19 ANSWER 40 OF 46 CANCERLIT

L8 ANSWER 8 OF 20 MEDLINE DUPLICATE 6
ACCESSION NUMBER: 2001246744 MEDLINE
DOCUMENT NUMBER: 21138433 PubMed ID: 11238996
TITLE: **Human securin**, hPTTG, is associated with Ku heterodimer, the regulatory subunit of the DNA-dependent protein kinase.
AUTHOR: Romero F; Multon M C; Ramos-Morales F; Dominguez A; Bernal J A; Pintor-Toro J A; Tortolero M.
CORPORATE SOURCE: Departamento de Microbiologia, Facultad de Biologia, Universidad de Sevilla, Apdo. 1095, 41080-Sevilla, Spain.. frport@cica.es
SOURCE: NUCLEIC ACIDS RESEARCH, (2001 Mar 15) 29 (6) 1300-7. Journal code: O8L; 0411011. ISSN: 1362-4962.
PUB. COUNTRY: England: United Kingdom
Journal; Article; (JOURNAL ARTICLE)
LANGUAGE: English
FILE SEGMENT: Priority Journals
ENTRY MONTH: 200105
ENTRY DATE: Entered STN: 20010517
Last Updated on STN: 20010521
Entered Medline: 20010510

AB We have previously isolated the hpttg proto-oncogene, which is expressed in normal tissues containing proliferating cells and in several kinds of tumors. In fact, expression of hPTTG correlates with cell proliferation in a cell cycle-dependent manner. Recently it was reported that PTTG is a vertebrate analog of the yeast **securins** Pds1 and Cut2, which are involved in sister chromatid separation. Here we show that hPTTG binds to Ku, the regulatory subunit of the DNA-dependent protein kinase (DNA-PK). hPTTG and Ku associate both in vitro and in vivo and the DNA-PK catalytic subunit phosphorylates hPTTG in vitro. Furthermore, DNA double-strand breaks prevent hPTTG-Ku association and disrupt the hPTTG-Ku complexes, indicating that genome damaging events, which result in the induction of pathways that activate DNA repair mechanisms and halt cell cycle progression, might inhibit hPTTG-Ku interaction in vivo. We propose that hPTTG might connect DNA damage-response pathways with sister chromatid separation, delaying the onset of mitosis while DNA repair occurs.

L8 ANSWER 9 OF 20 MEDLINE DUPLICATE 7
ACCESSION NUMBER: 2001205082 MEDLINE
DOCUMENT NUMBER: 21099256 PubMed ID: 11179223

L14 ANSWER 31 OF 32 MEDLINE DUPLICATE 23
ACCESSION NUMBER: 1999027589 MEDLINE
DOCUMENT NUMBER: 99027589 PubMed ID: 9811450
TITLE: **hpttg**, a **human** homologue of rat **pttg**, is overexpressed in hematopoietic neoplasms. Evidence for a transcriptional activation function of **hPTTG**.
AUTHOR: Dominguez A; Ramos-Morales F; Romero F; Rios R M; Dreyfus F; Tortolero M; Pintor-Toro J A
CORPORATE SOURCE: Departamento de Microbiologia, Facultad de Biologia, Universidad de Sevilla, Spain.
SOURCE: ONCOGENE, **(1998 Oct 29)** 17 (17) 2187-93.
Journal code: ONC; 8711562. ISSN: 0950-9232.
PUB. COUNTRY: ENGLAND: United Kingdom
Journal; Article; (JOURNAL ARTICLE)
LANGUAGE: English
FILE SEGMENT: Priority Journals
OTHER SOURCE: GENBANK-AJ223953
ENTRY MONTH: 199811
ENTRY DATE: Entered STN: 19990106
Last Updated on STN: 19990106
Entered Medline: 19981116

AB We have isolated a **human** cDNA clone encoding a novel protein of 22 kDa that is a **human** counterpart of the rat oncoprotein **PTTG**. We show that the corresponding gene (**hpttg**) is overexpressed in Jurkat cells (a **human** T lymphoma cell line) and in samples from patients with different kinds of hematopoietic malignancies. Analysis of the sequence showed that **hPTTG** has an amino-terminal basic domain and a carboxyl-terminal acidic domain, and that it is a proline-rich protein with several putative SH3-binding sites.

Subcellular fractionation studies show that, although **hPTTG** is mainly a cytosolic protein, it is partially localized in the nucleus. In addition we demonstrate that the acidic carboxyl-terminal region of **hPTTG** acts as a transactivation domain when fused to a heterologous DNA binding domain, both in yeast and in mammalian cells.

L14 ANSWER 32 OF 32 LIFESCI COPYRIGHT 2002 CSA

L14 ANSWER 30 OF 32 BIOSIS COPYRIGHT 2002 BIOLOGICAL ABSTRACTS INC.
ACCESSION NUMBER: 1999:297096 BIOSIS
DOCUMENT NUMBER: PREV199900297096
TITLE: New pituitary oncogenes.
AUTHOR(S): Melmed, Shlomo (1)
CORPORATE SOURCE: (1) Cedars-Sinai Research Institute, UCLA School of Medicine, Los Angeles, CA USA
SOURCE: Journal of Endocrinology, (**March**, **1999**) Vol. 160, No. SUPPL., pp. S22.
Meeting Info.: 18th Joint Meeting of the British Endocrine Societies Bournemouth, England, UK April 12-15, 1999 British Endocrine Societies
. ISSN: 0022-0795.
DOCUMENT TYPE: Conference
LANGUAGE: English

L14 ANSWER 31 OF 32 MEDLINE DUPLICATE 23
ACCESSION NUMBER: 1999027589 MEDLINE

L14 ANSWER 29 OF 32 MEDLINE DUPLICATE 22
ACCESSION NUMBER: 1999107039 MEDLINE
DOCUMENT NUMBER: 99107039 PubMed ID: 9892021
TITLE: Structure, expression, and function of **human pituitary** tumor-**transforming gene** (**PTTG**).
AUTHOR: Zhang X; Horwitz G A; Prezant T R; Valentini A; Nakashima M; Bronstein M D; Melmed S
CORPORATE SOURCE: Cedars-Sinai Research Institute-UCLA School of Medicine, Los Angeles, California 90048, USA.
CONTRACT NUMBER: DK-50238 (NIDDK)
DK-7682 (NIDDK)
SOURCE: MOLECULAR ENDOCRINOLOGY, **(1999 Jan)** 13 (1) 156-66.
Journal code: NGZ; 8801431. ISSN: 0888-8809.
PUB. COUNTRY: United States
Journal; Article; (JOURNAL ARTICLE)
LANGUAGE: English
FILE SEGMENT: Priority Journals
ENTRY MONTH: 199903
ENTRY DATE: Entered STN: 19990326
Last Updated on STN: 19990326
Entered Medline: 19990316

AB Despite advances in characterizing the pathophysiology and genetics of pituitary tumors, molecular mechanisms of their pathogenesis are poorly understood. Recently, we isolated a transforming gene [**pituitary** tumor-**transforming gene** (**PTTG**)] from rat pituitary tumor cells. Here we describe the cloning of **human PTTG**, which is located on chromosome 5q33 and shares striking sequence homology with its rat counterpart. Northern analysis revealed **PTTG** expression in normal adult testis, thymus, colon, small intestine, brain, lung, and fetal liver, but most abundant levels of **PTTG** mRNA were observed in several carcinoma cell lines. Stable transfection of NIH 3T3 cells with **human PTTG** cDNA caused anchorage-independent transformation in vitro and induced in vivo tumor formation when transfectants were injected into athymic mice. Overexpression of **PTTG** in transfected NIH 3T3 cells also stimulated expression and secretion of basic fibroblast growth factor, a **human** pituitary tumor growth-regulating factor. A proline-rich region, which contains two PXXP motifs for the SH3 domain-binding site, was detected in the **PTTG** protein sequence. When these proline residues were changed by site-directed mutagenesis, **PTTG** in vitro transforming and in vivo tumor-inducing activity, as well as stimulation of basic fibroblast growth factor, was abrogated. These results indicate that **human PTTG**, a novel oncogene, may function through SH3-mediated signal transduction pathways and activation of growth factor(s).

L14 ANSWER 30 OF 32 BIOSIS COPYRIGHT 2002 BIOLOGICAL ABSTRACTS INC.

L14 ANSWER 28 OF 32 BIOSIS COPYRIGHT 2002 BIOLOGICAL ABSTRACTS INC.
ACCESSION NUMBER: 1999:480337 BIOSIS
DOCUMENT NUMBER: PREV199900480337
TITLE: Expression of **hPTTG** oncoprotein in malignant lymphomas.
AUTHOR(S): Pereda, T. (1); Saez, C. (1); Luque, R. J. (1); Luna, R.; Tortolero, M.; Pintor-Toro, J. A.; Segura, D. I. (1); Japon, M. A. (1)
CORPORATE SOURCE: (1) Dept. of Pathology, H. U. Virgen del Rocio, Seville Spain
SOURCE: Virchows Archiv, (**Sept.**, **1999**) Vol. 435, No. 3, pp. 265.
Meeting Info.: 17TH European Congress of Pathology and the XIXth Spanish Congress of Pathology Barcelona, Spain September 18-23, 1999
ISSN: 0945-6317.
DOCUMENT TYPE: Conference
LANGUAGE: English

L14 ANSWER 29 OF 32 MEDLINE DUPLICATE 22
ACCESSION NUMBER: 1999107039 MEDLINE

L14 ANSWER 27 OF 32 BIOSIS COPYRIGHT 2002 BIOLOGICAL ABSTRACTS INC.

ACCESSION NUMBER: 1999:525162 BIOSIS

DOCUMENT NUMBER: PREV199900525162

TITLE: **Human PTTG**: A new proto-oncogene family.

AUTHOR(S): Prezant, T. R. (1); Merkel, P. (1); Kadioglu, P. (1); Heaney, A. P. (1); Horwitz, G. (1); Melmed, S. (1)

CORPORATE SOURCE: (1) Dept Med, Div Endocrinology, Cedars-Sinai Medical Ctr, Los Angeles, CA USA

SOURCE: American Journal of Human Genetics, (**Oct., 1999**) Vol. 65, No. 4, pp. A316.
Meeting Info.: 49th Annual Meeting of the American Society of Human Genetics San Francisco, California, USA October 19-23, 1999 The American Society of Human Genetics . ISSN: 0002-9297.

DOCUMENT TYPE: Conference

LANGUAGE: English

L14 ANSWER 26 OF 32 MEDLINE DUPLICATE 21
ACCESSION NUMBER: 2000047911 MEDLINE
DOCUMENT NUMBER: 20047911 PubMed ID: 10580151
TITLE: Molecular cloning, genomic organization, and identification of the promoter for the **human pituitary** tumor **transforming gene** (**PTTG**).
AUTHOR: Kakar S S
CORPORATE SOURCE: Department of Physiology, University of Alabama at Birmingham, Birmingham, AL, USA.. kakar@phybio.bhs.uab.edu
CONTRACT NUMBER: CA60871 (NCI)
CA82511 (NCI)
SOURCE: GENE, **(1999 Nov 29)** 240 (2) 317-24.
Journal code: FOP; 7706761. ISSN: 0378-1119.
PUB. COUNTRY: Netherlands
Journal; Article; (JOURNAL ARTICLE)
LANGUAGE: English
FILE SEGMENT: Priority Journals
OTHER SOURCE: GENBANK-AF167560; GENBANK-AF167561; GENBANK-AF167562; GENBANK-AF167563; GENBANK-AF167564
ENTRY MONTH: 200001
ENTRY DATE: Entered STN: 20000114
Last Updated on STN: 20000114
Entered Medline: 20000106

AB Recently, we cloned and sequenced cDNA of a potent **pituitary** tumor **transforming gene** (**PTTG**) from **human** testis and showed that this gene is expressed highly in various **human** tumors, including tumors of the pituitary and adrenal glands, and the liver, kidney, endometrium, uterus, and ovary. To determine the genomic organization of the **PTTG** and its transcriptional regulation in tumors, we isolated the gene. The **PTTG** spans more than 10kb and contains five exons and four introns. Primer extension and RNA protection assays indicated a transcription start site at an adenine residue at 37 bases upstream of the translation start site (ATG). Analysis of the 5' flanking region of the gene revealed the existence of three SP1/GC boxes, three AP1 and one AP2 binding sequences, a cyclic AMP response element sequence, and an insulin response element sequence. The promoter activity of the **PTTG** was evaluated by transfecting a **human** ovarian tumor cell line (SKOV3) and a mouse fibroblast cell line (NIH 3T3) with a chimeric fusion construct containing the 5' flanking sequence (nucleotide from -1336 to +34) and luciferase reporter gene (pluc 1370). The promoter activity of this construct was 210-fold higher in SKOV3 and 20-fold higher in NIH 3T3 cells than the promoterless vector. Deletion of sequences at the 5' end of the pluc 1370 construct from nucleotide -1336 to -1157 (pluc 1190), from nucleotide -1336 to -977 (pluc 1010) and from nucleotide -1336 to -707 (pluc 740) further increased luciferase activity. Further deletion of the 5' sequence from nucleotide -1336 to -407 (pluc 440), and from nucleotide -1336 to -127 (pluc 160) decreased activity by 95%. These results suggest that the sequence from nucleotide -126 to +34 is sufficient for **PTTG** promoter activity and that the sequence between nucleotide -706 and -407 contains an enhancer element. **PTTG** promoter activity was eight- to ten-fold higher in SKOV3 cells than NIH 3T3 cells, suggesting a basis for the tumor-specific expression of the **PTTG**

. Knowledge of the genomic organization and the promoter region of the **human** tumor transforming gene will allow further studies of possible disorders of the **PTTG** as well as facilitate elucidation of the transcriptional control of **PTTG** expression in **human** tumors.

L14 ANSWER 27 OF 32 BIOSIS COPYRIGHT 2002 BIOLOGICAL ABSTRACTS INC.

L14 ANSWER 24 OF 32 MEDLINE DUPLICATE 20
ACCESSION NUMBER: 1999340303 MEDLINE
DOCUMENT NUMBER: 99340303 PubMed ID: 10411507
TITLE: Identification of a vertebrate sister-chromatid separation inhibitor involved in transformation and tumorigenesis.
COMMENT: Comment in: Science. 1999 Jul 16;285(5426):344-5
AUTHOR: Zou H; McGarry T J; Bernal T; Kirschner M W
CORPORATE SOURCE: Department of Cell Biology, Harvard Medical School, 240 Longwood Avenue, Boston, MA 02115, USA.
CONTRACT NUMBER: GM26875 (NIGMS)
SOURCE: SCIENCE, **(1999 Jul 16)** 285 (5426) 418-22.
Journal code: UJ7; 0404511. ISSN: 0036-8075.
PUB. COUNTRY: United States
Journal; Article; (JOURNAL ARTICLE)
LANGUAGE: English
FILE SEGMENT: Priority Journals
OTHER SOURCE: GENBANK-AF220426
ENTRY MONTH: 199908
ENTRY DATE: Entered STN: 19990816
Last Updated on STN: 19990816
Entered Medline: 19990804

AB A vertebrate securin (**vSecurin**) was identified on the basis of its biochemical analogy to the Pds1p protein of budding yeast and the Cut2p protein of fission yeast. The **vSecurin** protein bound to a vertebrate homolog of yeast separins Esp1p and Cut1p and was degraded by proteolysis mediated by an anaphase-promoting complex in a manner dependent on a destruction motif. Furthermore, expression of a stable Xenopus securin mutant protein blocked sister-chromatid separation but did not block the embryonic cell cycle. The **vSecurin** proteins share extensive sequence similarity with each other but show no sequence similarity to either of their yeast counterparts. **Human** securin is identical to the product of the gene called **pituitary** tumor-**transforming gene** (**PTTG**), which is overexpressed in some tumors and exhibits transforming activity in NIH 3T3 cells. The oncogenic nature of increased expression of **vSecurin** may result from chromosome gain or loss, produced by errors in chromatid separation.

L14 ANSWER 25 OF 32 LIFESCI

L14 ANSWER 23 OF 32 MEDLINE DUPLICATE 19
ACCESSION NUMBER: 1999145048 MEDLINE
DOCUMENT NUMBER: 99145048 PubMed ID: 10022450
TITLE: Pituitary tumor transforming gene (PTTG) expression in pituitary adenomas.
AUTHOR: Zhang X; Horwitz G A; Heaney A P; Nakashima M; Prezant T R;
Bronstein M D; Melmed S
CORPORATE SOURCE: Cedars-Sinai Research Institute-University of California School of Medicine, Los Angeles 90048, USA.
CONTRACT NUMBER: DK 50238 (NIDDK)
DK 7682 (NIDDK)
SOURCE: JOURNAL OF CLINICAL ENDOCRINOLOGY AND METABOLISM, **(1999 Feb)** 84 (2) 761-7.
Journal code: HRB; 0375362. ISSN: 0021-972X.
PUB. COUNTRY: United States
Journal; Article; (JOURNAL ARTICLE)
LANGUAGE: English
FILE SEGMENT: Abridged Index Medicus Journals; Priority Journals
ENTRY MONTH: 199902
ENTRY DATE: Entered STN: 19990311
Last Updated on STN: 19990311
Entered Medline: 19990225

AB We recently cloned a novel **pituitary** tumor **transforming gene** (**PTTG**). Here we report **PTTG** expression in **human** pituitary adenomas and in normal pituitary tissue. In situ hybridization revealed **PTTG** expression in nonfunctioning and in GH-secreting adenomas but not in normal pituitary tissue. Using a more sensitive detection method, RT-PCR, low level **PTTG** expression was detected in normal pituitary. However, when expression levels in normal pituitary tissue were compared with those in 54 pituitary tumors using comparative reverse transcription polymerase chain reaction (RT-PCR), we found that most tumor samples expressed higher levels of **PTTG**. More than 50% **PTTG** increases were observed in 23 of 30 nonfunctioning pituitary tumors, all 13 GH-producing tumors, 9 of 10 prolactinomas, and 1 ACTH-secreting tumor, with more than 10-fold increases evident in some tumors. Furthermore, higher **PTTG** expression (P = 0.03) was observed in hormone-secreting tumors that had invaded the sphenoid bone (stages III and IV; 95% CI 3.118-9.715) compared with hormone-secreting tumors that were confined to the pituitary fossa (stages I and II; 95% CI 1.681-3.051). Therefore, **PTTG** abundance is a molecular marker for invasiveness in hormone-secreting pituitary tumors. The ubiquitous and prevalent expression of pituitary adenoma **PTTG** suggests that **PTTG** plays a role in pituitary tumorigenesis and invasiveness.

L14 ANSWER 24 OF 32 MEDLINE DUPLICATE 20

L14 ANSWER 22 OF 32 MEDLINE DUPLICATE 18
ACCESSION NUMBER: 1999293595 MEDLINE
DOCUMENT NUMBER: 99293595 PubMed ID: 10365261
TITLE: Cloning and expression of **human** cDNA encoding **human** homologue of **pituitary** tumor **transforming gene**.
AUTHOR: Lee I A; Seong C; Choe I S
CORPORATE SOURCE: Molecular and Cellular Biology Research Group, Korea Research Institute of Bioscience and Biotechnology, Taejon, Korea.
SOURCE: BIOCHEMISTRY AND MOLECULAR BIOLOGY INTERNATIONAL, **(1999 May)** 47 (5) 891-7.
Journal code: BOD; 9306673. ISSN: 1039-9712.
PUB. COUNTRY: ENGLAND: United Kingdom
Journal; Article; (JOURNAL ARTICLE)
LANGUAGE: English
FILE SEGMENT: Priority Journals
ENTRY MONTH: 199908
ENTRY DATE: Entered STN: 19990910
Last Updated on STN: 19990910
Entered Medline: 19990823

AB Recently, a potent transforming gene which was exclusively expressed in rat pituitary tumor but not in normal pituitary had been isolated and named as **pituitary** tumor **transforming gene** (**PTTG**). A cDNA clone encoding **human** homologue of rat **PTTG** was isolated from **human** fetal liver cDNA library. It contained an open reading frame of 603 base pairs predicting a protein composed of 201 amino acids with a calculated molecular weight of 26 kDa. The deduced protein showed about 85% homology (78% identity, 7% favored substitution) with the rat **PTTG**. Northern blot analysis showed that the cDNA hybridized to 1.0 kb mRNA species which was expressed in fetal liver and several cancer cell lines. These results suggest that the presence of the **human** homologue of rat **PTTG** gene may not be restricted to pituitary tumor.

L14 ANSWER 23 OF 32 MEDLINE DUPLICATE 19

L14 ANSWER 21 OF 32 MEDLINE DUPLICATE 17
ACCESSION NUMBER: 1999182101 MEDLINE
DOCUMENT NUMBER: 99182101 PubMed ID: 10084610
TITLE: An intronless homolog of human proto-oncogene **hPTTG** is expressed in pituitary tumors: evidence for **hPTTG** family.
AUTHOR: Prezant T R; Kadioglu P; Melmed S
CORPORATE SOURCE: Division of Endocrinology and Metabolism, Cedars-Sinai Research Institute, University of California, Los Angeles, USA.
CONTRACT NUMBER: CA75979 (NCI)
SOURCE: JOURNAL OF CLINICAL ENDOCRINOLOGY AND METABOLISM, **(1999 Mar)** 84 (3) 1149-52.
Journal code: HRB; 0375362. ISSN: 0021-972X.
PUB. COUNTRY: United States
Journal; Article; (JOURNAL ARTICLE)
LANGUAGE: English
FILE SEGMENT: Abridged Index Medicus Journals; Priority Journals
OTHER SOURCE: GENBANK-AF116538
ENTRY MONTH: 199904
ENTRY DATE: Entered STN: 19990426
Last Updated on STN: 19990426
Entered Medline: 19990413

AB A novel proto-oncogene, **PTTG** (**Pituitary** Tumor **Transforming Gene**), was isolated in our laboratory by virtue of its increased expression in rat pituitary tumor cell lines. Cells which overexpress **human** or rat **PTTG** form tumors in athymic mice. **hPTTG** is highly expressed in cancer cell lines, pituitary adenomas and in normal testis, suggesting that **hPTTG** protein has different tissue-specific interactions in normal cells and in cancer. Alternatively, different **hPTTG** gene family members may be functional in normal development and in tumorigenesis. While mapping the chromosomal location of **hPTTG** to 5q33, we discovered a second gene, hPTTG2, which is intronless and maps to chromosome 4p12. Using gene-specific oligonucleotide hybridization in a PCR-ELISA assay, we determined that hPTTG2 is expressed in both normal and tumorous pituitary. However, high levels of **hPTTG** mRNA in cancer cell lines are due to increased expression of hPTTG1. Thus, this family of proto-oncogenes appears to differentially participate in tumor-specific pathogenesis.

L14 ANSWER 22 OF 32 MEDLINE DUPLICATE 18
ACCESSION NUMBER: 1999293595 MEDLINE

L14 ANSWER 20 OF 32 MEDLINE DUPLICATE 16
ACCESSION NUMBER: 2000015198 MEDLINE
DOCUMENT NUMBER: 20015198 PubMed ID: 10546001
TITLE: Early involvement of estrogen-induced pituitary tumor transforming gene and fibroblast growth factor expression in prolactinoma pathogenesis.
AUTHOR: Heaney A P; Horwitz G A; Wang Z; Singson R; Melmed S
CORPORATE SOURCE: Department of Medicine, Cedars-Sinai Research Institute, UCLA School of Medicine, Los Angeles, California 90048, USA.
CONTRACT NUMBER: CA75979 (NCI)
SOURCE: NATURE MEDICINE, **(1999 Nov)** 5 (11) 1317-21.
Journal code: CG5; 9502015. ISSN: 1078-8956.
PUB. COUNTRY: United States
Journal; Article; (JOURNAL ARTICLE)
LANGUAGE: English
FILE SEGMENT: Priority Journals
ENTRY MONTH: 199911
ENTRY DATE: Entered STN: 20000111
Last Updated on STN: 20000111
Entered Medline: 19991119

AB Pituitary tumors are commonly encountered, and result from clonal expansion of a single mutated cell. Hypothalamic hormones, local growth factors and circulating sex steroid hormones promote pituitary tumor growth and expansion into large invasive tumors. Estrogen acting directly through its receptor and by stimulation of fibroblast growth factor regulates prolactin synthesis and secretion. Fibroblast growth factor-2 (bFGF) modulates angiogenesis, tumor formation and progression in many tissues, including the anterior pituitary. A **pituitary** tumor-derived **transforming gene** (**PTTG**) has been isolated, which is tumorigenic in vivo, regulates bFGF secretion, and inhibits chromatid separation. The **human PTTG** family consists of at least three homologous genes, of which PTTG1 is located on chromosome 5q33 and is expressed at low levels in most normal **human** tissues but is highly expressed in malignant **human** cell lines and in pituitary tumors. We report here that pituitary **pttg** is regulated in vivo and in vitro by estrogen. Maximal induction of rat pituitary **pttg** mRNA in vivo occurred early in pituitary transformation (normal cell to hypertrophic/hyperplastic cell), coincident with bFGF and vascular endothelial growth factor induction and pituitary angiogenesis. We also demonstrate that **pttg** expression is induced by bFGF, and show concordant **pttg** and bFGF expression in experimental and **human** pituitary adenomas. As bFGF and estrogen both induce **pttg**, and **pttg** expression coincides with the early lactotrophic hyperplastic response, angiogenesis and prolactinoma development, we propose a previously unknown paracrine growth factor-mediated mechanism for pituitary tumor pathogenesis and potentially other estrogen-regulated tumors.

L14 ANSWER 21 OF 32 MEDLINE DUPLICATE 17

L14 ANSWER 19 OF 32 MEDLINE DUPLICATE 15
ACCESSION NUMBER: 1999115663 MEDLINE
DOCUMENT NUMBER: 99115663 PubMed ID: 9915854
TITLE: **Pituitary** tumor-**transforming gene** protein associates with ribosomal protein S10 and a novel **human** homologue of DnaJ in testicular cells.
AUTHOR: Pei L
CORPORATE SOURCE: Division of Endocrinology, Cedars-Sinai Research Institute,
UCLA School of Medicine, Los Angeles, California 90048, USA.
CONTRACT NUMBER: DK-02346 (NIDDK)
SOURCE: JOURNAL OF BIOLOGICAL CHEMISTRY, **(1999 Jan 29)** 274 (5) 3151-8.
Journal code: HIV; 2985121R. ISSN: 0021-9258.
PUB. COUNTRY: United States
Journal; Article; (JOURNAL ARTICLE)
LANGUAGE: English
FILE SEGMENT: Priority Journals
OTHER SOURCE: GENBANK-AF080569
ENTRY MONTH: 199903
ENTRY DATE: Entered STN: 19990316
Last Updated on STN: 19990316
Entered Medline: 19990303

AB **Pituitary** tumor-**transforming gene** (**PTTG**) is a recently characterized proto-oncogene that is expressed specifically in adult testis. In this study, we have used in situ hybridization and developmental Northern blot assays to demonstrate that **PTTG** mRNA is expressed stage-specifically in spermatocytes and spermatids during rat spermatogenic cycle. We have used the yeast two-hybrid system to identify proteins that interact with **PTTG** in testicular cells. Two positive clones were characterized. One of the clones is the ribosomal protein S10, the other encodes a novel **human** DnaJ homologue designated HSJ2. Northern blot analysis showed that testis contains higher levels of HSJ2 mRNA than other tissues examined, and the expression pattern of HSJ2 mRNA in postnatal rat testis is similar to **PTTG**. S10 mRNA levels do not vary remarkably among different tissues and remains unchanged during testicular germ cell differentiation. In vitro binding assays demonstrated that both S10 and HSJ2 bind to **PTTG** specifically and that **PTTG** can be co-immunoprecipitated with S10 and HSJ2 from transfected cells. Moreover, the binding sites for both proteins were located within the C-terminal 75 amino acids of the **PTTG** protein. These results suggest that **PTTG** may play a role in spermatogenesis.

L14 ANSWER 20 OF 32 MEDLINE DUPLICATE 16

L14 ANSWER 18 OF 32 MEDLINE DUPLICATE 14
ACCESSION NUMBER: 1999429954 MEDLINE
DOCUMENT NUMBER: 99429954 PubMed ID: 10498901
TITLE: **hpttg** is over-expressed in pituitary adenomas and other primary epithelial neoplasias.
AUTHOR: Saez C; Japon M A; Ramos-Morales F; Romero F; Segura D I; Tortolero M; Pintor-Toro J A
CORPORATE SOURCE: Departamento de Anatomia Patologica, Hospital Universitario
Virgen del Rocio, 41013-Sevilla, Spain.
SOURCE: ONCOGENE, **(1999 Sep 23)** 18 (39) 5473-6.
Journal code: ONC; 8711562. ISSN: 0950-9232.
PUB. COUNTRY: ENGLAND: United Kingdom
Journal; Article; (JOURNAL ARTICLE)
LANGUAGE: English
FILE SEGMENT: Priority Journals
ENTRY MONTH: 199910
ENTRY DATE: Entered STN: 20000111
Last Updated on STN: 20000111
Entered Medline: 19991029

AB The role of oncogenes in pituitary tumorigenesis remains elusive since few genetic changes have been identified so far in pituitary tumors. **Pituitary** tumor-**transforming gene** (**pttg**) has been recently cloned from rat GH4 pituitary tumor cells. We have previously isolated and characterized **hpttg** from **human** thymus. In the present study, we analyse the expression of **hpttg** mRNA in a series of **human** pituitary adenomas. We show that **hpttg** is highly expressed in the majority of pituitary adenomas while only very low levels of mRNA can be detected in normal pituitary gland by Northern blot analysis. **hPTTG** protein was immunolocalized mainly in the cytoplasm of adenoma cells. Other common extra-cranial malignant tumors were also analysed by immunohistochemistry. Interestingly, strong **hPTTG** immunoreactivity was detected in most adenocarcinomas of mammary and pulmonary origins.

L14 ANSWER 19 OF 32 MEDLINE DUPLICATE 15
ACCESSION NUMBER: 1999115663 MEDLINE

L14 ANSWER 17 OF 32 MEDLINE DUPLICATE 13
ACCESSION NUMBER: 2000267846 MEDLINE
DOCUMENT NUMBER: 20267846 PubMed ID: 10806349
TITLE: Identification of the **human pituitary** tumor **transforming gene** (**hPTTG**) family: molecular structure, expression, and chromosomal localization.
AUTHOR: Chen L; Puri R; Lefkowitz E J; Kakar S S
CORPORATE SOURCE: Department of Physiology and Biophysics, University of Alabama at Birmingham, Birmingham, AL 35294, USA.
CONTRACT NUMBER: CA82511 (NCI)
SOURCE: GENE, **(2000 May 2)** 248 (1-2) 41-50.
Journal code: FOP; 7706761. ISSN: 0378-1119.
PUB. COUNTRY: Netherlands
Journal; Article; (JOURNAL ARTICLE)
LANGUAGE: English
FILE SEGMENT: Priority Journals
OTHER SOURCE: GENBANK-AF200719; GENBANK-AF200720
ENTRY MONTH: 200007
ENTRY DATE: Entered STN: 20000714
Last Updated on STN: 20000714
Entered Medline: 20000706

AB In an attempt to determine the mechanism of human tumorigenesis, we have searched for oncogenes and recently reported the molecular cloning of a potent oncogene (**hPTTG**) from human testis. **hPTTG** mRNA is expressed at high levels in various human tumors and tumor cell lines. Overexpression of **hPTTG** in the mouse fibroblast cell line (NIH 3T3) results in an increase in cell proliferation, induces cellular transformation in vitro, and promotes tumor formation in nude mice. The **hPTTG** gene isolated from the human genomic library consists of five exons and four introns and spans over 10kb. In the studies reported here, we further investigated the possibility of the presence of additional genes homologous to **hPTTG** in the human genome, which was first indicated by Southern blot analysis of the human genomic DNA and chromosomal mapping of the **hPTTG** gene using DNA from humanxhamster hybrid cell lines in PCR. Sequencing and restriction map analysis of the additional genomic clones identified two intronless genes homologous to **hPTTG**. This finding was confirmed by the chromosomal location of the second gene to chromosome 4p15.1 and the third gene to chromosome 8q13.1. Based on the similarity in sequences, we proposed that **hPTTG** be renamed hPTTG1 and the new genes be named hPTTG2 and hPTTG3. hPPTG2 was found to be 91% identical and hPPTG3 89% identical with hPPTG1 at the amino acid level. Northern blot and reverse transcriptase/polymerase chain reaction (RT/PCR) analyses of the mRNA from various human tissues revealed differential expression of the hPTTG2 and hPTTG3 genes in normal and tumor tissues, suggesting that these genes may be associated with tumorigenesis.

L14 ANSWER 18 OF 32 MEDLINE DUPLICATE 14

L14 ANSWER 15 OF 32 MEDLINE DUPLICATE 12
ACCESSION NUMBER: 2000120481 MEDLINE
DOCUMENT NUMBER: 20120481 PubMed ID: 10656688
TITLE: Cell cycle regulated expression and phosphorylation of **hpttg** proto-oncogene product.
AUTHOR: Ramos-Morales F; Dominguez A; Romero F; Luna R; Multon M C;
Pintor-Toro J A; Tortolero M
CORPORATE SOURCE: Departamento de Microbiologia, Facultad de Biologia, Universidad de Seville, Spain.
SOURCE: ONCOGENE, **(2000 Jan 20)** 19 (3) 403-9.
Journal code: ONC; 8711562. ISSN: 0950-9232.
PUB. COUNTRY: ENGLAND: United Kingdom
Journal; Article; (JOURNAL ARTICLE)
LANGUAGE: English
FILE SEGMENT: Priority Journals
ENTRY MONTH: 200002
ENTRY DATE: Entered STN: 20000218
Last Updated on STN: 20000218
Entered Medline: 20000210

AB We recently isolated a cDNA for **hpttg**, the **human** homolog of rat **pituitary** tumor **transforming gene**. Now we have analysed the expression of **hpttg** as a function of cell proliferation. **hPTTG** protein level is up-regulated in rapidly proliferating cells, is down-regulated in response to serum starvation or cell confluence, and is regulated in a cell cycle-dependent manner, peaking in mitosis. In addition, we show that **hPTTG** is phosphorylated during mitosis. Immunodepletion and in vitro phosphorylation experiments, together with the use of a specific inhibitor, indicate that Cdc2 is the kinase that phosphorylates **hPTTG**. These results suggest that **hpttg** is induced by, and may have a role in, regulatory pathways involved in the control of cell proliferation.

L14 ANSWER 16 OF 32 BIOSIS COPYRIGHT 2002 BIOLOGICAL ABSTRACTS INC.
ACCESSION NUMBER: 2000:252266 BIOSIS
DOCUMENT NUMBER: PREV200000252266

L14 ANSWER 14 OF 32 MEDLINE DUPLICATE 11
ACCESSION NUMBER: 2001074910 MEDLINE
DOCUMENT NUMBER: 20388582 PubMed ID: 10935539
TITLE: Pituitary tumor transforming gene (PTTG) regulates placental JEG-3 cell division and survival: evidence from live cell imaging.
AUTHOR: Yu R; Ren S G; Horwitz G A; Wang Z; Melmed S
CORPORATE SOURCE: Division of Endocrinology, Cedars-Sinai Research Institute-UCLA School of Medicine, Los Angeles, California 90048, USA.
CONTRACT NUMBER: CA-75979 (NCI)
SOURCE: MOLECULAR ENDOCRINOLOGY, **(2000 Aug)** 14 (8) 1137-46.
Journal code: NGZ. ISSN: 0888-8809.
PUB. COUNTRY: United States
Journal; Article; (JOURNAL ARTICLE)
LANGUAGE: English
FILE SEGMENT: Priority Journals
ENTRY MONTH: 200101
ENTRY DATE: Entered STN: 20010322
Last Updated on STN: 20010322
Entered Medline: 20010104

AB The **pituitary transforming gene, PTTG,** is abundantly expressed in endocrine neoplasms. **PTTG** has recently been recognized as a mammalian securin based on its biochemical homology to Pds1p. **PTTG** expression and intracellular localization were therefore studied during the cell cycle in **human** placental JEG-3 cells. **PTTG** mRNA and protein expressions were low at the G1/S border, gradually increased during S phase, and peaked at G2/M, but **PTTG** levels were attenuated as cells entered G1. In interphase cells, wild-type **PTTG**, an epitope-tagged **PTTG** , and a **PTTG**-EGFP conjugate all localized to both the nucleus and cytoplasm, but in mitotic cells, **PTTG** was not observed in the chromosome region. **PTTG**-EGFP colocalized with mitotic spindles in early mitosis and was degraded in anaphase. Intracellular fates of **PTTG**-EGFP and a conjugate of EGFP and a mutant inactivated **PTTG** devoid of an SH3-binding domain were observed by real-time visualization of the EGFP conjugates in live cells. The same cells were continuously observed as they progressed from G1/S border to S, G2/M, and G1. Most cells (67%) expressing **PTTG**-EGFP died by apoptosis, and few cells (4%) expressing **PTTG**-EGFP divided, whereas those expressing mutant **PTTG**-EGFP divided. **PTTG** -EGFP, as well as the mutant **PTTG**-EGFP, disappeared after cells divided. The results show that **PTTG** expression and localization are cell cycle-dependent and demonstrate that **PTTG** regulates endocrine tumor cell division and survival.

L14 ANSWER 15 OF 32 MEDLINE DUPLICATE 12

L14 ANSWER 11 OF 32 MEDLINE DUPLICATE 9
ACCESSION NUMBER: 2001082652 MEDLINE
DOCUMENT NUMBER: 20538375 PubMed ID: 11013229
TITLE: Pituitary tumor transforming gene causes aneuploidy and p53-dependent and p53-independent apoptosis.
AUTHOR: Yu R; Heaney A P; Lu W; Chen J; Melmed S
CORPORATE SOURCE: Cedars-Sinai Research Institute, UCLA School of Medicine, Los Angeles, California 90048, USA.
CONTRACT NUMBER: CA75979 (NCI)
SOURCE: JOURNAL OF BIOLOGICAL CHEMISTRY, **(2000 Nov 24)** 275 (47) 36502-5.
Journal code: HIV. ISSN: 0021-9258.
PUB. COUNTRY: United States
Journal; Article; (JOURNAL ARTICLE)
LANGUAGE: English
FILE SEGMENT: Priority Journals
ENTRY MONTH: 200101
ENTRY DATE: Entered STN: 20010322
Last Updated on STN: 20010322
Entered Medline: 20010108

AB The **pituitary** tumor **transforming gene, PTTG,** is abundantly expressed in several neoplasms. We recently showed that **PTTG** overexpression is associated with apoptosis and therefore have now studied the role of p53 in this process. In MCF-7 breast cancer cells that express wild type p53, **PTTG** overexpression caused apoptosis. p53 was translocated to the nuclei in cells expressing **PTTG**. Overexpression of p53, along with **PTTG,** augmented apoptosis, whereas expression of the **human** papillomavirus E6 protein inhibited **PTTG**-induced apoptosis. In MG-63 osteosarcoma cells that are deficient in p53, **PTTG** caused cell cycle arrest and subsequent apoptosis that was inhibited by caspase inhibitors. A proteasome inhibitor augmented **PTTG** expression in stable **PTTG** transfectants, suggesting that down-regulated **PTTG** expression is required for cell survival. Finally, MG-63 cells expressing **PTTG** showed signs of aneuploidy including the presence of micronuclei and multiple nuclei. These results indicate that **PTTG** overexpression causes p53-dependent and p53-independent apoptosis. In the absence of p53, **PTTG** causes aneuploidy. These results may provide a mechanism for **PTTG**-induced tumorigenesis whereby **PTTG** mediates aneuploidy and subsequent cell transformation.

L14 ANSWER 12 OF 32 MEDLINE DUPLICATE 10

L14 ANSWER 9 OF 32 MEDLINE DUPLICATE 8
ACCESSION NUMBER: 2001140933 MEDLINE
DOCUMENT NUMBER: 21097585 PubMed ID: 11163117
TITLE: Molecular cloning of pituitary tumor transforming gene 1 from ovarian tumors and its expression in tumors.
AUTHOR: Puri R; Tousson A; Chen L; Kakar S S
CORPORATE SOURCE: James Graham Brown Cancer Center, University of Louisville, KY 40202, USA.
CONTRACT NUMBER: CA82511 (NCI)
SOURCE: CANCER LETTERS, **(2001 Feb 10)** 163 (1) 131-9.
Journal code: CMX; 7600053. ISSN: 0304-3835.
PUB. COUNTRY: Ireland
Journal; Article; (JOURNAL ARTICLE)
LANGUAGE: English
FILE SEGMENT: Priority Journals
ENTRY MONTH: 200103
ENTRY DATE: Entered STN: 20010404
Last Updated on STN: 20010404
Entered Medline: 20010308

AB **Pituitary** tumor **transforming gene** 1 (PTTG1) recently cloned from **human** testis is a potent oncogene and is highly expressed in all the tumors analyzed to date. However, primary structure of PTTG1 and the cell types that express PTTG1 in tumors remained undescribed. We have used the reverse transcriptase-polymerase chain reaction technique to clone PTTG1 from ovarian tumors. Nucleotide sequencing of the PTTG1 cDNAs from various ovarian tumors showed identity with that of the **human** testis PTTG1. To determine the cell types that express PTTG1 in normal and tumor tissues, we performed in situ hybridization using digoxigenin-labeled cRNA as a probe. Our studies revealed a high level of expression of PTTG1 mRNA in both seminomatous and non-seminomatous testicular tumors; epithelial, sex-cord and stromal cell, and germ cell tumors of the ovary; and invasive ductal, ductal in situ and infiltrating ductal carcinoma of the breast. In normal tissues, expression of PTTG1 mRNA was very low or undetectable except in testis, where PTTG1 mRNA was found to be localized to spermatocytes and spermatids. Tumors that expressed high levels of PTTG1 mRNA also exhibited high levels of expression of basic fibroblast growth factor (bFGF), suggesting a correlation between PTTG1 and bFGF expression, and further suggesting that the PTTG1 protein may be involved in tumor angiogenesis and mitogenesis.

L14 ANSWER 10 OF 32 MEDLINE

L14 ANSWER 8 OF 32 MEDLINE DUPLICATE 7
ACCESSION NUMBER: 2002013858 MEDLINE
DOCUMENT NUMBER: 21307052 PubMed ID: 11414475
TITLE: Oncogene activation in pituitary tumors.
AUTHOR: Yu R; Melmed S
CORPORATE SOURCE: Cedars-Sinai Research Institute-UCLA School of Medicine, Los Angeles, CA 90048, USA.
CONTRACT NUMBER: CA75979 (NCI)
SOURCE: BRAIN PATHOLOGY, **(2001 Jul)** 11 (3) 328-41. Ref: 91
Journal code: 9216781. ISSN: 1015-6305.
PUB. COUNTRY: Switzerland
Journal; Article; (JOURNAL ARTICLE)
General Review; (REVIEW)
(REVIEW, ACADEMIC)
LANGUAGE: English
FILE SEGMENT: Priority Journals
ENTRY MONTH: 200112
ENTRY DATE: Entered STN: 20020121
Last Updated on STN: 20020121
Entered Medline: 20011204

AB Pituitary tumors constitute 10% of intracranial neoplasms and are mostly benign, monoclonal adenomas derived from single mutant cells. Pituitary oncogenes have been intensively studied and three of them, gsp, ccnd1, and **PTTG** are abundant in significant numbers of cases. gsp is present in approximately 40% of Caucasian patients with GH-secreting tumors and results from a mutated, constitutively active alpha subunit of Gs protein.

Persistent activation of the cAMP-PKA-CREB pathway may lead to uncontrolled cell proliferation and GH secretion. ccnd1 is overexpressed cyclin D1, and cyclin D1 gene is amplified in some pituitary tumors. **PTTG** is expressed in most pituitary tumors. **PTTG** is localized to both the nucleus and cytoplasm and interacts with several protein partners. At least three tumorigenesis mechanisms are proposed for **human PTTG**. 1) **PTTG** and FGF form a positive feedback loop and stimulate tumor vascularity. 2) **PTTG** transactivates c-myc or other pro-proliferation genes. 3) **PTTG** overexpression causes aneuploidy. **PTTG** expression activates p53 and causes p53-dependent and -independent apoptosis. Due to lack of functional **human** pituitary cell cultures and appropriate animal models for pituitary tumors, many of the results reviewed here are obtained from heterologous systems.

L24 ANSWER 2 OF 5 BIOSIS COPYRIGHT 2002 BIOLOGICAL ABSTRACTS INC.
ACCESSION NUMBER: 2001:270789 BIOSIS
DOCUMENT NUMBER: PREV200100270789
TITLE: **Aneuploidy** in spermatozoa after PEB **chemotherapy** used in testicular cancers.
AUTHOR(S): De Mas, P. (1); Daudin, M.; Vincent, M. C. (1); Calvas, P. (1); Bourrouillou, G. (1); Bujan, L.
CORPORATE SOURCE: (1) Service de Genetique Medicale, Hopital Purpan, Toulouse
France
SOURCE: Journal of Andrology, (May June, 2001) No. Supplement, pp. 169. print.
Meeting Info.: VIIth International Congress of Andrology Montreal, Canada June 15-19, 2001
ISSN: 0196-3635.
DOCUMENT TYPE: Conference
LANGUAGE: English
SUMMARY LANGUAGE: English

L24 ANSWER 3 OF 5 BIOSIS COPYRIGHT 2002 BIOLOGICAL ABSTRACTS INC.

L24 ANSWER 4 OF 5 BIOSIS COPYRIGHT 2002 BIOLOGICAL ABSTRACTS INC.
ACCESSION NUMBER: 1998:156067 BIOSIS
DOCUMENT NUMBER: PREV199800156067
TITLE: Evaluating **aneuploidy** induction by NOVP **chemotherapeutics** using sperm fluorescence in situ hybridization (FISH) in mice.
AUTHOR(S): Bishop, J. B. (1); Lowe, Xiu; Clark, J. A. (1); Myers, P. H. (1); Marchetti, F.; Sanders, C.; Wyrobek, A. J.
CORPORATE SOURCE: (1) NIEHS, RTP, NC USA
SOURCE: Environmental and Molecular Mutagenesis, (1998) Vol. 31, No. SUPPL. 29, pp. 59.
Meeting Info.: 29th Annual Meeting of the Environmental Mutagen Society Anaheim, California, USA March 21-26, 1998 Environmental Mutagen Society
. ISSN: 0893-6692.
DOCUMENT TYPE: Conference
LANGUAGE: English

L24 ANSWER 5 OF 5 CANCERLIT

L24 ANSWER 3 OF 5 BIOSIS COPYRIGHT 2002 BIOLOGICAL ABSTRACTS INC.
ACCESSION NUMBER: 2000:156568 BIOSIS
DOCUMENT NUMBER: PREV200000156568
TITLE: Mice are less susceptible than humans to induction of germ cell **aneuploidy** by NOVP cancer **chemotherapy** as measured by sperm-FISH.
AUTHOR(S): Bishop, J. B. (1); Clark, J. A. (1); Myers, P. H. (1); Lowe, X.; Marchetti, F.; Wyrobek, A. J.
CORPORATE SOURCE: (1) National Institute of Environmental Health Sciences, Research Triangle Park, NC USA
SOURCE: Environmental and Molecular Mutagenesis., (2000) Vol. 35, No. Suppl. 31, pp. 13.
Meeting Info.: Thirty-First Annual Meeting of the Environmental Mutagen Society. New Orleans, Louisiana, USA April 08-13, 2000 Environmental Mutagen Society
. ISSN: 0893-6692.
DOCUMENT TYPE: Conference
LANGUAGE: English
SUMMARY LANGUAGE: English

L19 ANSWER 41 OF 46 CANCERLIT
ACCESSION NUMBER: 80664792 CANCERLIT
DOCUMENT NUMBER: 80664792
TITLE: THE ROLE OF DNA DAMAGE AND REPAIR IN CELL KILLING INDUCED BY IONIZING RADIATION.
AUTHOR: Painter R B
CORPORATE SOURCE: Lab. Radiobiology, Univ. California, San Francisco, CA, 94143.
SOURCE: Non-serial, (1980). Radiation Biology in Cancer Research, Proceedings of the University of Texas System Cancer Center, M. D. Anderson Hospital and Tumor Institute 32nd Annual Symposium on Fundamental Cancer Research. Houston Texas., 665, pp., 1980. :.
DOCUMENT TYPE: Book; (MONOGRAPH)
FILE SEGMENT: ICDB
LANGUAGE: English
ENTRY MONTH: 198007

AB There is excellent evidence that DNA is the principal target for the **killing** of mammalian cells by ionizing radiation. Correlations between DNA repair systems in mammalian cells (an extremely complex process) and cell survival have not yet been established. Species differences in DNA repair mechanisms have been discovered. Chromosome aberrations are the chief cause of cell death in irradiated dividing cells. **Aneuploid cell** lines seem more capable of existing with additional **aneuploidy** than diploid **cell** lines. The ultimate DNA lesion that precedes a chromosome aberration is an unrepaired double-strand break (DSB). The frequency of unrepaired DSB in bacteriophage DNA increases with increasing linear energy transfer radiation. Unrepaired or nonrepairable DSB's are probably of the complex lesion type. DNA synthesis may play a role in the formation of unrepaired DSB's. Many cell types are most sensitive to x-rays at the G1/S border. If DNA replication enhances DSB formation and fixes DNA damage, the probability of cell **killing** should be inversely proportional to the fraction of S phase completed; this has been observed in several cell types. Agents that delay the onset of the S phase are radiosensitizing agents. Other DNA lesions are probably also involved in cell **killing**. A high fraction of radiation-induced base damage may be repaired at biological radiation doses (less than or equal to 1,000 rads), but saturation of the base-excision repair system may play an important role in radiation-induced interphase death. (43 Refs)

L19 ANSWER 14 OF 46 CANCERLIT
ACCESSION NUMBER: 96646899 CANCERLIT
DOCUMENT NUMBER: 96646899
TITLE: Detection of mitotic aneuploidy in interphase cells (Meeting abstract).
AUTHOR: Wilcox P; Presland K; Partheniou F; Wootton A; Stemp G; Tweats D
CORPORATE SOURCE: Glaxo Research and Development, Ware, Herts, UK.
SOURCE: Environ Mol Mutagen, (1995). Vol. 25, Suppl. 25, pp. 57. ISSN: 0893-6692.
DOCUMENT TYPE: (MEETING ABSTRACTS)
FILE SEGMENT: ICDB
LANGUAGE: English
ENTRY MONTH: 199607

AB The use of chromosome specific centromeric probes coupled with interphase scoring shows promise as a practical method for detecting chemically induced mitotic **aneuploidy** in cultured **cells**. We are evaluating this approach using a human lymphoblastoid cell line (558B), which has a normal, male karyotype, and fluorescent centromeric probes for chromosomes 13/21, 18 and X. The 13/21 probe is FITC labeled and is used with a propidium iodide counterstain. The 18 and X probes, which are used in combination, are labeled with CY3 and FITC, respectively, and are used with a DAPI counterstain. In order to provide an accurate estimate of spontaneous aneuploidy, assessments were made from an untreated culture, counting 500 or 1000 interphase cells/slide, for 4-5 slides. Results indicate that using the 13/21 probe approximately 15% of interphases appeared to be abnormal with respect to copy number of the labeled chromosomes, with a similar frequency of loss and gain. With the 18/X probes, approximately 9% of interphases were abnormal and the frequency of specific aneuploid events was loss of 18 (5.9%), gain of 18 (1.1%), gain of 2 18s (0.12), loss of X (0.48), gain of X (0.9%), gain of 2 18s and X [polyploidy?] (0.7%). Counts based on 1000 interphase cells appear to give an accurate estimate, as the frequency of the various aneuploid events did not change significantly on counting an additional 1, 2, 3 or 4 thousand cells. The high frequency of spontaneous aneuploidy observed could be the results of an unstable karyotype for this transformed cell line, or could be due to signal artefacts associated with this method. To further investigate these possibilities, experiments are in progress in which spontaneous aneuploidy is being assessed using these probes in a large number of demecolcine-arrested metaphase cells, located with the aid of an automatic metaphase finder. Analysis of metaphases should help to assess the frequency of 'rogue' signals which are not associated with chromatin material. In addition, the experiment is being repeated using long-term primary lymphocyte cultures (stimulated with IL2 and freeze **killed** B cells) to see whether primary cells show a higher degree of karyotype stability.

L19 ANSWER 15 OF 46 MEDLINE DUPLICATE 11
ACCESSION NUMBER: 93292578 MEDLINE

L19 ANSWER 8 OF 46 MEDLINE DUPLICATE 5
ACCESSION NUMBER: 1999186192 MEDLINE
DOCUMENT NUMBER: 99186192 PubMed ID: 10086273
TITLE: Cancer chemo-endocrine therapy and its cell biological basis.
AUTHOR: Nishiya I
CORPORATE SOURCE: Morioka Red Cross Hospital, Japan.
SOURCE: HUMAN CELL, (1998 Sep) 11 (3) 109-14. Ref: 0
Journal code: AY1; 8912329. ISSN: 0914-7470.
PUB. COUNTRY: Japan
Journal; Article; (JOURNAL ARTICLE)
General Review; (REVIEW)
(REVIEW, TUTORIAL)
LANGUAGE: Japanese
FILE SEGMENT: Priority Journals
ENTRY MONTH: 199905
ENTRY DATE: Entered STN: 19990607
Last Updated on STN: 20000303
Entered Medline: 19990525

AB The aim of our cell kinetic studies is to better understand the effects of chemo-endocrine therapy at the cell biological and molecular level. Cancer cell growth is characterized by uncontrolled proliferation, resulting in DNA distribution pattern in which, at any time, more cells are not G1 phase but in S, G2 and M phase of a shortened cycle. In a recent progress, flow cytometry (FCM) has become a powerful tool for the quantitative analysis of cell cycle parameters by measuring nuclear DNA content in large cell population with high speed. With the aid of FCM in earlier work about 60-80% of ovarian cancers were found to contain **aneuploid cells**. Now, multi-parameter FCM linked to a computer is available to measure fluorescent intensities not only no base total DNA (Propidium iodide) but also A-T (Hoechst 33342) and G-C (Mithramycin) base pairs in solid cancer nuclei. Since cisplatinum (CDDP) is the most important drug in the treatment of ovarian cancer, we have studied the relationship of CDDP cytotoxicity, pertubations cell cycle kinetis and DNA damage in ovarian adenocarcinoma cells in vitro & in vivo. We employed both CDDP sensitive cell line (KFt) and resistant cell line (KFr) derived from human serous cystoadenocarcinoma of the ovary by Kikuchi et al (JNCI 1986). Comparing cell kinetic pertubations of experimental cells demonstrates a decrease in G1 phase cells concomitant increase in S phase cells. The KFr cells had distinctly a shorter S-phase block up to 24 hrs not A-T but G-C preference in a quick response followed repairing of DNA damage to 48 hrs. However, some fractions of CDDP resistant cell population showed a later onset of G2, M phase accumulation. Comparison with the increase in early S phase cells of KFr in detailed analysis suggests only those damaged cells that are not **killed** immediately may proceed to G1 phase and start into DNA synthesis in S phase. Measurement of labeling index (L. I.) with Bromodeoxyuridine (BrdU) support our interpretation of differences between sensitivity and resistance to anti-cancer drug. Additionally, we discuss a targeting chemotherapy by coupling cytotoxic drugs with estrogen

based on increasing DNA damage into apoptosis and interfares with DNA repair process.

L19 ANSWER 9 OF 46 MEDLINE DUPLICATE 6

L19 ANSWER 5 OF 46 BIOSIS COPYRIGHT 2002 BIOLOGICAL ABSTRACTS INC.
ACCESSION NUMBER: 2000:184784 BIOSIS
DOCUMENT NUMBER: PREV200000184784
TITLE: Cell cycle analysis and pathological changes of malignant tumors treated with electrochemical therapy.
AUTHOR(S): Liu Jiyan (1); Wei Yuquan; Luo Feng; Lu Shichun; Peng Yulan; Lei Song; Zhao Xia; Yan Yonghua
CORPORATE SOURCE: (1) Center of Oncology, First Affiliated Hospital, WCUMS, Chengdu, 610041 China
SOURCE: Journal of West China University of Medical Sciences, (March, 2000) Vol. 31, No. 1, pp. 104-106. ISSN: 0257-7712.
DOCUMENT TYPE: Article
LANGUAGE: Chinese
SUMMARY LANGUAGE: Chinese; English
AB To investigate the mechanism and to observe the effectiveness of electrochemical therapy(ECT),33 patients of late stage cancers which treated by ECT were included in this study. Flow cytometry (FCM) and pathology were used to observe the changes of tumor cells before and after ECT. Tumor cells of G1, G2/M, S phases and **aneuploid cells** were found to be **killed** almostly and the ratio of apoptosis was elevated greatly after ECT. Also, pathological evidence proved the death of tumor cells and some characters of apoptosis. So, ECT can non-selectively **kill** tumor cells and induce the apoptosis of them, and FCM was a way to evaluate the effectiveness of ECT.

L19 ANSWER 6 OF 46 MEDLINE DUPLICATE 3

L19 ANSWER 28 OF 46 CANCERLIT
ACCESSION NUMBER: 88639628 CANCERLIT
DOCUMENT NUMBER: 88639628
TITLE: EVALUATION OF THE RESPONSE OF SOMATIC AND GERMINAL CELLS TO
INDUCTION OF CHROMOSOME ABERRATIONS AFTER SUBCHRONIC EXPOSURE TO BENZENE IN MALE MICE.
AUTHOR: Rithidech K
CORPORATE SOURCE: University of Texas Grad. Sch. of Biomed. Sci. at Galveston

SOURCE: Diss Abstr Int (Sci), (1987). Vol. 48, No. 3, pp. 644. ISSN: 0419-4217.
DOCUMENT TYPE: (THESIS)
FILE SEGMENT: ICDB
LANGUAGE: English
ENTRY MONTH: 198802

AB Benzene, a ubiquitous environmental contaminant, has been shown to induce cancer in multiple organs of rodents. Therefore, benzene may be capable of inducing genomic damage in multiple somatic cell types and perhaps even in germinal cells that are led to long-term consequences. The objective of this study was to investigate the somatic-cell and germinal-cell damages in male mice after being exposed subchronically to benzene. The somatic-cell damages were determined by chromosome aberrations in spleen lymphocytes and micronuclei in normochromatic erythrocytes. The germinal-cell damages were determined by chromosome aberrations in spermatogonia and in spermatocytes of treated spermatogonia. The urinary metabolite pattern was also investigated to correlate the presence of metabolites with the genotoxicity of benzene. Four groups of 10 mice were given a solution of benzene (in olive oil) daily by the oral route for 2 wk (with no treatment on days 5 and 10), and doses were 0 (olive oil only), 36.6, 73.2 and 146.4 mg/kg body wt, respectively. Urine samples were collected for metabolite analysis every 24 hr during the treatment period. Blood smears (from the tail vein of each animal) were done every third day during treatment for micronucleus analysis. Five mice in each group were **killed** after a 2-wk treatment for aberration analyses in spleen lymphocytes, in spermatogonia and in derived spermatocytes. The rest of the mice were **killed** at 60 days after the treatment for aberration analysis in derived spermatocytes of treated spermatogonia. Significant dose-dependent increases in the frequencies of chromatid breaks and abnormal cells in lymphocytes (p less than 0.001) and in spermatogonia (p less than 0.05) were observed. Micronucleus frequencies showed dose- and time-dependent increases (p less than 0.001). Stable chromosome aberrations (translocations) were detected in spermatocytes of treated spermatogonia (both differentiated and stem cells). The spindle-fiber disruptive activity of benzene was observed as evident by the presence of polyploid and **aneuploid cells** in lymphocytes and in derived spermatocytes, respectively. Major metabolites such as phenol, catechol, hydroquinone and muconic acid were observed. Among the most important information from this study is the detection of para-benzoquinone in the urine of treated mice. The amounts of unconjugated para-benzoquinone, unconjugated hydroquinone and unconjugated muconic acid were highly correlated with the frequency of micronuclei. (Full text available from University Microfilms International, Ann Arbor,

MI, as Order No: AAD87-12585)

Both probes hybridized to the transcripts of *Pp1α-96A* [2.3 kb (*26*)] and *rox8* [3 to 3.3 kb (*11*)] only, and no detectable differences in the expression of these genes between st-1 and j-1 were observed. It seems that inversion *2j* neither disrupted any transcriptional unit nor affected the expression of the closest genes, ruling out a relation between the mutational effect of the inversion and its adaptive value (*29*).

References and Notes

1. C. B. Krimbas and J. R. Powell, Eds., Drosophila *Inversion Polymorphism* (CRC Press, Boca Raton, FL, 1992).
2. J. R. Powell, *Progress and Prospects in Evolutionary Biology: The* Drosophila *Model* (Oxford Univ. Press, New York, 1997).
3. W. R. Engels and C. R. Preston, *Genetics* **107**, 657 (1984); S. Schneuwly, A. Kuroiwa, W. J. Gehring, *EMBO J.* **6**, 201 (1987); E. A. Montgomery, S.-M. Huang, C. H. Langley, B. H. Judd, *Genetics* **129**, 1085 (1991); J. K. Lim and M. J. Simmons, *Bioessays* **16**, 269 (1994); V. Ladeveze, S. Aulard, N. Chaminade, G. Periquet, F. Lemeunier, *Proc. R. Soc. London Ser. B* **265**, 1157 (1998).
4. T. W. Lyttle and D. S. Haymer, *Genetica* **86**, 113 (1992).
5. C. S. Wesley and W. F. Eanes, *Proc. Natl. Acad. Sci. U.S.A.* **91**, 3132 (1994); S. Cirera, J. M. Martin-Campos, C. Segarra, M. Aguadé, *Genetics* **139**, 321 (1995).
6. M. Wasserman, in (*1*), pp. 455–541; A. Ruiz and M. Wasserman, *Heredity* **70**, 582 (1993).
7. A. Fontdevila, A. Ruiz, G. Alonso, J. Ocaña, *Evolution* **35**, 148 (1981); A. Ruiz, H. Naveira, A. Fontdevila, *Genet. Iber.* **36**, 13 (1984); E. Hasson *et al.*, *J. Evol. Biol.* **8**, 369 (1995).
8. J. M. Ranz, C. Segarra, A. Ruiz, *Genetics* **145**, 281 (1997); J. M. Ranz, M. Cáceres, A. Ruiz, *Chromosoma* **108**, 32 (1999).
9. E. Sawruk, C. Udri, H. Betz, B. Schmitt, *FEBS Lett.* **273**, 177 (1990).
10. For the construction of genomic libraries, ~30 μg of high molecular weight genomic DNA were partially digested with Sau 3AI and electrophoresed on a 0.4% agarose gel. Fragments in the size range 15 to 23 kb were eluted from the gel, ligated with LambdaGEM-11 Bam HI arms, and packaged in vitro using Packagene extracts (Promega).
11. S. Brand and H.-M. Bourbon, *Nucleic Acids Res.* **21**, 3699 (1993).
12. I. Busseau, A. Pelisson, A. Bucheton, *Mol. Gen. Genet.* **218**, 222 (1989); N. Nassif and W. R. Engels, *Proc. Natl. Acad. Sci. U.S.A.* **90**, 1262 (1993).
13. D. J. Finnegan, *Trends Genet.* **5**, 103 (1989); P. Capy, C. Bazin, D. Higuet, T. Langin, *Dynamics and Evolution of Transposable Elements* (Springer-Verlag, Heidelberg, 1998).
14. The insertions at the *2j* inversion breakpoints do not show homology at the nucleotide level to any known sequence in the databases and thus appear to correspond to a previously undescribed TE. We have named this TE after the Italian astronomer, mathematician, and physicist Galileo Galilei (1564–1642).
15. A 5-kb probe of the λj3.1 proximal end that contains most of the *BD* insertion was in situ hybridized to the polytene chromosomes of seven *D. buzzatii* lines. The total number of euchromatic signals found per genome was 55 in st-1, 44 in st-3, 47 in st-4, 34 in j-1, 34 in j-8, 37 in j-11, and 28 in j-13 (*23*). On average, 11.8% of each line's signals were exclusive.
16. K. O'Hare and G. M. Rubin, *Cell* **34**, 25 (1983); R. D. Streck, J. E. MacGaffey, S. K. Beckendorf, *EMBO J.* **5**, 3615 (1986).
17. I. Marín and A. Fontdevila, *Mol. Gen. Genet.* **248**, 423 (1995).
18. G. S. Roeder and G. R. Fink, in *Mobile Genetic Elements*, J. Shapiro, Ed. (Academic Press, Orlando, FL, 1983), pp. 299–328; T. D. Petes and C. W. Hill, *Annu. Rev. Genet.* **22**, 147 (1988).
19. D. Lakich, H. H. Kazazian, S. E. Antonarakis, J. Gitschier, *Nature Genet.* **5**, 236 (1993); J. A. Naylor *et al.*, *Hum. Mol. Genet.* **4**, 1217 (1995); K. Small, J. Iber, S. T. Warren, *Nature Genet.* **16**, 96 (1997).
20. W. B. Eggleston, N. R. Rim, J. K. Lim, *Genetics* **144**, 647 (1996).
21. Y. Komoda, M. Enomoto, A. Tominaga, *ibid.* **129**, 639 (1991); M.-L. Daveran-Mingot, N. Campo, P. Ritzenthaler, P. le Bourgeois, *J. Bacteriol.* **180**, 4834 (1998).
22. K. D. Mathiopoulos, A. della Torre, V. Predazzi, V. Petrarca, M. Coluzzi, *Proc. Natl. Acad. Sci. U.S.A.* **95**, 12444 (1998).
23. The *D. buzzatii* lines used are homokaryotypic for four different chromosome arrangements: *2st*, *2j*, $2jz^3$, and $2jq^7$ ($2jz^3$ and $2jq^7$ derive from the *2j* arrangement and bear inversions $2z^3$ and $2q^7$, respectively). Their geographic origins cover a major part of the species distribution; lines that were sequenced are indicated in boldface. Spain: **st-1**, st-2, **j-1**, j-2, j-3, j-4, j-5, j-6, jz^3-1, jz^3-2, and jq^7-1 (Carboneras), j-7 and jq^7-3 (Caldetas), and jq^7-2 (Mogan, Canary Islands). Tunisia: jz^3-3 (Kariouan). Argentina: **st-3** (Vipos), **j-8** (San Luis), j-9 (Quilmes), j-10 (Palo Labrado), and jq^7-4 (Otamendi). Bolivia: **j-11** (Los Negros). Brazil: **st-4**, **j-12**, and j-13 (Guaritas, RS). Australia: **j-14**. All lines (except jq^7-3 and jq^7-4) were made isogenic by repeated sib-mating or by using the second chromosome balancer stock *Antp/Δ5* [J. S. F. Barker, *Genetica* **92**, 165 (1994)].
24. The PCR products were purified from 1% agarose gels, reamplified with one of the sequencing primers shown in Fig. 2, and sequenced in an ALFexpress DNA automated sequencer (Pharmacia Biotech). Both strands of each fragment were sequenced completely using primers separated by 323 to 466 nucleotides.
25. M. Nei, *Molecular Evolutionary Genetics* (Columbia Univ. Press, New York, 1987).
26. V. Dombrádi *et al.*, *Eur. J. Biochem.* **194**, 739 (1990).
27. Two sets of primers were used to amplify simultaneously a 271-bp 5′ fragment of the *Pp1α-96A* cDNA and 438 bp of the *Gapdh* cDNA (internal control) from the total cDNA. In both cases the primer sites were selected to span introns (of 61 bp and 69 bp, respectively). *Gapdh* primers were designed on the basis of the sequence of *D. hydei* [K. M. Wojtas, L. von Kalm, J. R. Weaver, D. T. Sullivan, *Genetics* **132**, 789 (1992)]. PCRs were performed with varying amounts of the reverse transcription reaction product as template and different concentrations of the two sets of primers.
28. The Northern blot hybridization was done with ~30 μg of total RNA from embryos, larvae, pupae, and adults of the st-1 and j-1 lines as described [A.-K. Rost, in *Quantitation of mRNA by Polymerase Chain Reaction: Nonradioactive PCR Methods*, Th. Köhler *et al.*, Eds. (Springer-Verlag, Berlin, 1995), pp. 93–114].
29. A. Ruiz *et al.*, *Genetics* **128**, 739 (1991); E. Betrán, M. Santos, A. Ruiz, *Evolution* **52**, 144 (1998).
30. W. R. Engels, D. M. Johnson-Schlitz, W. B. Eggleston, J. Sved, *Cell* **62**, 515 (1990); R. H. A. Plasterk, *EMBO J.* **10**, 1919 (1991); E. Takasu-Ishikawa, M. Yoshihara, Y. Hotta, *Mol. Gen. Genet.* **232**, 17 (1992).

31. Supported by a doctoral fellowship and a travel grant from the Comissionat per a Universitats i Recerca (Generalitat de Catalunya, Spain) (M.C.) and grant PB95-0607 from the Dirección General de Investigación Científica y Técnica (Ministerio de Educación y Cultura, Spain) (A.R.). We thank J. Zhang for his help in the RNA work; J. Barbé, O. Cabré, and A. Tapias for material and technical help; B. Schmitt for the *nAcRβ-96A* clone; J. S. F. Barker, E. Betrán, A. Fontdevila, and F. M. Sene for *D. buzzatii* stocks; and M. Aguadé, M. Ashburner, A. Berry, F. Brunet, B. Charlesworth, and R. de Frutos for valuable comments and helpful discussions.

4 February 1999; accepted 9 June 1999

Identification of a Vertebrate Sister-Chromatid Separation Inhibitor Involved in Transformation and Tumorigenesis

Hui Zou, Thomas J. McGarry, Teresita Bernal, Marc W. Kirschner*

A vertebrate securin (vSecurin) was identified on the basis of its biochemical analogy to the Pds1p protein of budding yeast and the Cut2p protein of fission yeast. The vSecurin protein bound to a vertebrate homolog of yeast separins Esp1p and Cut1p and was degraded by proteolysis mediated by an anaphase-promoting complex in a manner dependent on a destruction motif. Furthermore, expression of a stable *Xenopus* securin mutant protein blocked sister-chromatid separation but did not block the embryonic cell cycle. The vSecurin proteins share extensive sequence similarity with each other but show no sequence similarity to either of their yeast counterparts. Human securin is identical to the product of the gene called pituitary tumor-transforming gene (*PTTG*), which is overexpressed in some tumors and exhibits transforming activity in NIH 3T3 cells. The oncogenic nature of increased expression of vSecurin may result from chromosome gain or loss, produced by errors in chromatid separation.

The metaphase to anaphase transition is the final discrete event in duplication and separation of the genetic material of a cell. Its timing is regulated by the activation of the anaphase-promoting complex (APC), which mediates selective proteolysis of various mitotic regulators (*1*–*3*). Experiments with *Xenopus* egg extracts indicated that a putative protein factor might exist whose degradation was required for the onset of sister-chromatid separation (*4*). Proteins with such an activity

Department of Cell Biology, Harvard Medical School, 240 Longwood Avenue, Boston, MA 02115, USA.

*To whom correspondence should be addressed. E-mail: marc@hms.harvard.edu

were subsequently found in both budding yeast and fission yeast, encoded by the genes *PDS1* and *CUT2*, respectively (*5–7*). Both proteins are APC substrates and their degradation is required for chromatid separation (*8, 9*). Pds1p and Cut2p associate with the yeast separin proteins Esp1p and Cut1p, respectively (*10, 11*), and prevent the separins from promoting chromatid separation. Because of their similar cell cycle functions, Pds1p and Cut2p are also called anaphase inhibitors or securins (*12*).

The regulation of sister-chromatid separation in metazoans might be similar. Unfortunately, Pds1p and Cut2p show no sequence similarity to each other, and currently no sequence in the GenBank and EST databases shows any similarity to either of them. The COOH-terminus of a putative human separin homolog (hESP1), found by cDNA sequencing (*13*), has 28% identity with budding yeast Esp1p and 30% identity with fission yeast Cut1p (*11*). There is no similarity in the NH_2-terminus. We therefore attempted to identify the human securin homolog through its expected association with the putative human separin.

Antibodies to hESP1 were raised to a 269–amino acid fragment at the COOH-terminal region of hESP1 (*14*). After affinity purification, the antibodies were covalently coupled to protein A beads (*15*). Using these antibodies, we looked for proteins that coimmunoprecipitated with hESP1 proteins that were present in extracts of cells in metaphase but not in extracts of cells in anaphase, the expected properties of a human securin homolog. These extracts were prepared by release of human HeLa S3 cells from nocodazole-induced metaphase arrest (*16*). At various times, extracts were prepared and immunoprecipitated with anti-hESP1 (*17*). Immunoprecipitated proteins were separated by SDS–polyacrylamide gel electrophoresis (PAGE) and detected by silver staining. Among the many proteins that immunoprecipitated, two had apparent molecular sizes of 28 kD (EAP1, for hESP1-associated protein 1) and 42 kD (EAP2, for hESP1-associated protein 2). Both proteins were present in constant amounts in extracts prepared at various times up to 90 min after removing nocodazole. Neither protein was present in extracts prepared 4 hours after release from metaphase arrest (Fig. 1A). As a temporal control for progress through M phase, amounts of cyclin B1 were monitored by protein immunoblot analysis. Like EAP1 and EAP2, cyclin B1 was stable up to 90 min after release but was not detected at the 4-hour time point (Fig. 1A), indicating that the APC-mediated proteolysis pathway became active between 90 min and 4 hours after release. The coincidence between the loss of association of EAP1 and EAP2 with hESP1 and the activation of APC suggests that EAP1 and EAP2 could be candidates for a human securin-like molecule.

We had also isolated *Xenopus* APC substrates by small-pool expression cloning (*18, 19*). In this approach, small pools of cDNA clones from a *Xenopus* blastula library (*20*) were translated and labeled in vitro in rabbit reticulocyte lysates. Each pool was divided and incubated in mitotic extract or interphase extract. The cDNA clones corresponding to proteins that were proteolyzed in mitotic extract but not in interphase extract were isolated. We identified various cyclin Bs and geminin, an inhibitor of DNA replication degraded upon exit from mitosis (*19*). Two other proteins were identified in this screen: a 70-kD kinesin-like protein and a 25-kD protein (p25). The primary structure of *Xenopus* p25 shares extensive similarity with a human protein encoded by a gene called pituitary tumor-transforming gene (*PTTG*) (*21–23*). The open reading frame of *PTTG* from a human fetal thymus cDNA library was isolated and antibody to full-length PTTG protein was prepared (*14*). The following evidence suggested that EAP1 might be identical to PTTG. First, in vitro–translated PTTG protein migrated with the same mobility as EAP1 on SDS-PAGE (*24*). Second, PTTG also associated with hESP1. Endogenous PTTG coimmunoprecipitated with antibody to hESP1 in HeLa cell extract as detected by the antibody to PTTG (Fig. 1B). Endogenous hESP1 also coimmunoprecipitated with antibody to the Myc tag in extracts prepared from 293T cells transiently expressing Myc-tagged PTTG (Fig. 1C). Furthermore, hESP1 and PTTG from HeLa cell extracts cofractionated on both anionic exchange (*24*) and gel filtration columns (Fig. 1D). Thus, PTTG appears to be a vertebrate APC substrate that is associated with a vertebrate separin until activation of the APC. Therefore, we tentatively

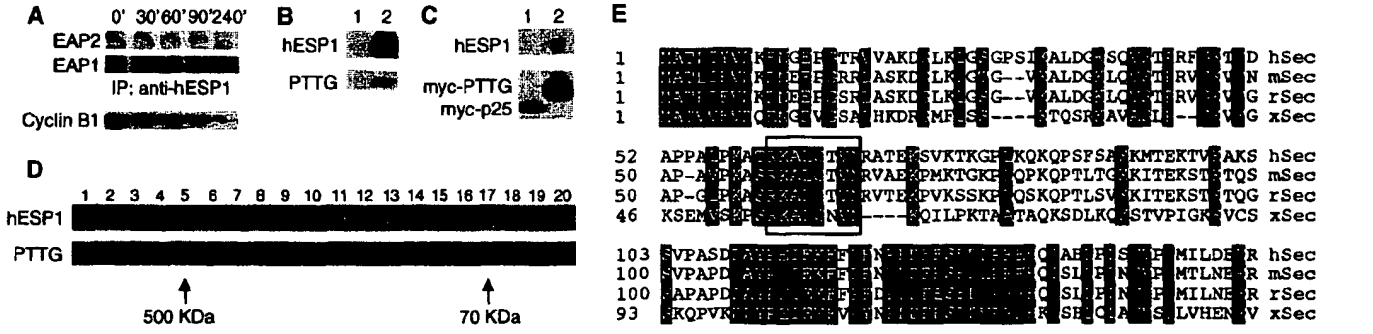

Fig. 1. Identification of an APC substrate associated with human EPS1. **(A)** Extracts were made from synchronized HeLa S3 cells. The time after release from nocodazole arrest is indicated in minutes. ESP1-associated proteins were coimmunoprecipitated with anti-hESP1. Beads were washed four times in lysis buffer and proteins were analyzed by SDS-PAGE. The amounts of cyclin B1 were determined by protein immunoblotting. **(B)** Immunoprecipitation with anti-hESP1 from extracts of HeLa S3 cells. As a control, preimmune antiserum (lane 1) was used in parallel with anti-hESP1 (lane 2). Both hESP1 and PTTG were detected by protein immunoblotting with respective antibodies. **(C)** Immunoprecipitations with antibody to the Myc tag (Santa Cruz) were performed in extracts prepared form 293T cells transfected with either Myc-tagged human PTTG (lane 2) or Myc-tagged *Xenopus* p25 (lane 1). Protein immunoblotting was performed to detect hESP1. We were unable to immunoprecipitate hESP1 with antibody to full-length PTTG, presumably because the binding sites on PTTG for ESP1 and the antibody overlap. **(D)** The fractions from a Superdex 200 column (*33*) were analyzed by protein immunoblotting to detect hESP1 and PTTG. Most of the PTTG cofractionated with hESP1 at an apparent molecular size of ~500 kD. Some PTTG was detected in fractions corresponding to ~70 kD, the same elution position of recombinant PTTG protein (*24*). **(E)** Sequence alignment of vertebrate securins (*25*). The hSecurin h(Sec) sequence obtained in this study (*14*) is identical to that of the human PTTG (*21*). The sequences of mouse securin (mSec) and rat securin (rSec) were obtained from GenBank (accession numbers AF069051 and U73030, respectively) (xSec, *Xenopus* securin). Amino acid sequence alignment was obtained with MegaAlign (DNAStar) by the clustal method. Residues that are identical or conserved among all four proteins are shaded in black. The conserved D-box is boxed.

named EAP1/PTTG as hSecurin and *Xenopus* p25 as xSecurin.

Among the vertebrate securins, sequence similarity was observed throughout the entire sequence (Fig. 1E). A conserved motif [RKALG(T or N)VN] (*25*) matches the destruction box (D-box) [RX(A or V or T)LGXXXN] shared by many APC substrates (*26*). The vertebrate securins share no sequence similarity with their yeast counterparts. In fact, the frog securin displays unusual diversity from its mammalian homologs (about 30% identity); most other cell cycle proteins are more than 80% identical in sequence. Nonetheless, there are conserved sequence features shared by all securins. All securins contain clusters of acidic and basic domains. The NH_2-terminal half of the proteins is rich in lysine residues surrounding the D-box. This is common for D-box–containing APC substrates, presumably because lysine is the residue that forms a covalent isopeptide linkage with ubiquitin.

To characterize the cell cycle function of vertebrate securins, we determined their abundance at various stages of the cell cycle. HeLa S3 cells were synchronized by release from a double-thymidine block, and extracts were prepared during the following 12 hours. Securin was detected by anti-hSecurin as two closely spaced bands. The amount of securin begins to accumulate at the onset of S phase and peaks at G_2-M phases in parallel with cyclin B1. As expected, its level drops precipitously when APC is activated, indicated by the decline of cyclin B1 (Fig. 2A).

Genetic studies in yeast and biochemical experiments in *Xenopus* egg extracts using yeast Pds1p and Cut2p suggested that Pds1p and Cut2p are ubiquitinated by the APC in a D-box–dependent manner (*8, 27*). To determine whether the putative D-box of the vertebrate securin is functional, we mutated the RKAL residues to AKAA (*25*) by site-directed mutagenesis. Mutated xSecurin (xSecurin^{dm}) was stable in mitotic extracts, confirming that the RKAL sequence is required for degradation (Fig. 2B). Similar observations were made with hSecurin (*24*). Furthermore, xSecurin was stabilized in the presence of an excess of an NH_2-terminal fragment of cyclin B1 that contains a D-box. However, the same cyclin B1 fragment lacking a D-box motif did not affect the degradation of xSecurin (Fig. 2C). Conversely, an excess of wild-type xSecurin, but not xSecurin^{dm}, inhibited the degradation of cyclin B1 (Fig. 2D). Taken together, these results demonstrate that the abundance of xSecurin is regulated by APC-mediated proteolysis in a D-box–dependent manner.

In yeast, the securins (Pds1p and Cut2p) function as inhibitors of chromatid separation. We therefore tested the effects of xSecurin^{dm} on sister-chromatid separation in *Xenopus* egg extracts (*4, 28*). In these experiments, we allowed extracts to go through one full cell cycle and observed chromatid separation at the following anaphase. Approximately 1 μl of purified xSecurin^{dm} protein (0.5 mg/ml) was added with *Xenopus* sperm nuclei and rhodamine tubulin to a 10-μl portion of a freshly prepared egg extract arrested at a metaphase-like stage (unfertilized egg extract). For comparison, equal amounts of bovine serum albumin were added to a separate sample of the same extract. The extracts were released into interphase by addition of calcium to allow DNA replication and then driven into mitosis by addition of unfertilized egg extract (2.5 μl) to allow the formation of the metaphase spindle. To prevent chromosome decondensation, which makes detection of the chromosomes difficult at late anaphase, we also added a nondegradable cyclin B1 lacking the NH_2-terminal 90 amino acids

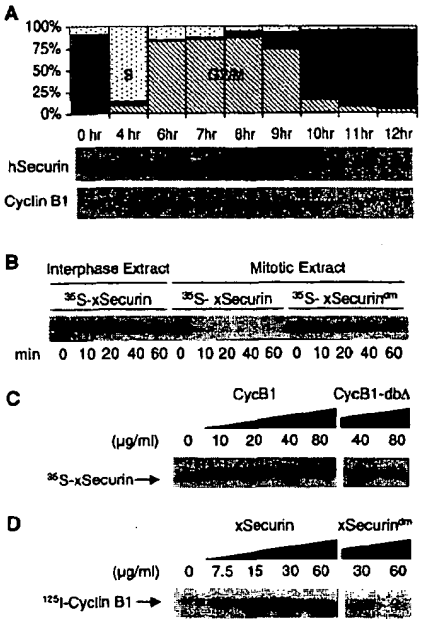

Fig. 2. Degradation of the vertebrate homolog of Pds1p by APC-mediated proteolysis. (**A**) HeLa S3 cells were synchronized at the G_1-S transition by a double-thymidine block. After release from arrest, extracts were prepared at various times up to 12 hours. The bottom two panels show the amounts of hSecurin and cyclin B1 analyzed by protein immunoblotting. The top graph indicates the percentage of cells in the G_1, S, and G_2-M phase of the cell cycle at the corresponding time points, as determined by FACS analysis. (**B**) Both xSecurin and xSecurin^{dm} protein were translated in vitro in the presence of [^{35}S]methionine. A portion of the translation mixture (2 μl) was added into interphase or mitotic extracts (7 μl) supplemented with bovine ubiquitin (10 μg). The reaction was incubated at room temperature for the time (minutes) indicated below the autoradiograph. (**C**) In vitro–translated xSecurin (1.5 μl) was added to mitotic extract (10 μl) supplemented with ubiquitin (10 μg) and incubated for 15 min. As competitors, a purified *Xenopus* cyclin B1 NH_2-terminal fragment (amino acids 1 to 102) and NH_2-terminal fragments lacking the D-box (CycB1-dbΔ) (*34*) were added to the reaction mixture. The final concentrations of competitors are indicated above the autoradiograph. (**D**) The same as in (**B**), except that *Xenopus* cyclin B1 NH_2-terminal fragments were labeled by iodination, and xSecurin or xSecurin^{dm} were used as competitors.

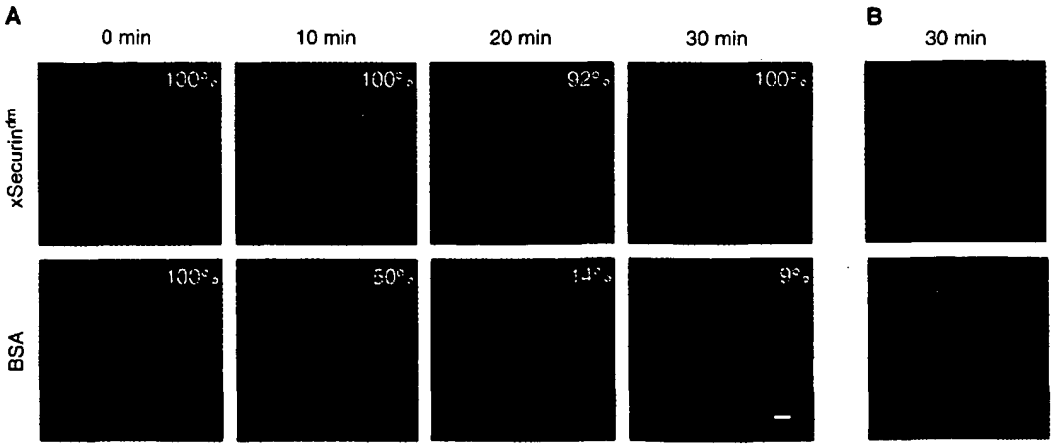

Fig. 3. Inhibition of chromatid separation by *Xenopus* securin. Anaphase was induced in extracts in the presence of (**A**) and in the absence of (**B**) nondegradable Δ90 cyclin B1. Photographs show the Hoechst 33342–stained chromosomes (blue) and rhodamine-labeled mitotic spindle (red) at various times after metaphase release. The percentage of spindles at metaphase for each time point (10 to 25 total spindles) is indicated. The white bar in the lower right panel of (**A**) represents 10 μm.

(Δ90 cyclin B1) (final concentration, 20 μg/ml). In this system, the cell cycle is arrested at metaphase and can be released into anaphase by addition of calcium. Anaphase movement of chromosomes can be monitored by the positions of the mitotic chromosomes, which were detected by DNA-specific fluorescent dye. We did not observe any differences in interphase nucleus formation, chromosome condensation, or nuclear envelope breakdown between extracts to which xSecurin^{dm} had been added and control extracts. Within 10 min of the second addition of calcium, chromosomes in control extracts had begun to move to the spindle poles (5 out of 10 spindles). No movement was seen in extracts containing xSecurin^{dm} even after 30 min, whereas at the same time in control extracts, 48% (11 out of 23) of the spindles were at late anaphase and 43% (10 out of 23) were at telophase (Fig. 3A).

In budding yeast, Pds1p has been suggested to be part of a checkpoint pathway that arrests the cell cycle at metaphase in the presence of DNA damage that occurs after G_1 (*7*). However, this function of Pds1p may reflect the unique properties of the budding yeast S-phase DNA damage checkpoint. Other eukaryotes, such as fission yeast and vertebrates, arrest the cell cycle at the G_2-M boundary in response to DNA damage occurring after G_1 by inhibiting the activation of the CDC2 cyclin-dependent kinase.

To test whether xSecurin inhibits any aspect of the anaphase progression other than chromatid separation, we performed the above assay with xSecurin^{dm} without the addition of Δ90 cyclin B1 and tested for inhibition of spindle disassembly, chromosome decondensation, and nuclear membrane reformation. No chromatid separation was observed in extracts containing xSecurin^{dm} up to 15 min after the second addition of calcium (eight spindles). Between 15 and 20 min after the second calcium addition, extracts had begun to decondense chromosomes and disassemble spindles. After 25 to 30 min, interphase nuclei were detected in both extracts (Fig. 3B). Protein immunoblot analysis with antibodies to xSecurin and cyclin B1 revealed that cyclin B1 is degraded in the presence of xSecurin^{dm} (*24*). These data demonstrate that xSecurin^{dm} does not interfere with assembly or disassembly of the spindle, with condensation or decondensation of chromosomes, or with breakdown or reformation of the nuclear envelope and thus appears not to interfere with the cycle of CDC2 cyclin-dependent kinase activation and inactivation. Instead, xSecurin specifically inhibits chromatid separation in *Xenopus* egg extracts. It remains possible that the checkpoint pathway is absent in frog embryos and that the vertebrate somatic cells have a checkpoint mechanism involving securins.

The vertebrate securin proteins have been implicated in transformation and tumorigenesis. Overexpression of securins led to the transformation of NIH 3T3 cells, and resulting transformants induced tumors when implanted into nude mice (*22–23*). In addition, expression of hSecurin is high in all carcinoma cell lines that have been tested, and in one case, the levels of hSecurin expression correlate with the malignancy of disease (*29*). The finding that a vertebrate securin has tumorigenic activity is somewhat anticipated because chromosome missegregation has been predicted to be a major source of genetic instability with profound consequences for cancer (*30*). On the basis of its function reported here, the simplest explanation is that tumor formation is the result of aneuploidy caused by defects in the sister-chromatid separation. In yeast, aneuploidy often occurs in mutants defective in sister-chromatid separation (*6, 31, 32*). Chromosome missegregation could lead to increases in the dosage of proto-oncogenes or loss of heterozygosity of tumor suppressors. Alternatively, the tumorigenic activity could result from an unknown function (*21*).

Our results indicate that, despite the low level of conservation among the securins, the basic process of chromatid separation is conserved in all eukaryotes. Identification of human securin as an oncogene suggests that misregulation of chromatid separation may contribute to the generation of malignant tumors.

References and Notes

1. S. Tugendreich, J. Tomkiel, W. Earnshaw, P. Hieter, *Cell* **81**, 261 (1995).
2. R. W. King *et al.*, *ibid.*, p. 279.
3. S. Irniger, S. Piatti, C. Michaelis, K. Nasmyth, *ibid.*, p. 269.
4. S. L. Holloway, M. Glotzer, R. W. King, A. W. Murray, *ibid.* **73**, 1393 (1993).
5. T. Hirano, S. Funahashi, T. Uemura, M. Yanagida, *EMBO J.* **5**, 2973 (1986).
6. A. Yamamoto, V. Guacci, D. Koshland, *J. Cell. Biol.* **133**, 85 (1996).
7. ———, *ibid.*, p. 99.
8. O. Cohen-Fix, J. M. Peters, M. W. Kirschner, D. Koshland, *Genes Dev.* **10**, 3081 (1996).
9. H. Funabiki *et al.*, *Nature* **381**, 438 (1996).
10. R. Ciosk *et al.*, *Cell* **93**, 1067 (1998).
11. H. Funabiki, K. Kumada, M. Yanagida, *EMBO J.* **15**, 6617 (1996).
12. A. Toth *et al.*, *Genes Dev.* **13**, 320 (1999).
13. T. Nagase, N. Seki, K. Ishikawa, A. Tanaka, N. Nomura, *DNA Res.* **3**, 17 (1996).
14. All human genes were cloned by polymerase chain reaction (PCR) from a human fetal thymus cDNA library (Clontech). A fragment of hESP1 cDNA was amplified with a pair of primers (5′-CGGAATTCAATGTCAGAGCCCTCTAAGACTCAG-3′ and 5′-CCCGCTCGAGGGTAGAAAGACCAGTGGCTAC-3′). This cDNA was cloned into the pET28b expression vector to create an NH_2-terminal $(His)_6$ fusion. A 269–amino acid recombinant protein was expressed in *Escherichia coli* according to the protocol provided by the manufacture (Novagen). Recombinant protein was purified up to 90% with Ni–nitrilotriacetic acid (NTA) beads (Qiagen). Full-length hSecurin (or PTTG) was isolated with primers 5′-ATGGCTACTCTGATCTATGTTGATAAGG-3′ and 5′-TTAAATATCTATGTCACAGCAAACAGGTG-3′. The PCR product was then cloned into a modified version of pCS2 for in vitro translation and transfection into mammalian cells. The same fragment was also cloned into a modified pET28a vector to express recombinant protein in *E. coli*. Protein more than 90% pure was obtained by affinity purification with Ni-NTA beads (Qiagen) followed by Resource Q column chromatography. Rabbit polyclonal antibodies to the 269–amino acid hESP1 fragment and full-length hSecurin (or PTTG) were made by Zymed with purified recombinant proteins as antigen. Crude sera were affinity-purified by passing them through affinity AffiGel-10 (Bio-Rad) columns coupled with corresponding antigens. Antibodies were eluted from the affinity-columns by 100 mM glycine (pH 2.5) followed by 100 mM triethylamine (pH 11.5). Affinity-purified antibody to hESP1 (anti-hESP1) cross-reacts with Myc tag. This antibody does not bind to in vitro–translated hSecurin (*24*). The anti-cyclin B1 used in this study was a rabbit antibody purchased from Santa Cruz Biotechnology.
15. E. Harlow and D. Lane, *Antibodies: A Laboratory Manual* (Cold Spring Harbor Laboratory Press, Cold Spring Harbor, NY, 1988).
16. Cells were arrested at metaphase with a thymidine-nocodazole block protocol and at the G_1-S transition with a double-thymidine block protocol (*34*). To determine the cell cycle distribution of each sample, we stained a small portion of the cells with propidium iodide and analyzed them by fluorescence-activated cell sorting (FACS). According to their DNA content, cells were classified as G_1 (N), S (between N and 2N), and G_2-M (2N), and the percentage for each stage of the cell cycle was calculated.
17. Harvested cells were washed with phosphate-buffered saline (PBS) and lysed in 10 volumes of lysis buffer [100 mM KCl, 0.1% NP-40, 20 mM tris (pH 8.0), 2 mM $MgCl_2$, 1 mM EDTA, 1 mM dithiothreitol, and 10% glycerol] supplemented with 1 μM microcystin and leupeptin, pepstatin, and chymostatin (each at 10 μg/ml). Dounce homogenization was used to maximize cell breakage. Cell debris was then removed by ultracentrifugation at 100,000*g* to make high-speed supernatant (S100). For immunoprecipitation, affinity-purified antibodies were covalently coupled onto protein A beads (*14*) at a concentration of about 1 mg/mL. The crude extracts were first incubated with beads coupled to preimmune rabbit immunoglobulin G. Then antibody beads were added into the extract and incubated at 4°C for 3 hours. Unless noted in the text, the beads were washed twice in 100 mM KCl and 0.5% NP-40 wash buffer in the presence of 20 mM tris (pH 8.0), 2 mM $MgCl_2$, 1 mM EDTA, 1 mM dithiothreitol, insulin (0.1 mg/ml), and 10% glycerol (same below); once in 300 mM KCl and 0.5% NP-40 wash buffer; and once in 500 mM KCl and 0.5% NP-40 wash buffer.
18. R. W. King, K. D. Lustig, P. T. Stukenberg, T. J. McGarry, M. W. Kirschner, *Science* **277**, 973 (1997).
19. T. J. McGarry and M. W. Kirschner, *Cell* **93**, 1043 (1998).
20. K. L. Kroll, A. N. Salic, L. M. Evans, M. W. Kirschner, *Development* **125**, 3247 (1998).
21. A. Dominguez *et al.*, *Oncogene* **17**, 2187 (1998).
22. L. Pei and S. Melmed, *Mol. Endocrinol.* **11**, 433 (1997).
23. X. Zhang *et al.*, *ibid.* **13**, 156 (1999).
24. H. Zou and W. M. Kirschner, unpublished observation.
25. Single-letter abbreviations for the amino acid residues are as follows: A, Ala; C, Cys; D, Asp; E, Glu; F, Phe; G, Gly; H, His; I, Ile; K, Lys; L, Leu; M, Met; N, Asn; P, Pro; Q, Gln; R, Arg; S, Ser; T, Thr; V, Val; W, Trp; and Y, Tyr.
26. R. W. King, M. Glotzer, M. W. Kirschner, *Mol. Biol. Cell* **7**, 1343 (1996).
27. H. Funabiki *et al.*, *EMBO J.* **16**, 5977 (1997).
28. C. E. Shamu and A. W. Murray, *J. Cell. Biol.* **117**, 921 (1992).
29. X. Zhang *et al.*, *J. Clin. Endocrinol. Metab.* **84**, 761 (1999).
30. C. Lengauer, K. W. Kinzler, B. Vogelstein, *Nature* **396**, 643 (1998).
31. J. T. McGrew, L. Goetsch, B. Byers, P. Baum, *Mol. Biol. Cell* **3**, 1443 (1992).
32. S. Uzawa, I. Samejima, T. Hirano, K. Tanaka, M. Yanagida, *Cell* **62**, 913 (1990).
33. Extract prepared from nocodazole-arrested HeLa S3 cells was fractionated on a Resource Q column with

a KCl concentration gradient from 100 mM to 1 M in the lysis buffer. Human ESP1 was eluted at about 250 mM KCl. Fractions containing hESP1 were pooled and loaded onto a Superdex 200 column.

34. G. Fang, H. Yu, M. W. Kirschner, *Mol. Cell* 2, 163 (1998).

35. We thank C. Pfleger and S. Rankin for comments on the manuscript; G. Fang, H. Yu, and other members of the Kirschner laboratory for helpful discussion and technical assistance; C. Pfleger and E. Lee for providing modified pCS2 and pET28a vectors; and Q. Zang for mammalian cell transfection. H.Z. is a fellow of The Jane Coffin Childs Memorial Fund for Medical Research. T.J.M. was supported by a Physician Postdoctoral Grant from the Howard Hughes Medical Institute and a Mentored Clinical Scientist Development Award from the National Heart, Lung, and Blood Institute. Supported by grants GM39023 and GM26875 from NIH awarded to M.W.K.

31 March 1999; accepted 18 May 1999

Different Trajectories of Parallel Evolution During Viral Adaptation

H. A. Wichman,[1]* M. R. Badgett,[2] L. A. Scott,[1] C. M. Boulianne,[1] J. J. Bull[2,3]

The molecular basis of adaptation is a major focus of evolutionary biology, yet the dynamic process of adaptation has been explored only piecemeal. Experimental evolution of two bacteriophage lines under strong selection led to over a dozen nucleotide changes genomewide in each replicate. At least 96 percent of the amino acid substitutions appeared to be adaptive, and half the changes in one line also occurred in the other. However, the order of these changes differed between replicates, and parallel substitutions did not reflect the changes with the largest beneficial effects or indicate a common trajectory of adaptation.

The wealth of molecular data now available reveals that genetic variation is virtually ubiquitous not only between species but also within species. Yet the extent to which this variation is adaptive is enigmatic. This question has taken on new importance as molecular data find increasing use to deduce the mechanism of drug resistance, monitor pathogen populations for incidence of resistance, and compare molecular responses to different drugs and treatment regimes. DNA sequence comparisons are commonly used to address this question, because they carry legacies of their histories that may reflect adaptive change. For example, historical occurrences of adaptive evolution can sometimes be recognized by the high rate of nonsynonymous to synonymous substitution in coding regions, which is a statistical landmark adaptive change (*1*–*4*). However, for two reasons, this statistical approach may be less useful for looking at contemporary adaptation of pests and pathogens. First, adaptive responses to strong selection may require too few changes at the molecular level to leave such "statistical tracks." Second, these methods reveal the occurrence but not the identity of adaptive changes. Parallel evolution—the same change having evolved repeatedly and independently—is also regarded as evidence of adaptation and can reveal the identity of at least some adaptive amino acid substitutions (*5*–*8*). In fact, parallel evolution is a standard criterion used to identify the amino acid substitutions responsible for drug resistance. Although some believe that organisms have too many degrees of freedom to allow this type of predictability, it is not out of the question that the short-term course of adaptation in response to specific selective agents can be predicted, and the short-term course is the one most relevant to human health and infectious disease. It is thus important to determine the extent to which parallel evolution allows us to predict the mechanisms and dynamics of evolution. Here we assess the genomewide dynamics of evolution to examine the molecular basis for and process of adaptation in a viral population under strong selection.

The single-stranded DNA bacteriophage ϕX174 was adapted to high temperature and a novel host (*Salmonella typhimurium*) in a two-stage chemostat for about 1000 population doublings over 10 days. Methods were as described (*9*) except that the temperature was 43.5°C throughout the 10 days of selection.

To guard against contamination, which could be misinterpreted as parallel evolution, we grew replicate lineages in our geographically separated laboratories; we refer to them as the TX and ID replicates. The chemostats were sampled every 24 hours, and isolates from these daily samples were archived into microtiter plates for later analysis. Population sizes in the chemostats were typically in excess of 10^7 except during the first few days of the TX chemostat, when population sizes were closer to 10^4. Our goal was to observe the process of adaptation in a very strong selective environment rather than to dissect responses to specific conditions in the environment. These conditions—large population size and strong selection—are highly favorable to adaptation.

In previous experiments (*9*), we found that adaptation to these conditions resulted in over a dozen substitutions genomewide, with 25 to 50% of them occurring in parallel between any two replicates. On the basis of this parallel evolution alone, we concluded that substitutions were adaptive at more than one-third of the sites where differences were detected. However, the underlying dynamics of evolution and the extent of genetic differentiation within populations was unknown. At one extreme, substitutions might quickly sweep through the population to fixation, so that most genotypes in the population are very similar at any point in time; at the other extreme, there could be multiple competing genotypes present throughout the history of the population. Furthermore, it is not known to what extent high levels of parallel evolution are a signature of similarity of adaptation at the phenotypic level.

Adaptation to chemostat conditions was evident by massive improvements in phage growth rates at the high temperature (Fig. 1). Phage population growth rates were measured as doublings of phage concentration per hour at 43°C under defined conditions (*9*); this assay measures a major component of fitness in the chemostat but does not measure all relevant fitness components. The population growth rate of the ID replicate increased from −5 to 7.1 over the course of the 10 days of selection, with no gain detectable after day 4. This corresponds to a 4000-fold improvement in the number of descendants per hour. The population growth rate of the TX replicate increased from −5 to 12.5 (about 18,000-fold) over the course of the 10 days of selection, with major improvements at several time points. A difference in correlated response to selection was also detected: ID lost its ability to plate on *Escherichia coli* C, whereas TX retained this ability. From this fitness evidence alone, it is obvious that both replicates accumulated changes but that they followed at least somewhat different pathways.

The genetic basis of adaptation was studied at both a nucleotide level and a population level over time. To identify substitutions at high frequency at the end of selection, we obtained complete genome sequences from polymerase chain reaction products amplified

[1]Department of Biological Sciences, University of Idaho, Moscow, ID 83844, USA. [2]Department of Zoology and [3]Institute of Cellular and Molecular Biology, University of Texas, Austin, TX 78712, USA.

*To whom correspondence should be addressed. E-mail: hwichman@uidaho.edu

30. G. Herrmann, T. Lindahl, P. Schar, *EMBO J.* **17**, 4188 (1998).
31. W. Ramos, G. Liu, C. N. Giroux, A. E. Tomkinson, *Nucleic Acids Res.* **26**, 5676 (1998).
32. S. Marcand, E. Gilson, D. Shore, *Science* **275**, 986 (1997).
33. A. Ray and K. W. Runge, *Proc. Natl. Acad. Sci. U.S.A.* **96**, 15044 (1999).
34. D. J. Burke, *Curr. Opin. Genet. Dev.* **10**, 26 (2000).
35. J. K. Tyler *et al.*, *Nature* **402**, 555 (1999).
36. S. Enomoto, P. D. McCune-Zierath, M. Gerami-Nejad, M. A. Sanders, J. Berman, *Genes Dev.* **11**, 358 (1997).
37. P. D. Kaufman, R. Kobayashi, B. Stillman, *Genes Dev.* **11**, 345 (1997).
38. E. K. Monson, D. de Bruin, V. A. Zakian, *Proc. Natl. Acad. Sci. U.S.A.* **94**, 13081 (1997).
39. S. Le, C. Davis, J. B. Konopka, R. Sternglanz, *Yeast* **13**, 1029 (1997).
40. A. Verreault, P. D. Kaufman, R. Kobayashi, B. Stillman, *Cell* **87**, 95 (1996).
41. A. Taddei, D. Roche, J. B. Sibarita, B. M. Turner, G. Almouzni, *J. Cell Biol.* **147**, 1153 (1999).
42. J. G. Moggs *et al.*, *Mol. Cell. Biol.* **20**, 1206 (2000); Z. Kelman and J. Hurwitz, *Trends Biochem. Sci.* **23**, 236 (1998).
43. K. W. Runge, R. J. Wellinger, V. A. Zakian, *Mol. Cell. Biol.* **11**, 2919 (1991).

REVIEW

Splitting the Chromosome: Cutting the Ties That Bind Sister Chromatids

Kim Nasmyth,* Jan-Michael Peters, Frank Uhlmann

In eukaryotic cells, sister DNA molecules remain physically connected from their production at S phase until their separation during anaphase. This cohesion is essential for the separation of sister chromatids to opposite poles of the cell at mitosis. It also permits chromosome segregation to take place long after duplication has been completed. Recent work has identified a multisubunit complex called cohesin that is essential for connecting sisters. Proteolytic cleavage of one of cohesin's subunits may trigger sister separation at the onset of anaphase.

Back to Basics: Chromosome Mechanics

Instructions for the behavior of every cell in the bodies of worms, flies, and humans will soon reside in public databases for all to read. A complete set of such instructions, packaged as chromosomes, is inherited by most cells in our body. Because of this, many if not most somatic nuclei in mammals are totipotent; that is, they are capable of programming all of mammalian development when injected into enucleated eggs (*1*). The cloning of Dolly had dramatic practical consequences, but its feasibility was never improbable on theoretical grounds. How cells inherit two complete packages of the genome at each cell division is one of the most fundamental questions in biology (Fig. 1A).

Recent studies of the chromosome cycle have concentrated on control mechanisms, such as the crucial part played by cyclin-dependent protein kinases in triggering chromosome duplication and segregation (*2*) and surveillance mechanisms (checkpoints) that monitor the fidelity of these two processes (*3*). This focus on "control" is, however, a recent phenomenon. Earlier studies, largely cytological in nature, concentrated on the mechanics of chromosome segregation (*4*–*7*). What, for example, was "the nature of the initial act of doubling of the spireme thread (chromosome)" (*5*, p. 109), and how were the sister threads moved to opposite poles of the cell during mitosis?

The elucidation of DNA's structure largely answered the first of these questions (*8*), and work on cytoskeletal proteins like tubulin and the spindle fibers assembled from it has gone a long way toward solving the mystery of chromosome movement. In contrast, until recently the mechanisms by which sister chromatids are tied together after chromosome duplication and then separated at the metaphase-to-anaphase transition was largely neglected, despite being equally crucial for the mitotic process (*9*).

Importance of Sister Cohesion

The ability of eukaryotic cells to delay segregation of chromosomes until long after their duplication distinguishes their cell cycle from that of bacteria, in which chromosome segregation starts soon after the initiation of DNA replication (*10*). This temporal separation forms the basis for the cell cycle's partition into four phases—G_1, S, G_2, and M—and it has played a central role in the evolution of eukaryotic organisms. Meiosis, during which two rounds of chromosome segregation follow a single round of duplication, requires separable S and M phases. Furthermore, mitotic chromosome condensation, without which large genomes cannot be partitioned between daughter cells at cell division, would not be possible if chromosome segregation coincided with DNA replication. A gap between S and M phases therefore made possible the evolution of large genomes. It is sister chromatid cohesion that permits chromosome segregation to take place long after duplication. Cohesion provides a memory of a duplication process that may have occurred long ago (up to 50 years in the case of human oocytes)—a memory that defines which chromatids within a nucleus are to be parted from each other at cell division. Were chromatids to drift apart before building a mitotic spindle, there would be no way for cells to determine whether chromatids were sisters (to be segregated to opposite poles) as opposed to being merely homologous chromosomes, a distinction that is crucial for all diploid organisms.

The structures holding sister chromatids together are responsible for generating bilaterally symmetrical chromosomes during mitotic divisions. The bilateral symmetry of chromosomes underlies the symmetry of the spindle apparatus and hence forms the basis for the exact and symmetrical partition of chromosomes and the roughly equal partition of most other cell constituents at cell division. In addition, tying sister chromatids together generates a centromere geometry that favors the attachment of sister kinetochores to spindles that extend to opposite poles. Only those kinetochore-spindle connections that result in tension are stabilized, which enables the chromosome alignment process to be proofread (*11*). Despite its importance, the mechanism by which sister chromatids are tied together is still poorly understood.

Chromatid Separation Independent of the Spindle Apparatus

The chromatid separation process has also remained mysterious. It is an autonomous process that does not directly depend on the mitotic spindle (*5*, *7*). This is most vividly seen in cells whose spindles have been destroyed by spindle poisons such as colchicine. In many organisms, in particular in plant cells, the cell cycle delay induced by colchicine is only transient, and chromatids eventually split apart in the complete absence of a mitotic spindle (*12*, *13*) (Fig. 2).

Research Institute of Molecular Pathology (IMP), Dr. Bohr-Gasse 7, A-1030 Vienna, Austria.

*To whom correspondence should be addressed. E-mail: nasmyth@nt.imp.univie.ac.at

Mitosis in the presence of colchicine or colcemid (known as c-mitosis) leads to the production of daughter cells with twice the normal complement of chromosomes. This process is routinely used for manipulating plant genomes and may contribute to the therapeutic effects of Taxol in treating breast cancer.

A Tense Period in the Cell Cycle

Changes in the interaction between sister chromatids, as opposed to changes in the activity of spindle fibers, are thought to trigger the sudden movement of chromatids to the poles at the metaphase-to-anaphase transition. Destroying the spindle fiber that connects a chromosome to one pole by using ultraviolet (*14*) or laser microbeams (*15*) causes the entire chromosome (i.e., both chromatids) to move rapidly to the opposite pole. The implication is that sister chromatid pairs on the metaphase plate are under tension. Sisters are being pulled away from each other by spindles attached to oppositely oriented sister kinetochores. The apparatus that will move chromatids to the poles during anaphase is therefore already engaged during metaphase. Metaphase is therefore viewed as a state of equilibrium in which traction exerted on kinetochores by spindle fibers is opposed by cohesion between sister chromatids (Fig. 1B) (*7*).

Loss of sister chromatid cohesion would therefore be sufficient for the sudden movement of chromatids to opposite poles at the metaphase-to-anaphase transition. According to this hypothesis, a specific apparatus binds chromatids together during replication, holds them in an orientation that facilitates the attachment of sister kinetochores to spindles extending to opposite poles, and resists the splitting force that results from this bipolar attachment to the spindle. Destruction of this specialized cohesive structure triggers movement of chromatids to opposite poles at the onset of anaphase.

In the absence of molecular details, this notion has remained a working hypothesis only. Indeed, until recently there has been little direct evidence that chromosome separation is due to the loss of cohesion as opposed to the onset of chromatid repulsion (*7*, *16*). An affinity between sister chromatids might be sufficient to resist their tendency to be split by spindle forces up to and during metaphase. Anaphase could be triggered by a repulsive force that overcomes the sister's "natural" affinity. The notion that the midzone of anaphase spindles [or Belar's Stemmkörper (*17*)] might exert this repulsion is now discredited, but unknown repulsive forces may yet lurk in the crevices between sisters.

Ties That Bind Chromatids Together

In many organisms, the regions around centromeres have a special role in holding sister chromatids together during metaphase. Flourescence in situ hybridization shows that most sister DNA sequences separate from each other (at least a short distance) soon after DNA replication (*18*). Nevertheless, sister chromatids usually do not acquire morphologically separate axes until prometaphase, well after the onset of chromosome condensation. Human chromosomes, for example, appear as undivided "sausages" during prophase even though they are already highly condensed (*19*) (Fig. 3A). When sister chromatid arms eventually emerge as separate entities during prometaphase, sister centromeric sequences still hug each other in a compact embrace known as the central constriction (Fig. 3, B and C). When late-mitotic events are inhibited by treatment with spindle poisons, separation of arm sequences continues while that of centromeres is blocked (*20*). The consequence is sister chromatid pairs connected only at centromeres, which though an artefact of drug treatment, is a classic image of mitotic chromosomes.

The robust cohesion at centromeres may be due more to their heterochromatic nature than to their ability to form attachments to the mitotic spindle. Other heterochromatic chromosome domains, like the entire Y

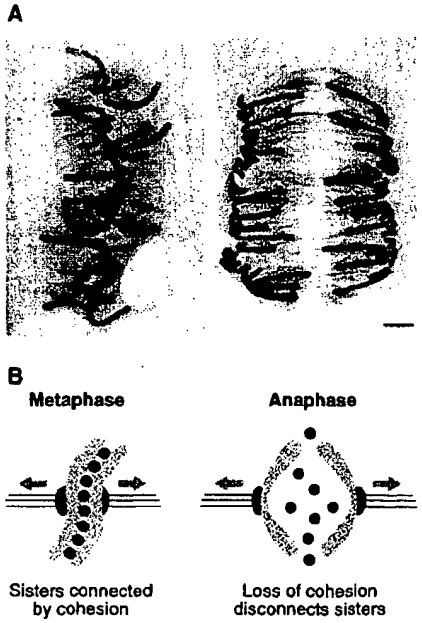

Fig. 1. The metaphase-to-anaphase transition. (**A**) Light micrographs of mitotic figures in endosperm of the African blood lily *Haemanthus katherinae* Bak. Microtubules are stained in red and chromosomes in blue. In metaphase (left), centromere regions are aligned on the spindle equator, whereas in anaphase (right), the arms of separated sister chromatids trail behind centromere regions, which move poleward. Bar, 10 μm. [Reprinted from (*97*) with permission] (**B**) A model depicting how cohesion structures (red dots) physically connect sister chromatids (light blue) during metaphase. Cohesion antagonizes the pulling forces exerted by spindle microtubules (green) on kinetochores (dark blue). During anaphase, loss of cohesion liberates sister chromatids for poleward movement.

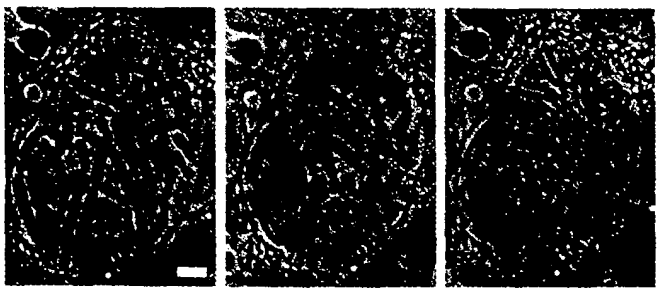

Fig. 2. Sister chromatid separation does not depend on the mitotic spindle. Light micrographs of mitosis in living flattened endosperm from *H. katherinae* Bak treated with colchicine (c-mitosis). The micrographs were taken at 10-min intervals. Bar, 10 μm. [Reprinted from (*12*) with permission]

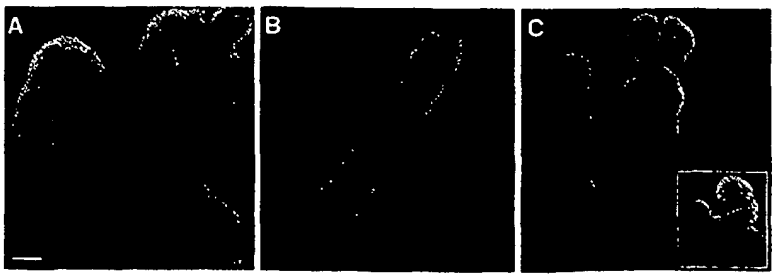

Fig. 3. Chromosome arms begin to separate in prometaphase. Scanning electron micrographs of human chromosomes isolated from cells in prophase (**A**), prometaphase (**B**), metaphase (**C**), and early anaphase [inset in (**C**)]. Bar, 1 μm. [Reprinted from (*19*) with permission]

chromosome in flies, also remain tightly stuck together during mitotic arrest (*21*). A relation between heterochromatin and stickiness is also seen during normal mitoses. Human chromatid pairs move to the poles during anaphase with different kinetics, and the laggards are invariably chromosomes with the greatest amount of centromeric heterochromatin (*22*).

Despite the extra stickiness of centromeres, it is often this region which splits first at the onset of a normal anaphase. Traction exerted at centromeres peels sisters apart, with distal regions of chromosome arms being the last to separate (*5*, *20*). In several organisms, including budding yeast (*23*, *24*), diatoms (*25*), and the crustacean *Ulophysema öresundense* (*26*), sister centromeres are pulled most of the way to the poles even during metaphase, long before arm sequences separate. In these organisms, it appears that loss of cohesion along chromosome arms and not at centromeres is what triggers anaphase (*20*).

Despite these valuble insights, over a century of cytological observation has shed little light on the identity of the sister chromatid cohesion apparatus. In the absence of a biochemical approach, one way forward was inspired guesswork. Once it appeared likely that chromosomes contained one double-stranded DNA molecule, it was proposed that the central constriction might be due to the late replication of centromeric DNA. However, pulse-labeling experiments suggest that little or no DNA is replicated during mitosis (*27*). Another ingenious idea is that sister chromatids are held together by the intertwining (catenation) of sister DNA molecules that arises when two replication forks converge (*28*). According to this notion, increased topoisomerase II (Topo II) activity triggers the final decatenation of sister DNA molecules at the onset of anaphase. Though Topo II is clearly essential to disentangle chromatids (*29*), there is evidence for an independent cohesion apparatus. First, circular mini-chromosomes in yeast are held together in nocodazole-treated cells without any intertwining of sister molecules (*30*). Second, centromeres (though not entire chromosomes) disengage from each other and move to the poles in the absence of any detectable Topo II activity in fission yeast (*31*). Third, addition of Topo II inhibitors to mammalian cells in metaphase fails to block separation of sister centromeres at the onset of anaphase (*32*, *33*).

Cohesin and Its Friends

Genetics is the method of last resort when other approaches reach their limits. The identification of mutants such as desynaptic in maize (*34*) and MeiS332 in *Drosophila* (*35*, *36*), in which sister chromatids dissociate prematurely during meiosis, provided the first inkling that sister chromatid cohesion might be mediated by special proteins (*37*). Despite its important role during meiosis, MeiS332 is dispensable for mitotic divisions and is therefore unlikely to be a universal component of the cohesion apparatus.

Genetic studies in yeast have meanwhile uncovered a multisubunit complex called cohesin that is essential for sister chromatid cohesion not only in yeast (*38*) but also in vertebrates (*39*). An important breakthrough in the identification of cohesin was the discovery that proteolysis (*40*), mediated by a ubiquitin protein ligase responsible for destroying mitotic cyclins (*41*, *42*), is needed for sister chromatid separation. This ligase, known as the anaphase-promoting complex (APC) or cyclosome (*43*), was initially thought to mediate proteolysis of cohesion proteins. Its role in sister chromatid separation turns out to be less direct; it in fact mediates destruction of an inhibitor of the sister-separating apparatus (*44*–*47*). Nevertheless, the premise that the APC destroyed cohesion proteins provided a new impetus to the search for proteinaceous bridges connecting sister chromatids. Screens for mutations that permitted separation of sister chromatids in cells lacking APC activity have now identified at least eight proteins essential for sister chromatid cohesion (*38*, *48*–*51*). Remarkably, the function of all these proteins seem to be intimately connected (Fig. 4A).

Four of these proteins, Smc1, Smc3, Scc1 (also called Mcd1 and Rad21), and Scc3, form a multisubunit complex called cohesin (*38*, *39*). Indeed, Mcd1/Scc1 was independently isolated as a dosage suppressor of an Smc1 mutation (*49*). All four cohesin subunits are required both for establishing cohesion during S phase and (at least in yeast) for maintaining it until the onset of anaphase. Two other proteins, Scc2 (Mis4) and Scc4, form a separate complex that is required for the association of cohesin with chromosomes (*52*). Cohesin binds to specific chromosomal loci (including centromeres) for much of interphase (*53*–*55*), but it can only establish cohesion between sister chromatids during DNA replication, possibly when sister DNA molecules emerge from replication forks (*56*). Establishment of sister cohesion is therefore an integral part of S phase.

Another protein, Spo76, is required for orderly sister chromatid cohesion in *Sordaria* (*57*), a genus of fungi. Spo76 has homologs in many organisms, called Pds5 in budding yeast (*58*) and BimD in *Aspergillus nidulans* (*59*). It is not yet understood how Spo76/Pds5 cooperates with cohesin. In budding yeast a protein called Eco1 or Ctf7 is essential for establishing cohesion during S phase but not for maintaining it during G_2 or M phases (*38*, *51*). Its fission yeast homolog Eso1 is also required for establishing sister chromatid cohesion (*60*). Of all known cohesion proteins, the cohesin complex may lie at the heart of the cohesion process because cleavage of one

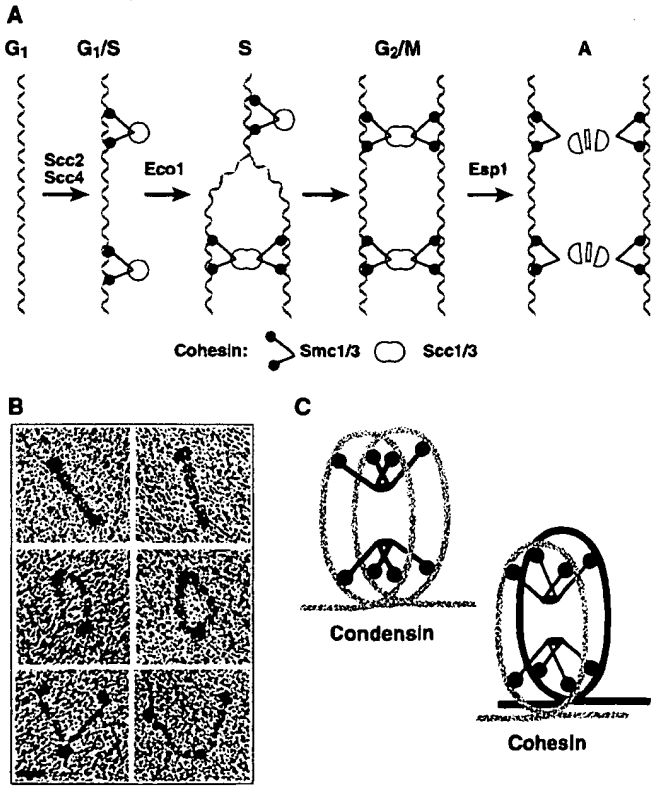

Fig. 4. Cohesin and friends. (**A**) A model illustrating how yeast proteins required for cohesion connect sister chromatids during DNA replication and maintain this association until the onset of anaphase. (**B**) Electron micrographs of homodimers of the *Bacillus subtilis* SMC protein. Three commonly observed conformations are shown. Bar, 20 nm. [Reprinted from (*63*) with permission] (**C**) A speculative model for how cohesin might join sister chromatids together, which is based on the premise that cohesin forms large supercoiled loops analogous to those proposed for condensin (shown alongside).

of its subunits is essential for the separation of sister chromatids, at least in yeast (*61*). *Xenopus* cohesin is also needed for proper sister chromatid cohesion (*39*). Nevertheless, it is still uncertain how, or indeed whether, cohesin holds sisters together during metaphase in animal cells, as most of it dissociates from chromosomes by prometaphase (*39*). It is therefore possible that other important players remain to be identified.

Two cohesin subunits, Smc1 and Smc3, are members of a large family of related proteins whose evolution predates the split between eukaryotes and bacteria (*62*). All Smc proteins have related globular domains at their NH_2- and COOH-termini, joined by two long stretches of α-helical coiled-coil, which are linked by a central flexible hinge. Bacterial Smc proteins form antiparallel homodimers whose terminal globular domains are proposed to form an active adenosine triphosphatase (ATPase). The flexibility of the hinge region allows the Smc homodimer to adopt either a V or a linear shape (Fig. 4B) (*63*). It remains to be seen whether cohesin contains an Smc1/Smc3 heterodimer or Smc1 and Smc3 homodimers.

Little is known about the properties of cohesin in vitro, except that fragments from the COOH-terminal domain of Smc3 and its coiled-coil region can bind DNA (*64*). Smc1 and Smc3 belong to a subfamily of eukaryotic Smc proteins, which includes Smc2 and Smc4. The latter two proteins are components of the condensin complex, which is necessary for mitotic chromosome condensation (*65–67*). Condensin possesses ATPase activity and is capable of forming large supercoiled loops by introducing a global positive writhe (*68*). These positive supercoils might be the driving force for mitotic chromosome condensation. The presence of a pair of Smc proteins in both condensin and cohesin suggests that these two complexes might have similar although not identical activities. Cohesin might, for example, introduce large constrained supercoils, like those produced by condensin, at equivalent positions on each sister chromatid. The Scc1 subunit of cohesin might help link together equivalent coils from each sister (Fig. 4C). An ability to coil chromosomes would explain how cohesin contributes to chromosome compaction (*49*).

In animal cells, condensin binds to chromosomes at about the same time that most cohesin dissociates from them (*39*), between prophase and prometaphase. It is possible that condensin's ability to condense chromosomes as cells enter mitosis depends on the prior dissociation of most cohesin. The connections between sister DNA molecules might otherwise interfere with the locally processive coiling of each chromatid on itself. Cohesin could also contribute to chromosome compaction during interphase and early stages of mitosis by providing longitudinal links along chromatids as well as horizontal ones between sisters (*49*).

Securin: A Protein Whose Destruction by the APC Controls Sister Chromatid Separation

Destruction of mitotic cyclins occurs at or shortly before sister chromatid separation but is not required for this process (*40*, *69*). The discovery that the ubiquitin protein ligase responsible for destroying cyclins was also required for separating sister chromatids (*41*) led to a hunt for other APC targets whose destruction might be necessary for sister separation. Two candidates soon emerged: Pds1 from budding yeast and Cut2 from fission yeast. Destruction of Pds1 and Cut2 proteins at the onset of anaphase depends on APC and is essential for sister chromatid separation (*44–46*). Although these two proteins have rather dissimilar primary sequences, it appears that they are members of a class of anaphase-inhibitory proteins existing in all eukaryotes and now called securins because of their role in controlling the onset of sister separation (Fig. 5).

The human securin protein (*70*) is overproduced in many tumor cells (*71*) and is thought to be an oncogene (*72*). Increased securin levels might cause missegregation of chromosomes and thereby facilitate genome instability. A possible candidate for the securin homolog in *Drosophila* is the pimples protein, which like yeast and vertebrate securins is destroyed at the metaphase-to-anaphase transition (*73*). In budding yeast, Pds1 is only essential for proliferation at high temperatures (*74*), and its elimination permits sister separation in the absence of APC activity (*44*, *47*). So, destruction of securin might be the APC's sole role in the triggering of sister separation, at least in yeast.

Separin: An Endopeptidase Necessary for Separating Chromatids?

The budding yeast securin has what appears to be a single stable partner, a 180-kD protein called Esp1 (*47*). In fission yeast, Cut2 had previously been found to be associated with Cut1, an Esp1 homolog (*75*). Vertebrate securins are likewise associated with an Esp1 homolog (*70*). Esp1/Cut1-like proteins, now known as separins, are found in most if not all eukaryotes. They are usually large proteins, with molecular sizes from 180 to 200 kD, containing a conserved COOH-terminal "separin" domain. In budding yeast (*47*, *76*), fission yeast (*75*), and *Aspergillus* (*77*), separins are essential for sister chromatid separation. Despite failing to separate sister chromatids, separin mutants proceed with most if not all other aspects of the cell cycle. It has been proposed that separins are dedicated "sister-separating" proteins whose activity is held in check by their association with securins. According to this hypothesis, the APC mediates sister chromatid separation by liberating separin from its inhibitory embrace by securin (Fig. 5) (*47*).

A clue to the mechanism by which separin splits sister chromatids was the observation that in budding yeast (contrary to most other eukaryotic cells) most Scc1 remains bound to chromosomes until the metaphase-to-anaphase transition (*48*). The dissociation of Scc1 from chromosomes at the onset of anaphase depends on separin (*47*) and is accompanied by the proteolytic cleavage of Scc1, both in vivo and in vitro (*61*). Separin induces Scc1 cleavage at two related sites, each with an arginine in the P1 position. Mutation of either arginine to aspartic acid abolishes cleavage at that site but is not lethal to the cell. However, simultaneous mutation of both sites is lethal and prevents both sister chromatid separation and Scc1's dissociation from chromosomes (*61*). Similar potential cleavage sites are found in Rad21, the fission yeast Scc1 homolog, and their simultaneous (but not single) mutation also blocks chromosome segregation (*78*). Cleavage of cohesin's Scc1 subunit might therefore be a conserved feature of sister chromatid separation, at least in fungi (Fig. 5).

With the recent addition of several other separins to the databases, the conserved amino acid residues within the separin domain have been identified. They include a universally conserved histidine and cysteine resi-

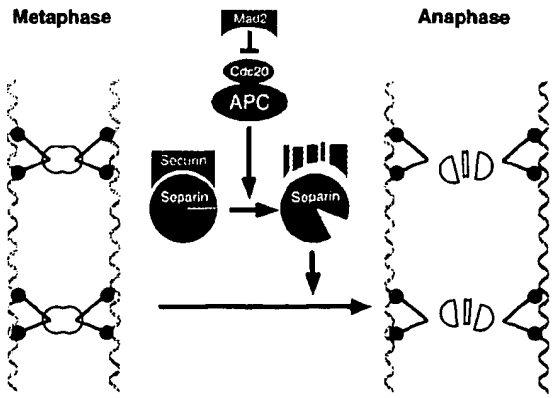

Fig. 5. The APC-separin pathway. A model illustrating how APC^{Cdc20} initiates anaphase through the activation of separin and subsequent cleavage of a cohesin subunit.

due, which is a hallmark of cysteine endopeptidases (*79*). The sequences flanking these two residues are characteristic of cysteine endopeptidases of the CD subclass, which includes caspases, legumains, and two bacterial proteases, gingipain and clostripain, (*80*). Thus, separin might indeed be the protease that cleaves Scc1. Whether cohesin's Scc1 subunit is the sole target of separin is presently unclear but certainly possible, for the only other yeast protein to contain good matches to the Scc1/Rad21 consensus is Rec8, a related protein that replaces Scc1 in the cohesin complex during meiosis (*81*). It will be crucial to address whether cleavage of Scc1 alone is sufficient to trigger anaphase in yeast and whether sister separation in animal and plant cells also depends on cleavage of cohesion proteins.

The proposed COOH-terminal catalytic domain of separin depends (at least for in vivo activity) on a long NH_2-terminal domain, which is bound by its inhibitory securin chaperone (*82*). Securin must do more than just inhibit separin, because sister separation fails to occur in cut2 (*75*) and pimples (*73*) mutants and is inefficient in pds1 securin mutants (*47*). Securin might either target separin to its future sites of action in the cell or help separin adopt a potentially active conformation, which is only unleashed on the cell when securins are destroyed by the APC.

Cutting the Gordian Knot

Could proteolytic cleavage of a cohesin subunit really be a universal trigger for sister separation? If so, how does one explain the dissociation of the bulk of cohesin from chromosomes during prometaphase in organisms other than yeast (*39*)? In vertebrates, this process clearly occurs in the absence of APC activity and is therefore presumably not due to separin activity (*83*). The implication is that two separate pathways must exist for removing cohesin from chromosomes: one, thus far detected only in yeast, involving Scc1 cleavage at the metaphase-to-anaphase transition; and a second, possibly absent in yeast, that removes cohesin from chromosomes during prometaphase in the absence of cleavage (Fig. 6). It is of course possible that Scc1 is simply not cleaved at all by separin in animal cells and that some as yet unidentified cohesion protein that does indeed persist on chromosomes until metaphase is separin's true target. Given the conservation of cell cycle mechanisms, it seems more likely that eukaryotic cells in fact possess both the cleavage and noncleavage cohesin-removal pathways and that separin's target is a residual amount of Scc1 associated with metaphase chromosomes, in particular in centromeric regions. Consistent with this hypothesis, a small fraction of cohesin remains associated with metaphase chromosomes in human cells, and a similar fraction of Scc1 is cleaved around anaphase (*84*). Let us therefore explore this working hypothesis further, bearing in mind that what applies to cohesin could equally apply to other as yet unidentified cohesion proteins.

The noncleavage pathway would remove most cohesin during prophase/prometaphase by an as yet obscure mechanism. This pathway could involve phosphorylation of a cohesin subunit by mitotic protein kinases, because vertebrate cohesins rebind to chromatin in telophase when mitotic kinases are inactivated and chromosomes decondense (*39*). The dissociation of cohesin from chromatin during prophase coincides with, but does not depend on, the association of condensin with chromosomes. This first phase of cohesin removal may be crucial (possibly along with the arrival of condensin) for the initial splitting of chromosomes into two morphologically separable chromatids.

Although it commences during prophase, the noncleavage pathway possibly does not complete its task before separins are activated after congression of all chromatid pairs to the metaphase plate. This would explain why cohesion between chromosome arms is the last to be peeled away during undisturbed mitoses and why arm cohesion appears to be sufficient for orderly chromosome segregation when centromeric cohesion has been destroyed by a laser beam (*20*). Nevertheless, given sufficient time, the noncleavage pathway is capable of removing all cohesin from chromosome arms, which explains why sister chromatid arms fully separate whereas centromeres remain connected in cells treated with spindle poisons (*13*) or in *Drosophila* mutants lacking either the APC activator Fizzy/Cdc20 (*21*) or the putative securin pimples (Fig. 6B) (*73*).

According to our hypothesis, something prevents the full removal of cohesin from heterochromatic regions, including all centromeres, where the interface between sister chromatids during metaphase is far more extensive than along chromosome arms (*85*, *86*). The final disentanglement of sister chromatids can only be achieved by cleavage of the "gordian knot" by separin. If as proposed by this hypothesis, cleavage of Scc1-like proteins is crucial for the final act of sister separation in all eukaryotic cells, this Achilles heal of the cohesion system deserves a nobler name ("gordin," for example) than the current ragbag of three-letter words inherited from different organisms. It is currently unclear what property of heterochromatin might protect cohesin (or other cohesion proteins for that matter) from the noncleavage dissociation pathway during metaphase. It is possible that the fairly widespread pathological phenomenon of premature centromere division (*87*), which is thought to cause aneuploidy and is found in patients with Roberts syndrome (*88*), might be caused by centromeric cohesion becoming susceptible to the noncleavage pathway.

Controlled Cutting

As Mazia noted in 1961, "metaphase strikes us as an interruption of the flow of events, during which the mitotic apparatus is waiting for something to happen" and that "chromosome splitting can be viewed as an event timed by a signal given by the cell and one that that does not depend on the mitotic ap-

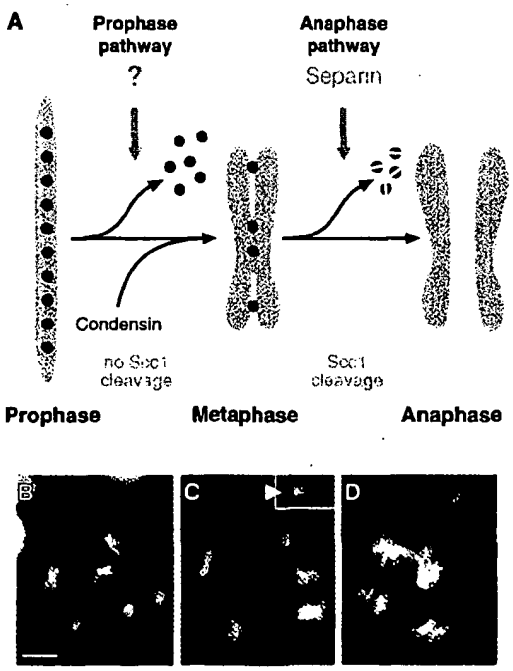

Fig. 6. (A) A two-step model for the sequential loss of sister chromatid cohesion in animal cells. The bulk of cohesion proteins may be removed from condensing chromosomes during prophase by a separin-independent pathway, which might involve mitotic kinases such as Cdk1, Polo, and Aurora. Activation of the separin pathway then initiates anaphase by cleaving residual cohesion proteins that remain on chromosomes, in particular at centromeres. (B to D) Mitotic chromosomes from wild-type *Drosophila* cells (B) and pimples mutant cells after one (C) and two (D) rounds of re-replication after possible failure of the separin pathway. [Reprinted from (*73*) with permission] Chromatids of autosomes are held together solely in pericentric heterochromatic regions but along the entire Y chromosome [inset in (C)]. Bar, 5 μm.

paratus" (*7*, p. 233). Mazia's "signal" is presumably the liberation of separin from its inhibition by securin. If so, what initiates this process? Time-lapse photography of mitosis supplied the answer: "Chromosomes that have already reached the equator wait for chromosomes delayed at one pole" (i.e., those that have not yet formed bipolar attachments to the spindle) "and only when the metaphase plate contains all the chromosomes does anaphase begin" (*7*, p. 268). This is a fairly clear description written over 40 years ago of the chromosome-alignment surveillance mechanism, which is also called the spindle assembly checkpoint (*89*). In most, but not all, eukaryotic cells, unaligned or lagging chromosomes transmit a signal by way of the protein Mad2, which inhibits the APC and its activator protein Cdc20 and thereby prevents the proteolysis of both B-type cyclins and securins. It is the block to securin destruction that prevents Scc1 cleavage and thereby sister chromatid separation (Fig. 5) (*90*).

The Mad2 pathway is thought to be essential for regulating mitosis in somatic cells of many organisms. In its absence, chromatin bridges, lagging chromosomes, and chromosome fragmentation are observed during anaphase (*91*). Most tumor cells are highly aneuploid and moreover have unstable karyotypes, which might be caused by defects in the Mad2 pathway (*92*). Nevertheless, destruction of securin by the APC is tightly regulated by mechanisms that are independent of Mad2. These involve the accumulation of Cdc20 protein only as cells enter mitosis (*93*, *94*) and phosphorylation of APC by mitotic kinases, which enables the complex to respond to Cdc20 (*95*, *96*). Strikingly, sister chromatid separation remains tightly regulated in budding yeast mutants lacking securin (*90*), suggesting that other mechanisms regulate cleavage of Scc1.

Summary

The veil of mystery surrounding the sister separation process for over a century is finally lifting. There is now convincing evidence that the sudden movement of chromosomes to the poles at the onset of anaphase is triggered by cleavage of specific sister chromatid cohesion proteins. Future research must address the structural basis of cohesion and how it is established only at replication forks. It must also address the generality of mechanisms that dismantle cohesion at the metaphase-to-anaphase transition and how mistakes in this process contribute to human disease.

References and Notes

1. I. Wilmut, A. E. Schnieke, J. McWhir, A. J. Kind, K. H. Campbell, *Nature* **385**, 810 (1997).
2. P. Nurse, *Nature* **344**, 503 (1990).
3. L. H. Hartwell and T. A. Weinert, *Science* **246**, 629 (1989).
4. W. Flemming, *Arch. Mikrosk. Ana.* **18**, 151 (1879).
5. E. B. Wilson, *The Cell in Development and Heredity* (Macmillan, New York, ed. 3, 1925).
6. F. Schrader, *Mitosis* (Columbia Univ. Press, New York, 1944).
7. D. Mazia, *Mitosis and the Physiology of Cell Division*, J. Brachet and A. E. Mirsky, Eds. (Academic Press, New York, 1961), vol. 3.
8. J. D. Watson and F. H. C. Crick, *Nature* **171**, 964 (1953).
9. M. P. Maguire, *Biochem. Cell Biol.* **68**, 1231 (1990).
10. D. C. Lin and A. D. Grossman, *Cell* **92**, 675 (1998).
11. R. B. Nicklas and S. C. Ward, *J. Cell Biol.* **126**, 1241 (1994).
12. J. Mole-Bajer, *Chromosoma* **9**, 332 (1958).
13. C. L. Rieder and R. E. Palazzo, *J. Cell Sci.* **102**, 387 (1992).
14. K. Izutsu, *Mie Med. J.* **9**, 15 (1959).
15. P. A. McNeill and M. W. Berns, *J. Cell Biol.* **88**, 543 (1981).
16. C. D. Darlington, *The Evolution of Genetic Systems* (Basic Books, New York, 1939).
17. K. Belar, *Wilhelm Roux Arch. Entwicklungsmech. Org.* **118**, 359 (1929).
18. S. Selig, K. Okumura, D. C. Ward, H. Cedar, *EMBO J.* **11**, 1217 (1992).
19. A. T. Sumner, *Chromosoma* **100**, 410 (1991).
20. C. L. Rieder and R. Cole, *J. Cell Sci.* **112**, 2607 (1999).
21. S. Sigrist, H. Jacobs, R. Stratmann, C. F. Lehner, *EMBO J.* **14**, 4827 (1995).
22. B. K. Vig, *Hum. Genet.* **57**, 247 (1981).
23. T. Tanaka and K. Nasmyth, personal communication.
24. G. Goshima and M. Yanagida, *Cell* **100**, 619 (2000).
25. D. H. Tippet, J. D. Pickett-Heaps, R. L. Leslie, *J. Cell Biol.* **86**, 402 (1980).
26. Y. Melander, *Heriditas* **36**, 233 (1950).
27. D. E. Comings, *Science* **154**, 1463 (1966).
28. A. W. Murray and J. W. Szostak, *Annu. Rev. Cell Biol.* **1**, 289 (1985).
29. S. Dinardo, K. A. Voelkel, R. L. Sternglanz, *Proc. Natl. Acad. Sci. U.S.A.* **81**, 2616 (1984).
30. D. Koshland and L. Hartwell, *Science* **238**, 1713 (1987).
31. H. Funabiki, I. Hagan, S. Uzawa, M. Yanagida, *J. Cell Biol.* **121**, 961 (1993).
32. C. S. Downes, A. M. Mullinger, R. T. Johnson, *Proc. Natl. Acad. Sci. U.S.A.* **88**, 8895 (1991).
33. G. J. Gorbsky, *Cancer Res.* **54**, 1042 (1994).
34. M. P. Maguire, A. M. Paredes, R. W. Riess, *Genome* **34**, 879 (1991).
35. B. K. Davis, *Mol. Gen. Genet.* **113**, 251 (1971).
36. L. S. B. Goldstein, *Chromosoma* **78**, 79 (1980).
37. A. W. Kerrebrock, D. P. Moore, J. S. Wu, T. L. Orr-Weaver, *Cell* **83**, 247 (1995).
38. A. Toth *et al.*, *Genes Dev.* **13**, 320 (1999).
39. A. Losada, M. Hirano, T. Hirano, *Genes Dev.* **12**, 1986 (1998).
40. S. L. Holloway, M. Glotzer, R. W. King, A. W. Murray, *Cell* **73**, 1393 (1993).
41. S. Irniger, S. Piatti, C. Michaelis, K. Nasmyth, *Cell* **81**, 269 (1995).
42. R. W. King *et al.*, *Cell* **81**, 279 (1995).
43. W. Zachariae and K. Nasmyth, *Genes Dev.* **13**, 2039 (1999).
44. A. Yamamoto, V. Guacci, D. Koshland, *J. Cell Biol.* **133**, 99 (1996).
45. O. Cohen-Fix, J.-M. Peters, M. W. Kirschner, D. Koshland, *Genes Dev.* **10**, 3081 (1996).
46. H. Funabiki *et al.*, *Nature* **381**, 438 (1996).
47. R. Ciosk, *et al.*, *Cell* **93**, 1067 (1998).
48. C. Michaelis, R. Ciosk, K. Nasmyth, *Cell* **91**, 35 (1997).
49. V. Guacci, D. Koshland, A. Strunnikov, *Cell* **91**, 47 (1997).
50. K. Furuya, K. Takahashi, M. Yanagida, *Genes Dev.* **12**, 3408 (1998).
51. R. V. Skibbens, L. B. Corson, D. Koshland, P. Hieter, *Genes Dev.* **13**, 307 (2000).
52. R. Ciosk *et al.*, *Mol. Cell* **5**, 1 (2000).
53. T. Tanaka, M. P. Cosma, K. Wirth, K. Nasmyth, *Cell* **98**, 847 (1999).
54. Y. Blat and N. Kleckner, *Cell* **98**, 249 (1999).
55. P. C. Megee, C. Mistrot, V. Guacci, D. Koshland, *Mol. Cell* **4**, 445 (1999).
56. F. Uhlmann and K. Nasmyth, *Curr. Biol.* **8**, 1095 (1998).
57. D. van Heemst, H. James, S. Pöggeler, V. Berteaux-Lecellier, D. Zickler, *Cell* **98**, 261 (1999).
58. http://genome-www.stanford.edu/Saccharomyces/
59. S. H. Denison, E. Kafer, G. S. May, *Genetics* **134**, 1085 (1993).
60. K. Tanaka *et al.*, *Mol. Cell. Biol.* **20**, 3459 (2000).
61. F. Uhlmann, F. Lottspeich, K. Nasmyth, *Nature* **400**, 37 (1999).
62. T. Hirano, *Genes Dev.* **13**, 11 (1999).
63. T. E. Melby, C. N. Ciampaglio, G. Briscoe, H. P. Erickson, *J. Cell Biol.* **142**, 1595 (1998).
64. A. T. Akhmedov, B. Gross, R. Jessberger, *J. Biol. Chem.* **274**, 38216 (1999).
65. T. Hirano and T. J. Mitchison, *Cell* **79**, 449 (1994).
66. Y. Saka *et al.*, *EMBO J.* **13**, 4938 (1994).
67. T. Hirano, R. Kobayashi, M. Hirano, *Cell* **89**, 511 (1997).
68. K. Kimura, V. V. Rybenkov, N. J. Crisona, T. Hirano, N. R. Cozzarelli, *Cell* **98**, 239 (1999).
69. U. Surana *et al.*, *EMBO J.* **12**, 1969 (1993).
70. H. Zou, T. J. McGarry, T. Bernal, M. W. Kirschner, *Science* **285**, 418 (1999).
71. C. Saez *et al.*; *Oncogene* **18**, 5473 (1999).
72. L. Pei and S. Melmed, *Mol. Endocrinol.* **11**, 433 (1997).
73. R. Stratmann and C. F. Lehner, *Cell* **84**, 25 (1996).
74. A. Yamamoto, V. Guacci, D. Koshland, *J. Cell Biol.* **133**, 85 (1996).
75. H. Funabiki, K. Kumada, M. Yanagida, *EMBO J.* **15**, 6617 (1996).
76. J. T. McGrew, L. Goetsch, B. Byers, P. Baum, *Mol. Biol. Cell* **3**, 1443 (1992).
77. G. S. May, C. A. McGoldrick, C. L. Holt, S. H. Denison, *J. Biol. Chem.* **267**, 15737 (1992).
78. K. Nagao, F. Uhlmann, K. Nasmyth, M. Yanagida, unpublished results
79. A. J. Barrett, N. D. Rawlings, J. F. Woessner, Eds., *Handbook of Proteolytic Enzymes* (Academic Press, London, 1998).
80. J. M. Chen, N. D. Rawlings, R. A. Stevens, A. J. Barrett, *FEBS Lett.* **441**, 361 (1998).
81. F. Klein *et al.*, *Cell* **98**, 91 (1999).
82. K. Kumada *et al.*, *Curr. Biol.* **8**, 633 (1998).
83. I. Sumara and J.-M. Peters, personal communication.
84. I. Waizenegger, S. Hauf, J.-M. Peters, personal communication.
85. L. M. Lica, S. Narayanswami, B. A. Hamkalo, *J. Cell Biol.* **103**, 1145 (1986).
86. J. B. Rattner, *Bioessays* **13**, 51 (1991).
87. P. H. Fitzgerald, A. F. Pickering, J. M. Mercer, P. M. Miethke, *Ann. Hum. Genet.* **38**, 417 (1975).
88. D. Tomkins, A. Hunter, M. Roberts, *Am. J. Med. Genet.* **4**, 17 (1979).
89. A. Amon, *Curr. Opin. Genet. Dev.* **9**, 69 (1999).
90. G. Alexandru, W. Zachariae, A. Schleiffer, K. Nasmyth, *EMBO J.* **18**, 2707 (1999).
91. J. Basu *et al.*, *J. Cell Biol.* **146**, 13 (1999).
92. D. P. Cahill, *et al.*, *Nature* **392**, 300 (1998).
93. J. Weinstein, *J. Biol. Chem.* **272**, 28501 (1997).
94. M. Shirayama, W. Zachariae, R. Ciosk, K. Nasmyth, *EMBO J.* **17**, 1336 (1998).
95. M. Shteinberg, Y. Protopopov, T. Listovsky, M. Brandeis, A. Hershko, *Biochem. Biophys. Res. Commun.* **260**, 193 (1999).
96. E. R. Kramer, N. Scheuringer, A. V. Podtelejnikov, M. Mann, J.-M. Peters, *Mol. Biol. Cell* **11**, 1555 (2000).
97. A. Khodjakov, R. W. Cole, A. S. Bajer, C. L. Rieder, *J. Cell Biol.* **132**, 1093 (1996).

98. We thank E. Koonin for first pointing out the conserved His and Cys residues in the separin sequences. We also thank K. Nagao, I. Sumara, S. Hauf, I. Waizenegger, and M. Yanagida for communicating unpublished results; D. Schweizer and H. Tkadletz for help with the figures; A. Bajer, H. Erickson, C. Lehner, J. Mole-Bajer, C. Rieder, and A. Sumner for providing micrographs; S. Vrba for library support; and M. Glotzer, C. Lehner, A. Nasmyth, C. Rieder, D. Schweizer, and T. Skern for discussions and comments on the manuscript. Supported by grants from the Austrian Industrial Research Promotion Fund (FFF) and the Austrian Science Promotion Fund (FWF) to K.N. and J.-M.P.